

**Probing the Interaction Mechanisms among Asphaltenes, Fine Solids, Water-Oil
Emulsions and Pipeline Surfaces in Oil Sands Production**

by

Lu Gong

A thesis submitted in partial fulfillment of the requirements for the degree of

Doctor of Philosophy

In

Chemical Engineering

Department of Chemical & Materials Engineering

University of Alberta

© Lu Gong, 2020

Abstract

Fouling problem has been one of the most challenging problems in oil industries. Asphaltenes, fine solids, and water-oil emulsions have been regarded as the major components in the fouling phenomena during oil production. Investigating the interactions between foulants (e.g., asphaltenes, fine solids, and water-oil emulsions) and substrate surfaces is of both fundamental and practical importance in understanding the fouling mechanisms and developing efficient antifouling strategies. In this thesis, the atomic force microscope (AFM) colloidal and drop probe techniques have been employed to directly quantify the surface interactions among asphaltenes, silica particles, water-oil emulsions and selected substrates. The commonly used iron substrate and remarkable electroless nickel-phosphorus (EN) coating have been included.

The interaction forces between silica or asphaltene-coated silica particles and iron or EN substrate in aqueous solutions were measured using the AFM colloidal probe technique. The effects of salinity, pH and divalent ions (i.e. Ca^{2+}) were investigated. The obtained force profiles were analyzed using the classic Derjaguin-Landau-Verwey-Overbeek (DLVO) theory. It was noticed that the attractive van der Waals (VDW) force between the particle and the substrate contributed to the attachment of particles, which finally led to the fouling phenomena, whereas the repulsive electric double layer (EDL) force played the important role in the antifouling property. The high salinity in the solutions could significantly compress the electric double layer and minimize the

strength of the EDL repulsion. Basic pH could deprotonate the surface chemical groups and result in more negative surface potentials, thus strengthening the repulsive EDL force. The presence of Ca^{2+} ions could weaken the EDL repulsion because of the high positive charge density of divalent ions and the strong electric screening effect. Meanwhile, the asphaltene-coated silica particle was detected to have stronger adhesion with iron and EN substrates than silica particle due to the functional groups of asphaltenes. The adhesion between silica or asphaltene-coated silica particle and EN coating was much weaker than that with iron substrate, which suggested the easier removal of asphaltenes from EN surface. Moreover, the conducted bulk fouling tests in silica and asphaltene-coated silica particle suspensions showed less fouling of silica and asphaltenes on EN coating, which were consistent with force measurement results.

The interaction forces between water-oil emulsions and iron or EN substrates were investigated using the AFM drop probe technique. In oil-in-water emulsion case, the interaction forces between toluene drops with asphaltenes adsorbed at the interface and iron or EN substrate in aqueous solutions were investigated under effects of asphaltene concentration, salinity, pH and divalent ions. The measured force profiles were theoretically analyzed using the model combining Reynolds lubrication theory and augmented Young-Laplace equation. The results showed that the attractive VDW force played an important role in the fouling phenomena, while the repulsive EDL force prevented the contact between toluene drop and substrate surface, hence contributing to the antifouling property. Besides, the high salinity, acidic pH and presence of Ca^{2+} ions in aqueous solutions were demonstrated to weaken the EDL repulsion and promote

the contact of oil drops on substrate surface. Compared with iron substrate, the surface potential of EN coating in aqueous solution was more negative and thus led to stronger EDL repulsion with oil drops, indicating the difficult contact of oil drops on EN coating surface.

In water-in-oil emulsion case, the interaction forces between water drops with interfacial asphaltenes and iron or EN substrates in organic media were investigated, and the effects of asphaltenes, aging time, solvent type, loading force and contact time were explored. The measured results showed that more interfacially adsorbed asphaltenes, better solvent type, longer aging time, increased loading force and prolonged contact time could result in a stronger adhesion, which was due to the aggregation and the conformational change of interfacial asphaltenes. Moreover, it was noticed that the adhesion between water drops and EN substrate was much weaker than that with iron substrate, suggesting the easier removal of asphaltenes from EN coating surface. Furthermore, the bulk fouling tests of iron and EN substrates in both oil-in-water and water-in-oil emulsions were conducted and the results showed that there was much less asphaltenes on EN coating surface than that on iron substrate, which agreed well with the force measurement results.

This work sheds useful insights into the interaction mechanisms between various foulants (e.g., asphaltenes, fine solids, and water-oil emulsions) and different substrates as well as the fundamental understandings of fouling problems, with the implications for the development of novel efficient antifouling coatings in oil industries.

Preface

Chapter 3 of this thesis has been published as Lu Gong, Jingyi Wang, Ling Zhang, Vahdoddin Fattapour, Mahdi Mahmoudi, Morteza Roostaei, Brent Fermaniuk, Jing-Li Luo and Hongbo Zeng, “Fouling Mechanisms of Fine Solids and Asphaltenes on Carbon Steel in Oil Production and Antifouling Strategies via Electroless Nickel-Phosphorus Coating”, *Fuel*, 252, 188-199. I conducted the force measurements, bulk fouling tests, result analysis, and manuscript composition. Jingyi Wang and Ling Zhang helped me with the experiments. Vahdoddin Fattapour, Mahdi Mahmoudi, and Brent Fermaniuk provided the experimental materials and corresponding characterization. Dr. Jing-Li Luo contributed to the manuscript edits. Dr. Hongbo Zeng was the corresponding author and involved in the manuscript composition.

Chapter 4 of this thesis has been published as Lu Gong, Xiaoyong Qiu, Ling Zhang, Jun Huang, Wenjihao Hu, Li Xiang, Da Zhu, Reza Sabbagh, Mahdi Mahmoudi, Vahdoddin Fattapour, Jing-Li Luo and Hongbo Zeng, “Probing the Interaction Mechanism between Oil-in-Water Emulsions and Electroless Nickel-Phosphorus Coating with Implications for Antifouling in Oil Production”, *Energy & Fuels*, 33, 3764-3775. I was responsible for the AFM experiments and data analysis, as well as the manuscript composition. Xiaoyong Qiu, Ling Zhang and Jun Huang conducted the bulk fouling tests. Wenjihao Hu and Li Xiang and I collaborated in the surface energy measurements. Da Zhu, Reza Sabbagh, Mahdi Mahmoudi, and Vahdoddin Fattapour provided the metal substrates. Dr. Jing-Li Luo contributed to the manuscript edits. Dr.

Hongbo Zeng was the supervisor and contributed in the manuscript composition.

Chapter 5 of this thesis has been submitted as Lu Gong, Ling Zhang, Li Xiang, Jiawen Zhang, Vahdoddin Fattapour, Mahdi Mahmoudi, Morteza Roostaei, Brent Fermaniuk, Jing-Li Luo and Hongbo Zeng, “Surface Interactions between Water-in-Oil Emulsions with Asphaltenes and Electroless Nickel-Phosphorus Coating”, *Langmuir*. I and Ling Zhang conducted the force measurements. Li Xiang and Jiawen Zhang were responsible for the material preparation and characterization. Vahdoddin Fattapour, Mahdi Mahmoudi, Morteza Roostaei, and Brent Fermaniuk provided the experimental materials. Dr. Jing-Li Luo contributed to the manuscript edits. Dr. Hongbo Zeng was the corresponding author and supervisor, who was involved in the manuscript composition.

Chapter 1, 2 and 6 are originally written by Lu Gong, and have never been published before.

Acknowledgement

First of all, I want to sincerely express my greatest gratitude to my supervisor, Prof. Hongbo Zeng, for his solid support, valuable guidance and inspiring thoughts during my Ph.D program. He helped me every time when I came into difficulties in the past five years. His dedication and passion in the scientific researches always encouraged me to keep learning and investigating all the phenomena that I have observed. The insightful discussions with Prof. Zeng also let me to think more and more, which would be beneficial for my entire life. I also would like to thank my co-supervisor Dr. Jing-Li Luo for all her help and guidance in my research project.

Secondly, I wish to thank all my group members for their support and help in my Ph.D study. I would like to express my special thanks to Dr. Jingyi Wang, Mr. Li Xiang, Dr. Jiawen Zhang, and Dr. Ling Zhang for their precious supports and contributions to the accomplishment of my Ph.D program. I also want to appreciate the kind help from the RGL Reservoir Management Inc. (RGL).

Thirdly, I would like to acknowledge the Natural Sciences and Engineering Research Council of Canada (NSERC), RGL Reservoir Management Inc. (RGL), Canada Foundation for Innovation (CFI), and the Canada Research Chairs Program (H. Zeng).

Finally, I would like to thank my parents for their support, encouragement and confidence to me. I would never be able to continue and finish my Ph.D study without their company.

Table of Contents

Abstract.....	ii
Preface.....	v
Acknowledgement	vii
List of Tables.....	xiii
List of Figures.....	xv
List of Acronyms.....	xxiii
List of Symbols.....	xxiv
Chapter 1 Introduction	1
1.1 Fouling problems in oil industries.....	1
1.1.1 Fouling problems	1
1.1.2 Foulant compositions	3
1.1.3 Interaction and adsorption mechanisms of asphaltenes on substrate surfaces	7
1.2 Protective methods to pipelines	8
1.3 Techniques to investigate the interaction and adsorption of asphaltenes on substrate surfaces	11
1.3.1 Contact angle measurement	11
1.3.2 Quartz crystal micro-balance with dissipation (QCM-D).....	12
1.3.3 Surface forces apparatus (SFA).....	12
1.3.4 Atomic force microscope (AFM).....	14
1.4 Objectives.....	15

1.5 Structure of the thesis.....	16
Reference	18
Chapter 2 Materials and Experimental Techniques.....	42
2.1 Electroless nickel-phosphorus (EN) coating	42
2.2 Atomic force microscope colloidal probe technique.....	43
2.2.1 Experimental setup.....	43
2.2.2 Theoretical analysis.....	45
2.3 Atomic force microscope drop probe technique.....	47
2.3.1 Experimental setup.....	47
2.3.2 Theoretical analysis.....	49
2.4 Quartz crystal micro-balance with dissipation monitoring technique.....	51
2.5 Three probe liquid technique.....	54
Reference	55
Chapter 3 Fouling Mechanisms of Asphaltenes and Fine Solids on Bare and Coated Carbon Steel in Oil Production.....	59
3.1 Introduction.....	59
3.2 Materials and Methodology	61
3.2.1 Materials.....	61
3.2.2 Preparation of Electroless Nickel-phosphorus (EN) Coating.....	62
3.2.3 Preparation of silica and asphaltenes probes.....	63
3.2.4 Force measurements using colloidal probe technique.....	64
3.2.5 Bulk fouling tests.	67

3.3 Results and Discussion.....	68
3.3.1 Characterization of EN coating.....	68
3.3.2 Effect of electrolyte (NaCl) concentration.....	69
3.3.3 Effect of pH.....	76
3.3.4 Effect of calcium ion.....	79
3.3.5 Bulk fouling tests in silica and asphaltenes-coated silica suspensions.....	82
3.4 Conclusions.....	89
3.5 Supporting information.....	90
Reference.....	95
Chapter 4 Probing the Interaction Mechanism Between Oil-in-Water Emulsions and Electroless Nickel-phosphorus (EN) Coating with Implications for Antifouling in Oil Production	116
4.1 Introduction.....	116
4.2 Experimental Section	118
4.2.1 Materials.....	118
4.2.2 Preparation of iron and EN substrates.....	119
4.2.3 Surface energies of Fe/EN substrates using Lifshitz-van der Waals Acid/Base approach.....	120
4.2.4 Force measurements using drop probe AFM technique.....	121
4.2.5 Theoretical analysis of force profiles.....	122
4.2.6 Bulk fouling tests in oil-in-water emulsions with asphaltenes.....	124
4.3 Results and Discussion.....	125
4.3.1 Surface properties of Fe/EN substrates.....	125

4.3.2 Effects of salinity on surface forces.	127
4.3.3 Effects of asphaltenes.....	132
4.3.4 Effects of pHs.....	136
4.3.5 Effects of Ca ²⁺ ions.....	138
4.3.6 Fouling tests in toluene-in-water emulsions.....	140
4.4 Conclusions.....	141
Reference	143
Chapter 5 Surface Interactions between Water-in-Oil Emulsions with Asphaltenes and Electroless Nickel-phosphorus Coating.....	
5.1 Introduction.....	151
5.2 Materials and Experimental Methods	154
5.2.1 Materials.....	154
5.2.2 Preparation of Fe and EN coating substrates.....	155
5.2.3 AFM force measurements.	155
5.2.4 Bulk fouling tests.	158
5.3 Results and Discussion.....	159
5.3.1 Characterization of Fe and EN substrates.	159
5.3.2 Effect of asphaltene concentrations.....	160
5.3.3 Effect of solvent type.	164
5.3.4 Effect of aging time.....	166
5.3.5 Effect of contact time.	168
5.3.6 Effect of loading force.....	169

5.3.7 Bulk fouling tests	170
5.4 Conclusions.....	172
5.5 Support information	174
Reference	186
Chapter 6 Conclusions and Future Works.....	195
6.1 Major conclusions	195
6.2 Original contributions	197
6.3 Suggestions for future work.....	200
Bibliography	202

List of Tables

Table 2.1 Bath compositions and environmental conditions for deposition of EN coating.....	43
Table 3.1 Bath compositions and reaction conditions for EN coating deposition	63
Table 3.2 The Hamaker constants and surface potentials of silica, asphaltenes, L80 and EN in 1, 10 and 100 mM NaCl solutions.	74
Table 3.3 The surface potentials of silica, asphaltenes, L80 and EN in 1 mM NaCl solutions at pH of 5.5, 8.0 and 10.5.	78
Table 3.4 The surface potentials of silica, asphaltenes, L80 and EN in 1 mM NaCl solutions at pH 8.0 with the addition of 0, 1 and 10 mM Ca ²⁺	81
Table 3.S1 The Hamaker constants and surface potentials of silica and asphaltenes in 1, 10 and 100 mM NaCl solutions.	91
Table 3.S2 The surface potentials of silica and asphaltenes in 1 mM NaCl solutions at pH of 5.5, 8.0 and 10.5.....	92
Table 3.S3 The surface potentials of silica and asphaltene surfaces in 1 mM NaCl solutions with 0, 1 mM and 10 mM Ca ²⁺ (pH=8.0).....	93
Table 4.1 Bath compositions and environmental conditions for deposition of EN coating.....	119
Table 4.2 Surface energy components of water, DIM and DMSO.....	121
Table 4.3 Calculated surface energies of Fe and EN substrates.	127
Table 4.4 Theoretical fitted Hamaker constant (based on the surface force profiles	

measured in 100 mM NaCl) and theoretical Hamaker constant of a toluene drop and Fe/EN substrate in aqueous solutions.	131
Table 5.1 The compositions of the bath solution for EN coating.	155

List of Figures

Figure 1.1 Schematic illustration of the asphaltenes fouling process on metal substrate.	7
Figure 2.1 Schematic illustration of the atomic force microscope (AFM) colloidal probe technique.....	45
Figure 2.2 Schematic illustration of the AFM drop probe technique.....	49
Figure 2.3 Schematic illustration of quartz crystal microbalance with dissipation monitoring technique.	52
Figure 3.1 Schematic of AFM colloidal probe technique in aqueous solution. The inset shows the SEM image of a typical silica probe (Scale bar: 5 μm).....	64
Figure 3.2 (A) SEM image of EN coating deposited on L80. (B) EDS spectrum of EN coating. (C) SEM image of the cross section of the EN coating. (D, E, F) EDS elemental mapping of the cross section of EN coating for elements Fe, P and Ni.....	69
Figure 3.3 Topographic AFM image of (A) EN coating and (B) L80 substrate. The root-mean-square (rms) roughness is 21.9 nm for EN and 12.5 nm for L80.	69
Figure 3.4 Normalized surface interaction forces during approaching in 1, 10 and 100 mM NaCl solutions for (A) silica probe vs. L80 substrate, (B) silica probe vs. EN substrate, (C) asphaltenes-coated silica probe vs. L80 substrate, and (D) asphaltenes-coated probe vs. EN substrate.....	70

Figure 3.5 Normalized surface interaction forces during approaching in 1 mM NaCl solution at pH of 5.5, 8.0 and 10.5 for (A) silica probe vs. L80 substrate, (B) silica probe vs. EN substrate, (C) asphaltenes-coated silica probe and L80 substrate, and (D) asphaltenes-coated silica probe and EN substrate..... 76

Figure 3.6 Normalized surface interaction forces during approaching in 1 mM NaCl solutions at pH 8.0 with the addition of 0, 1 and 10 mM Ca²⁺ for (A) silica probe vs. L80 substrate, (B) silica probe and EN substrate, (C) asphaltenes-coated silica probe and L80 substrate, and (D) asphaltenes-coated silica probe and EN substrate..... 80

Figure 3.7 Optical images of L80 and EN substrates after bulk fouling tests in silica and asphaltenes suspensions with 1, 10 and 100 mM NaCl. (A) L80 substrates in silica suspensions. (B) EN substrates in silica suspensions. (C) L80 substrates in asphaltenes-coated silica suspensions. (D) EN substrates in asphaltenes-coated silica suspensions. (The size of substrates 8×8×3 mm.) 83

Figure 3.8 SEM and EDS results of L80 and EN substrates after bulk fouling tests in silica and asphaltenes suspensions with 100 mM NaCl. (A, B) L80 substrate in silica suspensions. (C, D) EN substrate in silica suspensions. (E, F) L80 substrate in asphaltenes suspensions. (G, H) EN substrate in asphaltenes suspensions. (Scale bar: 25 μm)..... 85

Figure 3.9 Optical images of L80 and EN substrates after bulk fouling tests in silica and asphaltenes suspensions with 1mM NaCl solution and pH of 5.5, 8.0 and 10.5. (A) L80 substrates in silica suspensions. (B) EN substrates in silica

suspensions. (C) L80 substrates in asphaltenes-coated silica suspensions. (D) EN substrates in asphaltenes-coated silica suspensions. (The dimensions of substrates are: 8×8×3 mm.).....86

Figure 3.10 Images of L80 and EN substrates after bulk fouling tests in silica and asphaltenes suspensions in 1mM NaCl solution with 0, 1 mM and 10 mM Ca²⁺ ions. (A) L80 substrates in silica suspensions. (B) EN substrates in silica suspensions. (C) L80 substrates in asphaltenes-coated silica suspensions. (D) EN substrates in asphaltenes-coated silica suspensions. (The dimensions of substrates are: 8×8×3 mm.).....88

Figure 3.S1 Typical scanning electron microscopy (SEM) images of silica probe (A) and asphaltenes probe (B).90

Figure 3.S2 Normalized surface interaction forces during approaching in 1, 10 and 100 mM NaCl solutions for (A) silica probe and silica wafer, and (B) asphaltenes-coated silica probe and silica wafer.....91

Figure 3.S3 Normalized surface interaction forces during approaching in NaCl solutions at pH of 5.5, 8.0 and 10.5 for (A) silica probe and silica wafer, and (B) asphaltenes-coated silica probe and silica wafer.92

Figure 3.S4 Normalized surface interaction forces during approaching in 1 mM NaCl solutions at pH 8.0 with 0, 1 and 10 mM Ca²⁺ for (A) silica probe and silica wafer, and (B) asphaltenes-coated silica probe and silica wafer.93

Figure 3.S5 (A) Optical images of original L80 substrate (left) and EN coating substrate (right). (B) SEM image of L80 substrate. (C) EDS results of L80

substrate.94

Figure 4.1 Schematic of experimental setup for surface force measurements between an oil drop and a substrate using the drop probe AFM technique. The inset (up) shows the central interaction region between an oil drop and a flat substrate, and the inset (left) shows a microscopic image of a typical drop probe prepared (Scale bar 100 μm).....122

Figure 4.2 AFM topographic images of silicon wafer (A), iron substrate (B), and EN coating (C). (D) SEM section image of EN coating. The thickness of the EN coating is measured to be about 1.6 μm . (E) Elemental EDX mapping images of iron and silicon for deposited Fe substrate. (F) Elemental EDX mapping images of nickel, phosphate, and iron for the as-prepared EN substrate.126

Figure 4.3 Contact angles of water, DIM, and DMSO on Fe substrate (A) and EN substrate (B) in air.....127

Figure 4.4 Interaction force profiles of a toluene drop and Fe substrate (A, B) and EN substrate (C, D) in 1 mM and 100 mM NaCl solutions (pH=5.8). The hollow black symbols were experiment data, and solid red lines were theoretical calculation results.....128

Figure 4.5 (A) Calculated profiles of VDW, EDL, hydrodynamic and disjoining pressures between a toluene drop and Fe substrate in 1 mM aqueous NaCl solution. (B) Calculated emulsion drop profile and confined water film thickness under maximum loading condition during force measurements

between a toluene drop and solid substrates (i.e., Fe, EN) in 1 mM NaCl solution. (C, D, E, F) Interaction force-separation profiles of a toluene drop and Fe substrate (C, D) and EN substrate (E, F) in 1 mM and 100 mM NaCl solutions (pH=5.8).	132
Figure 4.6 Interaction force profiles of a toluene drop and Fe substrate (A, B, E, F) and EN substrate (C, D, G, H) in the presence of 10 ppm and 100 ppm asphaltenes in 1 mM and 100 mM NaCl solutions.	134
Figure 4.7 Interaction force profiles of a toluene drop (10 ppm asphaltenes) and Fe substrate (A, B) and EN substrate (C, D) in 1 mM NaCl solutions of pH of 3 (A, C) and pH 10 (B, D).	137
Figure 4.8 Interaction force profiles of a toluene drop (10 ppm asphaltenes) and Fe substrate (A, B) and EN substrate (C, D) in 1 mM NaCl solutions with the addition of 1 mM and 10 mM CaCl ₂	139
Figure 4.9 (A) Schematic process of fouling tests of selected substrates in oil-in-water emulsions based on toluene dissolved with 100 ppm asphaltenes and 100 mM NaCl solution (pH 5.8) at room temperature (22 °C) for 24 hours. Images of Fe and EN substrates before (B) and after (C) fouling test in the emulsions. (Scale bar 1 μm).....	141
Figure 5.1 (A) The preparation of Fe and EN substrates. (B) The schematic of drop probe atomic force microscope (AFM) technique. The ΔX shows the piezo displacement. (C) A microscope image showing a water drop was anchored on the tipless AFM cantilever in toluene for the force measurements.....	156

Figure 5.2 Schematic of bulk fouling tests for Fe and EN substrates in water-in-oil emulsions with asphaltenes.....	159
Figure 5.3 Oil contact angles (OCAs) in water for (A) silica substrate, (B) Fe substrate, (C) EN substrate. Water contact angles (WCAs) in oil for (D) silica substrate, (E) Fe substrate, (F) EN substrate.....	160
Figure 5.4 Measured force profiles between a water drop and Fe substrate in toluene after aged in (A) 0 and (B) 10 mg/L asphaltene solutions for 5 min. The open dots are experimental data. The arrows show the movements of water drops.....	161
Figure 5.5 The normalized adhesion of a water drop on Fe substrate and EN coating substrate in toluene after aged in asphaltene solutions with different concentrations.	163
Figure 5.6 The normalized adhesion of a water drop on Fe substrate and EN coating substrate in toluene and heptol.....	166
Figure 5.7 (A) The normalized adhesion of a water drop on Fe and EN substrate in 50% heptol after being aged in 100 mg/L asphaltene solution for 1, 2, 5, 10, 20 and 30 min, respectively. (B) Measured dynamic interfacial tension curve of water and 50% heptol with 100 mg/L asphaltenes dissolved.	167
Figure 5.8 (A) The normalized adhesion between a water drop and Fe or EN substrate in 50% heptol after aged in 100 mg/L asphaltenes solutions for 5 min with the contact time of 0, 1, 2, 5 and 10 s, respectively. (B) Schematic of conformational change of confined asphaltenes during contact with the	

substrate.	169
Figure 5.9 The normalized adhesion between the water drop and Fe or EN substrate in 50% heptol after aged in 100 mg/L asphaltenes solutions for 5 min under the loading force of 1, 2, 4, 10, 20 and 40 nN, respectively.	170
Figure 5.10 (A) Optical images of Fe and EN substrates before and after bulk fouling tests. AFM surface image of Fe (B) and EN (C) substrate after bulk fouling tests.	171
Figure 5.S1 AFM images of (A) silica substrate, (B) Fe substrate and (C) EN substrate. The SEM images (D, F) and EDS results (E, G) of Fe and EN substrate. (H) The SEM image of the cross section of EN substrate.	175
Figure 5.S2 Measured force profiles between a water drop and Fe substrate in toluene after aged in (A) 20, (B) 50, (C) 100, (D) 200, and (E) 500 mg/L asphaltene solutions for 5 min. The open dots are experimental data. The arrows show the movements of water drops.	176
Figure 5.S3 Measured force profiles between a water drop and EN substrate in toluene after aged in (A) 0, (B) 10, (C) 20, (D) 50, (E) 100, (F) 200, and (G) 500 mg/L asphaltene solutions for 5 min.	177
Figure 5.S4 Measured force profiles between a water drop and Fe substrate in (A) heptol with 75% volume fraction of toluene (denoted as 75% heptol), (B) 50% heptol, (C) 25% heptol and (D) heptane, after aged in 100 mg/L asphaltene solutions for 5 min. The percentage is the volume ratio of toluene.	178
Figure 5.S5 Measured force profiles between the water drop and EN substrate in	

(A) heptol with 75% volume fraction of toluene (denoted as 75% heptol), (B) 50% heptol, (C) 25% heptol and (D) heptane, after aged in 100 mg/L asphaltene solutions for 5 min. The percentages in the figures are the volume ratios of toluene.	179
Figure 5.S6 Measured force profiles of a water drop with Fe substrate (A-F) and EN substrate (G-L) in 50% heptol, after aged in 100 mg/L asphaltenes solutions for 1, 2, 5, 10, 20 and 30 min.	181
Figure 5.S7 Measured force profiles of a water drop with Fe substrate (A-E) and EN substrate (F-J) in 50% heptol, after aged in 100 mg/L asphaltenes solutions for 5 min, with the contact time of 0, 1, 2, 5 and 10 s.	183
Figure 5.S8 Measured force profiles of a water drop with Fe substrate (A-F) and EN substrate (G-L) in 50% heptol, after aged in 100 mg/L asphaltenes solutions for 5 min, with the loading force of 1, 2, 4, 10, 20 and 40 nN....	185
Figure 5.S9 SEM images, EDS element analysis and obtained elemental weight percentages for Fe (A, B and C) and EN (D, E and F) substrates after the bulk fouling tests.	185

List of Acronyms

AFM	Atomic force microscope
SFA	Surface force apparatus
DLVO	Derjaguin-Landau-Verwey-Overbeek
VDW	Van der Waals
EDL	Electric double layer
rms	Root-mean-squared
QCM-D	Quartz crystal microbalance with dissipation
OTS	Octadecyltrichlorosilane

List of Symbols

A	Hamaker constant
h	Thickness of confined liquid film
D	Separation between two surfaces
R	Radius of a particle or a drop
F	Interaction force
F_{ad}	Adhesion
T	Temperature
k_B	Boltzman constant
Ψ	Surface potential
γ	Interfacial tension
κ	Inverse of Debye length
K	Spring constant
σ	Surface charge density
e	Elementary charge
C	Bulk concentration of the electrolyte
ε	Relative permittivity
ε_0	Permittivity of the vacuum
Π	Pressure
L	Characteristic length of the brush
s	Mean distance between two polymers

Δf	Frequency change
Δm	Mass change
ΔD	Dissipation energy change
ρ	Density
η	Viscosity
μ	Shear modulus
v	Shear wave velocity in quartz

Chapter 1 Introduction

1.1 Fouling problems in oil industries

1.1.1 Fouling problems

As the demand of the energy increases and the conventional oil reservoir reduces,¹⁻² more and more attention of oil industries has been paid to non-conventional sources, such as oil sands and crude oil.³⁻⁷ Every year, the oil industries in Alberta of Canada provide billions of barrels of crude oil to the world, and it is also estimated that trillions of barrels of crude oil can be economically recovered.⁸⁻¹¹ In Canada, there are various *in-situ* techniques applied in the extraction of crude oil, and the steam assisted gravity drainage (SAGD) operation has been regarded as the most promising method due to its less environmental damages than conventional surface mining operations.¹²⁻¹³ Nowadays, more than 80% of the oil sands in Alberta are extracted using the SAGD operation.¹⁴⁻¹⁵

In the typical SAGD operation, two horizontal paralleled wells are drilled into the crude oil formation of the deep ground, and the pipes with sand control devices (i.e., slots) are put in the wells. The steam with high temperature and high pressure is continuously pumped through the upper slotted pipes to heat the crude oil and reduce its viscosity. The fluidized oil is drained using the lower pipes and then pumped out to the ground.^{12-13, 15-18} It is noted that the performance and reliability of the slotted liners determine the extraction efficiency of crude oil. However, during the oil production, many detrimental problems, especially the fouling phenomena, could happen to plug and damage the slotted liners.¹⁹⁻²⁴ The undesired depositions

of foulants on liner surfaces could significantly increase the heat resistance and pressure drop, thus leading to the great waste of energy.²⁵⁻²⁷ The inorganic and organic foulants could also be one of the reasons for the erosion and corrosion of the liner surface, which cause serious damages to the liners.²⁸⁻³⁰ The growing foulants would finally cause the total plugging of the liners and the failure of the related facilities.³¹⁻³³

In industries, there are many strategies or methods being developed to control or reduce these serious fouling problems. For example, adding chemical inhibitors in the flowing system could effectively prevent the contact of foulants on pipe surfaces.³⁴⁻³⁷ Those inhibitors are commonly expensive and some of them could cause serious environment issues. Ion exchange technology is also an effective method to control fouling problems by preventing foulants entering the systems, which, however, can only solve the problems only due to inorganic materials (e.g., calcium carbonate).³⁸⁻³⁹ Physical treatment methods including magnetic conditioners, electronic conditioners and ultrasonic treatment technologies have been applied to deal with fouling problems in water treatments and membrane industries.⁴⁰⁻⁴⁵ The mechanisms of these methods are to either change the potential of the facility surface for foulant depositions or inhibit the growth processes of fouling phenomena. It is found that the deposition or fouling of inorganic materials (e.g., calcium carbonate and silica) have been effectively reduced. As to the organic materials (e.g., bitumen or asphaltenes) or in soft systems (e.g., emulsions), the performances are not satisfactory.⁴⁶⁻⁴⁷ Surface modification technologies, such as coating methods, have also been widely used to produce surfaces with low fouling phenomena.⁴⁸⁻⁵⁰ Because of the low expense, convenient processes, and the excellent physical or chemical properties of the coatings, surface modification technologies are becoming more and more

popular in industries.

1.1.2 Foulant compositions

Fouling phenomena in oil production are usually attributed by the deposition of organic and inorganic materials and the corrosion products on liner surfaces.⁵¹⁻⁵⁵ Because of the complex flowing system in liners, bitumen (or asphaltenes), fine solids, and emulsions have been identified to contact the liner surfaces and contribute to the fouling problems.⁵⁶⁻⁵⁸

Bitumen contains large quantities of asphaltenes, resins, fatty acids, and wax crystals.⁵⁹⁻⁶² Generally, asphaltenes are often believed to account for the deposition phenomena and fouling problems in oil production.⁶³⁻⁶⁶ Asphaltenes, as the largest, densest, and surface-active fraction of bitumen, are defined by its solubility that is soluble in aromatic solvents such as toluene or benzene, but insoluble in alkanes such as pentane (C5) or heptane (C7).⁶⁷⁻⁷⁰ This definition based on the solubility suggest that asphaltenes are not a well-defined chemical material but a complicated mixture of various molecules within the same solubility regime.⁷¹⁻⁷³ The accurate composition of asphaltenes changes with the source, the processing conditions and extraction method.⁷³⁻⁷⁵ Nevertheless, large amount of researches have been conducted to study asphaltenes from different oil samples, and theoretical models, such as Yen-Mullins model,^{72-73, 76} have been proposed to describe the molecular compositions of asphaltenes, understand the molecular and interfacial interactions. In the Yen-Mullins model, the typical asphaltenes molecules consists of a polyaromatic core decorated with alkyl linkages, aliphatic side chains and different functional groups, including thiophene, sulfidic, sulfoxide, pyrrolic, pyridine, quinolone, hydroxyl, carboxyl and carbonyl.^{71, 73} These molecules tend to interact with each other and form

nanoaggregates, and these nanoaggregates can further associate into clusters.⁷⁷⁻⁷⁸ Experiment results show that the size of nanoaggregates is about 2 nm, and the size of clusters is ranging between 3 and 10 nm.⁷⁹ It has been reported that the clusters are the precursors for the precipitation and deposition, which finally develop into serious fouling problems.⁷¹ With so many functional groups and diverse molecular assemblies, the asphaltenes-related interactions are the complicated combination of acid-base interactions, hydrogen bonding, van der Waals force, π - π interaction and cation/anion- π interactions,⁸⁰⁻⁸² all of which play the important role in the asphaltenes-asphaltene interactions and asphaltenes-surface interactions. The former interactions lead to the formation of large asphaltene particles, whilst the later interactions can facilitate the adsorption of asphaltenes onto a substrate surface. During oil extraction, transportation, and refinery, asphaltene molecules and aggregates often cause the great adsorption on equipment surfaces, formation of stable water-oil emulsions, sedimentation phenomena, and final fouling problems.

Fine solids, such as silica and clay, are also present in the extracted crude oil, which originate from the reservoir.⁸³⁻⁸⁶ It is reported that these solids could be treated as the active surfaces for asphaltene adsorption.⁸⁷⁻⁸⁸ Therefore, after the presence in crude oil for some time, the naturally hydrophilic particles could become oleophilic, which has a tremendous influence in the stability of water-oil emulsions and the existence of fine solids in produced crude oil.⁶² To protect the facilities, the limitation on the weight percentages of fine solids was set to be 0.5 wt% for pipeline specification and 0.3 wt% for refinery feed.⁸⁹⁻⁹⁰ Silica, as the commonest model of fine solids, has been widely studied in the previous researches.⁷¹ Many effects of temperature, surface chemical groups, water chemistry and organic solvents were investigated

in the adsorption of asphaltenes on silica surface.⁹¹⁻⁹⁸ It is discovered that the asphaltenes adsorption on silica surface was largely determined by the surface silica hydroxyl groups.⁹⁹⁻¹⁰⁰ The silica surface with higher hydroxyl group density adsorbs more asphaltenes.¹⁰¹⁻¹⁰² In fouling problems, the silica particles, which have asphaltenes adsorbed on them, are found to be almost impossible to be separated and could be the main materials to plug the pipelines.^{62, 64} However, the interaction and adsorption mechanisms between silica particle with the presence of asphaltenes and substrate surfaces (i.e., liner surface) have been seldom reported.

Emulsions are the liquid dispersion of water and oil. It can be the water drops dispersed in oil media or the oil drops dispersed in water, with the drop size usually ranging in several micrometers.¹⁰³⁻¹⁰⁴ Typically, emulsions are stabilized by the surfactants or the surface-active materials, which adsorb at the oil-water interface to prevent drops coalesce and stabilize the emulsions. In the emulsions of oil industries, asphaltenes and asphaltene-coated particles often play the role of surfactants to stabilize water-in-oil and oil-in-water emulsions.¹⁰⁵⁻¹⁰⁷ It has been reported that the adsorptions of asphaltenes at water-oil interfaces are very stable and irreversible, indicating the difficulty to remove asphaltenes from the interfaces.¹⁰⁸⁻¹¹⁰ The stable water-in-oil and oil-in-water emulsions can cause many challenging problems during the oil production, such as fouling and plugging in pipelines, upgrading equipment and heat exchangers.^{73, 111-113} Many researches have been conducted to investigate the stability mechanisms of asphaltene-stabilized emulsions under the effects including water chemistry (i.e., salinity, pH and divalent ions), organic media (i.e., good solvent and bad solvent), and adsorption behaviors of asphaltenes.¹¹⁴⁻¹¹⁷ The results indicated that interfacially adsorbed asphaltenes in oil-in-water emulsions could strengthen the electric double layer repulsion, whereas the in water-in-oil

emulsions, asphaltenes could generate strong steric repulsion between drops.¹¹⁴⁻¹¹⁵ Such repulsive interactions contribute significantly to the stability of emulsions. Moreover, the interfacially adsorbed asphaltenes can form strong bonding with the other asphaltenes and substrate surfaces via mentioned asphaltene-asphaltene interactions and asphaltene-surface interactions, thus leading to fouling problems.

In practical oil sands production, the foulants are much more complex. Other organic components in crude oil, such as the wax crystals, are also discovered in the recovered foulants from oil wells.¹¹⁸⁻¹²⁰ The depositions of carbonate or bicarbonate salts on pipe surfaces (also known as scaling) are regarded as the major materials to plug the pipes for water stream in SAGD operations.¹²¹⁻¹²³ Due to the changing flowing conditions and parameters (e.g., flow rate, temperature, and pressure) along the pipelines, the stability of the water-oil emulsions could be altered.¹²⁴⁻¹²⁶ Besides, all of these organic and inorganic materials are mixed in the pipelines during oil production. Hence, the synergic effects of different foulants should also be taken into consideration. To study the complex fouling problems, the model systems should be firstly investigated to have fundamental understandings on fouling mechanisms in oil sands production. Thus, the fouling phenomena of asphaltenes, silica particles, and water-oil emulsions stabilized by asphaltenes on pipeline surfaces will be included. Since in natural water, sodium chloride (NaCl) is the most common salt and calcium (Ca^{2+}) ion usually has highest concentration among divalent ions,¹²⁷⁻¹³⁰ the effects of NaCl concentration and the addition of CaCl_2 will be explored.

1.1.3 Interaction and adsorption mechanisms of asphaltenes on substrate surfaces

The interaction and adsorption mechanisms between asphaltenes and substrate surface are important in this work, which have the direct relevance to the fouling problems in oil production. However, there are only several studies on the asphaltenes-surface interactions and adsorptions, such as gold, steel, iron and alumina.¹³¹⁻¹³⁴ The adsorption isotherm for asphaltenes on gold surface, even though the system is not practical, still provided the valuable and fundamental information on the adsorption behaviors and mechanisms including the influences of conditions (e.g., temperature and surface hydrophilicity) and deposition dynamics.¹³⁵⁻¹³⁷ The adsorption capacity can be as large as 7.1 mg/m^2 .¹³⁵ As to the cases of steel, iron and alumina, the adsorptions of asphaltenes in toluene have been investigated and the highest capacity of asphaltenes reached 2.7 mg/m^2 for steel, 1.35 mg/m^2 for iron and 0.25 mg/m^2 for alumina, respectively.^{131, 138-139} Using the scanning electron microscopy (SEM), it has been concluded that the different adsorption capacities on the substrate with the same materials are largely attributed to the surface morphologies.¹³³

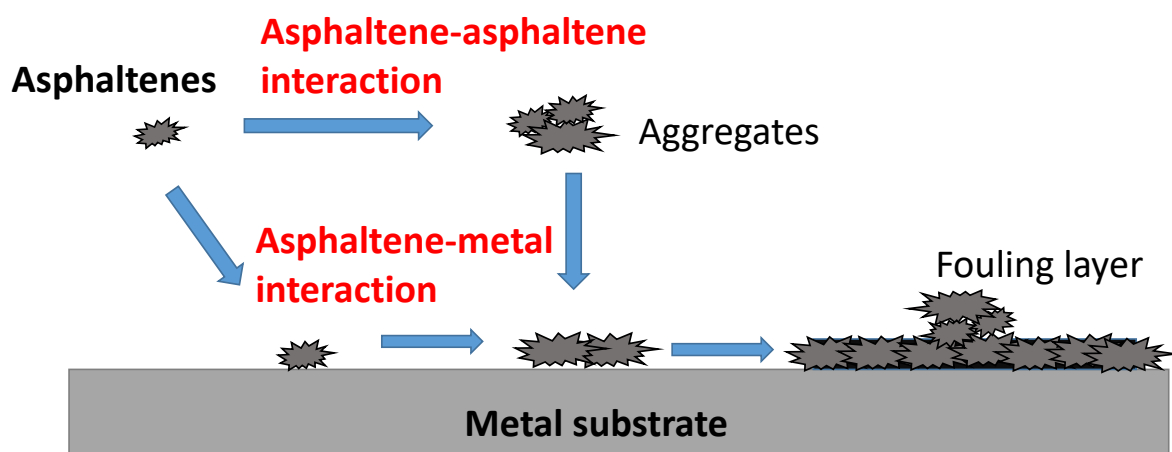


Figure 1.1 Schematic illustration of the asphaltenes fouling process on metal substrate.

Recently, a model on the asphaltenes deposition behavior has been proposed by Karan *et al.* as shown in Figure 1.1.¹⁴⁰⁻¹⁴³ Firstly, the precipitation of asphaltenes, due to the intrinsic aggregation behavior of asphaltenes and the changes of the environmental conditions, could form bigger particles via the intermolecular interactions. Then, some particles could diffuse to the vicinity of a metal surface and adhere to the surface via asphaltene-surface interactions. Besides, the asphaltenes-asphaltene interactions could result in the continuous deposition of other asphaltene particles on the deposited asphaltene layer, forming multilayer structure. In reality, the deposition behaviors and mechanisms should be much more complicated, as more materials as well as their various states (e.g., asphaltene aggregates) would be included in the adsorption and many effects are not well understood. Investigating the interaction mechanisms between asphaltene-stabilized emulsion drops and substrate surfaces could help to fundamentally understand the interaction and adsorption mechanisms in fouling phenomena and develop efficient antifouling strategies.

1.2 Protective methods to pipelines

Iron material is one of the most common constructive materials used in various industries. For example, the carbon steel is the most widely used material in oil wells.¹⁴⁴⁻¹⁴⁵ However, because of the weak resistances to the fouling, corrosion, and erosion, millions of tons of carbon steel materials would be damaged and wasted.¹⁴⁶⁻¹⁴⁸ This damage would be aggravated when the working conditions become extremely harsh, such as in SAGD.¹⁴⁹⁻¹⁵⁰ Nowadays, a variety of surface treatments to the steel materials have been developed and exploited to improve the resistances of corrosion and erosion, such as plasma enhanced chemical vapor deposition

(PECVD) technique, polymeric coatings, ion implantation and electroless plating.^{50, 151-153} The PECVD techniques can generate a thick and passivating layer on substrate surfaces at a very high deposition rate.¹⁵⁴⁻¹⁵⁶ However, the extreme operation conditions and harsh requirements to facilities limit the application of this technique in industries. Polymeric coatings have become more and more attractive in the past decades due to their uncountable species and versatile properties. Their instability and poor performances of polymer materials in extreme conditions (e.g., high temperature and high pressure in SAGD operations) are still the major problems for academics and industries.¹⁵⁷⁻¹⁵⁹ Ion implantation technique can introduce inert atoms onto the substrate surfaces, thus lowering the surface potentials for chemical and/or electrochemical corrosion reactions.¹⁶⁰⁻¹⁶³ This technique is quite expensive and the corrosion protective performances are found to be limited under high temperature. Electroless plating became more and more popular in the past decades, due to the low cost and convenient operation conditions.^{153, 164-165} In the commercial and industrial aspects, the electroless nickel-phosphorus (EN) coating is outstanding due to its unique properties, low cost, and ease of control.¹⁶⁶⁻¹⁶⁸

The EN coating was first noted by Wurtz in 1844.¹⁶⁹ In 1946, Brenner and Riddell accidentally re-discovered this plating process and improved the bathing processes.¹⁷⁰⁻¹⁷¹ Since then, the EN coating and its derivatives are gradually catching increasing attention from the academic researchers and industries. Another advantage of EN coating technique is that this coating can be achieved on interior surfaces of pipes, valves and other hard-to-reach surfaces.¹⁷²⁻¹⁷³ According to the typical weight percentage of phosphorus content, the EN coatings can be classified as the low ($\leq 5\%$), medium (5-8%), and high ($\geq 9\%$).¹⁷⁴⁻¹⁷⁵ It has been noticed that the state of the deposition and surface micro-structure changed with the phosphorus

content, which were related to the properties. Low phosphorus EN coating has the micro-crystalline nickel, which was believed to be nickel phosphide (Ni_3P), with very limited composition of amorphous nickel.¹⁷⁶ Medium phosphorus EN coating has the mixture of micro-crystalline and amorphous structure.¹⁷⁷ High phosphorus EN coating is almost amorphous and consisting of multiple compound phases.¹⁷⁸ Therefore, the low phosphorus coating has high mechanical strength, while high phosphorus EN coating shows better corrosion resistance.^{167,}¹⁷⁹ It has also been noted that the increasing percentage of phosphorus content could reduce the hardness of the coating. Though diverse EN coatings have been developed and applied, the high-phosphorus EN coatings are preferred because of the fast deposition rates, better stability, and improved properties.¹⁸⁰

Recently, the original EN coatings show more and more weakness especially when they are used in complex conditions. To fulfill different requests and improve some special property, one or more metallic elements, metal oxides, and carbon derivatives have been added in the bath during the coating process, such as Cu, Mo, W, Sn, TiO_2 , Al_2O_3 , ZrO_2 , SiC, carbon nanotubes, and graphite.¹⁸¹⁻¹⁸⁸ For instance, the addition of W in the EN coating was found to have better corrosion resistance.¹⁸⁹ The Al_2O_3 particles could prevent the occurrence of delamination during plating and improve the stability and abrasion resistance.¹⁹⁰ The coating with ZrO_2 has been proved to have hydrophobic wettability, as well as better corrosion resistance.¹⁹¹ The EN coatings prepared with SiC, WC and B_4C nano-composites exhibited significantly improved micro-hardness and excellent corrosion resistance.^{183, 188}

As there is the urgency and necessity to protect the equipment from corrosion, erosion, abrasion and clay plugging in oil processing, EN coating has been considered as an effective

method to protect carbon steel substrate in oil production.¹⁹² The field testing results showed that the EN coating significantly reduced the corrosion occurrence and scaling deposition.^{22, 192} However, the antifouling property of the EN coating has been scarcely investigated. Therefore, it is of practical importance to study the antifouling property of EN coatings in oil industries, which could help to facilitate the new EN coatings with efficient antifouling performances.

1.3 Techniques to investigate the interaction and adsorption of asphaltenes on substrate surfaces

Various techniques have been applied to investigate the adsorption of crude oil (e.g., bitumen or asphaltenes) on a surface, such as contact angle measurement, quartz crystal micro-balance with dissipation (QCM-D), surface forces apparatus (SFA), and atomic force microscope (AFM).

1.3.1 Contact angle measurement

The contact angle of a liquid drop on a substrate surface in air or liquid provides the information in the affinity of the liquid to the substrate. The contact angle measurement has been used by Buckley *et al.* to study the interactions between crude oil drops and a steel surface in aqueous solutions to reveal the adsorption behaviors.¹⁹³⁻¹⁹⁵ The measured contact angles showed that asphaltenes were easy to adsorb on the steel surface. It also indicated that the direct contact of crude oil drops and pipeline surface allowed the adsorption of asphaltenes on substrate surface and resulted in the reversed wettability of the metallic surfaces. The presence of a stable thin aqueous film between crude oil and pipeline surface could prevent the direct contact and stop the adsorption of asphaltenes. Besides, the salinity, such as NaCl, in aqueous

solutions had significant influence in the film stability.¹⁹⁴ However, the contact angle measurement only provides the information in macro-scale and the interactions between silica particles and steel surface cannot be directly measured.

1.3.2 Quartz crystal micro-balance with dissipation (QCM-D)

The quartz crystal micro-balance with dissipation (QCM-D) monitoring technique has been popularly used in to study the adsorption behaviors and mechanisms between asphaltenes and steel surfaces in organic solvents.^{137, 196-197} The obtained results showed that the adsorption behaviors of asphaltenes on steel surface started at a rapid rate and could reached a plateau due to the limited surface area. The continuous adsorption behavior of asphaltenes after the saturation was also observed. It was also demonstrated that the asphaltenes-surface interactions and asphaltenes-asphaltene interactions attribute to the adsorption behaviors.¹³⁴ The more asphaltenes were present in the bulk solutions, the more asphaltenes were adsorbed on steel surface. The asphaltenes dissolved in good solvents, such as toluene, would have a less adsorption amount, while the asphaltenes in bad solvents, such as toluene, would have a greater adsorption amount.¹⁹⁷⁻¹⁹⁸ This result proved that the precipitated asphaltene aggregates were the major reason for the asphaltene adsorption on a surface, which finally could lead to the fouling and plugging problems. However, the QCM-D monitoring technique also cannot directly and quantitatively measure the interactions between asphaltenes and steel surface.

1.3.3 Surface forces apparatus (SFA)

The surface forces apparatus (SFA) has been applied to directly measure the interaction forces between asphaltene surfaces in both aqueous solutions and organic media.^{113, 115, 117, 199-}

²⁰¹ With the analysis of fringes of equal chromatic order (FECO), SFA can provide the accurate information on the absolute separation between two surfaces with a high resolution. The reported studies showed that the interactions between two asphaltene surfaces in aqueous solutions were affected by the solution pH, salinity and addition of divalent ions (i.e., Ca^{2+}).²⁰⁰ Basic pH of the solution led to the deprotonation of the functional groups of asphaltenes and thus rendered the surface with a more negative surface potential. High salinity in the solution resulted in the more compressed electric double layer (EDL) on the surface. Divalent ions had a higher charge density, which suggested a stronger electric shielding effect and lowered surface potential. As the consequence, acidic pH, high salinity and presence of divalent ions could result in the weakened EDL repulsion between asphaltene surfaces. Also, it has been found that the presence of Ca^{2+} ions in the solution could change the morphology of adsorbed asphaltenes and influence the stability of asphaltenes film. In the case of organic solvents, the obtained forces showed that the strong repulsive steric interactions between asphaltene surfaces in good solvent (i.e., toluene) dominated the interfacial interactions and prevented the contact of asphaltenes. However, the interaction forces became attractive when the solvent was bad solvent (i.e., heptane), which was due to the attractive VDW force between asphaltenes and the significantly weakened steric repulsion.^{113, 115, 117} These results were in consistence with the fact that the adsorption of asphaltenes in good solvents was much lower than that in bad solvents. SFA can provide the fundamental understandings on the intermolecular and surface interactions between asphaltenes under different conditions. However, using SFAs to measure the interfacial interactions with the involvement of emulsion drops is almost impossible. Due to the limitation of FECO system and the opaque property of some materials (e.g., iron), it is difficult to exploit

SFAs in the investigation of fouling problems in oil production.

1.3.4 Atomic force microscope (AFM)

Atomic force microscope (AFM) has been widely used to detect the surface morphology of a substrate and measure the interaction forces of two objects in the nano-scale. In reported literatures, various AFM based techniques have been applied to directly and quantitatively measure the interaction forces between two surfaces in both aqueous solutions and organic solvents, including asphaltenes, silica particles, water drops, oil drops, and silica substrates.^{114-116, 201-204} For example, the interaction forces between silica substrate and asphaltene surface in aqueous solutions and organic solvents have been investigated using AFM colloidal probe technique.^{92, 205-206} The measured force profiles showed that the effects of electrolyte salinity, solution pH, divalent ions, loading force and surface morphologies are significant. The VDW force, EDL force, steric force, and hydrophobic force contributed to the measured force profiles. The interaction forces in AFM experiments are obtained from the deflection of a cantilever using the Hooke's spring.²⁰⁷⁻²⁰⁹ When the interacting objects are rigid enough that the surface deformation can be ignored, the separation distance between two surfaces can be calculated straightforward from the cantilever deflection and piezo deformation, which suggest that this separation is not absolute or directly obtained. Except for the solid surfaces, the interaction forces between emulsion drops with the presence of asphaltenes have also been investigated using the AFM drop probe technique, including the interactions between two toluene drops in aqueous solutions, and the interactions between two water drops in organic media.^{114, 116, 202, 204} The theoretical model combining the augmented Young-Laplace equation and Reynolds

lubrication theory has been developed to interpret the measured force profiles.²¹⁰⁻²¹² Because of the deformation of the drops and bubbles, the separation distance between two surfaces was difficult to be directly measured. Recently, the reflection interference contrast microscopy (RICM) coupled with AFM bubble probe technique was used to simultaneously probe the interactions and the spatiotemporal evolution of the confined thin film between a bubble and mica surface in aqueous solutions.²¹³ This work showed that the measured thickness of the confined thin film and the calculated results of the separation distance agreed with each other, which demonstrated the validity of AFM bubble probe technique. Therefore, it is feasible and reliable to use the AFM colloidal and drop probe techniques to investigate the interactions among asphaltenes, silica particles, water-oil emulsions and pipeline surfaces and understand the fouling mechanisms and antifouling properties.

1.4 Objectives

As discussed above, although the fouling problems have caused serious damages to the oil industries, the fundamental understandings on the interaction mechanisms of fouling phenomena and antifouling properties are still limited. Therefore, the main objectives of this thesis are to directly and quantitatively investigate the interaction mechanisms among asphaltenes, silica particles, water drops, oil drops and substrate surfaces in both aqueous solutions and organic media, and to evaluate the performance of industrial coating with implications to develop efficient antifouling coatings and strategies in oil production. The detailed objectives are as follows.

- (1) Investigate the interaction mechanisms of fine solids and asphaltenes on carbon steel

surface with electroless nickel-phosphorus (EN) coating in aqueous solutions using the AFM colloidal probe technique under effects of asphaltenes, salinity, pH and presence of Ca^{2+} , which will provide the fundamental information on the fouling mechanisms of silica and asphaltenes on substrate surfaces, and evaluate the antifouling performances of EN coating.

(2) Probe the interaction mechanisms of oil drops on iron surface with or without EN coating in NaCl solutions using the AFM oil drop probe technique and study the effects of asphaltenes, salinity, pH and presence of Ca^{2+} . The theoretical model combining augmented Young-Laplace equation and Reynolds lubrication equation will be applied to analyze the measured force profiles. Besides, the bulk fouling tests of iron substrate and EN coating in water-oil emulsions will be conducted.

(3) Measure the interaction mechanisms of water drops on iron substrate with or without EN coating in organic media using the AFM water drop probe technique. The influences of interfacial asphaltenes, aging time, asphaltenes concentration, solvent type, aging time, loading force and contact time will be studied.

1.5 Structure of the thesis

Chapter 1 overviews the fouling issues in oil industries, discusses the current methods used to study related problems and introduces the objectives of this thesis.

Chapter 2 presents the preparation of experimental materials, techniques used in this project, and theoretical models for the data analysis.

Chapter 3 describes the interaction forces between silica particles and carbon steel substrates in aqueous solutions using AFM colloidal probe technique. The classic DLVO theory is validate

to analyze the measured force profiles. The major driving forces accounting for the fouling phenomena and antifouling properties will be determined.

Chapter 4 presents the results of the interaction forces between oil-in-water emulsions and iron surface or EN coating with the presence of asphaltenes using AFM drop probe technique. The water chemistries including salinity, pH and Ca^{2+} ions are studied, and the corresponding bulk fouling tests are conducted.

Chapter 5 compares the measured adhesions between water drops with the presence of asphaltenes and iron/EN surface in organic solvents. The effects of asphaltenes density, molecular conformation, solvent quality, loading force and contact time have been investigated. The results provide the fundamental information of asphaltenes-metal interactions.

The overall conclusions of this project and future works are outlined in Chapter 6.

Reference

1. Campbell, C. J., The assessment and importance of oil depletion. *Energy exploration & exploitation* **2002**, 20 (6), 407-435.
2. Kokal, S.; Al-Kaabi, A., Enhanced oil recovery: challenges & opportunities. *World Petroleum Council: Official Publication* **2010**, 64.
3. Hirschberg, A.; DeJong, L.; Schipper, B.; Meijer, J., Influence of temperature and pressure on asphaltene flocculation. *Society of Petroleum Engineers Journal* **1984**, 24 (03), 283-293.
4. Bentley, R. W., Global oil & gas depletion: an overview. *Energy policy* **2002**, 30 (3), 189-205.
5. Méjean, A.; Hope, C., Modelling the costs of non-conventional oil: A case study of Canadian bitumen. *Energy Policy* **2008**, 36 (11), 4205-4216.
6. Sorrell, S.; Speirs, J.; Bentley, R.; Brandt, A.; Miller, R., Global oil depletion: A review of the evidence. *Energy Policy* **2010**, 38 (9), 5290-5295.
7. Owen, N. A.; Inderwildi, O. R.; King, D. A., The status of conventional world oil reserves—Hype or cause for concern? *Energy policy* **2010**, 38 (8), 4743-4749.
8. Stringham, G., Energy developments in Canada's oil sands. In *Developments in Environmental Science*, Elsevier: 2012; Vol. 11, pp 19-34.
9. Söderbergh, B.; Robelius, F.; Aleklett, K., A crash programme scenario for the Canadian oil sands industry. *Energy policy* **2007**, 35 (3), 1931-1947.
10. Giacchetta, G.; Leporini, M.; Marchetti, B., Economic and environmental analysis of a Steam Assisted Gravity Drainage (SAGD) facility for oil recovery from Canadian oil sands. *Applied Energy* **2015**, 142, 1-9.

11. Isaacs, E., Canadian Oil Sands: development and future outlook. *Alberta Energy Research Institute, Calgary* **2005**.
12. Shin, H.; Polikar, M. In *Optimizing the SAGD process in three major Canadian oil-sands areas*, SPE Annual Technical Conference and Exhibition, Society of Petroleum Engineers: 2005.
13. McLennan, A.; Deutsch, C. V., SAGD reservoir characterization using geostatistics: Application to the Athabasca oil sands, Alberta, Canada. *Canadian Heavy Oil Association handbook, 2d ed.: Canadian Heavy Oil Association* **2005**, 321-340.
14. Schneider, R.; Dyer, S., *Death by a thousand cuts: impacts of in situ oil sands development on Alberta's boreal forest*. Pembina Institute Calgary, AB, Canada: 2006.
15. Shin, H.; Polikar, M., Fast-SAGD application in the Alberta oil sands areas. *Journal of Canadian Petroleum Technology* **2006**, 45 (09).
16. Stalder, J. L. In *Test of SAGD Flow Distribution Control Liner System, Surmont Field, Alberta, Canada*, SPE Western Regional Meeting, Society of Petroleum Engineers: 2012.
17. Edmunds, N.; Chhina, H., Economic optimum operating pressure for SAGD projects in Alberta. *Journal of Canadian Petroleum Technology* **2001**, 40 (12).
18. Jimenez, J. In *The field performance of SAGD projects in Canada*, International petroleum technology conference, International Petroleum Technology Conference: 2008.
19. Lightbown, V., New SAGD technologies show promise in reducing environmental impact of oil sand production. *Journal of Environmental Solutions for Oil, Gas, and Mining* **2015**, 1 (1), 47-58.
20. Pugsley, T.; Pernitsky, D.; Grundler, J.; Johnsen, E. In *Fouling of heat transfer surfaces in a steam assisted gravity drainage (SAGD) in situ facility for the recovery of oil sands bitumen*,

International Conference on Heat Exchanger Fouling and Clearing, 2013.

21. Acosta, E., Achieving sustainable, optimal SAGD operations. *Journal of Petroleum Technology* **2010**, 62 (11), 24-28.
22. Zhu, D.; Uzcategui, A.; Gong, L.; Qiu, X.; Huang, J.; Sun, C.; Luo, J.-L.; Zeng, H. In *Investigation of Electroless Nickel-Phosphorus Coating as an Alternative to Corrosion/Fouling Resistant Alloys in Downhole Service*, OTC Brasil, Offshore Technology Conference: 2017.
23. Alipour, M.; Kurian, V.; Dhir, S.; Gupta, R., Analysis of syngas cooler fouling from asphaltene gasification. *Fuel Processing Technology* **2016**, 152, 7-14.
24. Thibault, Y.; McEvoy, J. G.; Mortazavi, S.; Smith, D.; Doiron, A., Characterization of fouling processes in ceramic membranes used for the recovery and recycle of oil sands produced water. *Journal of Membrane Science* **2017**, 540, 307-320.
25. Bell, I. H.; Groll, E. A., Air-side particulate fouling of microchannel heat exchangers: experimental comparison of air-side pressure drop and heat transfer with plate-fin heat exchanger. *Applied Thermal Engineering* **2011**, 31 (5), 742-749.
26. Sarafraz, M.; Hormozi, F., Heat transfer, pressure drop and fouling studies of multi-walled carbon nanotube nano-fluids inside a plate heat exchanger. *Experimental Thermal and Fluid Science* **2016**, 72, 1-11.
27. Hesselgreaves, J., An approach to fouling allowances in the design of compact heat exchangers. *Applied Thermal Engineering* **2002**, 22 (7), 755-762.
28. Little, B.; Wagner, P.; Mansfeld, F., Microbiologically influenced corrosion of metals and alloys. *International Materials Reviews* **1991**, 36 (1), 253-272.
29. Lee, W.; Lewandowski, Z.; Nielsen, P. H.; Hamilton, W. A., Role of sulfate - reducing

- bacteria in corrosion of mild steel: a review. *Biofouling* **1995**, 8 (3), 165-194.
30. Somerscales, E. F., Fundamentals of corrosion fouling. *Experimental thermal and fluid science* **1997**, 14 (4), 335-355.
31. Finnie, I., Erosion of surfaces by solid particles. *wear* **1960**, 3 (2), 87-103.
32. Safaei, M.; Mahian, O.; Garoosi, F.; Hooman, K.; Karimipour, A.; Kazi, S.; Gharehkhani, S., Investigation of micro-and nanosized particle erosion in a 90 pipe bend using a two-phase discrete phase model. *The scientific world journal* **2014**, 2014.
33. Barton, D.; Wallace, R., Effects of eroding oil sand and periodic flooding on benthic macroinvertebrate communities in a brown-water stream in northeastern Alberta, Canada. *Canadian Journal of Zoology* **1979**, 57 (3), 533-541.
34. Heggs, P., Heat exchanger fouling-mitigation and cleaning technologies by Hans Muller-Steinhager. *TCE CHEMICAL ENGINEER* **2001**, 49-49.
35. Egan, S.; James, S.; Kjelleberg, S., Identification and characterization of a putative transcriptional regulator controlling the expression of fouling inhibitors in *Pseudoalteromonas tunicata*. *Appl. Environ. Microbiol.* **2002**, 68 (1), 372-378.
36. Müller-Steinhagen, H.; Malayeri, M.; Watkinson, A., Heat exchanger fouling: environmental impacts. Taylor & Francis: 2009.
37. Chen, T.; Chan, S.-H., Novel biological inhibitors of fouling and scale formation on heat transfer surfaces through genetic engineering. *Microscale Thermophysical Engineering* **2000**, 4 (2), 103-108.
38. Gönder, Z. B.; Kaya, Y.; Vergili, I.; Barlas, H., Capacity loss in an organically fouled anion exchanger. *Desalination* **2006**, 189 (1-3), 303-307.

39. Ming, F.; Howell, J.; Acosta, F.; Hubble, J., Study on separation of conalbumin and lysozyme from high concentration fresh egg white at high flow rates by a novel ion - exchanger. *Biotechnology and bioengineering* **1993**, *42* (9), 1086-1090.
40. Wang, Y.; Babchin, J.; Chernyi, L.; Chow, R.; Sawatzky, R., Rapid onset of calcium carbonate crystallization under the influence of a magnetic field. *Water Research* **1997**, *31* (2), 346-350.
41. Vermeiren, T., Magnetic treatment of liquids for scale and corrosion prevention. *Anti-Corrosion Methods and Materials* **1958**, *5* (7), 215-219.
42. Cho, Y.; Choi, B.-G., Validation of an electronic anti-fouling technology in a single-tube heat exchanger. *International Journal of Heat and Mass Transfer* **1999**, *42* (8), 1491-1499.
43. Cho, Y. I.; Fan, C.; Choi, B.-G., Use of electronic anti-fouling technology with filtration to prevent fouling in a heat exchanger. *International journal of heat and mass transfer* **1998**, *41* (19), 2961-2966.
44. Kobayashi, T.; Chai, X.; Fujii, N., Ultrasound enhanced cross-flow membrane filtration. *Separation and Purification Technology* **1999**, *17* (1), 31-40.
45. Chen, D.; Weavers, L. K.; Walker, H. W. In *Using ultrasound to reduce ceramic membrane fouling by silica particles*, National Meeting of the American Chemical Society, Orlando, USA, 2002; pp 166-169.
46. Pan, Y.; Wang, T.; Sun, H.; Wang, W., Preparation and application of titanium dioxide dynamic membranes in microfiltration of oil-in-water emulsions. *Separation and purification technology* **2012**, *89*, 78-83.
47. Bates, D.; Patist, A., Industrial applications of high power ultrasonics in the food, beverage

- and wine industry. In *Case Studies in Novel Food Processing Technologies*, Elsevier: 2010; pp 119-138.
48. Zhang, H.; Chiao, M., Anti-fouling coatings of poly (dimethylsiloxane) devices for biological and biomedical applications. *Journal of medical and biological engineering* **2015**, *35* (2), 143-155.
49. Förster, M.; Augustin, W.; Bohnet, M., Influence of the adhesion force crystal/heat exchanger surface on fouling mitigation. *Chemical Engineering and Processing: Process Intensification* **1999**, *38* (4-6), 449-461.
50. Müller-Steinhagen, H.; Zhao, Q., Investigation of low fouling surface alloys made by ion implantation technology. *Chemical Engineering Science* **1997**, *52* (19), 3321-3332.
51. Allen, E. W., Process water treatment in Canada' s oil sands industry: I. Target pollutants and treatment objectives. *Journal of Environmental Engineering and Science* **2008**, *7* (2), 123-138.
52. Duyvesteyn, W. P.; Budden, J. R.; Picavet, M. A., Extraction of bitumen from bitumen froth and biotreatment of bitumen froth tailings generated from tar sands. Google Patents: 1999.
53. Epstein, N. In *Fouling in heat exchangers*, Sixth International Heat Transfer Conference., 1977; pp 235-253.
54. Speight, J. G., *Fouling in refineries*. Gulf Professional Publishing: 2015.
55. Wu, X.; Chung, K., Hydrotreater feed filter fouling and its remedy. *Energy & fuels* **2007**, *21* (3), 1212-1216.
56. Irani, M. In *On Subcool Control in the SAGD Producers. Part II: Localized Hot Spots Effects and Optimization of Flow-Control-Devices*, SPE Thermal Well Integrity and Design

Symposium, Society of Petroleum Engineers: 2018.

57. Ezeuko, C. C.; Wang, J.; Gates, I. D., Investigation of emulsion flow in steam-assisted gravity drainage. *SPE Journal* **2013**, *18* (03), 440-447.

58. Kar, T.; Williamson, M.; Hascakir, B. In *The role of asphaltenes in emulsion formation for steam assisted gravity drainage (SAGD) and expanding solvent-SAGD (ES-SAGD)*, SPE Heavy and Extra Heavy Oil Conference: Latin America, Society of Petroleum Engineers: 2014.

59. Edwards, Y.; Isacson, U., Wax in bitumen: part 1—classifications and general aspects. *Road materials and pavement design* **2005**, *6* (3), 281-309.

60. Sheu, E. Y., Petroleum asphaltene properties, characterization, and issues. *Energy & Fuels* **2002**, *16* (1), 74-82.

61. Lee, R. F., Agents which promote and stabilize water-in-oil emulsions. *Spill Science & Technology Bulletin* **1999**, *5* (2), 117-126.

62. Langevin, D.; Poteau, S.; Hénaut, I.; Argillier, J., Crude oil emulsion properties and their application to heavy oil transportation. *Oil & gas science and technology* **2004**, *59* (5), 511-521.

63. Watkinson, A.; Wilson, D., Chemical reaction fouling: A review. *Experimental Thermal and Fluid Science* **1997**, *14* (4), 361-374.

64. Wiehe, I. A.; Kennedy, R. J.; Dickakian, G., Fouling of nearly incompatible oils. *Energy & fuels* **2001**, *15* (5), 1057-1058.

65. Stark, J. L.; Asomaning, S., Crude oil blending effects on asphaltene stability in refinery fouling. *Petroleum science and technology* **2003**, *21* (3-4), 569-579.

66. Bennett, C. A., A theory describing asphaltene adhesion fouling inside heat exchanger tubes. *Heat Transfer Engineering* **2012**, *33* (15), 1246-1250.

67. FAN, M.; SUN, X.-w.; XU, Z.-m.; ZHAO, S.-q., Characterization of Residue (C5-C7) Asphaltene (Soluble in n-Heptane but Insoluble in n-Pentane)[J]. *Journal of Petrochemical Universities* **2011**, *3*.
68. Goual, L., Petroleum asphaltenes. In *Crude Oil Emulsions-Composition Stability and Characterization*, InTech: 2012.
69. Dufour, J.; Calles, J. A.; Marugán, J.; Giménez-Aguirre, R.; Peña, J. L.; Merino-García, D., Influence of hydrocarbon distribution in crude oil and residues on asphaltene stability. *Energy & Fuels* **2009**, *24* (4), 2281-2286.
70. Strausz, O. P.; Jha, K. N.; Montgomery, D. S., Chemical composition of gases in Athabasca bitumen and in low-temperature thermolysis of oil sand, asphaltene and maltene. *Fuel* **1977**, *56* (2), 114-120.
71. Adams, J. J., Asphaltene adsorption, a literature review. *Energy & Fuels* **2014**, *28* (5), 2831-2856.
72. Mullins, O. C.; Sabbah, H.; Eyssautier, J.; Pomerantz, A. E.; Barré, L.; Andrews, A. B.; Ruiz-Morales, Y.; Mostowfi, F.; McFarlane, R.; Goual, L., Advances in asphaltene science and the Yen–Mullins model. *Energy & Fuels* **2012**, *26* (7), 3986-4003.
73. Mullins, O. C., The asphaltenes. *Annual review of analytical chemistry* **2011**, *4*, 393-418.
74. Ancheyta, J.; Centeno, G.; Trejo, F.; Marroquin, G.; Garcia, J.; Tenorio, E.; Torres, A., Extraction and characterization of asphaltenes from different crude oils and solvents. *Energy & Fuels* **2002**, *16* (5), 1121-1127.
75. Alboudwarej, H.; Beck, J.; Svrcek, W.; Yarranton, H.; Akbarzadeh, K., Sensitivity of asphaltene properties to separation techniques. *Energy & Fuels* **2002**, *16* (2), 462-469.

76. Dutta Majumdar, R.; Gerken, M.; Mikula, R.; Hazendonk, P., Validation of the Yen–Mullins model of Athabasca oil-sands asphaltenes using solution-state ¹H NMR relaxation and 2D HSQC spectroscopy. *Energy & Fuels* **2013**, *27* (11), 6528-6537.
77. Mullins, O. C.; Seifert, D. J.; Zuo, J. Y.; Zeybek, M., Clusters of asphaltene nanoaggregates observed in oilfield reservoirs. *Energy & Fuels* **2012**, *27* (4), 1752-1761.
78. Mullins, O. C., The modified Yen model. *Energy & Fuels* **2010**, *24* (4), 2179-2207.
79. Simon, S.; Jestin, J.; Palermo, T.; Barré, L. c., Relation between solution and interfacial properties of asphaltene aggregates. *Energy & Fuels* **2008**, *23* (1), 306-313.
80. Long, J.; Xu, Z.; Masliyah, J. H., Single molecule force spectroscopy of asphaltene aggregates. *Langmuir* **2007**, *23* (11), 6182-6190.
81. Moschopedis, S. E.; Speight, J. G., Investigation of hydrogen bonding by oxygen functions in Athabasca bitumen. *Fuel* **1976**, *55* (3), 187-192.
82. Lopez-Chavez, E.; Pacheco-Sánchez, J.-H.; Martínez-Magadán, J.-M.; Castillo-Alvarado, F. d. L.; Soto-Figueroa, C.; Garcia-Cruz, I., Methodology for predicting the phase envelope of a heavy crude oil and its asphaltene deposition onset. *Petroleum science and technology* **2007**, *25* (1-2), 19-39.
83. Sparks, B.; Kotlyar, L.; O'Carroll, J.; Chung, K., Athabasca oil sands: effect of organic coated solids on bitumen recovery and quality. *Journal of Petroleum Science and Engineering* **2003**, *39* (3-4), 417-430.
84. Masliyah, J.; Zhou, Z. J.; Xu, Z.; Czarnecki, J.; Hamza, H., Understanding water - based bitumen extraction from Athabasca oil sands. *The Canadian Journal of Chemical Engineering* **2004**, *82* (4), 628-654.

85. Yan, N.; Gray, M. R.; Masliyah, J. H., On water-in-oil emulsions stabilized by fine solids. *Colloids and Surfaces A: Physicochemical and Engineering Aspects* **2001**, *193* (1-3), 97-107.
86. Kotlyar, L.; Sparks, B.; Woods, J.; Chung, K., Solids associated with the asphaltene fraction of oil sands bitumen. *Energy & fuels* **1999**, *13* (2), 346-350.
87. Jada, A.; Debih, H., Hydrophobation of clay particles by asphaltene adsorption. *Composite Interfaces* **2009**, *16* (2-3), 219-235.
88. Binks, B. P.; Desforges, A.; Duff, D. G., Synergistic stabilization of emulsions by a mixture of surface-active nanoparticles and surfactant. *Langmuir* **2007**, *23* (3), 1098-1106.
89. Bensebaa, F.; Kotlyar, L. S.; Sparks, B. D.; Chung, K. H., Organic coated solids in Athabasca bitumen: Characterization and process implications. *The Canadian Journal of Chemical Engineering* **2000**, *78* (4), 610-616.
90. Nikakhtari, H.; Wolf, S.; Choi, P.; Liu, Q.; Gray, M. R., Migration of fine solids into product bitumen from solvent extraction of Alberta oilsands. *Energy & Fuels* **2014**, *28* (5), 2925-2932.
91. Abraham, T.; Christendat, D.; Karan, K.; Xu, Z.; Masliyah, J., Asphaltene– Silica Interactions in Aqueous Solutions: Direct Force Measurements Combined with Electrokinetic Studies. *Industrial & engineering chemistry research* **2002**, *41* (9), 2170-2177.
92. Liu, J.; Zhang, L.; Xu, Z.; Masliyah, J., Colloidal interactions between asphaltene surfaces in aqueous solutions. *Langmuir* **2006**, *22* (4), 1485-1492.
93. Fritschy, G.; Papirer, E., Interactions between a bitumen, its components and model fillers. *Fuel* **1978**, *57* (11), 701-704.
94. Liu, J.; Xu, Z.; Masliyah, J., Interaction forces in bitumen extraction from oil sands. *Journal of colloid and interface science* **2005**, *287* (2), 507-520.

95. Wang, S.; Liu, J.; Zhang, L.; Masliyah, J.; Xu, Z., Interaction forces between asphaltene surfaces in organic solvents. *Langmuir* **2009**, *26* (1), 183-190.
96. Wang, J.; Li, C.; Zhang, L.; Que, G.; Li, Z., The properties of asphaltenes and their interaction with amphiphiles. *Energy & Fuels* **2009**, *23* (7), 3625-3631.
97. Peltonen, P. V., Road aggregate choice based on silicate quality and bitumen adhesion. *Journal of transportation engineering* **1992**, *118* (1), 50-61.
98. Long, J.; Zhang, L.; Xu, Z.; Masliyah, J. H., Colloidal interactions between Langmuir–Blodgett bitumen films and fine solid particles. *Langmuir* **2006**, *22* (21), 8831-8839.
99. Jada, A.; Chaou, A. A.; Bertrand, Y.; Moreau, O., Adsorption and surface properties of silica with transformer insulating oils. *Fuel* **2002**, *81* (9), 1227-1232.
100. Wang, S.; Segin, N.; Wang, K.; Masliyah, J. H.; Xu, Z., Wettability control mechanism of highly contaminated hydrophilic silica/alumina surfaces by ethyl cellulose. *The Journal of Physical Chemistry C* **2011**, *115* (21), 10576-10587.
101. Cortés, F. B.; Mejía, J. M.; Ruiz, M. A.; Benjumea, P.; Riffel, D. B., Sorption of asphaltenes onto nanoparticles of nickel oxide supported on nanoparticulated silica gel. *Energy & Fuels* **2012**, *26* (3), 1725-1730.
102. Zahabi, A.; Gray, M. R.; Dabros, T., Kinetics and properties of asphaltene adsorption on surfaces. *Energy & Fuels* **2012**, *26* (2), 1009-1018.
103. Becher, P.; Hamor, W. A., *Emulsions: theory and practice*. Reinhold New York: 1957; Vol. 135.
104. Berg, J. C., *An introduction to interfaces & colloids: the bridge to nanoscience*. World Scientific: 2010.

105. Khristov, K.; Taylor, S.; Czarnecki, J.; Masliyah, J., Thin liquid film technique—application to water–oil–water bitumen emulsion films. *Colloids and Surfaces A: Physicochemical and Engineering Aspects* **2000**, *174* (1-2), 183-196.
106. Yan, Z.; Elliott, J. A.; Masliyah, J. H., Roles of various bitumen components in the stability of water-in-diluted-bitumen emulsions. *Journal of colloid and interface science* **1999**, *220* (2), 329-337.
107. Gao, S.; Moran, K.; Xu, Z.; Masliyah, J., Role of bitumen components in stabilizing water-in-diluted oil emulsions. *Energy & Fuels* **2009**, *23* (5), 2606-2612.
108. Freer, E.; Radke, C., Relaxation of asphaltenes at the toluene/water interface: diffusion exchange and surface rearrangement. *The Journal of Adhesion* **2004**, *80* (6), 481-496.
109. Acevedo, S.; Ranaudo, M. A.; García, C.; Castillo, J.; Fernández, A., Adsorption of asphaltenes at the toluene– silica interface: A kinetic study. *Energy & fuels* **2003**, *17* (2), 257-261.
110. Langevin, D.; Argillier, J.-F., Interfacial behavior of asphaltenes. *Advances in colloid and interface science* **2016**, *233*, 83-93.
111. Tsamantakis, C.; Masliyah, J.; Yeung, A.; Gentzis, T., Investigation of the interfacial properties of water-in-diluted-bitumen emulsions using micropipette techniques. *Journal of colloid and interface science* **2005**, *284* (1), 176-183.
112. Kralova, I.; Sjöblom, J.; Øye, G.; Simon, S.; Grimes, B. A.; Paso, K., Heavy crude oils/particle stabilized emulsions. *Advances in colloid and interface science* **2011**, *169* (2), 106-127.
113. Natarajan, A.; Xie, J.; Wang, S.; Liu, Q.; Masliyah, J.; Zeng, H.; Xu, Z., Understanding

molecular interactions of asphaltenes in organic solvents using a surface force apparatus. *The Journal of Physical Chemistry C* **2011**, *115* (32), 16043-16051.

114. Shi, C.; Zhang, L.; Xie, L.; Lu, X.; Liu, Q.; Mantilla, C. A.; van den Berg, F. G.; Zeng, H., Interaction mechanism of oil-in-water emulsions with asphaltenes determined using droplet probe AFM. *Langmuir* **2016**, *32* (10), 2302-2310.

115. Zhang, L.; Shi, C.; Lu, Q.; Liu, Q.; Zeng, H., Probing molecular interactions of asphaltenes in heptol using a surface forces apparatus: Implications on stability of water-in-oil emulsions. *Langmuir* **2016**, *32* (19), 4886-4895.

116. Shi, C.; Zhang, L.; Xie, L.; Lu, X.; Liu, Q.; He, J.; Mantilla, C. A.; Van den Berg, F. G.; Zeng, H., Surface interaction of water-in-oil emulsion droplets with interfacially active asphaltenes. *Langmuir* **2017**, *33* (5), 1265-1274.

117. Natarajan, A.; Kuznicki, N.; Harbottle, D.; Masliyah, J.; Zeng, H.; Xu, Z., Understanding mechanisms of asphaltene adsorption from organic solvent on mica. *Langmuir* **2014**, *30* (31), 9370-9377.

118. Bott, T. R., Aspects of crystallization fouling. *Experimental thermal and fluid science* **1997**, *14* (4), 356-360.

119. Fernandez-Torres, M.; Fitzgerald, A.; Paterson, W.; Wilson, D., A theoretical study of freezing fouling: limiting behaviour based on a heat and mass transfer analysis. *Chemical Engineering and Processing: Process Intensification* **2001**, *40* (4), 335-344.

120. Rogel, E.; Ovalles, C.; Vien, J.; Moir, M., Asphaltene characterization of paraffinic crude oils. *Fuel* **2016**, *178*, 71-76.

121. MacAdam, J.; Parsons, S. A., Calcium carbonate scale formation and control. *Re/Views*

in Environmental Science & Bio/Technology **2004**, 3 (2), 159-169.

122. Chen, T.; Neville, A.; Yuan, M., Calcium carbonate scale formation—assessing the initial stages of precipitation and deposition. *Journal of Petroleum Science and Engineering* **2005**, 46 (3), 185-194.

123. Ramstad, K.; Tydal, T.; Askvik, K. M.; Fotland, P., Predicting carbonate scale in oil producers from high temperature reservoirs. *SPE Journal* **2005**, 10 (04), 363-373.

124. Jones, T.; Neustadter, E.; Whittingham, K., Water-in-crude oil emulsion stability and emulsion destabilization by chemical demulsifiers. *Journal of Canadian Petroleum Technology* **1978**, 17 (02).

125. Kokal, S. L., Crude oil emulsions: A state-of-the-art review. *SPE Production & facilities* **2005**, 20 (01), 5-13.

126. Sullivan, A. P.; Kilpatrick, P. K., The effects of inorganic solid particles on water and crude oil emulsion stability. *Industrial & Engineering Chemistry Research* **2002**, 41 (14), 3389-3404.

127. Gillis, P. L., Assessing the toxicity of sodium chloride to the glochidia of freshwater mussels: Implications for salinization of surface waters. *Environmental Pollution* **2011**, 159 (6), 1702-1708.

128. Blanchard, G.; Maunaye, M.; Martin, G., Removal of heavy metals from waters by means of natural zeolites. *Water research* **1984**, 18 (12), 1501-1507.

129. Hem, J. D.; Survey, G., Study and interpretation of the chemical characteristics of natural water. **1989**.

130. Fattahpour, V.; Mahmoudi, M.; Roostaei, M.; Cheung, S.; Gong, L.; Qiu, X.; Huang,

J.; Velayati, A.; Kyanpour, M.; Alkough, A. In *Evaluation of the Scaling Resistance of Different Coating and Material for Thermal Operations*, SPE International Heavy Oil Conference and Exhibition, Society of Petroleum Engineers: 2018.

131. Nassar, N. N., Asphaltene adsorption onto alumina nanoparticles: kinetics and thermodynamic studies. *Energy & Fuels* **2010**, *24* (8), 4116-4122.

132. Mohammadi, M.; Sedighi, M.; Hashemi Kiasari, H.; Hosseini, S. M., Genetic algorithm development for prediction of modified Langmuir isotherm parameters of asphaltene adsorption onto metal surfaces: using novel quartz crystal nanobalance. *Journal of Dispersion Science and Technology* **2015**, *36* (3), 384-392.

133. Alboudwarej, H.; Pole, D.; Svrcek, W. Y.; Yarranton, H. W., Adsorption of asphaltenes on metals. *Industrial & engineering chemistry research* **2005**, *44* (15), 5585-5592.

134. Rudrake, A. Investigations of Asphaltene-Metal Interactions. 2008.

135. Ekholm, P.; Blomberg, E.; Claesson, P.; Auflem, I. H.; Sjöblom, J.; Kornfeldt, A., A quartz crystal microbalance study of the adsorption of asphaltenes and resins onto a hydrophilic surface. *Journal of colloid and interface science* **2002**, *247* (2), 342-350.

136. Goual, L.; Horváth-Szabó, G.; Masliyah, J. H.; Xu, Z., Adsorption of bituminous components at oil/water interfaces investigated by quartz crystal microbalance: Implications to the stability of water-in-oil emulsions. *Langmuir* **2005**, *21* (18), 8278-8289.

137. Rudrake, A.; Karan, K.; Horton, J. H., A combined QCM and XPS investigation of asphaltene adsorption on metal surfaces. *Journal of colloid and interface science* **2009**, *332* (1), 22-31.

138. Abdallah, W.; Taylor, S., Surface characterization of adsorbed asphaltene on a stainless

steel surface. *Nuclear Instruments and Methods in Physics Research Section B: Beam Interactions with Materials and Atoms* **2007**, 258 (1), 213-217.

139. Balabin, R. M.; Syunyaev, R. Z.; Schmid, T.; Stadler, J.; Lomakina, E. I.; Zenobi, R., Asphaltene adsorption onto an iron surface: combined near-infrared (NIR), Raman, and AFM study of the kinetics, thermodynamics, and layer structure. *Energy & Fuels* **2010**, 25 (1), 189-196.

140. Karan, K.; Hammami, A.; Flannery, M.; Artur Stankiewicz, B., Evaluation of asphaltene instability and a chemical control during production of live oils. *Petroleum science and technology* **2003**, 21 (3-4), 629-645.

141. Papadimitriou, N.; Romanos, G.; Charalambopoulou, G. C.; Kainourgiakis, M.; Katsaros, F.; Stubos, A., Experimental investigation of asphaltene deposition mechanism during oil flow in core samples. *Journal of petroleum science and engineering* **2007**, 57 (3-4), 281-293.

142. Eskin, D.; Ratulowski, J.; Akbarzadeh, K.; Pan, S., Modelling asphaltene deposition in turbulent pipeline flows. *The Canadian Journal of Chemical Engineering* **2011**, 89 (3), 421-441.

143. Buckley, J. S., Asphaltene deposition. *Energy & Fuels* **2012**, 26 (7), 4086-4090.

144. Kermani, M.; Harrop, D., The impact of corrosion on oil and gas industry. *SPE Production & Facilities* **1996**, 11 (03), 186-190.

145. Wu, S.; Cui, Z.; Zhao, G.; Yan, M.; Zhu, S.; Yang, X., EIS study of the surface film on the surface of carbon steel from supercritical carbon dioxide corrosion. *Applied Surface Science* **2004**, 228 (1-4), 17-25.

146. Finšgar, M.; Jackson, J., Application of corrosion inhibitors for steels in acidic media for the oil and gas industry: a review. *Corrosion Science* **2014**, *86*, 17-41.
147. Migahed, M.; Mohamed, H.; Al-Sabagh, A., Corrosion inhibition of H-11 type carbon steel in 1 M hydrochloric acid solution by N-propyl amino lauryl amide and its ethoxylated derivatives. *Materials chemistry and physics* **2003**, *80* (1), 169-175.
148. Ren, C.; Liu, D.; Bai, Z.; Li, T., Corrosion behavior of oil tube steel in simulant solution with hydrogen sulfide and carbon dioxide. *Materials chemistry and physics* **2005**, *93* (2-3), 305-309.
149. Nasr, T.; Beaulieu, G.; Golbeck, H.; Heck, G. In *Novel expanding solvent-SAGD process "ES-SAGD"*, Canadian International Petroleum Conference, Petroleum Society of Canada: 2002.
150. Singh, D.; Sirkar, K. K., Desalination of brine and produced water by direct contact membrane distillation at high temperatures and pressures. *Journal of Membrane Science* **2012**, *389*, 380-388.
151. Droes, S. R.; Kudas, T. T.; Hampden-Smith, M. J., Plasma-Enhanced Chemical Vapor Deposition (PECVD). In *Carbide, Nitride and Boride Materials Synthesis and Processing*, Springer: 1997; pp 579-603.
152. Schultz, M. P., Frictional resistance of antifouling coating systems. *Transactions of the ASME-I-Journal of Fluids Engineering* **2004**, *126* (6), 1039-1047.
153. Cheng, Y.; Zou, Y.; Cheng, L.; Liu, W., Effect of the microstructure on the anti-fouling property of the electroless Ni-P coating. *Materials letters* **2008**, *62* (27), 4283-4285.
154. Alayo, M.; Pereyra, I.; Scopel, W. L.; Fantini, M. C. d. A., On the nitrogen and oxygen

incorporation in plasma-enhanced chemical vapor deposition (PECVD) SiO_xN_y films. *Thin Solid Films* **2002**, 402 (1-2), 154-161.

155. Miyajima, S.; Irikawa, J.; Yamada, A.; Konagai, M., High quality aluminum oxide passivation layer for crystalline silicon solar cells deposited by parallel-plate plasma-enhanced chemical vapor deposition. *Applied Physics Express* **2009**, 3 (1), 012301.

156. Park, K. C.; Moon, J. H.; Jang, J.; Oh, M. H., Deposition of hydrogen - free diamond - like carbon film by plasma enhanced chemical vapor deposition. *Applied physics letters* **1996**, 68 (25), 3594-3595.

157. Wang, Y.; Fei, W.; An, L., Oxidation/Corrosion of Polymer - Derived SiAlCN Ceramics in Water Vapor. *Journal of the American Ceramic Society* **2006**, 89 (3), 1079-1082.

158. Marcus, P., *Corrosion mechanisms in theory and practice*. CRC press: 2011.

159. Mansfeld, F. B., *Corrosion mechanisms*. CRC Press: 1986; Vol. 28.

160. Wang, W.; Booske, J.; Baum, C.; Clothier, C.; Zjaba, N.; Zhang, L., Modification of bearing steel surface by nitrogen plasma source ion implantation for corrosion protection. *Surface and Coatings Technology* **1999**, 111 (1), 97-102.

161. Stroosnijder, M., Ion implantation for high temperature corrosion protection. *Surface and Coatings Technology* **1998**, 100, 196-201.

162. Karimi, M. V.; Sinha, S.; Kothari, D.; Khanna, A.; Tyagi, A., Effect of ion implantation on corrosion resistance and high temperature oxidation resistance of Ti deposited 316 stainless steel. *Surface and Coatings Technology* **2002**, 158, 609-614.

163. Smidt, F., Recent advances in the application of ion implantation to corrosion and wear protection. *Nuclear Instruments and Methods in Physics Research Section B: Beam Interactions*

with *Materials and Atoms* **1985**, *10*, 532-538.

164. Barish, J. A.; Goddard, J. M., Anti-fouling surface modified stainless steel for food processing. *Food and Bioproducts processing* **2013**, *91* (4), 352-361.

165. Zhao, Q.; Liu, Y.; Müller-Steinhagen, H.; Liu, G., Graded Ni–P–PTFE coatings and their potential applications. *Surface and Coatings Technology* **2002**, *155* (2-3), 279-284.

166. Keong, K.; Sha, W.; Malinov, S., Crystallisation kinetics and phase transformation behaviour of electroless nickel–phosphorus deposits with high phosphorus content. *Journal of Alloys and Compounds* **2002**, *334* (1-2), 192-199.

167. Keong, K.; Sha, W.; Malinov, S., Hardness evolution of electroless nickel–phosphorus deposits with thermal processing. *Surface and Coatings Technology* **2003**, *168* (2-3), 263-274.

168. Brown, R. J.; Brewer, P. J.; Milton, M. J., The physical and chemical properties of electroless nickel–phosphorus alloys and low reflectance nickel–phosphorus black surfaces. *Journal of Materials Chemistry* **2002**, *12* (9), 2749-2754.

169. Wurtz, A., *Hebd. Sciences Acad. Sci* **1844**, *18*, 702.

170. Brenner, A.; Riddell, G. E., Deposition of nickel and cobalt by chemical reduction. *J. Res. Nat. Bur. Stand* **1947**, *39*, 385-395.

171. Brenner, A.; Riddell, G. E., Nickel plating on steel by chemical reduction. *Plating and surface finishing* **1998**, *85* (8), 54-55.

172. Ashassi-Sorkhabi, H.; Rafizadeh, S. H., Effect of coating time and heat treatment on structures and corrosion characteristics of electroless Ni–P alloy deposits. *Surface and coatings Technology* **2004**, *176* (3), 318-326.

173. Dai, K.; Xiong, Y.; Yin, J., Electroless Ni - P coating on Cu substrate with strike nickel

activation and its corrosion resistance. *Materialwissenschaft und Werkstofftechnik* **2013**, *44* (11), 918-921.

174. Cui, G.; Li, N.; Li, D.; Zheng, J.; Wu, Q., The physical and electrochemical properties of electroless deposited nickel–phosphorus black coatings. *Surface and Coatings Technology* **2006**, *200* (24), 6808-6814.

175. Mai, Q.; Daniels, R.; Harpalani, H., Structural changes induced by heating in electroless nickel-phosphorus alloys. *Thin Solid Films* **1988**, *166*, 235-247.

176. Lambert, M. R.; Duquette, D. J., A study of electroless nickel coatings containing low phosphorus. *Thin Solid Films* **1989**, *177* (1-2), 207-223.

177. Kumar, P. S.; Nair, P. K., Studies on crystallization of electroless Ni–P deposits. *Journal of Materials Processing Technology* **1996**, *56* (1-4), 511-520.

178. Erming, M.; Shoufu, L.; Pengxing, L., A transmission electron microscopy study on the crystallization of amorphous Ni-P electroless deposited coatings. *Thin Solid Films* **1988**, *166*, 273-280.

179. Wang, J. J.; Li, S. R.; Su, X. J.; Hou, G. L.; Song, B.; Liu, C. H. In *Study on Wear Resistance of Two Types of Low Phosphorus Electroless Nickel Plating on 30CrMnSi*, Advanced Materials Research, Trans Tech Publ: 2017; pp 178-182.

180. Balaraju, J.; Seshadri, S., Synthesis and characterization of electroless nickel-high phosphorus coatings. *Metal Finishing* **1999**, *97* (7), 8-13.

181. Wang, Y.; Shu, X.; Wei, S.; Liu, C.; Gao, W.; Shakoor, R.; Kahraman, R., Duplex Ni–P–ZrO₂/Ni–P electroless coating on stainless steel. *Journal of Alloys and Compounds* **2015**, *630*, 189-194.

182. Karthikeyan, S.; Ramamoorthy, B., Effect of reducing agent and nano Al₂O₃ particles on the properties of electroless Ni–P coating. *Applied Surface Science* **2014**, *307*, 654-660.
183. Bigdeli, F.; Allahkaram, S. R., An investigation on corrosion resistance of as-applied and heat treated Ni–P/nanoSiC coatings. *Materials & Design* **2009**, *30* (10), 4450-4453.
184. Xu, H.; Yang, Z.; Li, M.-K.; Shi, Y.-L.; Huang, Y.; Li, H.-L., Synthesis and properties of electroless Ni–P–Nanometer Diamond composite coatings. *Surface and coatings technology* **2005**, *191* (2-3), 161-165.
185. Ranganatha, S.; Venkatesha, T.; Vathsala, K., Process and properties of electroless Ni–Cu–P–ZrO₂ nanocomposite coatings. *Materials Research Bulletin* **2012**, *47* (3), 635-645.
186. Sadreddini, S.; Afshar, A., Corrosion resistance enhancement of Ni-P-nano SiO₂ composite coatings on aluminum. *Applied Surface Science* **2014**, *303*, 125-130.
187. Araghi, A.; Paydar, M., Electroless deposition of Ni–W–P–B₄C nanocomposite coating on AZ91D magnesium alloy and investigation on its properties. *Vacuum* **2013**, *89*, 67-70.
188. Luo, H.; Leitch, M.; Behnamian, Y.; Ma, Y.; Zeng, H.; Luo, J.-L., Development of electroless Ni–P/nano-WC composite coatings and investigation on its properties. *Surface and Coatings Technology* **2015**, *277*, 99-106.
189. Tsai, Y.-Y.; Wu, F.-B.; Chen, Y.-I.; Peng, P.-J.; Duh, J.-G.; Tsai, S.-Y., Thermal stability and mechanical properties of Ni–W–P electroless deposits. *Surface and Coatings Technology* **2001**, *146*, 502-507.
190. Balaraju, J.; Rajam, K., Influence of particle size on the microstructure, hardness and corrosion resistance of electroless Ni–P–Al₂O₃ composite coatings. *Surface and Coatings*

Technology **2006**, 200 (12-13), 3933-3941.

191. Zielińska, K.; Stankiewicz, A.; Szczygieł, I., Electroless deposition of Ni–P–nano-ZrO₂ composite coatings in the presence of various types of surfactants. *Journal of colloid and interface science* **2012**, 377 (1), 362-367.

192. Zhu, D.; Leitch, M.; Wang, J.; Shi, X.; Gong, L.; Aghaie, E.; Luo, J.-l.; Zeng, H. In *Evaluation of an Advanced Metal Bonded Coating Technology for Improved SAGD Performance*, SPE Latin America and Caribbean Heavy and Extra Heavy Oil Conference, Society of Petroleum Engineers: 2016.

193. Buckley, J.; Morrow, N. In *Characterization of crude oil wetting behavior by adhesion tests*, SPE/DOE Enhanced Oil Recovery Symposium, Society of Petroleum Engineers: 1990.

194. Buckley, J. S. In *Chemistry of the crude oil/brine interface*, Proc. 3rd International Symposium on Evaluation of Reservoir Wettability and Its Effect on Oil Recovery, 1994; pp 33-38.

195. Buckley, J.; Liu, Y.; Monsterleet, S., Mechanisms of wetting alteration by crude oils. *SPE journal* **1998**, 3 (01), 54-61.

196. Abudu, A.; Goual, L., Adsorption of crude oil on surfaces using quartz crystal microbalance with dissipation (QCM-D) under flow conditions. *Energy & Fuels* **2008**, 23 (3), 1237-1248.

197. Xie, K.; Karan, K., Kinetics and thermodynamics of asphaltene adsorption on metal surfaces: A preliminary study. *Energy & fuels* **2005**, 19 (4), 1252-1260.

198. Harbottle, D.; Chen, Q.; Moorthy, K.; Wang, L.; Xu, S.; Liu, Q.; Sjoblom, J.; Xu, Z., Problematic stabilizing films in petroleum emulsions: Shear rheological response of

viscoelastic asphaltene films and the effect on drop coalescence. *Langmuir* **2014**, *30* (23), 6730-6738.

199. Wang, J.; van der Tuuk Opedal, N.; Lu, Q.; Xu, Z.; Zeng, H.; Sjöblom, J., Probing molecular interactions of an asphaltene model compound in organic solvents using a surface forces apparatus (SFA). *Energy & Fuels* **2011**, *26* (5), 2591-2599.

200. Zhang, L.; Xie, L.; Shi, C.; Huang, J.; Liu, Q.; Zeng, H., Mechanistic Understanding of Asphaltene Surface Interactions in Aqueous Media. *Energy & Fuels* **2016**, *31* (4), 3348-3357.

201. Wang, S.; Liu, J.; Zhang, L.; Xu, Z.; Masliyah, J., Colloidal interactions between asphaltene surfaces in toluene. *Energy & Fuels* **2008**, *23* (2), 862-869.

202. Xie, L.; Shi, C.; Cui, X.; Huang, J.; Wang, J.; Liu, Q.; Zeng, H., Probing the interaction mechanism between air bubbles and bitumen surfaces in aqueous media using bubble probe atomic force microscopy. *Langmuir* **2017**, *34* (3), 729-738.

203. Liu, J.; Wang, J.; Huang, J.; Cui, X.; Tan, X.; Liu, Q.; Zeng, H., Heterogeneous Distribution of Adsorbed Bitumen on Fine Solids from Solvent-Based Extraction of Oil Sands Probed by AFM. *Energy & Fuels* **2017**, *31* (9), 8833-8842.

204. Mao, X.; Gong, L.; Xie, L.; Qian, H.; Wang, X.; Zeng, H., Novel Fe₃O₄ based superhydrophilic core-shell microspheres for breaking asphaltenes-stabilized water-in-oil emulsion. *Chemical Engineering Journal* **2019**, *358*, 869-877.

205. Gong, L.; Wang, J.; Zhang, L.; Fattahpour, V.; Mamoudi, M.; Roostaei, M.; Fermaniuk, B.; Luo, J.-L.; Zeng, H., Fouling mechanisms of asphaltenes and fine solids on bare and electroless nickel-phosphorus coated carbon steel. *Fuel* **2019**, *252*, 188-199.

206. Liu, J.; Xu, Z.; Masliyah, J., Studies on bitumen– silica interaction in aqueous

solutions by atomic force microscopy. *Langmuir* **2003**, *19* (9), 3911-3920.

207. Hutter, J. L.; Bechhoefer, J., Calibration of atomic - force microscope tips. *Review of Scientific Instruments* **1993**, *64* (7), 1868-1873.

208. Meyer, G.; Amer, N. M., Novel optical approach to atomic force microscopy. *Applied physics letters* **1988**, *53* (12), 1045-1047.

209. Giessibl, F. J., Advances in atomic force microscopy. *Reviews of modern physics* **2003**, *75* (3), 949.

210. Chan, D. Y.; Klaseboer, E.; Manica, R., Dynamic deformations and forces in soft matter. *Soft Matter* **2009**, *5* (15), 2858-2861.

211. Chan, D. Y.; Klaseboer, E.; Manica, R., Film drainage and coalescence between deformable drops and bubbles. *Soft Matter* **2011**, *7* (6), 2235-2264.

212. Chan, D. Y.; Klaseboer, E.; Manica, R., Theory of non-equilibrium force measurements involving deformable drops and bubbles. *Advances in colloid and interface science* **2011**, *165* (2), 70-90.

213. Shi, C.; Cui, X.; Xie, L.; Liu, Q.; Chan, D. Y.; Israelachvili, J. N.; Zeng, H., Measuring forces and spatiotemporal evolution of thin water films between an air bubble and solid surfaces of different hydrophobicity. *ACS nano* **2014**, *9* (1), 95-104.

Chapter 2 Materials and Experimental Techniques

2.1 Electroless nickel-phosphorus (EN) coating

The electroless nickel-phosphorus coating was conducted on the iron surfaces or the carbon steel L80 substrates, which were provided by the RGL Reservoir Management Inc. (RGL, Canada), using the reported EN coating bath.¹ In details, the carbon steel L80 substrates were cut from a pipeline into smaller pieces with the size around 8 mm×8 mm×3 mm. These substrates were firstly polished by sand papers to minimize the effect of surface roughness. Then, cleaning procedure was conducted to remove the inorganic and organic contaminations from the surfaces. The substrates were clean and sonicated for 10 min in DI water, ethanol, acetone and toluene. The substrates were dried using pure nitrogen. Following the washing, the substrates were immersed in NaOH solution (20 wt%) and heated to 70 °C for 15 min to remove all cutting fluids, grease and oil from the surface. The DI water was used to wash the substrate and nitrogen was used to dry them. Finally, the substrates were immersed in hydrochloride acid solution (10 wt%) for 1 min to activate for EN plating process.

The EN coating bath solution was firstly prepared before the cleaning of carbon steel substrates. The bath compositions were listed in the Table 2.1. During EN coating process, the bath solution was heated to 80 °C for 5 min and the agitation using a magnetic stir was set to 200 rpm. Then, a cleaned and activated substrate was put and hanged in the bath solution. The plating was kept for 30 min. If a greater thickness of

EN coating was needed, the plating time could be more than 1 hour. After the plating, the substrates were washed using DI water and ethanol, and dried using pure nitrogen. The atomic force microscope (AFM) surface imaging, scanning electron microscopy (SEM), and energy dispersive X-ray spectroscopy (EDS) were used to confirm the successful deposition of EN coating on carbon steel surface.

Table 2.1 Bath compositions and environmental conditions for deposition of EN coating.

Composition	Concentration
NiSO₄·6H₂O	25 g/L
NaH₂PO₂·H₂O	16 g/L
NH₄Cl	40 g/L
CH₃COONa	10 g/L
Citric acid	15 g/L
Plating conditions:	
Temperature: 80~85 °C	
pH: 8~9	
Agitation: 200 rpm	
Time: 30 min	

2.2 Atomic force microscope colloidal probe technique

2.2.1 Experimental setup

In this project, the atomic force microscope (AFM) colloidal probe technique has been used to directly and quantitatively probe the interactions between silica particles

or asphaltenes-coated silica particles and pipeline substrates in both aqueous solutions and organic media. All the force measurements in this study were conducted using an MFP-3D AFM system (Asylum Research, Santa Barbara, CA). The experimental setups and details are followed.²⁻⁴

Prior to force measurements, the silica probe was firstly prepared. The silica microspheres (radius around 2.5 μm) were suspended in DI water by sonication for 15 min to make a concentration less than 0.1 wt%. The drop of silica suspension with 10 μL was spread on a clean glass substrate and left to dry in ambient condition. With the assistance of AFM, a tipless AFM cantilever (NP-O10, Bruker, Santa Barbara, CA) was driven by the piezo to firstly pick up some two-component epoxy glue (EP2LV, MasterBond, USA) at the top of the probe, and then stick one silica microsphere spread on glass substrate. Finally, the silica probe was prepared and left in room temperature for 24 hours to dry. These silica probes were cleaned using DI water and ethanol before used in the experiments. The asphaltenes-coated silica probe was prepared by immersing silica probe in 20 mg/L asphaltenes in toluene solution for 2 days. This probe was then carefully washed using ethanol and dried in pure nitrogen.

During force measurements, the prepared and cleaned silica probe was stalled in the probe holder, and the pipeline substrate was immersed in the fluid cell filled with aqueous solution or organic solvent. Then, this silica probe was carefully immersed in the fluid cell. The laser was adjusted to point at the tip of the probe and reflected to a photo screen, which could monitor the deflection of the cantilever. The spring constant of the silica probe was calibrated using the thermal tune method. Afterwards, the silica

probe was moved to place above the substrate with a proper distance. The force measurement began when the silica probe was driven by the piezo at a velocity of 1 $\mu\text{m/s}$ to approach the substrate till a maximum loading force of 10 nN was reached. Then, the probe was withdrawn to the original position. During this approach and withdraw process, the deflection of the cantilever was monitored by the photo screen and the force data was obtained with the calibrated spring constant. After each force measurement, the profiles containing the force and separation could be exported from the AFM software, and used in the following theoretical analysis.

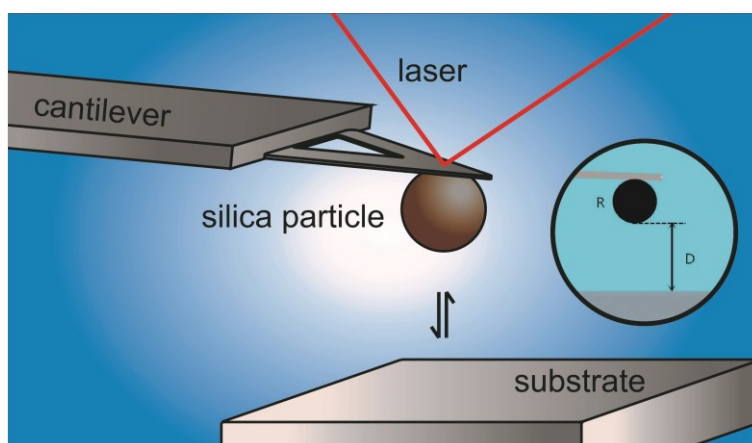


Figure 2.1 Schematic illustration of the atomic force microscope (AFM) colloidal probe technique.

2.2.2 Theoretical analysis

The Derjaguin-Landau-Verwey-Overbeek (DLVO) theory was used to analyze the measured force profiles using the AFM colloidal probe technique.⁵⁻⁷ This DLVO theory describes the interfacial and intermolecular interactions between charged surfaces in liquid medium using the van der Waals (VDW) force and electric double layer (EDL) force. In this project, the classic DLVO theory was used in the case of aqueous solutions

and the extended DLVO theory coupled with steric force was used in the case of organic media.

The VDW force is originated from the electromagnetic interactions among atoms and molecules, and physically exists between two objects. In this project, the VDW force F_{VDW} between a silica particle and pipeline substrate in liquid can be calculated using the following equation.⁸⁻⁹

$$F_{VDW} = -\frac{A_H R}{6D^2} \quad (2.1)$$

Here A_H is the Hamaker constant, R is the radius of silica microsphere, D is the separation distance between the microsphere and flat substrate. The Hamaker constant was calculated using the Lifshitz theory from the dielectric permittivity ϵ and reflex index n of the materials. The Hamaker constant between object 1 & 2 across medium 3 could be calculated using the following equation.⁸

$$A_H \approx \frac{3}{4} k_B T \left(\frac{\epsilon_1 - \epsilon_3}{\epsilon_1 + \epsilon_3} \right) \left(\frac{\epsilon_2 - \epsilon_3}{\epsilon_2 + \epsilon_3} \right) + \frac{3h\nu_e}{8\sqrt{2}} \frac{(n_1^2 - n_3^2)(n_2^2 - n_3^2)}{(n_1^2 + n_3^2)^{1/2} (n_2^2 + n_3^2)^{1/2} \left\{ (n_1^2 + n_3^2)^{1/2} + (n_2^2 + n_3^2)^{1/2} \right\}} \quad (2.2)$$

Here k_B is the Boltzmann constant, T is the temperature, h is the Planck constant, and ν_e is the resonance frequency with a typical value of $4 \times 10^{15} \text{ s}^{-1}$. The first term in the Equation 2.2 includes the Keesom and Debye dipolar contributions of the VDW interaction, and the second term describes the dispersion energy contributed by the London energy.

The EDL force occurs between two charged surfaces in electrolyte solution (typically water). In this project, the EDL force F_{EDL} between the silica probe and pipeline

substrate in aqueous solution could be calculated using the following equation.^{6, 8-9}

$$F_{EDL} = \frac{\pi}{\varepsilon\varepsilon_0\kappa^2} \left[(\sigma_P^2 + \sigma_S^2) (e^{-2\kappa D} + 2\kappa D - 1) e^{-2\kappa D} + 4\sigma_P\sigma_S (e^{-\kappa D} + \kappa D - 1) e^{-\kappa D} \right] \quad (2.3)$$

$$\sigma = \sqrt{8\varepsilon\varepsilon_0 \cdot k_B T \cdot CN_A} \sinh\left(\frac{e\Psi}{2k_B T}\right) \quad (2.4)$$

Here ε is the relative permittivity of medium, ε_0 is the vacuum permittivity, κ is the Debye length, σ_p is the surface charge density of probe, σ_s is the substrate surface charge density, C is the bulk concentration of ions, N_A is the Avogadro's number, e is the elementary charge, and Ψ is the surface potential.

In organic medium (e.g. toluene), the asphaltenes adsorbed at the interface could stretched out into the bulk and behave like the polymer brush. Therefore, the steric force could occur when the asphaltenes-coated silica probe was brought to contact pipeline substrate in organic solvent. In this project, the steric force F_{STE} can be calculated using the following equation.¹⁰⁻¹²

$$\frac{F_{ste}}{R} = 200 \frac{k_B T L_0}{s^3} \exp\left(-\pi \frac{D}{L_0}\right) \quad (2.5)$$

Here L_0 is the characteristic thickness of coating layer on the surface, s is the mean distance between two grafting points of polymer on the surface.

2.3 Atomic force microscope drop probe technique

2.3.1 Experimental setup

In this project, the AFM drop probe technique has been used to probe the interactions between oil droplet and pipeline substrate in aqueous solutions and the interactions

between water droplet and pipeline substrate in organic solvent. The force measurements in this study were conducted using an MFP-3D AFM system (Asylum Research, Santa Barbara, CA). The experimental setups and details are followed.¹³⁻¹⁵

To pick up the oil droplet in aqueous solution, the custom-made rectangular tipless AFM cantilevers (size of $400 \times 70 \times 2 \mu\text{m}$) with a thin circular gold patch (diameter $\sim 65 \mu\text{m}$, thickness $\sim 10 \text{ nm}$) at one end was firstly hydrophobized using hydrophobic thiol (e.g. 1-decanethiol) to facilitate the stability of oil droplet on the cantilever. In the case of picking up water droplet, the AFM cantilevers was treated in UV ozone for 5 min to get a slight hydrophilicity. Before the force measurement, the oil (or water) drops were generated in the aqueous solution (or organic solvent) using a custom-made ultra-sharp glass pipette. The modified AFM cantilever was then driven to carefully pick up one drop with a proper size, thus creating the oil or water drop probe.

During each force measurement, both the prepared drop probe and the substrate were immersed in the AFM fluid cell filled with aqueous solutions and organic solvent. The drop probe was moved above the substrate with a proper distance. A laser reflection system was applied to monitor the deflection of the cantilever. The spring constant of the cantilever was calibrated using the thermal tune method. The drop anchored cantilever was driven by a piezo to move at a velocity of $1 \mu\text{m/s}$ approach to substrate till a certain deflection of $1 \mu\text{m}$ was reached. Then, the cantilever was withdrawn to move back to the original place. The maximum loading force, the contact time, and moving velocity could be changed as needed. During the movement of the cantilever, the force data could be recorded according to the deflection and the spring constant of

the cantilever. After each force measurement, the profiles containing the force, piezo movement and time were exported from the AFM software, and used in the further data analysis.

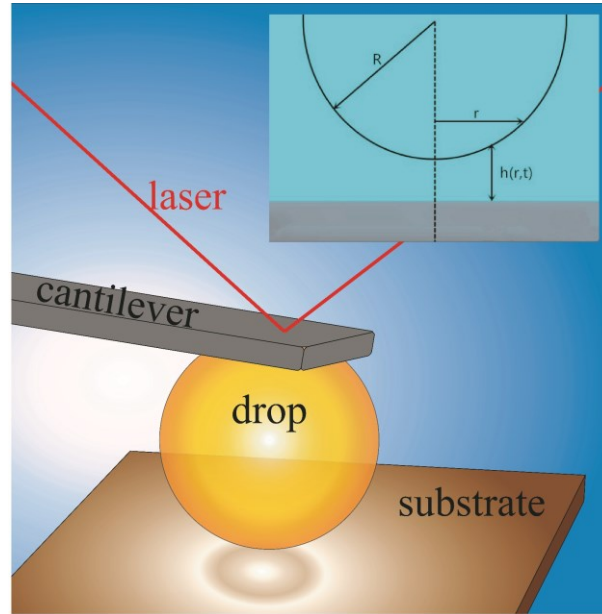


Figure 2.2 Schematic illustration of the AFM drop probe technique.

2.3.2 Theoretical analysis

Since the drop is deformable, the theoretical model combining the augmented Young-Laplace equation and the Reynolds lubrication theory was applied to analyze the measured force profiles measured using the AFM drop probe technique.¹⁶⁻¹⁸ With response to the external pressure including the hydrodynamic pressure and disjoining pressure, the water or oil drop would deform. The augmented Young-Laplace equation describes the deformation of a drop under the effect of external pressures within the force area, as following:¹⁶⁻¹⁷

$$\frac{\sigma}{r} \frac{\partial}{\partial r} \left(r \frac{\partial h}{\partial r} \right) = \frac{2\sigma}{R} - \Pi - p \quad (2.6)$$

Here, σ is the interfacial tension of the oil/water interface, r is the radial coordinate, h is the thickness of the water film confined between the drop and the substrate, R is the radius of the drop, Π is the disjoining pressure and p is the excess hydrodynamic pressure. The disjoining pressure could arise from van der Waals (VDW) interaction, electric double layer (EDL) interaction and other surface interactions in this project.

The VDW force can be calculated using the following equation.^{8, 13}

$$\Pi_{VDW} = -\frac{A_H}{6\pi h^3} \quad (2.7)$$

Here, A_H is the Hamaker constant between the drop and the substrate in aqueous solutions or organic solvent. The EDL force can be calculated using the following equation.⁸⁻⁹

$$\Pi_{EDL} = \frac{2\varepsilon\varepsilon_0\kappa^2 \left[(e^{\kappa D} + e^{-\kappa D})\Psi_1\Psi_2 - (\Psi_1^2 + \Psi_2^2) \right]}{(e^{\kappa D} - e^{-\kappa D})^2} \quad (2.8)$$

Where, κ is the inverse of Debye length, Ψ is the surface potential of the drop or substrates, ε_0 is the vacuum permittivity and ε is the dielectric constant of the liquid medium. The inverse of Debye length κ was calculated as:

$$\kappa = \sqrt{\frac{\sum \rho_0 e^2 z^2}{\varepsilon\varepsilon_0 k_B T}} \quad (2.9)$$

Where, ρ_0 is the number density of ions in aqueous solutions, e is the elementary charge, z is the valence of the ions, and k_B is the Boltzmann constant. When the drop was brought to the substrate in a liquid, the confined liquid film could be described using the Reynolds lubrication theory under the assumption of immobile boundary condition.¹⁶⁻¹⁷

$$\frac{\partial h}{\partial t} = \frac{1}{12\mu r} \frac{\partial}{\partial r} \left(rh^3 \frac{\partial p}{\partial r} \right) \quad (2.10)$$

Where, t is time and μ is the viscosity of the aqueous solutions. The overall interaction $F(t)$ can be calculated from the integration of the hydrodynamic pressure and the disjoining pressure based on Derjaguin approximation.

$$F(t) = 2\pi \int_0^{\infty} [p(r,t) + \Pi(r,t)] \cdot r dr \quad (2.11)$$

2.4 Quartz crystal micro-balance with dissipation monitoring technique

The quartz crystal micro-balance with dissipation (QCM-D) has been used in this project to study the dynamic adsorption of asphaltenes on iron surface and EN coating in organic solvent.¹⁹⁻²⁰ The QCM-D E1 system (Q-sense, Sweden) was used. The iron sensor was prepared by depositing a layer of iron (thickness about 90 nm) on the gold sensor surface using the electron beam evaporation (EBE) technique. A layer of chromium (thickness about 10 nm) was firstly deposited between the iron and gold surface to enhance the adhesive stability of iron. The EN sensor was prepared via electroless nickel-phosphorus (EN) coating on the iron sensor surface. The iron and EN sensors were calibrated before the adsorption experiments to make sure the feasibility of the sensors.

The sensor used in this study is AT-cut silica crystals coated with gold with the resonance frequency of 5 MHz. The electrodes connected on each side of the sensor could monitor the resonance frequency of the sensor when an AC voltage is applied. The material adsorbed onto the surface of the sensor would result in the changes of the

resonance frequency of the sensor.

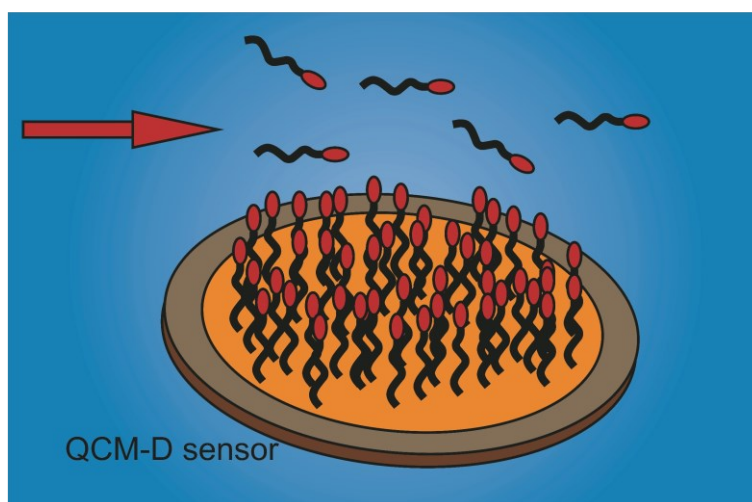


Figure 2.3 Schematic illustration of quartz crystal microbalance with dissipation monitoring technique.

During the QCM-D adsorption experiment, the sensors were thoroughly cleaned following a standard procedure using the DI water, ethanol, acetone and toluene. The asphaltenes solution in toluene and pure toluene were prepared and sonicated for at least 15 min. After the careful cleaning, the sensor was placed in the flow module of the QCM-D system and the testing system was applied to check the resonance frequencies of the sensor. The background solution (i.e. toluene) was then introduced using a peristaltic pump. The flow rate was set to be 350 $\mu\text{L}/\text{min}$, unless other specific effect was considered. The frequency change of the sensor will be monitored by the controller and defined to be zero as the baseline after the curve becomes stable and constant. The experiment started then. After about 3 min of the baseline, the as-prepared asphaltenes solution was pumped in at the same flow rate. The adsorption process was last for ~ 90 min and the pure toluene was applied to replace the asphaltenes solution to wash the unstably adsorbed asphaltenes from the sensor surface. The experiment

stooped when the adsorption curve became straight and unchanged. The frequency change Δf and dissipation energy change ΔD were recorded as a function of time.

There are two models used to calculate the mass Δm of adsorbed material on the sensor surface from the measured frequency change and dissipation energy change. The first model is the Sauerbrey equation.²⁰⁻²¹

$$\Delta m = -\frac{C}{n} \Delta f \quad (2.12)$$

where, C equals 17.1 ng/(Hz•cm²) for a 5 MHz quartz crystal sensor, n is the overtone number (n=1,3,5,7...). However, the Sauerbrey equation is only valid when the adsorbed layer of the material is evenly distributed, relatively thin and quite rigid. When the amount of adsorbed asphaltenes are large, asphaltenes layer is soft and not uniform. The conditions are not satisfied. Then, the Voigt viscoelastic model was used to describe the relationship between the mass of the adsorbed asphaltenes and both changes of frequency and dissipation as following.^{20, 22}

$$\Delta f \approx -\frac{1}{2\pi\rho_0 h_0} \left\{ \frac{\eta_2}{\delta_2} + \left[h_1 \rho_1 \omega - 2h_1 \left(\frac{\eta_2}{\delta_2} \right)^2 \frac{\eta_1 \omega^2}{\mu_1^2 + \eta_1 \omega^2} \right] \right\} \quad (2.13)$$

$$\Delta D \approx -\frac{1}{2\pi f \rho_0 h_0} \left\{ \frac{\eta_2}{\delta_2} + \left[2h_1 \left(\frac{\eta_2}{\delta_2} \right)^2 \frac{\eta_1 \omega^2}{\mu_1^2 + \eta_1 \omega^2} \right] \right\} \quad (2.14)$$

$$\delta_2 = \sqrt{\frac{2\eta_2}{\rho_2 \omega}} \quad (2.15)$$

Where, h is the adsorbed layer, ρ is the density, η is the viscosity, μ is the shear modulus, and ω is the circular frequency for the adsorbed layer (index 1), quartz crystal (index 0) and fluid phase (index 2).

2.5 Three probe liquid technique

The three probe liquid technique was applied in this study to study the surface energies of metal substrates. According to the van der Waals and acid-base theory, the surface energy of a substrate can be regarded as three components.²³

$$\gamma = \gamma^d + \gamma^p = \gamma^d + 2\sqrt{\gamma^+ \cdot \gamma^-} \quad (2.16)$$

Where, γ is the total surface energy, γ^d and γ^p are the apolar and polar components, γ^+ is the electron-acceptor parameter, and γ^- is the electron-donor parameter. These parameters can be obtained from the contact angles of three probe liquids with different polarities. The contact angle of a liquid on a substrate was measured by a standard goniometer (Model 250, Ramé-hart, USA). A drop of $\sim 3 \mu\text{L}$ probe liquid was gently and carefully placed on the substrate, and shape of the drop was imaged by the software. The contact angle was then obtained from fitting the outline of the drop shape. Using the Lifshitz-van der Waals/acid-base approach,²⁴ the surface energy of the substrate could be calculated.

$$\begin{bmatrix} 2\sqrt{\gamma_{L1}^d} & 2\sqrt{\gamma_{L1}^+} & 2\sqrt{\gamma_{L1}^-} \\ 2\sqrt{\gamma_{L2}^d} & 2\sqrt{\gamma_{L2}^+} & 2\sqrt{\gamma_{L2}^-} \\ 2\sqrt{\gamma_{L3}^d} & 2\sqrt{\gamma_{L3}^+} & 2\sqrt{\gamma_{L3}^-} \end{bmatrix} \cdot \begin{bmatrix} \sqrt{\gamma_S^d} \\ \sqrt{\gamma_S^-} \\ \sqrt{\gamma_S^+} \end{bmatrix} = \begin{bmatrix} \gamma_{L1}(1 + \cos \theta_{L1}) \\ \gamma_{L2}(1 + \cos \theta_{L2}) \\ \gamma_{L3}(1 + \cos \theta_{L3}) \end{bmatrix} \quad (2.17)$$

where, γ_S^d , γ_S^+ and γ_S^- are the surface energy components of the substrate, γ_L^d , γ_L^+ and γ_L^- are the surface energy components of the probe liquid, θ_L is the contact angle of probe liquid on the substrate.

Reference

1. Luo, H.; Leitch, M.; Behnamian, Y.; Ma, Y.; Zeng, H.; Luo, J.-L., Development of electroless Ni-P/nano-WC composite coatings and investigation on its properties. *Surface and Coatings Technology* **2015**, *277*, 99-106.
2. Wang, S.; Liu, J.; Zhang, L.; Masliyah, J.; Xu, Z., Interaction forces between asphaltene surfaces in organic solvents. *Langmuir* **2009**, *26* (1), 183-190.
3. Wang, S.; Liu, J.; Zhang, L.; Xu, Z.; Masliyah, J., Colloidal interactions between asphaltene surfaces in toluene. *Energy & Fuels* **2008**, *23* (2), 862-869.
4. Zhang, L.; Xie, L.; Shi, C.; Huang, J.; Liu, Q.; Zeng, H., Mechanistic Understanding of Asphaltene Surface Interactions in Aqueous Media. *Energy & Fuels* **2016**, *31* (4), 3348-3357.
5. Brant, J. A.; Childress, A. E., Membrane–colloid interactions: comparison of extended DLVO predictions with AFM force measurements. *Environmental Engineering Science* **2002**, *19* (6), 413-427.
6. Dorobantu, L. S.; Bhattacharjee, S.; Foght, J. M.; Gray, M. R., Analysis of force interactions between AFM tips and hydrophobic bacteria using DLVO theory. *Langmuir* **2009**, *25* (12), 6968-6976.
7. Freitas, A. M.; Sharma, M. M., Detachment of particles from surfaces: an AFM study. *Journal of colloid and interface science* **2001**, *233* (1), 73-82.
8. Israelachvili, J. N., *Intermolecular and surface forces*. Academic press: 2011.
9. Cappella, B.; Dietler, G., Force-distance curves by atomic force microscopy. *Surface science reports* **1999**, *34* (1-3), 1-104.

10. Butt, H.-J.; Kappl, M.; Mueller, H.; Raiteri, R.; Meyer, W.; R uhe, J., Steric forces measured with the atomic force microscope at various temperatures. *Langmuir* **1999**, *15* (7), 2559-2565.
11. Biggs, S., Steric and bridging forces between surfaces bearing adsorbed polymer: an atomic force microscopy study. *Langmuir* **1995**, *11* (1), 156-162.
12. Liu, J.; Cui, X.; Huang, J.; Xie, L.; Tan, X.; Liu, Q.; Zeng, H., Understanding the stabilization mechanism of bitumen-coated fine solids in organic media from non-aqueous extraction of oil sands. *Fuel* **2019**, *242*, 255-264.
13. Shi, C.; Zhang, L.; Xie, L.; Lu, X.; Liu, Q.; Mantilla, C. A.; van den Berg, F. G.; Zeng, H., Interaction mechanism of oil-in-water emulsions with asphaltenes determined using droplet probe AFM. *Langmuir* **2016**, *32* (10), 2302-2310.
14. Shi, C.; Zhang, L.; Xie, L.; Lu, X.; Liu, Q.; He, J.; Mantilla, C. A.; Van den Berg, F. G.; Zeng, H., Surface interaction of water-in-oil emulsion droplets with interfacially active asphaltenes. *Langmuir* **2017**, *33* (5), 1265-1274.
15. Xie, L.; Shi, C.; Cui, X.; Huang, J.; Wang, J.; Liu, Q.; Zeng, H., Probing the interaction mechanism between air bubbles and bitumen surfaces in aqueous media using bubble probe atomic force microscopy. *Langmuir* **2017**, *34* (3), 729-738.
16. Chan, D. Y.; Klaseboer, E.; Manica, R., Theory of non-equilibrium force measurements involving deformable drops and bubbles. *Advances in colloid and interface science* **2011**, *165* (2), 70-90.
17. Chan, D. Y.; Klaseboer, E.; Manica, R., Film drainage and coalescence between deformable drops and bubbles. *Soft Matter* **2011**, *7* (6), 2235-2264.

18. Shi, C.; Cui, X.; Xie, L.; Liu, Q.; Chan, D. Y.; Israelachvili, J. N.; Zeng, H., Measuring forces and spatiotemporal evolution of thin water films between an air bubble and solid surfaces of different hydrophobicity. *ACS nano* **2014**, *9* (1), 95-104.
19. Rudrake, A.; Karan, K.; Horton, J. H., A combined QCM and XPS investigation of asphaltene adsorption on metal surfaces. *Journal of colloid and interface science* **2009**, *332* (1), 22-31.
20. Tamiz Bakhtiari, M.; Harbottle, D.; Curran, M.; Ng, S.; Spence, J.; Siy, R.; Liu, Q.; Masliyah, J.; Xu, Z., Role of caustic addition in bitumen–clay interactions. *Energy & Fuels* **2015**, *29* (1), 58-69.
21. Vogt, B. D.; Lin, E. K.; Wu, W.-l.; White, C. C., Effect of film thickness on the validity of the Sauerbrey equation for hydrated polyelectrolyte films. *The Journal of Physical Chemistry B* **2004**, *108* (34), 12685-12690.
22. Malmström, J.; Agheli, H.; Kingshott, P.; Sutherland, D. S., Viscoelastic Modeling of Highly Hydrated Laminin Layers at Homogeneous and Nanostructured Surfaces: Quantification of Protein Layer Properties Using QCM-D and SPR. *Langmuir* **2007**, *23* (19), 9760-9768.
23. Wu, W.; Giese, R. F., Jr.; van Oss, C. J., Evaluation of the Lifshitz-van der Waals/Acid-Base Approach To Determine Surface Tension Components. *Langmuir* **1995**, *11* (1), 379-382.
24. Park, S.; Jang, E.; An, H.; Choi, W.; Kim, J.-H.; Lee, J.-H.; Choi, J.; Lee, J. S., The Lifshitz-van der Waals acid-base theory assisted fabrication of MFI-containing mixed matrix membranes for gas separations. *Microporous and Mesoporous Materials* **2018**,

264, 60-69.

Chapter 3 Fouling Mechanisms of Asphaltenes and Fine Solids on Bare and Coated Carbon Steel in Oil Production

3.1 Introduction

Fouling, defined as the adsorption and build-up of undesired materials on the surfaces of related substrates or equipment through physical or/and chemical interactions,¹⁻³ has caused significantly challenging problems to the chemical engineering and oil industries. The unexpected depositions of various materials on substrate surfaces in industrial operations result in negative impacts on the operational efficiency and generate significant economic losses.

Steam-Assisted Gravity Drainage (SAGD) technique is the most widely used in-situ recovery method to extract bitumen from the Canadian oil sands.⁴ In the SAGD operations, fouling on facilities such as pipelines and heat exchangers can lead to plugged liners, increased pressure drop, enlarged heat resistance and reduced bitumen extraction efficiency.⁵⁻⁷ Meanwhile, it costs billions of dollars for industries in the world to shut down and clean or replace related facilities.⁸ Disposal of the fouled devices and the related foulants could also lead to potential negative impacts on the environment. Therefore, it is important to characterize the foulant components and understand the fouling mechanisms in related industrial processes.

In previous studies, it has been reported that the major components of plugging foulants identified in SAGD operations include corrosion products (e.g., iron oxide),

clay particles (e.g., kaolinite), fine solids (e.g., silica) and organics (e.g., bitumen, asphaltenes).^{1, 9-11} Among these foulants, asphaltenes are the heaviest molecular fractions of crude oil with complex ring structures, which are insoluble in alkane solvents (e.g., heptane), but soluble in aromatic solvents (e.g., toluene).¹²⁻¹⁵ Asphaltenes are considered to be one of the major causes for the fouling issues in oil production.¹⁶⁻²⁰ It was well known that asphaltenes can easily deposit on various surfaces, such as silica and iron surfaces, via the van der Waals force, hydrogen bonds, cation/anion- π interactions and so on.²¹⁻²² Additionally, the aggregations of asphaltenes could act as the precursor for the coke formation, and the coke can lead to stronger fouling problems in oil production.²³⁻²⁷ Fine solids, originated from the reservoir ground or oil sands,²⁸⁻²⁹ were often presented with asphaltenes in bitumen extraction.³⁰⁻³¹ Thus, the adsorption of fine solids (i.e., silica) and organics (e.g., asphaltenes) contributes significantly to the fouling in oil production processes.

L80 carbon steel is one of the commonly used materials in pipe and joints for oil and gas industry.³²⁻³⁴ However, the limited corrosion and fouling resistance of L80 carbon steel makes antifouling treatments requisite for its service under harsh environment in industrial operations.³⁴⁻³⁶ Over past decades, various protective coating techniques on steels have been developed to extend their applications in different industrial processes,³⁷⁻⁴² such as plasma enhanced chemical vapor deposition, polymer coatings and electroless deposition.⁴³⁻⁴⁸ Among them, the electroless nickel-phosphorus (EN) coating shows great potential applications for its remarkable properties, such as high corrosion resistance, high wear resistance, great hardness, uniform thickness, and good

lubricity.⁴⁹⁻⁵¹ The EN coating on steel substrates could protect the steel during service under harsh operation environment.⁴⁹ Meanwhile, other materials, such as TiO₂, Al₂O₃, SiC, and ZrO₂, have been added in the EN coating to improve its performances (e.g., corrosion resistance).⁵²⁻⁵⁶ However, the evaluation and understanding of the antifouling property of EN coating in chemical and oil industries still remains very limited, which is one of the major focuses of this work.

In this study, for the *first* time, the fouling and antifouling behaviors and the interaction mechanisms of silica and asphaltenes on L80 carbon steel and L80 with EN coating in aqueous solutions have been investigated via quantitative force measurements using the atomic force microscope (AFM) colloidal probe technique and bulk fouling tests. The effects of salinity, pH and divalent ions (i.e., Ca²⁺) were also investigated. Our work studies the fundamental fouling and antifouling mechanisms of fine solids and organics on selected metal surfaces in chemical and oil industries, with implications for the development of effective antifouling strategies.

3.2 Materials and Methodology

3.2.1 Materials.

L80 carbon steel (L80) substrates were supplied by RGL Reservoir Management Inc. (RGL, Alberta, Canada). Silica microsphere particles (diameter 5 μm, Sigma-Aldrich, Canada) were used as fine solids in the force measurements. Asphaltenes were extracted from Athabasca bitumen by following a procedure reported previously.⁵⁷ Toluene (C₇H₈, 99.9%, HPLC grade, Sigma-Aldrich, Canada) was used as the solvent to dissolve

asphaltenes. Silica wafers with 0.5 μm thermal oxide layer purchased from NanoFAB, University of Alberta, were used in force measurements for the force calibration of AFM probes. Sodium chloride (NaCl , $\geq 99.5\%$, Sigma-Aldrich, Canada) was used to prepare the aqueous solutions. Calcium chloride dihydrate ($\text{CaCl}_2 \cdot 2\text{H}_2\text{O}$, ACS reagent, $\geq 99\%$, Sigma-Aldrich, Canada) was used as the source of Calcium ions to investigate the effect of divalent cations on fouling. Sodium hydroxide (NaOH , ACS reagent, $\geq 97\%$, Sigma-Aldrich, Canada) and hydrochloric acid (HCl , certified ACS Plus, Fisher Scientific, Canada) were used as pH modifiers. Aqueous solutions were prepared using Milli-Q water with a resistivity of $18.2 \text{ M}\Omega \cdot \text{cm}$ (BARNSTEAD Smart2Pure, Thermo Scientific, Canada). Silica particles (size $0.5\text{-}10 \mu\text{m}$, Sigma-Aldrich, Canada) were used to prepare the silica suspensions for fouling tests. Ethanol (99.5% , anhydrous, ACROS Organics, Canada) was used for washing and cleaning of the substrates.

3.2.2 Preparation of Electroless Nickel-phosphorus (EN) Coating.

The nickel-phosphorus (EN) coating used in this study was prepared by electroless deposition onto L80 carbon steel substrates from a piece of slotted liner using reported EN coating plating process.⁵⁸⁻⁵⁹ First, the bare L80 steel was soaked in NaOH solution ($20 \text{ wt}\%$) at $70 \text{ }^\circ\text{C}$ for 15 min to remove all cutting fluids, grease and oil from the surface. Then, it was washed by DI water and ethanol, and dried using pure nitrogen. A solution of $10 \text{ wt}\%$ hydrochloric acid was used to activate the L80 surface for the plating process. The details of bath compositions and reaction conditions are listed in Table 3.1. The activated L80 substrates were placed in the electroless plating solution for EN coating.

After the coating process was completed, the substrates were rinsed with DI water and ethanol, and dried using pure nitrogen.

Table 3.1 Bath compositions and reaction conditions for EN coating deposition

Composition	Concentration
NiSO₄·6H₂O	25 g L ⁻¹
NaH₂PO₂·H₂O	30 g L ⁻¹
Citric acid	20 g L ⁻¹
Lactic acid	20 ml L ⁻¹
Reaction Conditions:	
pH: 6.0	
Temperature: 85 °C	
Agitation: 250 rpm	
Time: 30 min	

3.2.3 Preparation of silica and asphaltenes probes.

The silica probe was prepared using two-component epoxy glue (EP2LV, MasterBond, USA) to attach a silica microsphere (radius ~2.5 μm) to the end of a tipless AFM cantilever (NP-O10, Bruker, Santa Barbara, CA). This glued silica probe was placed at room temperature (23 °C) for at least 24 h for epoxy curing. Before force measurements, the silica probe was treated in a UV-Ozone cleaner for 15 min to remove the possible organic contaminants, and then rinsed with DI water and ethanol, followed

by drying with pure nitrogen. Asphaltenes probe was prepared by immersing the cleaned silica probe in 20 ppm asphaltenes-in-toluene solution for 2 days. Figure 3.S1 shows the scanning electron microscopy (SEM) images of silica probe and asphaltenes-coated silica probe, demonstrating the successful deposition and full coverage of asphaltenes on the probe. Prior to force measurements, the asphaltenes probe was washed using toluene and dried with pure nitrogen.

3.2.4 Force measurements using colloidal probe technique.

The force measurements between silica or asphaltenes-coated silica probe and different substrates (i.e., L80, L80 with EN coating) in NaCl solutions were conducted with a Dimension Icon AFM (Bruker, Santa Barbara, CA, USA) using the colloidal probe technique, as illustrated in Figure 3.1. The details of experimental setup were reported elsewhere.^{7, 60-66}

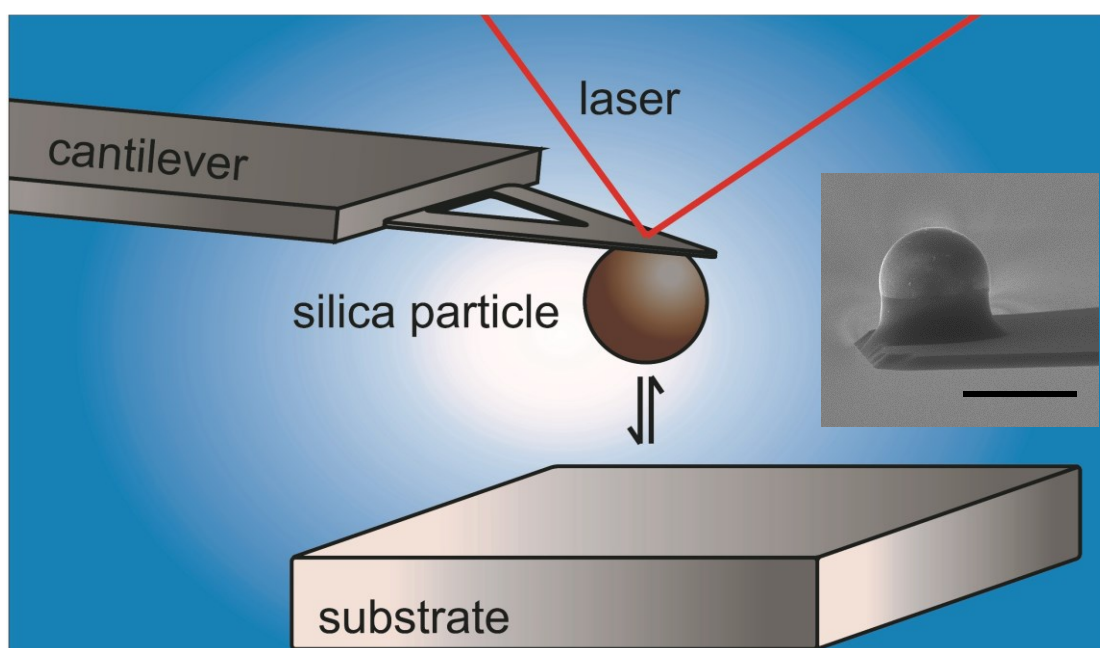


Figure 3.1 Schematic of AFM colloidal probe technique in aqueous solution. The inset

shows the SEM image of a typical silica probe (Scale bar: 5 μm).

During the force measurements, the substrate was firstly immersed in the aqueous solution. A silica or asphaltenes probe was installed in the tip holder of the AFM and then placed in the aqueous solution. The piezo sensitivity was calibrated from the linear regime of the force curves between the probe and a clean silica surface, and the spring constant of this probe was calibrated using the thermal tune method.⁶⁷ During each force measurement, the silica or asphaltenes probe was driven by a piezo to approach the substrate at a velocity of 1 $\mu\text{m s}^{-1}$ until a loading force of 10 nN was reached, and then it was retracted from the substrate. The deflection of the probe was detected by an optical laser beam detection system, and the interaction forces were calculated using the Hooke's law. The corresponding force profiles between the probe and the substrate were recorded by the AFM software. To obtain reproducible results, multiple force measurements were conducted with the probe on different positions (more than 50) of the same substrate, and two independently prepared substrates were tested. The measured force curves were analyzed and the average adhesion between the probe and the substrate was determined.

The force-separation profiles between the probe and substrate in NaCl solutions were measured and recorded by the AFM software. To theoretically analyze the measured interactions, the classical Derjaguin-Landau-Verwey-Overbeek (DLVO) model coupled with hydrodynamic interaction has been applied to fit the measured force data. The included van der Waals force (F_{vdw}) and electric double layer force (F_{edl}) are given by

Equations 1 and 2, respectively.⁶⁸⁻⁶⁹

$$F_{vdw} = -\frac{A_H R}{6D^2} \quad (1)$$

$$F_{edl} = \frac{\pi}{\varepsilon\varepsilon_0\kappa^2} \left[(\sigma_P^2 + \sigma_S^2) (e^{-2\kappa D} + 2\kappa D - 1) e^{-2\kappa D} + 4\sigma_P\sigma_S (e^{-\kappa D} + \kappa D - 1) e^{-\kappa D} \right] \quad (2)$$

$$\sigma = \sqrt{8\varepsilon\varepsilon_0 \cdot k_B T \cdot CN_A} \sinh\left(\frac{e\Psi}{2k_B T}\right) \quad (3)$$

where A_H is the Hamaker constant, R is the radius of silica microsphere, D is the separation distance between the microsphere and flat substrate, ε is the relative permittivity of medium, ε_0 is the vacuum permittivity, κ is the Debye length, σ_P is the surface charge density of colloidal probe, σ_S is the charge density of the flat substrate, k_B is the Boltzmann constant, T is the temperature, C is the bulk concentration of ions, N_A is the Avogadro's number, e is the elementary charge, and Ψ is the surface potential. In addition to the DLVO interactions, the hydrodynamic force (F_{hd}) was also included to analyze the measured force profile as given by Equation 4.⁷⁰

$$F_{hd} = -\frac{6\pi\eta R^2}{D} u, \text{ as } \frac{D}{R} \rightarrow 0 \quad (4)$$

where η is the fluid viscosity (0.001 N m⁻², 20 °C), and u is the approaching velocity of microsphere ($u=1 \mu\text{m s}^{-1}=1.0\times 10^{-6} \text{ m s}^{-1}$). Therefore, the total forces (F) can be given by Equation 5.

$$F = F_{vdw} + F_{edl} + F_{hd} \quad (5)$$

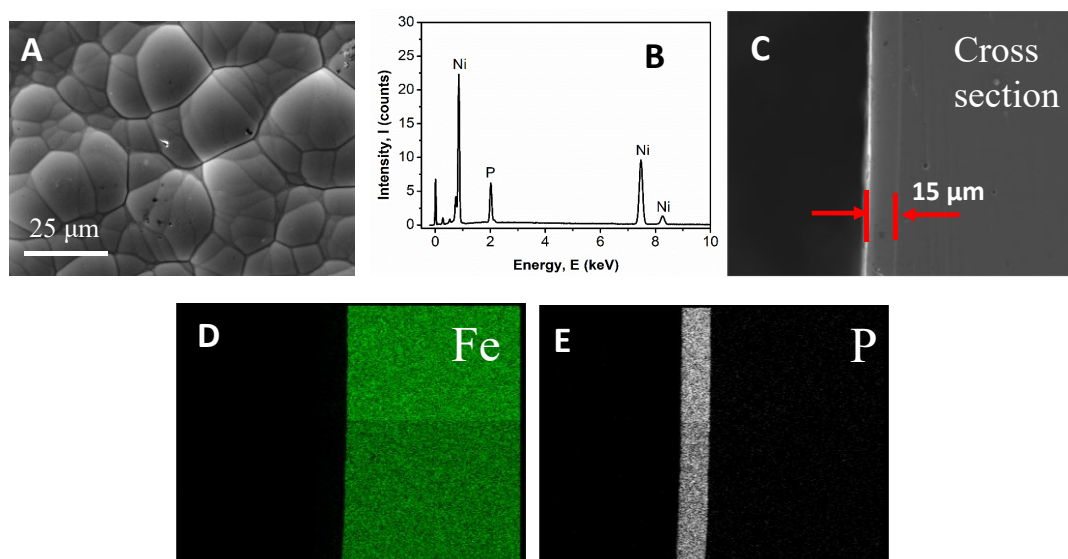
3.2.5 Bulk fouling tests.

The bulk fouling tests of L80 and EN coating in silica and asphaltenes-coated silica suspensions were conducted to evaluate their fouling and antifouling performances. Asphaltenes-coated silica particles were prepared by soaking silica particles (0.5~10 μm) in 20 ppm asphaltenes in toluene for 2 days. Then the liquid was removed after centrifugation. The solids were thoroughly washed by pure toluene and dried at room temperature (23 °C). Silica or asphaltenes-coated silica suspensions were prepared by dispersing 0.1 g particles in 100 mL NaCl solutions with different water chemistries (e.g., salinity, pH and Ca^{2+} ions) using an ultrasonic bath for 1 hour. L80 and EN substrates were separately immersed in the silica or asphaltenes-coated silica suspensions with a stirring speed of 300 rpm for 24 h at room temperature (23 °C). Then the treated substrates were washed with DI water and dried with pure nitrogen, and characterized using optical imaging, Scanning Electron Microscopy (SEM) and Energy Dispersive X-Ray Spectroscopy (EDS). The intensity signal of silicon element in the EDS spectra was determined to show the fouling of silica particles, and that of carbon element was examined for the fouling of asphaltenes-coated silica particles. It is noted that although EDS characterizations could not quantify the total amount of foulants adsorbed on substrates, they provide useful data for direct comparison of antifouling performance of different substrates under same experimental condition.

3.3 Results and Discussion

3.3.1 Characterization of EN coating.

Figure 3.2 shows the SEM and EDS results of EN coating on L80 substrate. The typical nodular structure of electroless nickel phosphorus⁵⁸ was detected on the flat substrate. The EDS element results of the EN coating show the presence of nickel and phosphorus elements, demonstrating the successful deposition of EN coating on L80 substrate. Figure 3.2C shows the SEM image of the cross section of EN coating, and Figure 3.2C, E and F show the EDS element mapping of iron, phosphate and nickel at the cross section. The thickness of the EN coating layer was determined to be ~15 μm . Figure 3.3 shows the topographic AFM images of the EN and L80 substrates, which have root-mean-square (rms) roughness of 21.9 nm and 12.5 nm, respectively.



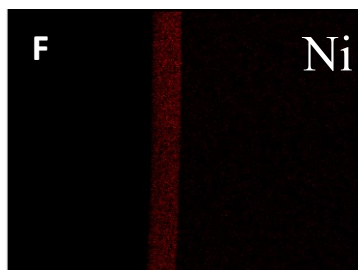


Figure 3.2 (A) SEM image of EN coating deposited on L80. (B) EDS spectrum of EN coating. (C) SEM image of the cross section of the EN coating. (D, E, F) EDS elemental mapping of the cross section of EN coating for elements Fe, P and Ni.

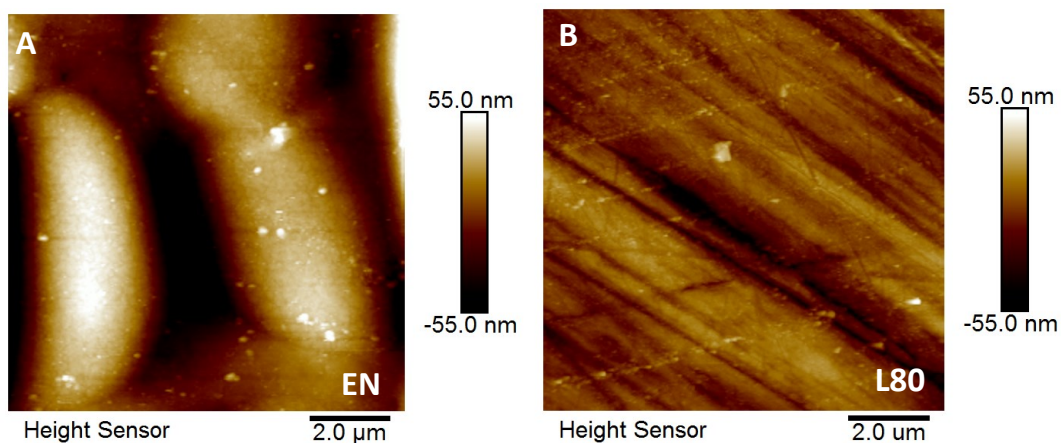


Figure 3.3 Topographic AFM image of (A) EN coating and (B) L80 substrate. The root-mean-square (rms) roughness is 21.9 nm for EN and 12.5 nm for L80.

3.3.2 Effect of electrolyte (NaCl) concentration.

The effects of electrolyte concentration on the surface interactions were investigated. The interaction forces between silica or asphaltenes-coated silica probe and L80 or EN substrates were measured in NaCl solutions of varying concentration: 1, 10, and 100 mM at natural pH of 5.8. The force results are shown in Figure 3.4.

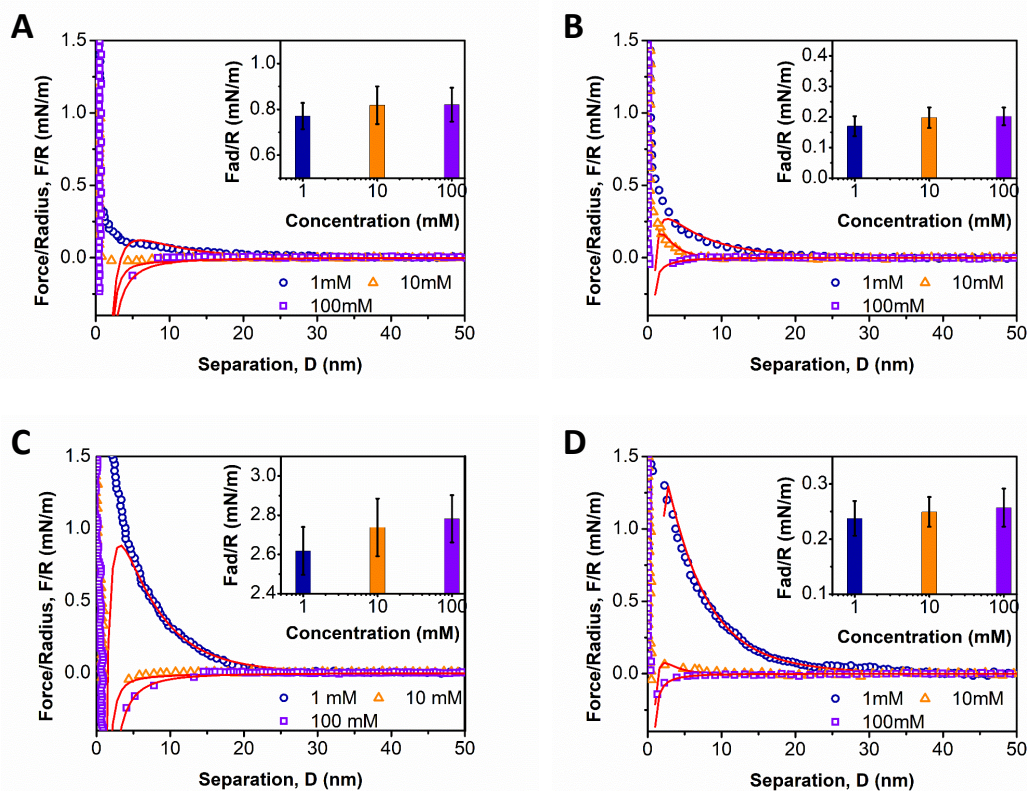


Figure 3.4 Normalized surface interaction forces during approaching in 1, 10 and 100 mM NaCl solutions for (A) silica probe vs. L80 substrate, (B) silica probe vs. EN substrate, (C) asphaltenes-coated silica probe vs. L80 substrate, and (D) asphaltenes-coated probe vs. EN substrate.

Figure 3.4A shows the normalized force profiles between silica probe and L80 substrate in 1, 10 and 100 mM NaCl solutions. Pure repulsive forces were measured between silica probe and L80 substrate in 1 mM NaCl. At low salinity (i.e., 1 mM), the Debye length is about 9.6 nm, and the electrical double layer (EDL) interaction contributes significantly to the long-range repulsion. In 10 mM NaCl solution, the long-range repulsion disappeared and repulsion was detected only at very short distances of $D < 2$ nm. At high salinity condition (i.e., 100 mM NaCl), no noticeable repulsion was

detected during approaching, while attraction was measured and an obvious “jump-in” behavior was observed at distance less than 10 nm. According to the classical DLVO theory, both the van der Waals (VDW) and electric double layer (EDL) interactions contribute to the surface interaction between the silica probe and L80 surface in NaCl solutions. Under high salinity (i.e., 100 mM) condition, the electric double layer was significantly compressed with a Debye length less than 1 nm, thus the VDW attraction dominates the interaction and leads to the “jump-in” behavior during approaching.⁶⁸ The inset in Figure 3.4A shows the normalized adhesion F_{ad}/R measured during the separation between the silica probe and L80 substrate under different NaCl concentration conditions, which were all around 0.8 mN m^{-1} and did not change significantly with salt concentration.

To better understand the interactions between silica probe and L80 substrate in NaCl solutions, the experimental data was theoretically analyzed based on the DLVO theory, as shown in the solid red curves of Figure 3.4A. For calibrating the surface property (i.e., surface potential) of silica, firstly, the interaction forces between silica probe and flat silica substrate were measured in 1, 10 and 100 mM NaCl solutions, as shown in Figure 3.S2A, which were fitted with the DLVO theory. The Hamaker constant between silica surfaces in NaCl solution was calculated as $6.28 \times 10^{-21} \text{ J}$ using the Lifshitz theory and assuming the dielectric constant and reflective index of silica and water.^{68, 71-72} It is found that the experimental data in 100 mM NaCl reasonably agrees with theoretical calculations based on the dominating VDW interactions, which validates the calculated Hamaker constant. Fitting the measured force curves between silica surfaces in 1 and

10 mM NaCl solutions using the DLVO theory gives the surface potentials of silica surface in 1 and 10 mM NaCl as -28.0 and -22.0 mV, respectively. The obtained surface potentials of silica fall within the value range reported previously,^{61, 73-74} as in Table 3.S1. The Hamaker constant and fitted surface potential values of silica were further applied to fit the measured force curves between silica probe and L80 surface in 1, 10 and 100 mM NaCl solutions. The fitted Hamaker constant between the silica probe and the L80 substrate in the 100 mM NaCl solution was 2.13×10^{-20} J based on the measured force curves. The reported Hamaker constants of silica, steel and water are 6.3×10^{-20} J, 3.0×10^{-19} J, and 3.7×10^{-20} J, respectively.^{68, 75} The Hamaker constant between silica and steel in aqueous solution was calculated as 2.08×10^{-20} J based on the combination relation which is very close to the fitted value. The surface potentials of L80 in 1 and 10 mM NaCl solutions were further fitted and calculated as -5.5 and -3.0 mV, respectively, as shown in Table 3.2, also close to the reported values.⁷⁶⁻⁷⁷ It is noted that the surface potentials of silica and L80 surfaces in NaCl solutions become less negative when the solution salinity increases.⁶⁸

Figure 3.4B shows the measured force curves between silica probe and EN substrate in 1, 10 and 100 mM NaCl solutions. Similar trend was observed as that in Figure 3.4A that the measured forces changed from the repulsion to attraction when the salinity increased from 1 mM to 100 mM. This tendency was also due to the compressed electric double layer interaction under high salinity condition. The inset in Figure 3.4B shows the normalized adhesion between silica probe and EN coating surface measured during separation, which was all around 0.2 mN m^{-1} . Comparing the force curves in Figure

3.4A and B, the interaction forces during approaching between silica probe and EN substrate are less attractive in 100 mM NaCl and more repulsive in 1 mM NaCl compared to those of the L80 substrate. Meanwhile the adhesion forces measured during separation are also much weaker. These results indicate that silica particles are more difficult to attach on EN coating than on L80 in NaCl solutions.

The measured force curves between silica probe and EN substrate in 1, 10 and 100 mM NaCl solutions were also theoretically analyzed using a similar approach used to obtain Figure 3.4A, and are shown by the solid curves in Figure 3.4B. The Hamaker constant between silica and EN substrate was determined to be 3.3×10^{-21} J from the force results under high salinity condition (i.e., 100 mM). This value was much smaller than the Hamaker constant between silica and L80 substrate, indicating that the VDW attraction between silica and EN substrate in NaCl solutions was weaker than that between silica and L80 substrate. The surface potentials of EN coating in 1 and 10 mM NaCl solutions were fitted to be -9.5 mV and -6.0 mV, respectively. These surface potentials were more negative than those of L80 substrate in NaCl solutions, demonstrating that the EDL repulsion between silica and EN substrate was stronger than that between silica and L80 substrate. The EN coating has nickel atoms and phosphorus atoms on its surface, which could attract more hydroxyl groups in aqueous solutions. Therefore, the more negative surface potentials, as well as the stronger EDL repulsions between EN substrate and silica probe, could be obtained.

Figure 3.4C and D show the measured force curves and theoretical fittings for interactions of asphaltenes probe with L80 and EN substrate in 1, 10 and 100 mM NaCl

solutions, respectively. Under low salinity (i.e., 1 mM NaCl), the force curves were repulsive due to the strong EDL repulsion. Under high salinity (i.e., 100 mM NaCl), the force curves became attractive because of the dominant role of VDW attraction. The measured adhesion between asphaltenes and L80 (around 2.7 mN m⁻¹) was much stronger than that between asphaltenes and EN coating (around 0.25 mN m⁻¹), suggesting that the asphaltenes was more difficult to attach to EN coating surface.

Table 3.2 The Hamaker constants and surface potentials of silica, asphaltenes, L80 and EN in 1, 10 and 100 mM NaCl solutions.

Hamaker constant A_H			
Silica probe-water-L80 substrate	2.13×10 ⁻²⁰ J		
Silica probe-water-EN substrate	3.3×10 ⁻²¹ J		
Asphaltenes probe-water-L80 substrate	2.31×10 ⁻²⁰ J		
Asphaltenes probe-water-EN substrate	3.5×10 ⁻²¹ J		
Surface potentials Ψ			
	1 mM	10 mM	100 mM
Silica	-28.0 mV	-22.0 mV	-
Asphaltenes	-55.0 mV	-18.0 mV	-
L80	-5.5 mV	-3.0 mV	-
EN	-9.5 mV	-6.0 mV	-

The measured force profiles were also theoretically analyzed based on the classic DLVO theory which is shown in the solid red curves of Figures 3.4C and D. For calibrating the surface property (i.e., surface potential) of asphaltenes-coated silica probe, the interaction forces between asphaltenes-coated silica probe and silica substrate were measured in 1, 10 and 100 mM NaCl solutions, as shown in Figure 3.S2B. The Hamaker constant between asphaltenes and silica in NaCl solution was found through fitting to be 6.55×10^{-21} J from the force curve at high salinity (i.e., 100 mM), which is close to the reported values.⁷⁸⁻⁷⁹ Then, fitting the force curves at 1 and 10 mM NaCl solutions gives the surface potentials of asphaltenes surface as -55.0 mV and -18.0 mV, respectively, as in Table 3.S1. The obtained surface potentials of asphaltenes were within the reported value range.^{73, 80} The Hamaker constant and fitted surface potentials were further used in the theoretical analysis of measured force curves between asphaltenes-coated silica probe and L80 or EN substrate. The Hamaker constants between asphaltenes-coated silica probe and L80 or EN substrates in NaCl solution were also found through fitting to be 2.31×10^{-20} J and 3.5×10^{-21} J, respectively. Based on the measured interaction forces at high salinity (i.e., 100 mM). The smaller Hamaker constant between asphaltenes-coated silica and EN substrate indicated a weaker VDW attraction than that between asphaltenes-coated silica and L80 substrate. With the fitted surface potentials of asphaltenes, L80 and EN substrates, it is noted that the experimental force curves between asphaltenes-coated silica and L80 or EN substrate in 1 and 10 mM NaCl solutions agree well with theoretical calculations based on the classical DLVO theory. These results further validate the fitted Hamaker

constants and surface potentials.

3.3.3 Effect of pH.

The effect of solution pH on the surface interactions was also investigated. The interaction forces between silica probe or asphaltenes-coated silica probe and L80 or EN substrate were measured in 1 mM NaCl solution at pH of 5.5, 8.0 and 10.5. The force results are shown in Figure 3.5.

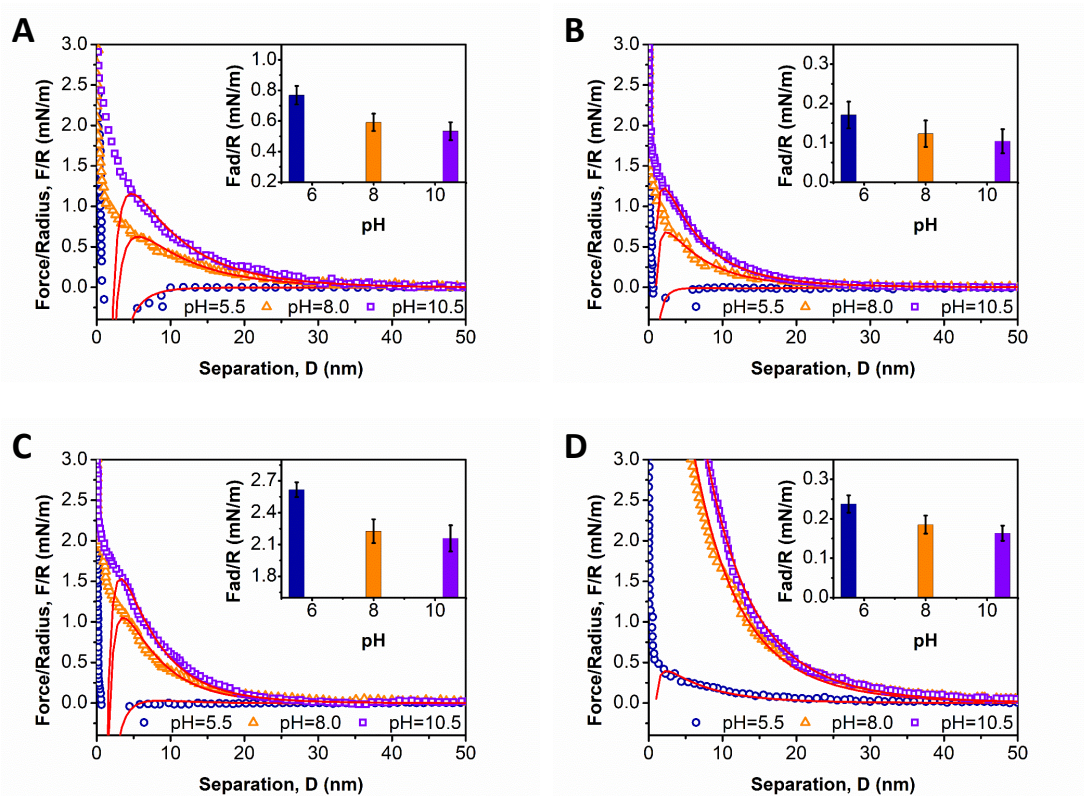


Figure 3.5 Normalized surface interaction forces during approaching in 1 mM NaCl solution at pH of 5.5, 8.0 and 10.5 for (A) silica probe vs. L80 substrate, (B) silica probe vs. EN substrate, (C) asphaltenes-coated silica probe and L80 substrate, and (D) asphaltenes-coated silica probe and EN substrate.

Figure 3.5A shows the normalized interaction forces between a silica probe and L80 substrate in 1 mM NaCl solutions at different pH of 5.5, 8.0 and 10.5. The long-range repulsive forces were detected at pH of 8.0 and 10.5. At pH of 5.5, the “jump-in” behavior was observed at distance less than 10 nm and attraction was measured. At alkaline pH (i.e., pH 10.5), more OH⁻ ions in the bulk solution could induce more adsorption of OH⁻ ions on the surface or promote the deprotonation of related surface chemical groups, which makes the substrate surface more negatively charged.⁶⁸ Therefore, alkaline pH of the NaCl solution induced stronger EDL repulsion between silica probe and L80 substrate. The inset in Figure 3.5A shows the normalized adhesions F_{ad}/R between silica probe and L80 substrate in 1 mM NaCl solutions at pH of 5.5, 8.0 and 10.5. The normalized adhesion F_{ad}/R decreases from 0.78 mN m⁻¹ at pH 5.5 to 0.60 mN m⁻¹ at pH 8.0 and finally to 0.58 mN m⁻¹ at pH 10.5, indicating that the alkaline pH leads to weaker adhesion between silica and L80 substrate. Thus, the solution pH has an influence on the adhesion between two surfaces. Figure 3.5B shows the normalized interaction forces between silica probe and EN substrate in 1 mM NaCl solutions at pH of 5.5, 8.0 and 10.5. A similar trend as in Figure 3.5A was observed. The measured normalized adhesions decreased from 0.17 mN m⁻¹ at pH 5.5 to 0.11 mN m⁻¹ at pH 10.5, which was also due to the alkaline pH. It was noticed that the adhesion forces between silica probe and EN substrate were weaker than those between silica and L80 substrate in NaCl solutions, indicating that it would be more difficult for silica particles to attach to EN surface.

Figures 3.5C and D show the normalized interaction forces between asphaltenes-

coated silica probe and L80 or EN substrate in 1 mM NaCl solutions at pH 5.5, 8.0 and 10.5. The obtained force curves are repulsive, except for the case of asphaltenes-coated silica probe and L80 substrate in 1 mM NaCl solution at pH 5.5, which showed a “jump-in” behavior at distances less than 4 nm. It was observed that the interaction forces between asphaltenes-coated silica probe and EN substrate were more repulsive than those between asphaltenes-coated silica probe and L80 substrate. This result was also due to the more negatively charged asphaltene surface at alkaline pH. Moreover, the normalized adhesion between asphaltenes and L80 or EN substrates became weaker at alkaline solution (i.e. pH 10.5), as shown in the insets of Figures 3.5C and D. Additionally, the adhesion between asphaltenes and EN coating was much weaker than that between asphaltenes and L80, suggesting the higher possibility for asphaltenes to adsorb on L80 surface.

Table 3.3 The surface potentials of silica, asphaltenes, L80 and EN in 1 mM NaCl solutions at pH of 5.5, 8.0 and 10.5.

	pH=5.5	pH=8.0	pH=10.5
Silica	-25.0 mV	-32.0 mV	-39.5 mV
Asphaltenes	-52.0 mV	-63.0 mV	-68.5 mV
L80	-3.0 mV	-6.0 mV	-6.5 mV
EN	-7.0 mV	-18.0 mV	-19.0 mV

The measured force profiles were also theoretically analyzed using the similar

approach, as shown by the solid red curves in Figure 3.5. For calibrating the surface property (i.e. surface potential) of silica and asphaltenes-coated silica, the interaction forces between silica probe or asphaltenes-coated silica probe and silica substrate in 1 mM NaCl solution at pH of 5.5, 8.0 and 10.5 were measured, as shown in Figure 3.S3. Since the Hamaker constants between silica probe or asphaltenes-coated silica probe and silica substrate in NaCl solution were known, the surface potentials of silica and asphaltenes were fitted and the results were listed in Table 3.S2. These values were within the value ranges reported previously.^{68, 73, 78, 80} Afterwards, the surface potentials of silica and asphaltenes were applied in the theoretical analysis of the measured interaction forces between silica probe or asphaltenes-coated silica probe and L80 or EN substrate. Thus, the surface potentials of L80 and EN substrates were fitted, as shown in Table 3.3. It was noted that the surface potentials of L80 and EN substrates became more negative when the solution pH turned to be alkaline, and the surface potentials of EN substrate were more negative than those of L80 substrate, suggesting a stronger EDL repulsion between silica or asphaltenes and EN substrate in NaCl solutions.

3.3.4 Effect of calcium ion.

Previous studies show that the presence of divalent ions could influence the aggregation behaviors and conformations of asphaltenes adsorbed at the oil-water interfaces, which would further impact the emulsion stability.⁸¹⁻⁸³ The effect of divalent ions (i.e., calcium ions) was also investigated. The interaction forces between silica

probe or asphaltenes-coated silica probe and L80 or EN substrate in 1mM NaCl at pH=8.0 with the addition of 0, 1 and 10 mM Ca^{2+} were measured, and the force results are shown in Figure 3.6.

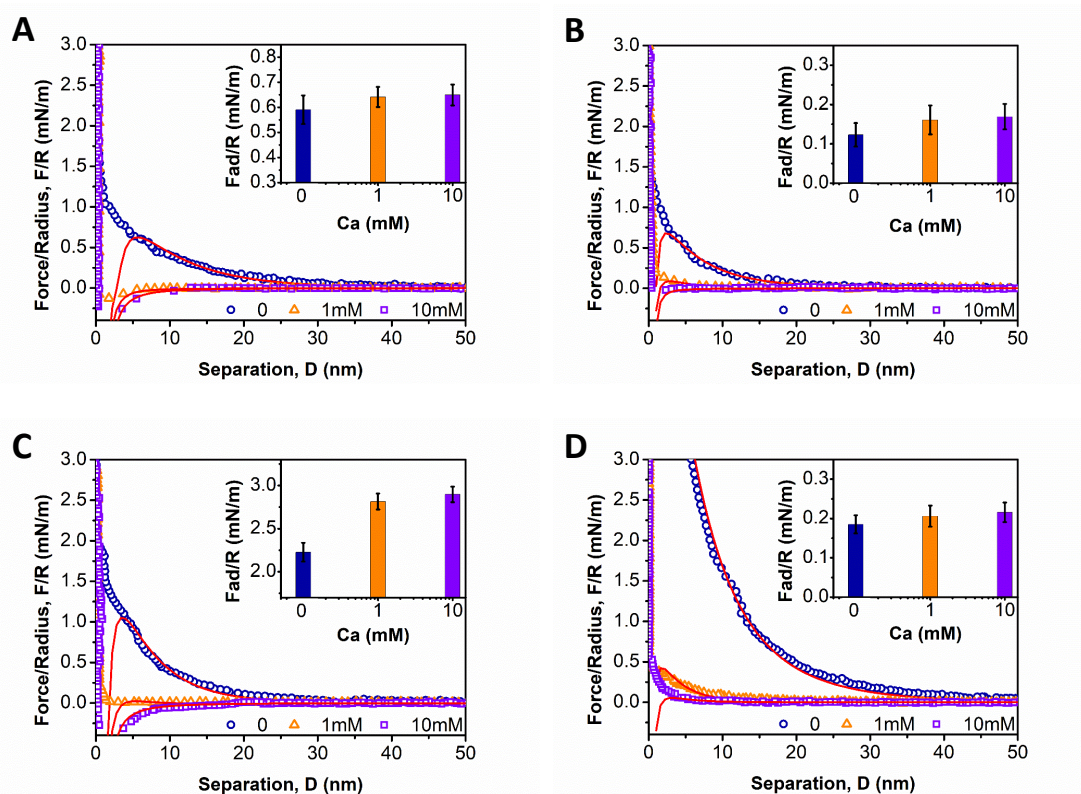


Figure 3.6 Normalized surface interaction forces during approaching in 1 mM NaCl solutions at pH 8.0 with the addition of 0, 1 and 10 mM Ca^{2+} for (A) silica probe vs. L80 substrate, (B) silica probe and EN substrate, (C) asphaltenes-coated silica probe and L80 substrate, and (D) asphaltenes-coated silica probe and EN substrate.

Figure 3.6A and B show the normalized interaction forces between the silica probe and L80 or EN substrate in 1 mM NaCl solution with the addition of 0, 1, and 10 mM Ca^{2+} ions. The measured force profiles exhibited a tremendously weakened repulsion with the addition of Ca^{2+} ions, which could be due to the significantly compressed

electrical double layer force. Divalent calcium ion has the stronger charge-shielding effect than monovalent sodium ions, which results in the more neutralized surface potentials and the weaker EDL repulsion.⁸⁴ It was also noted that the force profiles between the silica probe and L80 substrate in 1 and 10 mM Ca^{2+} ions were more attractive than those between silica probe and EN substrate, which was due to the stronger VDW attraction between silica and L80. Figure 3.6C and D show the normalized interaction forces between asphaltenes-coated silica probe and L80 or EN substrate in 1 mM NaCl solutions with the addition of 0, 1, and 10 mM Ca^{2+} ions. Similar trend of the force profiles with silica probe cases could be observed. The insets in Figure 3.6 show the normalized adhesions F_{ad}/R between silica probe or asphaltenes-coated silica probe and L80 or EN substrate in the presence of 0, 1 and 10 mM Ca^{2+} ions. The increased adhesion with the addition of Ca^{2+} ions demonstrates the significant influence of divalent ions (i.e., Ca^{2+} ions) in the surface interactions. The increased adhesion with the addition of Ca^{2+} ions demonstrates the significant influence of divalent ions (i.e., Ca^{2+} ions) in the surface interactions as the result of the strong shielding effect to weaken electric double layer interaction and bridging effect of Ca^{2+} ions between two negatively charged surfaces.⁸³ The relatively smaller adhesion between silica or asphaltenes and EN substrate than those between silica or asphaltenes and L80 substrate suggests the greater possibility to lower the fouling of silica and asphaltenes on EN coating surface.

Table 3.4 The surface potentials of silica, asphaltenes, L80 and EN in 1 mM NaCl

solutions at pH 8.0 with the addition of 0, 1 and 10 mM Ca²⁺.

	0	1 mM	10 mM
Silica	-32.0 mV	-15.0 mV	-5.0 mV
Asphaltenes	-63.0 mV	-28.0 mV	-16.0 mV
L80	-6.0 mV	-4.0 mV	-2.0 mV
EN	-18.0 mV	-6.0 mV	-3.0 mV

The measured force profiles were also analyzed by the theoretical approach discussed above, as shown by the solid red curves in Figure 3.6. The surface potentials of silica probe and asphaltenes-coated silica probe in 1 mM NaCl solutions with 0, 1 and 10 mM Ca²⁺ ions were firstly calibrated via force measurements with the silica substrate, as shown in Figure 3.S4. Based on the classical DLVO theory, the surface potentials of silica and asphaltenes were fitted and listed in Table 3.S3 and Table 3.4. Then, the surface potentials of L80 and EN were fitted from the measured force profiles and the results are also listed in Table 3.4. It is noted that the surface potentials became less negative when Ca²⁺ ions were added to the NaCl solution. The surface potentials of EN substrate was more negative than L80 substrate, suggesting a stronger EDL repulsion between EN coating and silica probe or asphaltenes-coated silica probe in NaCl solutions.

3.3.5 Bulk fouling tests in silica and asphaltenes-coated silica suspensions.

To examine the fouling and antifouling performance of L80 and EN substrates in

NaCl solutions, bulk fouling tests in silica and asphaltenes-coated silica suspensions were conducted under the effects of salinity, pH and Ca^{2+} ions. The optical images of L80 and EN substrates before the bulk fouling tests are shown in Figure 3.S5.

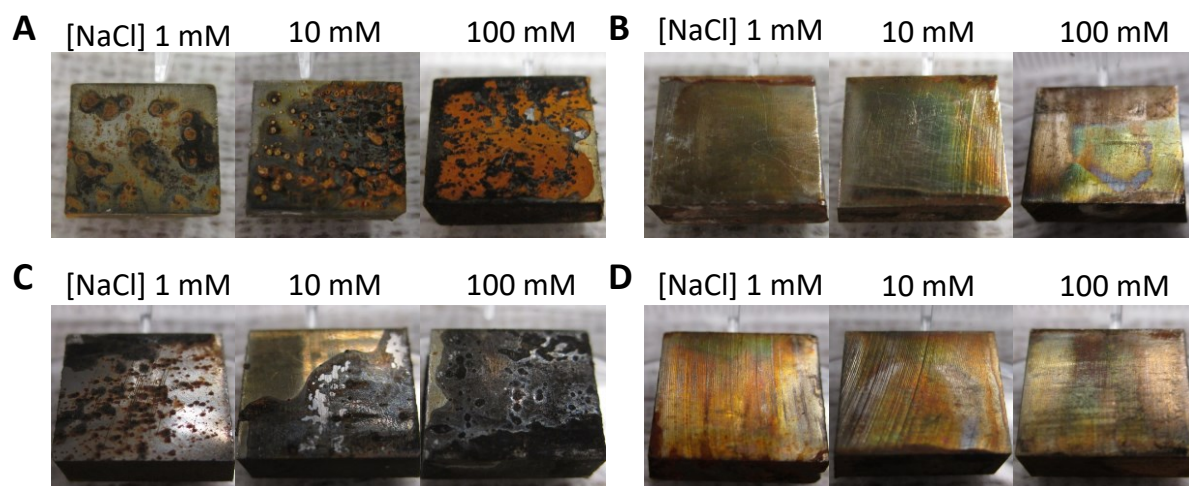
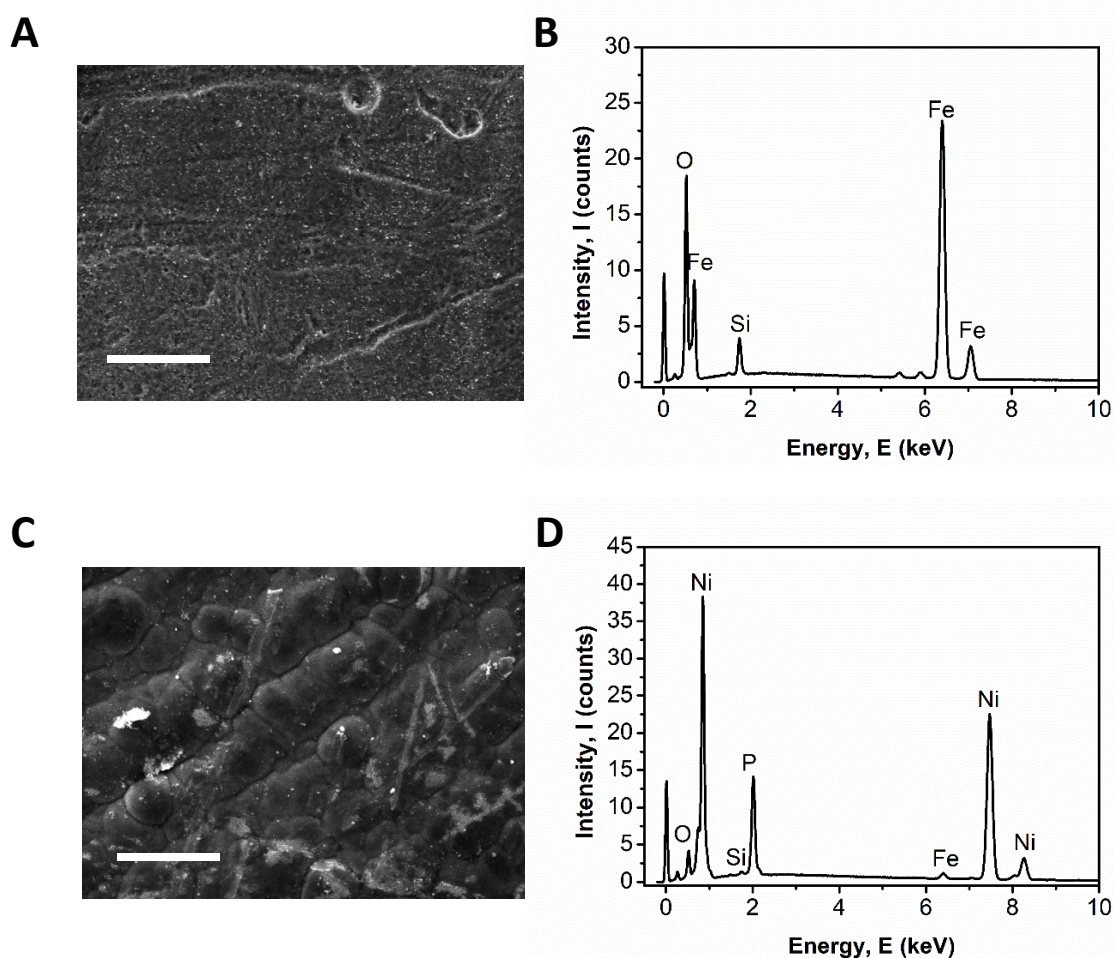


Figure 3.7 Optical images of L80 and EN substrates after bulk fouling tests in silica and asphaltenes suspensions with 1, 10 and 100 mM NaCl. (A) L80 substrates in silica suspensions. (B) EN substrates in silica suspensions. (C) L80 substrates in asphaltenes-coated silica suspensions. (D) EN substrates in asphaltenes-coated silica suspensions. (The size of substrates 8×8×3 mm.)

Figure 3.7A and C show the bulk fouling test results of L80 substrates in silica and asphaltenes-coated silica suspensions with 1, 10 and 100 mM NaCl, respectively. After performing the fouling tests, the L80 substrates showed increased corrosion and fouling products (yellow and black domains) on the surface with increasing solution salinity, indicating that the fouling of L80 substrate by silica particles and asphaltenes aggravated under higher salinity conditions. Therefore, high salinity (i.e., 100 mM

NaCl) promoted the fouling of silica and asphaltenes-coated silica particles on L80 surface. Figure 3.7B and D show the optical images of EN substrates after the bulk fouling tests in silica and asphaltenes-coated silica suspensions with 1, 10 and 100 mM NaCl. Unlike L80 substrates, there was no obvious fouling on EN substrates, suggesting that EN coating may possess an excellent antifouling property compared to L80.



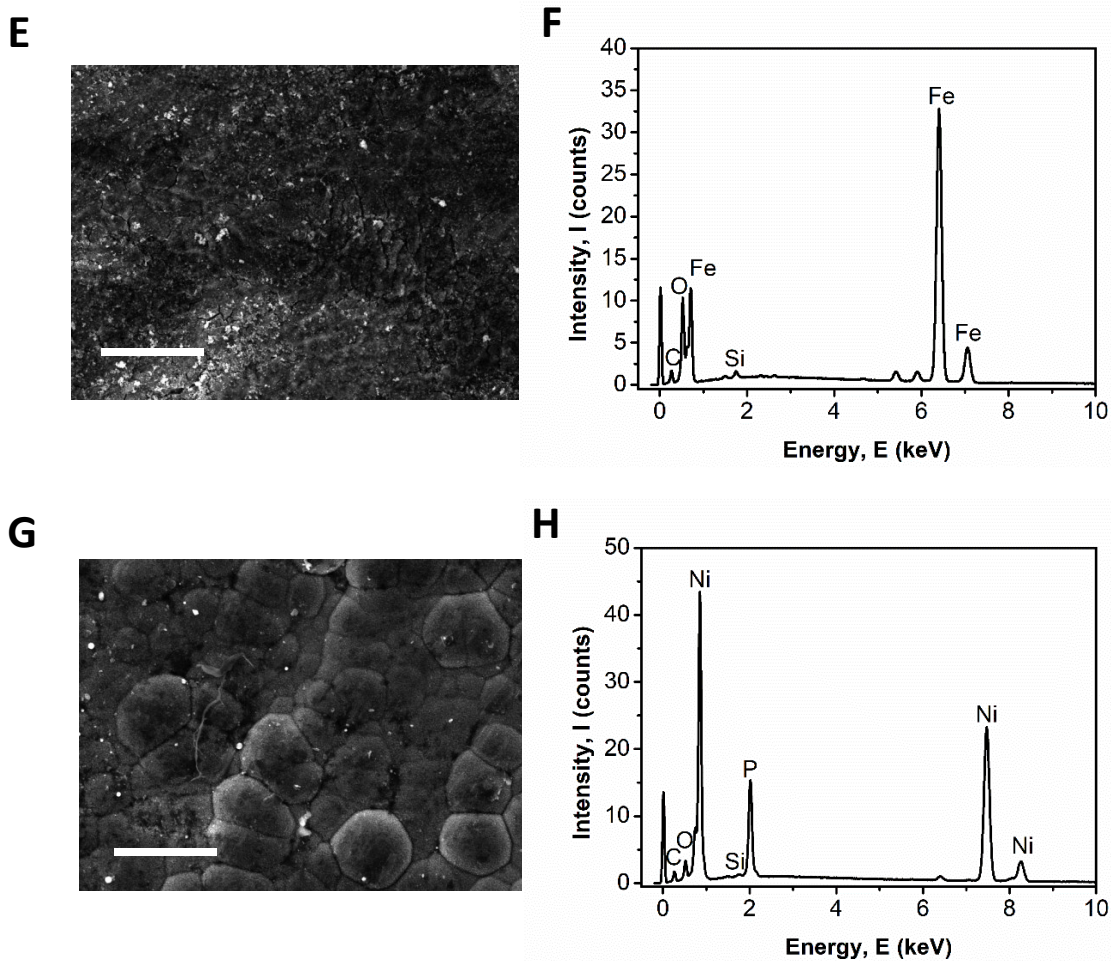


Figure 3.8 SEM and EDS results of L80 and EN substrates after bulk fouling tests in silica and asphaltene suspensions with 100 mM NaCl. (A, B) L80 substrate in silica suspensions. (C, D) EN substrate in silica suspensions. (E, F) L80 substrate in asphaltene suspensions. (G, H) EN substrate in asphaltene suspensions. (Scale bar: 25 μ m)

To evaluate the fouling phenomena, SEM and EDS were conducted to characterize L80 and EN substrates after the bulk fouling tests in silica and asphaltene suspensions with 100 mM NaCl, and the results are shown in Figure 3.8. The SEM images of L80 substrates (Figure 3.8A and E) showed that there were particles adsorbed on the

substrate surfaces, and the EDS results (Figure 3.8B and F) confirmed the presence of silicon element. It is noted that no silicon signal was detected from the EDS result of L80 substrate before fouling tests (Figure 3.S4C). Thus, the fouling of silica and asphaltenes-coated silica occurred on L80 surfaces. Figure 3.8C and G show the SEM images of EN substrates after bulk fouling tests. The EDS results (Figure 3.8D and H) show that only a very limited amount of silicon could be detected on the EN surfaces. The SEM and EDS results were consistent with the optical images in Figure 3.7. Therefore, these results demonstrate that the EN coating possesses a much better antifouling performance than L80 in silica and asphaltenes suspensions with different salinities. It is noted that EN coating (RMS roughness 21.9 nm) has the rougher surface morphology and lower surface energy than L80 substrate (RMS roughness 12.5 nm).⁷⁷ Previous reports demonstrated that large surface roughness and high surface energy could aggravate fouling phenomena.⁸⁵⁻⁸⁶ With high surface roughness and low surface energy, EN coating shows good antifouling property.

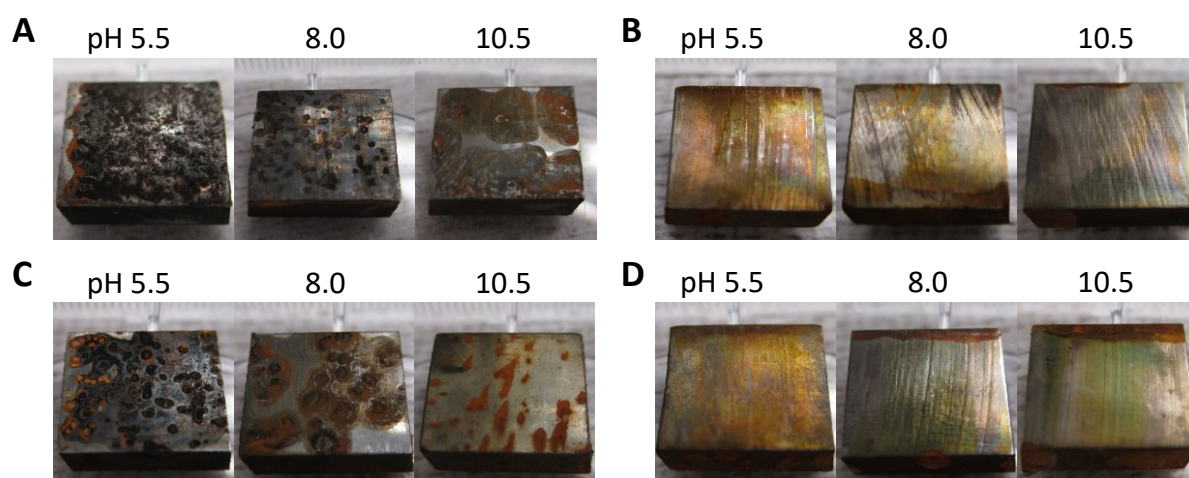


Figure 3.9 Optical images of L80 and EN substrates after bulk fouling tests in silica

and asphaltenes suspensions with 1mM NaCl solution and pH of 5.5, 8.0 and 10.5. (A) L80 substrates in silica suspensions. (B) EN substrates in silica suspensions. (C) L80 substrates in asphaltenes-coated silica suspensions. (D) EN substrates in asphaltenes-coated silica suspensions. (The dimensions of substrates are: 8×8×3 mm.)

Figure 3.9A and C show the optical images of L80 substrates after the bulk fouling tests in silica and asphaltenes suspensions with 1 mM NaCl and pH of 5.5, 8.0 and 10.5. It was observed that all the L80 substrates displayed yellow and black domains on the surfaces, indicating fouling occurrence. The fouling aggravated when the solution pH decreased to 5.5, suggesting that low acidic pH promoted the fouling of silica and asphaltenes-coated silica particles on L80 surface. Figure 3.9B and D show the optical images of EN substrates after the bulk fouling tests in silica and asphaltenes suspensions with 1 mM NaCl and pH of 5.5, 8.0 and 10.5. No obvious change was observed on EN surfaces. Therefore, EN coating possesses a better antifouling performance than L80 in silica and asphaltenes suspensions at different pH.

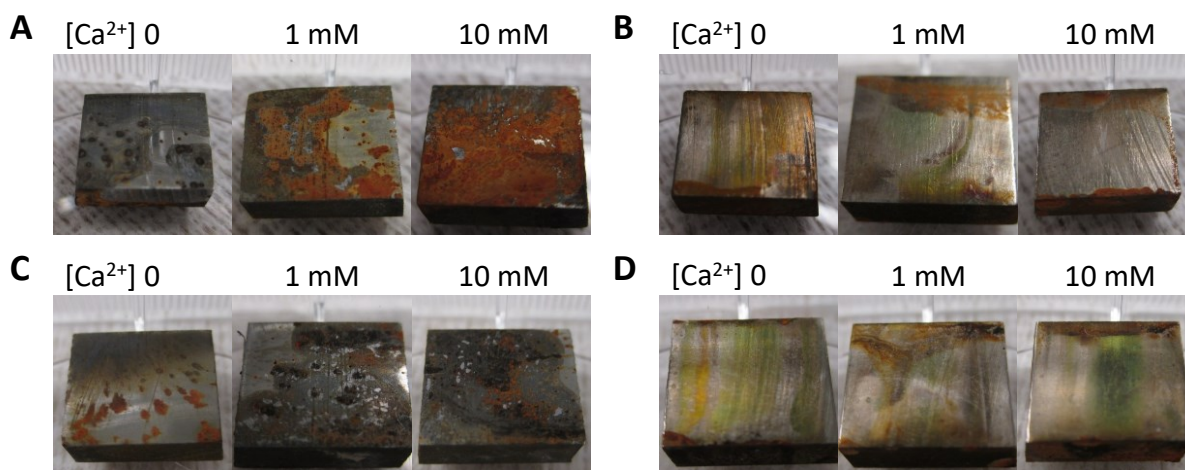


Figure 3.10 Images of L80 and EN substrates after bulk fouling tests in silica and asphaltenes suspensions in 1mM NaCl solution with 0, 1 mM and 10 mM Ca^{2+} ions. (A) L80 substrates in silica suspensions. (B) EN substrates in silica suspensions. (C) L80 substrates in asphaltenes-coated silica suspensions. (D) EN substrates in asphaltenes-coated silica suspensions. (The dimensions of substrates are: $8 \times 8 \times 3$ mm.)

Figure 3.10A and C show the optical images of L80 substrates after the bulk fouling tests in silica and asphaltenes suspensions in 1 mM NaCl solutions with 0, 1 and 10 mM Ca^{2+} ions. Fouling was visually detected on L80 surfaces and aggravated fouling could be detected when more Ca^{2+} ions was added in the NaCl solutions. Thus, the presence of Ca^{2+} ions promoted the fouling of silica and asphaltenes particles on the L80 surfaces. Figure 3.10B and D show the optical images of EN surfaces after the bulk fouling tests. Similarly, no obvious fouling was observed on the EN surfaces. Thus, EN coating shows a better antifouling performance than L80 in silica and asphaltenes suspensions in the presence of Ca^{2+} ions.

3.4 Conclusions

In this work, the fouling mechanisms and antifouling property of silica and asphaltenes-coated silica on L80 and EN substrates in NaCl solutions were directly quantified using the AFM colloidal probe technique. The effects of solution salinity, pH and presence of Ca^{2+} ions were investigated. The measured force curves were theoretically analyzed using the classic DLVO theory. The force results indicate that the attractive VDW interactions between silica probe or asphaltenes-coated silica probe and L80 or EN substrate in NaCl solutions contribute to the fouling phenomena, and the repulsive EDL interactions play an important role in their antifouling property. The surface force measurements also demonstrated that the EDL repulsion became weakened under high salinity condition, at low acidic pH and with the presence of divalent ions (i.e., Ca^{2+}). Compared with the L80 substrate, EN coating surface showed weaker VDW attraction and stronger EDL repulsion with silica and asphaltenes-coated silica in NaCl solutions. EN coating has nickel atoms and non-metal phosphorus atoms on its surface, which could adsorb more hydroxyl ions to carry more negative surface potential. Therefore, the stronger EDL repulsion, as well as the weaker VDW attraction, led to the excellent antifouling properties of EN in oil-in-water emulsions. Furthermore, bulk fouling tests of L80 and EN substrates in silica and asphaltenes suspensions were also conducted to evaluate their fouling and antifouling performances. The bulk fouling results agreed well with the surface force measurement results, which demonstrated that EN coating possessed excellent antifouling property. Our work has improved the fundamental understandings of the fouling mechanisms of silica particles and

asphaltenes on bare and EN-coated L80 surfaces in NaCl solutions, which provides useful insights on the antifouling behaviors of the EN coatings and the development of antifouling strategies for chemical and petroleum industries.

3.5 Supporting information

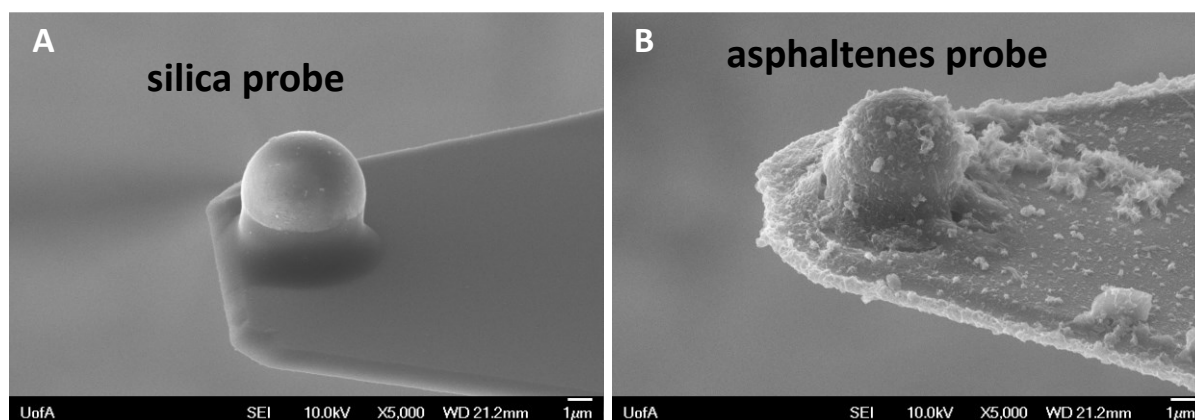


Figure 3.S1 Typical scanning electron microscopy (SEM) images of silica probe (A) and asphaltene probe (B).

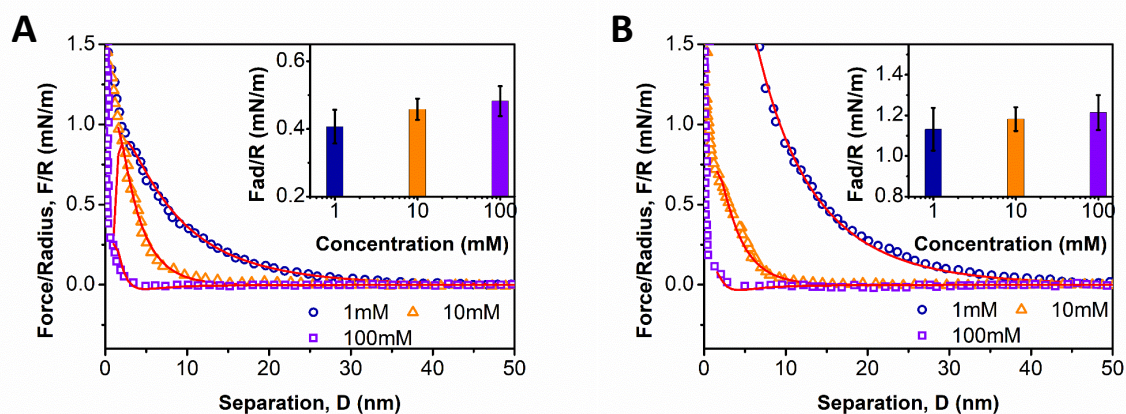


Figure 3.S2 Normalized surface interaction forces during approaching in 1, 10 and 100 mM NaCl solutions for (A) silica probe and silica wafer, and (B) asphaltenes-coated silica probe and silica wafer.

Table 3.S1 The Hamaker constants and surface potentials of silica and asphaltenes in 1, 10 and 100 mM NaCl solutions.

Hamaker constant A_H			
Silica probe-water-silica substrate	6.28×10^{-21} J		
Asphaltenes probe-water-silica substrate	6.55×10^{-21} J		
Surface potentials Ψ			
	1 mM	10 mM	100 mM
Silica	-28.0 mV	-22.0 mV	-
Asphaltenes	-55.0 mV	-18.0 mV	-

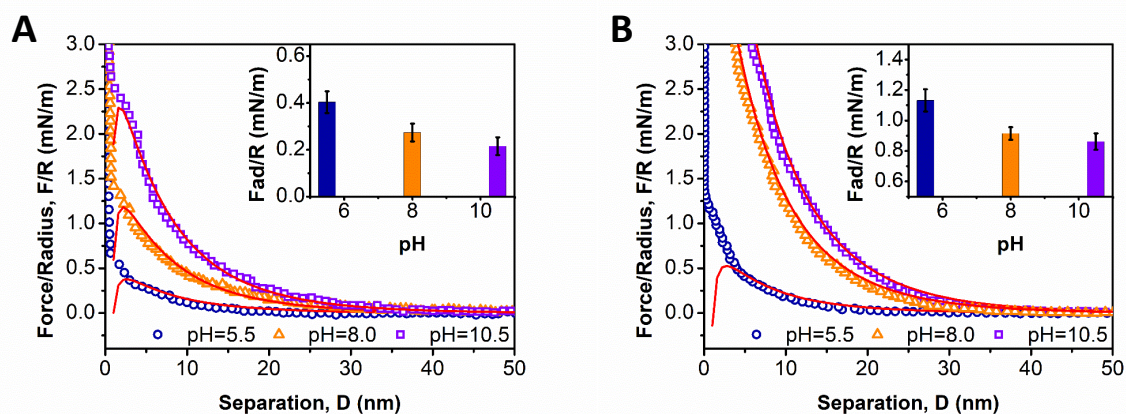


Figure 3.S3 Normalized surface interaction forces during approaching in NaCl solutions at pH of 5.5, 8.0 and 10.5 for (A) silica probe and silica wafer, and (B) asphaltenes-coated silica probe and silica wafer.

Table 3.S2 The surface potentials of silica and asphaltenes in 1 mM NaCl solutions at pH of 5.5, 8.0 and 10.5.

	pH=5.5	pH=8.0	pH=10.5
Silica	-25.0 mV	-32.0 mV	-39.5 mV
Asphaltenes	-52.0 mV	-63.0 mV	-68.5 mV

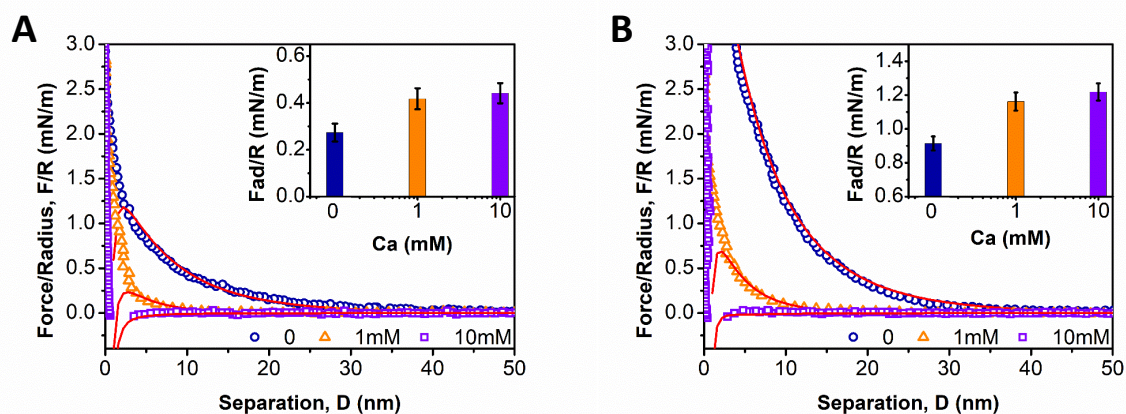
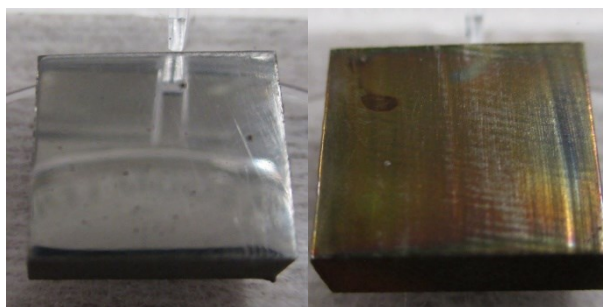


Figure 3.S4 Normalized surface interaction forces during approaching in 1 mM NaCl solutions at pH 8.0 with 0, 1 and 10 mM Ca^{2+} for (A) silica probe and silica wafer, and (B) asphaltenes-coated silica probe and silica wafer.

Table 3.S3 The surface potentials of silica and asphaltene surfaces in 1 mM NaCl solutions with 0, 1 mM and 10 mM Ca^{2+} (pH=8.0).

	0 Ca^{2+}	1 mM Ca^{2+}	10 mM Ca^{2+}
Silica	-32.0 mV	-15.0 mV	-5.0 mV
Asphaltenes	-63.0 mV	-28.0 mV	-16.0 mV

A



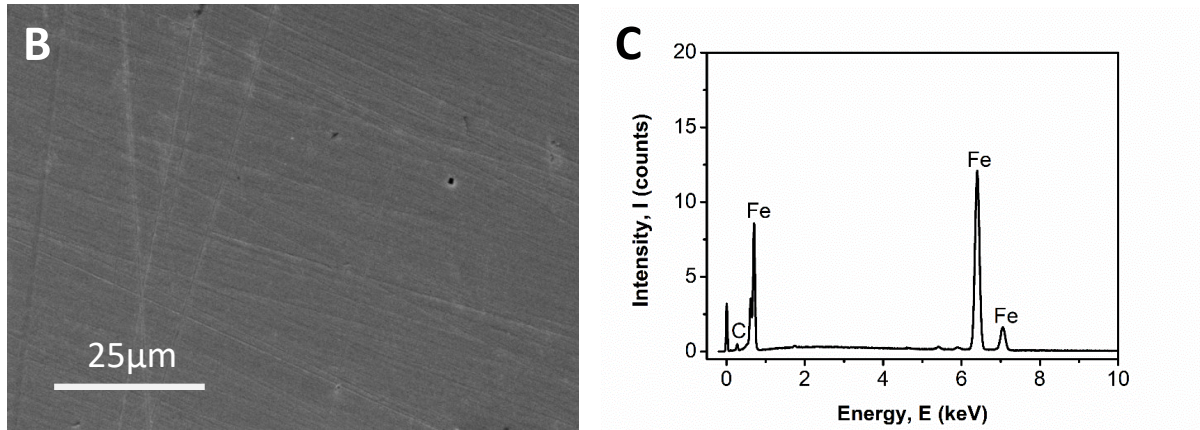


Figure 3.S5 (A) Optical images of original L80 substrate (left) and EN coating substrate (right). (B) SEM image of L80 substrate. (C) EDS results of L80 substrate.

Reference

1. Watkinson, A. P., Deposition from crude oils in heat exchangers. *Heat transfer engineering* **2007**, 28 (3), 177-184.
2. Hu, B.; Scott, K., Microfiltration of water in oil emulsions and evaluation of fouling mechanism. *Chemical Engineering Journal* **2008**, 136 (2-3), 210-220.
3. Amin, I. N. H. M.; Mohammad, A. W., Adsorptive fouling of organic solutes simulating sweetwater solutions on ultrafiltration membranes. *Chemical Engineering Journal* **2015**, 264, 470-478.
4. Acosta, E., Achieving sustainable, optimal SAGD operations. *Journal of Petroleum Technology* **2010**, 62 (11), 24-28.
5. Munoz, V.; Elliott, G.; Afara, M.; Mikula, R., Microscopy of Heat Exchanger Fouling During SAGD Operations. *Microsc. Microanal.* **2011**, 17 (S2), 1906.
6. Pugsley, T.; Pernitsky, D.; Grundler, J.; Johnsen, E. In *Fouling of heat transfer surfaces in a steam assisted gravity drainage (SAGD) in situ facility for the recovery of oil sands bitumen*, International Conference on Heat Exchanger Fouling and Clearing, 2013.
7. Zhu, D.; Leitch, M.; Wang, J.; Shi, X.; Gong, L.; Aghaie, E.; Luo, J.-l.; Zeng, H. In *Evaluation of an Advanced Metal Bonded Coating Technology for Improved SAGD Performance*, SPE Latin America and Caribbean Heavy and Extra Heavy Oil Conference, Society of Petroleum Engineers: 2016.
8. MacAdam, J.; Parsons, S. A., Calcium carbonate scale formation and control. *Re/Views in Environmental Science & Bio/Technology* **2004**, 3 (2), 159-169.

9. Das, S. K.; Butler, R. M., Mechanism of the vapor extraction process for heavy oil and bitumen. *Journal of Petroleum Science and Engineering* **1998**, *21* (1), 43-59.
10. Srinivasan, M. Heat exchanger fouling of some Canadian crude oils. University of British Columbia, 2008.
11. Lalchan, C. A.; Wiggins, C. B.; Moriyama, C. In *Formulation of an Emulsified Thermal Acid Blend for SAGD Applications in Eastern Alberta*, Canadian Unconventional Resources Conference, Society of Petroleum Engineers: 2011.
12. Adams, J. J., Asphaltene adsorption, a literature review. *Energy & Fuels* **2014**, *28* (5), 2831-2856.
13. Yarranton, H. W.; Masliyah, J. H., Molar mass distribution and solubility modeling of asphaltenes. *AIChE Journal* **1996**, *42* (12), 3533-3543.
14. Hoepfner, M. P.; Limsakoune, V.; Chuenmeechao, V.; Maqbool, T.; Fogler, H. S., A fundamental study of asphaltene deposition. *Energy & fuels* **2013**, *27* (2), 725-735.
15. Goual, L.; Firoozabadi, A., Measuring asphaltenes and resins, and dipole moment in petroleum fluids. *AIChE Journal* **2002**, *48* (11), 2646-2663.
16. Wang, J.; Buckley, J. S.; Creek, J. L., Asphaltene deposition on metallic surfaces. *J. Dispersion Sci. Technol.* **2004**, *25* (3), 287-298.
17. Deshannavar, U.; Rafeen, M.; Ramasamy, M.; Subbarao, D., Crude oil fouling: A review. *Journal of Applied Sciences(Faisalabad)* **2010**, *10* (24), 3167-3174.
18. Zhang, L.; Xie, L.; Shi, C.; Huang, J.; Liu, Q.; Zeng, H., Mechanistic Understanding of Asphaltene Surface Interactions in Aqueous Media. *Energy & Fuels* **2016**, *31* (4), 3348-3357.

19. Rocha, J.; Baydak, E.; Yarranton, H.; Sztukowski, D.; Ali-Marcano, V.; Gong, L.; Shi, C.; Zeng, H., Role of aqueous phase chemistry, interfacial film properties, and surface coverage in stabilizing water-in-bitumen emulsions. *Energy & Fuels* **2016**, *30* (7), 5240-5252.
20. Mao, X.; Gong, L.; Xie, L.; Qian, H.; Wang, X.; Zeng, H., Novel Fe₃O₄ based superhydrophilic core-shell microspheres for breaking asphaltenes-stabilized water-in-oil emulsion. *Chemical Engineering Journal* **2019**, *358*, 869-877.
21. Mullins, O. C., The asphaltenes. *Annual review of analytical chemistry* **2011**, *4*, 393-418.
22. Mullins, O. C.; Sheu, E. Y., *Structures and dynamics of asphaltenes*. Springer Science & Business Media: 2013.
23. Harji, A.; Koppel, P.; Mazurek, W.; Meysami, P. In *Processing Options for Bitumen Upgrading*, Canadian International Petroleum Conference, Petroleum Society of Canada: 2003.
24. Jian, C.; Tang, T.; Bhattacharjee, S., Probing the effect of side-chain length on the aggregation of a model asphaltene using molecular dynamics simulations. *Energy & Fuels* **2013**, *27* (4), 2057-2067.
25. Jian, C.; Zeng, H.; Liu, Q.; Tang, T., Probing the Adsorption of Polycyclic Aromatic Compounds onto Water Droplets Using Molecular Dynamics Simulations. *The Journal of Physical Chemistry C* **2016**, *120* (26), 14170-14179.
26. Goual, L.; Sedghi, M.; Zeng, H.; Mostowfi, F.; McFarlane, R.; Mullins, O. C., On the formation and properties of asphaltene nanoaggregates and clusters by DC-

- conductivity and centrifugation. *Fuel* **2011**, *90* (7), 2480-2490.
27. Kim, S.-H.; Kim, K.-D.; Lee, H.; Lee, Y.-K., Beneficial roles of H-donors as diluent and H-shuttle for asphaltenes in catalytic upgrading of vacuum residue. *Chemical Engineering Journal* **2017**, *314*, 1-10.
28. Thompson, D.; Taylor, A.; Graham, D., Emulsification and demulsification related to crude oil production. *Colloids and Surfaces* **1985**, *15*, 175-189.
29. Bobicki, E. R.; Liu, Q.; Xu, Z., Ligand-promoted dissolution of serpentine in ultramafic nickel ores. *Minerals Engineering* **2014**, *64*, 109-119.
30. Chalaturnyk, R. J.; Don Scott, J.; Özüm, B., Management of oil sands tailings. *Petroleum Science and Technology* **2002**, *20* (9-10), 1025-1046.
31. Liu, J.; Cui, X.; Huang, J.; Xie, L.; Tan, X.; Liu, Q.; Zeng, H., Understanding the stabilization mechanism of bitumen-coated fine solids in organic media from non-aqueous extraction of oil sands. *Fuel* **2019**, *242*, 255-264.
32. Carew, J.; Al-Sayegh, A.; Al-Hashem, A. In *The effect of water-cut on the corrosion behaviour L80 carbon steel under downhole conditions*, CORROSION-NATIONAL ASSOCIATION OF CORROSION ENGINEERS ANNUAL CONFERENCE-, NACE: 2000.
33. Choi, H. J.; Warnken, D.; Al Beheiri, F. I.; Al-Bannai, N. S. In *Field Corrosion Assessment of L80 Carbon Steel Downhole Production Tubing at Khuff Gas Wells*, CORROSION 2006, NACE International: 2006.
34. Sun, W.; Pugh, D.; Ling, S.; Reddy, R.; Pacheco, J.; Nisbet, R.; Nor, N.; Kersey, M.; Morshidi, L. In *Understanding and quantifying corrosion of L80 carbon steel in*

- sour environments*, CORROSION 2011, NACE International: 2011.
35. Deyab, M. A. M., Corrosion Inhibition and Adsorption Behavior of Sodium Lauryl Ether Sulfate on L80 Carbon Steel in Acetic Acid Solution and Its Synergism with Ethanol. *Journal of Surfactants and Detergents* **2015**, *18* (3), 405-411.
 36. Ye, Y.; Liu, Z.; Liu, W.; Zhang, D.; Zhao, H.; Wang, L.; Li, X., Superhydrophobic oligoaniline-containing electroactive silica coating as pre-process coating for corrosion protection of carbon steel. *Chemical Engineering Journal* **2018**, *348*, 940-951.
 37. Lalande, M.; Tissier, J.-P.; Corrieu, G., Fouling of a plate heat exchanger used in ultra-high-temperature sterilization of milk. *Journal of Dairy Research* **1984**, *51* (04), 557-568.
 38. Changani, S.; Belmar-Beiny, M.; Fryer, P., Engineering and chemical factors associated with fouling and cleaning in milk processing. *Exp. Therm Fluid Sci.* **1997**, *14* (4), 392-406.
 39. Visser, J.; Jeurink, T. J., Fouling of heat exchangers in the dairy industry. *Exp. Therm Fluid Sci.* **1997**, *14* (4), 407-424.
 40. Bansal, B.; Chen, X. D., A critical review of milk fouling in heat exchangers. *Comprehensive reviews in food science and food safety* **2006**, *5* (2), 27-33.
 41. Genzer, J.; Marmur, A., Biological and synthetic self-cleaning surfaces. *MRS Bull.* **2008**, *33* (08), 742-746.
 42. Mérian, T.; Goddard, J. M., Advances in nonfouling materials: perspectives for the food industry. *J. Agric. Food. Chem.* **2012**, *60* (12), 2943-2957.
 43. Beuf, M.; Rizzo, G.; Leuliet, J.; Müller-Steinhagen, H.; Yiantsios, S.; Karabelas,

A.; Benezech, T., Fouling and cleaning of modified stainless steel plate heat exchangers processing milk products. **2003**.

44. Rosmaninho, R.; Melo, L. F., Calcium phosphate deposition from simulated milk ultrafiltrate on different stainless steel-based surfaces. *International Dairy Journal* **2006**, *16* (1), 81-87.

45. Premathilaka, S.; Hyland, M.; Chen, X.; Bansal, B., A study of the effects of surface chemistry on the initial deposition mechanisms of dairy fouling. *Food and bioproducts processing* **2006**, *84* (4), 265-273.

46. Rosmaninho, R.; Santos, O.; Nylander, T.; Paulsson, M.; Beuf, M.; Benezech, T.; Yiantsios, S.; Andritsos, N.; Karabelas, A.; Rizzo, G., Modified stainless steel surfaces targeted to reduce fouling—evaluation of fouling by milk components. *J. Food Eng.* **2007**, *80* (4), 1176-1187.

47. Balasubramanian, S.; Puri, V., Thermal energy savings in pilot-scale plate heat exchanger system during product processing using modified surfaces. *J. Food Eng.* **2009**, *91* (4), 608-611.

48. Lin, J.; Wang, C.; Wang, S.; Chen, Y.; He, W.; Xiao, D., Initiation electroless nickel plating by atomic hydrogen for PCB final finishing. *Chemical Engineering Journal* **2016**, *306*, 117-123.

49. Gu, C.; Lian, J.; Li, G.; Niu, L.; Jiang, Z., High corrosion-resistant Ni–P/Ni/Ni–P multilayer coatings on steel. *Surf. Coat. Technol.* **2005**, *197* (1), 61-67.

50. Cheng, Y.; Zou, Y.; Cheng, L.; Liu, W., Effect of the microstructure on the anti-fouling property of the electroless Ni–P coating. *Materials letters* **2008**, *62* (27), 4283-

4285.

51. Wu, Y.; Liu, T.; Luo, S., Corrosion characteristics of electroless Ni–P coating in sulfur-bearing solution. *Mater. Corros.* **2009**, *60* (12), 987-990.
52. Karthikeyan, S.; Ramamoorthy, B., Effect of reducing agent and nano Al₂O₃ particles on the properties of electroless Ni–P coating. *Appl. Surf. Sci.* **2014**, *307*, 654-660.
53. Bigdeli, F.; Allahkaram, S. R., An investigation on corrosion resistance of as-applied and heat treated Ni–P/nanoSiC coatings. *Materials & Design* **2009**, *30* (10), 4450-4453.
54. Xu, H.; Yang, Z.; Li, M.-K.; Shi, Y.-L.; Huang, Y.; Li, H.-L., Synthesis and properties of electroless Ni–P–Nanometer Diamond composite coatings. *Surface and coatings technology* **2005**, *191* (2-3), 161-165.
55. Ranganatha, S.; Venkatesha, T.; Vathsala, K., Process and properties of electroless Ni–Cu–P–ZrO₂ nanocomposite coatings. *Mater. Res. Bull.* **2012**, *47* (3), 635-645.
56. Sadreddini, S.; Afshar, A., Corrosion resistance enhancement of Ni-P-nano SiO₂ composite coatings on aluminum. *Appl. Surf. Sci.* **2014**, *303*, 125-130.
57. Zhang, L. Y.; Lawrence, S.; Xu, Z.; Masliyah, J. H., Studies of Athabasca asphaltene Langmuir films at air–water interface. *Journal of colloid and interface science* **2003**, *264* (1), 128-140.
58. Luo, H.; Leitch, M.; Behnamian, Y.; Ma, Y.; Zeng, H.; Luo, J.-L., Development of electroless Ni–P/nano-WC composite coatings and investigation on its properties. *Surface and Coatings Technology* **2015**, *277*, 99-106.

59. Kar, K. K.; Sathiyamoorthy, D., Influence of process parameters for coating of nickel–phosphorous on carbon fibers. *journal of materials processing technology* **2009**, *209* (6), 3022-3029.
60. Xie, L.; Wang, J.; Shi, C.; Huang, J.; Zhang, H.; Liu, Q.; Liu, Q.; Zeng, H., Probing surface interactions of electrochemically active galena mineral surface using atomic force microscopy. *The Journal of Physical Chemistry C* **2016**, *120* (39), 22433-22442.
61. Wang, J.; Li, J.; Xie, L.; Shi, C.; Liu, Q.; Zeng, H., Interactions between elemental selenium and hydrophilic/hydrophobic surfaces: Direct force measurements using AFM. *Chemical Engineering Journal* **2016**, *303*, 646-654.
62. Xie, L.; Wang, J.; Shi, C.; Cui, X.; Huang, J.; Zhang, H.; Liu, Q.; Liu, Q.; Zeng, H., Mapping the nanoscale heterogeneity of surface hydrophobicity on the sphalerite mineral. *The Journal of Physical Chemistry C* **2017**, *121* (10), 5620-5628.
63. Liu, J.; Wang, J.; Huang, J.; Cui, X.; Tan, X.; Liu, Q.; Zeng, H., Heterogeneous Distribution of Adsorbed Bitumen on Fine Solids from Solvent-Based Extraction of Oil Sands Probed by AFM. *Energy & Fuels* **2017**, *31* (9), 8833-8842.
64. Wang, J.; Xie, L.; Zhang, H.; Liu, Q.; Liu, Q.; Zeng, H., Probing interactions between sphalerite and hydrophobic/hydrophilic surfaces: Effect of water chemistry. *Powder Technology* **2017**, *320*, 511-518.
65. Yang, D.; Xie, L.; Bobicki, E.; Xu, Z.; Liu, Q.; Zeng, H., Probing anisotropic surface properties and interaction forces of chrysotile rods by atomic force microscopy and rheology. *Langmuir* **2014**, *30* (36), 10809-10817.
66. Gao, Z.; Xie, L.; Cui, X.; Hu, Y.; Sun, W.; Zeng, H., Probing Anisotropic Surface

- Properties and Surface Forces of Fluorite Crystals. *Langmuir* **2018**, *34* (7), 2511-2521.
67. Hutter, J. L.; Bechhoefer, J., Calibration of atomic-force microscope tips. *Review of Scientific Instruments* **1993**, *64* (7), 1868-1873.
68. Israelachvili, J. N., *Intermolecular and surface forces*. Academic press: 2011.
69. Cappella, B.; Dietler, G., Force-distance curves by atomic force microscopy. *Surface science reports* **1999**, *34* (1-3), 1-104.
70. Tulpar, A.; Walz, J., Simultaneous measurement of structural and hydrodynamic forces between colloidal surfaces in complex fluids. *Colloids Surf., A* **2007**, *300* (3), 268-280.
71. Prieve, D. C.; Russel, W. B., Simplified predictions of Hamaker constants from Lifshitz theory. *Journal of Colloid and Interface Science* **1988**, *125* (1), 1-13.
72. Bergstrom, L.; Meurk, A.; Arwin, H.; Rowcliffe, D. J., Estimation of Hamaker constants of ceramic materials from optical data using Lifshitz theory. *Journal of the American Ceramic Society* **1996**, *79* (2), 339-348.
73. Wang, M.; Revil, A., Electrochemical charge of silica surfaces at high ionic strength in narrow channels. *Journal of colloid and interface science* **2010**, *343* (1), 381-386.
74. Wang, S.; Liu, J.; Zhang, L.; Xu, Z.; Masliyah, J., Colloidal interactions between asphaltene surfaces in toluene. *Energy & Fuels* **2008**, *23* (2), 862-869.
75. Chen, G.; Warmack, R.; Huang, A.; Thundat, T., Harmonic response of near-contact scanning force microscopy. *Journal of Applied Physics* **1995**, *78* (3), 1465-1469.
76. Boulangé-Petermann, L.; Doren, A.; Baroux, B.; Bellon-Fontaine, M.-N., Zeta

potential measurements on passive metals. *Journal of colloid and interface science* **1995**, *171* (1), 179-186.

77. Gong, L.; Qiu, X.; Zhang, L.; Huang, J.; Hu, W.; Xiang, L.; Zhu, D.; Sabbagh, R.; Mahmoudi, M.; Fattahpour, V., Probing the Interaction Mechanism between Oil-in-Water Emulsions and Electroless Nickel–Phosphorus Coating with Implications for Antifouling in Oil Production. *Energy & Fuels* **2018**.

78. Liu, J.; Xu, Z.; Masliyah, J., Studies on bitumen– silica interaction in aqueous solutions by atomic force microscopy. *Langmuir* **2003**, *19* (9), 3911-3920.

79. Wu, J.; Prausnitz, J. M.; Firoozabadi, A., Molecular thermodynamics of asphaltene precipitation in reservoir fluids. *AIChE journal* **2000**, *46* (1), 197-209.

80. Das, S.; Thundat, T.; Mitra, S. K., Analytical model for zeta potential of asphaltene. *Fuel* **2013**, *108*, 543-549.

81. Wang, J.; Lu, Q.; Harbottle, D.; Sjöblom, J.; Xu, Z.; Zeng, H., Molecular interactions of a polyaromatic surfactant C5Pe in aqueous solutions studied by a surface forces apparatus. *The Journal of Physical Chemistry B* **2012**, *116* (36), 11187-11196.

82. Chaisoontornyotin, W.; Haji-Akbari, N.; Fogler, H. S.; Hoepfner, M. P., Combined asphaltene aggregation and deposition investigation. *Energy & Fuels* **2016**, *30* (3), 1979-1986.

83. Shi, C.; Zhang, L.; Xie, L.; Lu, X.; Liu, Q.; Mantilla, C. A.; van den Berg, F. G.; Zeng, H., Interaction mechanism of oil-in-water emulsions with asphaltenes determined using droplet probe AFM. *Langmuir* **2016**, *32* (10), 2302-2310.

84. Mo, H.; Tay, K. G.; Ng, H. Y., Fouling of reverse osmosis membrane by protein

(BSA): effects of pH, calcium, magnesium, ionic strength and temperature. *Journal of Membrane Science* **2008**, *315* (1-2), 28-35.

85. Elimelech, M.; Zhu, X.; Childress, A. E.; Hong, S., Role of membrane surface morphology in colloidal fouling of cellulose acetate and composite aromatic polyamide reverse osmosis membranes. *Journal of membrane science* **1997**, *127* (1), 101-109.

86. Hamza, A.; Pham, V.; Matsuura, T.; Santerre, J., Development of membranes with low surface energy to reduce the fouling in ultrafiltration applications. *Journal of Membrane Science* **1997**, *131* (1-2), 217-227.

1. Watkinson, A. P., Deposition from crude oils in heat exchangers. *Heat transfer engineering* **2007**, *28* (3), 177-184.

2. Hu, B.; Scott, K., Microfiltration of water in oil emulsions and evaluation of fouling mechanism. *Chemical Engineering Journal* **2008**, *136* (2-3), 210-220.

3. Amin, I. N. H. M.; Mohammad, A. W., Adsorptive fouling of organic solutes simulating sweetwater solutions on ultrafiltration membranes. *Chemical Engineering Journal* **2015**, *264*, 470-478.

4. Acosta, E., Achieving sustainable, optimal SAGD operations. *Journal of Petroleum Technology* **2010**, *62* (11), 24-28.

5. Munoz, V.; Elliott, G.; Afara, M.; Mikula, R., Microscopy of Heat Exchanger Fouling During SAGD Operations. *Microsc. Microanal.* **2011**, *17* (S2), 1906.

6. Pugsley, T.; Pernitsky, D.; Grundler, J.; Johnsen, E. In *Fouling of heat transfer surfaces in a steam assisted gravity drainage (SAGD) in situ facility for the recovery of oil sands bitumen*, International Conference on Heat Exchanger Fouling and Clearing, 2013.
7. Zhu, D.; Leitch, M.; Wang, J.; Shi, X.; Gong, L.; Aghaie, E.; Luo, J.-l.; Zeng, H. In *Evaluation of an Advanced Metal Bonded Coating Technology for Improved SAGD Performance*, SPE Latin America and Caribbean Heavy and Extra Heavy Oil Conference, Society of Petroleum Engineers: 2016.
8. MacAdam, J.; Parsons, S. A., Calcium carbonate scale formation and control. *Re/Views in Environmental Science & Bio/Technology* **2004**, 3 (2), 159-169.
9. Das, S. K.; Butler, R. M., Mechanism of the vapor extraction process for heavy oil and bitumen. *Journal of Petroleum Science and Engineering* **1998**, 21 (1), 43-59.
10. Srinivasan, M. Heat exchanger fouling of some Canadian crude oils. University of British Columbia, 2008.
11. Lalchan, C. A.; Wiggins, C. B.; Moriyama, C. In *Formulation of an Emulsified Thermal Acid Blend for SAGD Applications in Eastern Alberta*, Canadian Unconventional Resources Conference, Society of Petroleum Engineers: 2011.
12. Adams, J. J., Asphaltene adsorption, a literature review. *Energy & Fuels* **2014**, 28 (5), 2831-2856.
13. Yarranton, H. W.; Masliyah, J. H., Molar mass distribution and solubility modeling of asphaltenes. *AIChE Journal* **1996**, 42 (12), 3533-3543.
14. Hoepfner, M. P.; Limsakoune, V.; Chuenmeechao, V.; Maqbool, T.; Fogler, H. S.,

- A fundamental study of asphaltene deposition. *Energy & fuels* **2013**, 27 (2), 725-735.
15. Goual, L.; Firoozabadi, A., Measuring asphaltenes and resins, and dipole moment in petroleum fluids. *AIChE Journal* **2002**, 48 (11), 2646-2663.
 16. Wang, J.; Buckley, J. S.; Creek, J. L., Asphaltene deposition on metallic surfaces. *J. Dispersion Sci. Technol.* **2004**, 25 (3), 287-298.
 17. Deshannavar, U.; Rafeen, M.; Ramasamy, M.; Subbarao, D., Crude oil fouling: A review. *Journal of Applied Sciences(Faisalabad)* **2010**, 10 (24), 3167-3174.
 18. Zhang, L.; Xie, L.; Shi, C.; Huang, J.; Liu, Q.; Zeng, H., Mechanistic Understanding of Asphaltene Surface Interactions in Aqueous Media. *Energy & Fuels* **2016**, 31 (4), 3348-3357.
 19. Rocha, J.; Baydak, E.; Yarranton, H.; Sztukowski, D.; Ali-Marcano, V.; Gong, L.; Shi, C.; Zeng, H., Role of aqueous phase chemistry, interfacial film properties, and surface coverage in stabilizing water-in-bitumen emulsions. *Energy & Fuels* **2016**, 30 (7), 5240-5252.
 20. Mao, X.; Gong, L.; Xie, L.; Qian, H.; Wang, X.; Zeng, H., Novel Fe₃O₄ based superhydrophilic core-shell microspheres for breaking asphaltenes-stabilized water-in-oil emulsion. *Chemical Engineering Journal* **2019**, 358, 869-877.
 21. Mullins, O. C., The asphaltenes. *Annual review of analytical chemistry* **2011**, 4, 393-418.
 22. Mullins, O. C.; Sheu, E. Y., *Structures and dynamics of asphaltenes*. Springer Science & Business Media: 2013.
 23. Harji, A.; Koppel, P.; Mazurek, W.; Meysami, P. In *Processing Options for Bitumen*

Upgrading, Canadian International Petroleum Conference, Petroleum Society of Canada: 2003.

24. Jian, C.; Tang, T.; Bhattacharjee, S., Probing the effect of side-chain length on the aggregation of a model asphaltene using molecular dynamics simulations. *Energy & Fuels* **2013**, *27* (4), 2057-2067.

25. Jian, C.; Zeng, H.; Liu, Q.; Tang, T., Probing the Adsorption of Polycyclic Aromatic Compounds onto Water Droplets Using Molecular Dynamics Simulations. *The Journal of Physical Chemistry C* **2016**, *120* (26), 14170-14179.

26. Goual, L.; Sedghi, M.; Zeng, H.; Mostowfi, F.; McFarlane, R.; Mullins, O. C., On the formation and properties of asphaltene nanoaggregates and clusters by DC-conductivity and centrifugation. *Fuel* **2011**, *90* (7), 2480-2490.

27. Kim, S.-H.; Kim, K.-D.; Lee, H.; Lee, Y.-K., Beneficial roles of H-donors as diluent and H-shuttle for asphaltenes in catalytic upgrading of vacuum residue. *Chemical Engineering Journal* **2017**, *314*, 1-10.

28. Thompson, D.; Taylor, A.; Graham, D., Emulsification and demulsification related to crude oil production. *Colloids and Surfaces* **1985**, *15*, 175-189.

29. Bobicki, E. R.; Liu, Q.; Xu, Z., Ligand-promoted dissolution of serpentine in ultramafic nickel ores. *Minerals Engineering* **2014**, *64*, 109-119.

30. Chalaturnyk, R. J.; Don Scott, J.; Özü, B., Management of oil sands tailings. *Petroleum Science and Technology* **2002**, *20* (9-10), 1025-1046.

31. Liu, J.; Cui, X.; Huang, J.; Xie, L.; Tan, X.; Liu, Q.; Zeng, H., Understanding the stabilization mechanism of bitumen-coated fine solids in organic media from non-

- aqueous extraction of oil sands. *Fuel* **2019**, *242*, 255-264.
32. Carew, J.; Al-Sayegh, A.; Al-Hashem, A. In *The effect of water-cut on the corrosion behaviour L80 carbon steel under downhole conditions*, CORROSION-NATIONAL ASSOCIATION OF CORROSION ENGINEERS ANNUAL CONFERENCE-, NACE: 2000.
33. Choi, H. J.; Warnken, D.; Al Beheiri, F. I.; Al-Bannai, N. S. In *Field Corrosion Assessment of L80 Carbon Steel Downhole Production Tubing at Khuff Gas Wells*, CORROSION 2006, NACE International: 2006.
34. Sun, W.; Pugh, D.; Ling, S.; Reddy, R.; Pacheco, J.; Nisbet, R.; Nor, N.; Kersey, M.; Morshidi, L. In *Understanding and quantifying corrosion of L80 carbon steel in sour environments*, CORROSION 2011, NACE International: 2011.
35. Deyab, M. A. M., Corrosion Inhibition and Adsorption Behavior of Sodium Lauryl Ether Sulfate on L80 Carbon Steel in Acetic Acid Solution and Its Synergism with Ethanol. *Journal of Surfactants and Detergents* **2015**, *18* (3), 405-411.
36. Ye, Y.; Liu, Z.; Liu, W.; Zhang, D.; Zhao, H.; Wang, L.; Li, X., Superhydrophobic oligoaniline-containing electroactive silica coating as pre-process coating for corrosion protection of carbon steel. *Chemical Engineering Journal* **2018**, *348*, 940-951.
37. Lalande, M.; Tissier, J.-P.; Corrieu, G., Fouling of a plate heat exchanger used in ultra-high-temperature sterilization of milk. *Journal of Dairy Research* **1984**, *51* (04), 557-568.
38. Changani, S.; Belmar-Beiny, M.; Fryer, P., Engineering and chemical factors associated with fouling and cleaning in milk processing. *Exp. Therm Fluid Sci.* **1997**,

14 (4), 392-406.

39. Visser, J.; Jeurink, T. J., Fouling of heat exchangers in the dairy industry. *Exp. Therm Fluid Sci.* **1997**, *14* (4), 407-424.

40. Bansal, B.; Chen, X. D., A critical review of milk fouling in heat exchangers. *Comprehensive reviews in food science and food safety* **2006**, *5* (2), 27-33.

41. Genzer, J.; Marmur, A., Biological and synthetic self-cleaning surfaces. *MRS Bull.* **2008**, *33* (08), 742-746.

42. Mérian, T.; Goddard, J. M., Advances in nonfouling materials: perspectives for the food industry. *J. Agric. Food. Chem.* **2012**, *60* (12), 2943-2957.

43. Beuf, M.; Rizzo, G.; Leuliet, J.; Müller-Steinhagen, H.; Yiantsios, S.; Karabelas, A.; Benezech, T., Fouling and cleaning of modified stainless steel plate heat exchangers processing milk products. **2003**.

44. Rosmaninho, R.; Melo, L. F., Calcium phosphate deposition from simulated milk ultrafiltrate on different stainless steel-based surfaces. *International Dairy Journal* **2006**, *16* (1), 81-87.

45. Premathilaka, S.; Hyland, M.; Chen, X.; Bansal, B., A study of the effects of surface chemistry on the initial deposition mechanisms of dairy fouling. *Food and bioproducts processing* **2006**, *84* (4), 265-273.

46. Rosmaninho, R.; Santos, O.; Nylander, T.; Paulsson, M.; Beuf, M.; Benezech, T.; Yiantsios, S.; Andritsos, N.; Karabelas, A.; Rizzo, G., Modified stainless steel surfaces targeted to reduce fouling—evaluation of fouling by milk components. *J. Food Eng.* **2007**, *80* (4), 1176-1187.

47. Balasubramanian, S.; Puri, V., Thermal energy savings in pilot-scale plate heat exchanger system during product processing using modified surfaces. *J. Food Eng.* **2009**, *91* (4), 608-611.
48. Lin, J.; Wang, C.; Wang, S.; Chen, Y.; He, W.; Xiao, D., Initiation electroless nickel plating by atomic hydrogen for PCB final finishing. *Chemical Engineering Journal* **2016**, *306*, 117-123.
49. Gu, C.; Lian, J.; Li, G.; Niu, L.; Jiang, Z., High corrosion-resistant Ni-P/Ni/Ni-P multilayer coatings on steel. *Surf. Coat. Technol.* **2005**, *197* (1), 61-67.
50. Cheng, Y.; Zou, Y.; Cheng, L.; Liu, W., Effect of the microstructure on the anti-fouling property of the electroless Ni-P coating. *Materials letters* **2008**, *62* (27), 4283-4285.
51. Wu, Y.; Liu, T.; Luo, S., Corrosion characteristics of electroless Ni - P coating in sulfur - bearing solution. *Mater. Corros.* **2009**, *60* (12), 987-990.
52. Karthikeyan, S.; Ramamoorthy, B., Effect of reducing agent and nano Al₂O₃ particles on the properties of electroless Ni-P coating. *Appl. Surf. Sci.* **2014**, *307*, 654-660.
53. Bigdeli, F.; Allahkaram, S. R., An investigation on corrosion resistance of as-applied and heat treated Ni-P/nanoSiC coatings. *Materials & Design* **2009**, *30* (10), 4450-4453.
54. Xu, H.; Yang, Z.; Li, M.-K.; Shi, Y.-L.; Huang, Y.; Li, H.-L., Synthesis and properties of electroless Ni-P-Nanometer Diamond composite coatings. *Surface and coatings technology* **2005**, *191* (2-3), 161-165.

55. Ranganatha, S.; Venkatesha, T.; Vathsala, K., Process and properties of electroless Ni–Cu–P–ZrO₂ nanocomposite coatings. *Mater. Res. Bull.* **2012**, *47* (3), 635-645.
56. Sadreddini, S.; Afshar, A., Corrosion resistance enhancement of Ni-P-nano SiO₂ composite coatings on aluminum. *Appl. Surf. Sci.* **2014**, *303*, 125-130.
57. Zhang, L. Y.; Lawrence, S.; Xu, Z.; Masliyeh, J. H., Studies of Athabasca asphaltene Langmuir films at air–water interface. *Journal of colloid and interface science* **2003**, *264* (1), 128-140.
58. Luo, H.; Leitch, M.; Behnamian, Y.; Ma, Y.; Zeng, H.; Luo, J.-L., Development of electroless Ni–P/nano-WC composite coatings and investigation on its properties. *Surface and Coatings Technology* **2015**, *277*, 99-106.
59. Kar, K. K.; Sathiyamoorthy, D., Influence of process parameters for coating of nickel–phosphorous on carbon fibers. *journal of materials processing technology* **2009**, *209* (6), 3022-3029.
60. Xie, L.; Wang, J.; Shi, C.; Huang, J.; Zhang, H.; Liu, Q.; Liu, Q.; Zeng, H., Probing surface interactions of electrochemically active galena mineral surface using atomic force microscopy. *The Journal of Physical Chemistry C* **2016**, *120* (39), 22433-22442.
61. Wang, J.; Li, J.; Xie, L.; Shi, C.; Liu, Q.; Zeng, H., Interactions between elemental selenium and hydrophilic/hydrophobic surfaces: Direct force measurements using AFM. *Chemical Engineering Journal* **2016**, *303*, 646-654.
62. Xie, L.; Wang, J.; Shi, C.; Cui, X.; Huang, J.; Zhang, H.; Liu, Q.; Liu, Q.; Zeng, H., Mapping the nanoscale heterogeneity of surface hydrophobicity on the sphalerite mineral. *The Journal of Physical Chemistry C* **2017**, *121* (10), 5620-5628.

63. Liu, J.; Wang, J.; Huang, J.; Cui, X.; Tan, X.; Liu, Q.; Zeng, H., Heterogeneous Distribution of Adsorbed Bitumen on Fine Solids from Solvent-Based Extraction of Oil Sands Probed by AFM. *Energy & Fuels* **2017**, *31* (9), 8833-8842.
64. Wang, J.; Xie, L.; Zhang, H.; Liu, Q.; Liu, Q.; Zeng, H., Probing interactions between sphalerite and hydrophobic/hydrophilic surfaces: Effect of water chemistry. *Powder Technology* **2017**, *320*, 511-518.
65. Yang, D.; Xie, L.; Bobicki, E.; Xu, Z.; Liu, Q.; Zeng, H., Probing anisotropic surface properties and interaction forces of chrysotile rods by atomic force microscopy and rheology. *Langmuir* **2014**, *30* (36), 10809-10817.
66. Gao, Z.; Xie, L.; Cui, X.; Hu, Y.; Sun, W.; Zeng, H., Probing Anisotropic Surface Properties and Surface Forces of Fluorite Crystals. *Langmuir* **2018**, *34* (7), 2511-2521.
67. Hutter, J. L.; Bechhoefer, J., Calibration of atomic - force microscope tips. *Review of Scientific Instruments* **1993**, *64* (7), 1868-1873.
68. Israelachvili, J. N., *Intermolecular and surface forces*. Academic press: 2011.
69. Cappella, B.; Dietler, G., Force-distance curves by atomic force microscopy. *Surface science reports* **1999**, *34* (1-3), 1-104.
70. Tulpar, A.; Walz, J., Simultaneous measurement of structural and hydrodynamic forces between colloidal surfaces in complex fluids. *Colloids Surf., A* **2007**, *300* (3), 268-280.
71. Prieve, D. C.; Russel, W. B., Simplified predictions of Hamaker constants from Lifshitz theory. *Journal of Colloid and Interface Science* **1988**, *125* (1), 1-13.
72. Bergstrom, L.; Meurk, A.; Arwin, H.; Rowcliffe, D. J., Estimation of Hamaker

- constants of ceramic materials from optical data using Lifshitz theory. *Journal of the American Ceramic Society* **1996**, *79* (2), 339-348.
73. Wang, M.; Revil, A., Electrochemical charge of silica surfaces at high ionic strength in narrow channels. *Journal of colloid and interface science* **2010**, *343* (1), 381-386.
74. Wang, S.; Liu, J.; Zhang, L.; Xu, Z.; Masliyah, J., Colloidal interactions between asphaltene surfaces in toluene. *Energy & Fuels* **2008**, *23* (2), 862-869.
75. Chen, G.; Warmack, R.; Huang, A.; Thundat, T., Harmonic response of near - contact scanning force microscopy. *Journal of Applied Physics* **1995**, *78* (3), 1465-1469.
76. Boulangé-Petermann, L.; Doren, A.; Baroux, B.; Bellon-Fontaine, M.-N., Zeta potential measurements on passive metals. *Journal of colloid and interface science* **1995**, *171* (1), 179-186.
77. Gong, L.; Qiu, X.; Zhang, L.; Huang, J.; Hu, W.; Xiang, L.; Zhu, D.; Sabbagh, R.; Mahmoudi, M.; Fattahpour, V., Probing the Interaction Mechanism between Oil-in-Water Emulsions and Electroless Nickel–Phosphorus Coating with Implications for Antifouling in Oil Production. *Energy & Fuels* **2018**.
78. Liu, J.; Xu, Z.; Masliyah, J., Studies on bitumen– silica interaction in aqueous solutions by atomic force microscopy. *Langmuir* **2003**, *19* (9), 3911-3920.
79. Wu, J.; Prausnitz, J. M.; Firoozabadi, A., Molecular thermodynamics of asphaltene precipitation in reservoir fluids. *AIChE journal* **2000**, *46* (1), 197-209.
80. Das, S.; Thundat, T.; Mitra, S. K., Analytical model for zeta potential of asphaltene. *Fuel* **2013**, *108*, 543-549.

81. Wang, J.; Lu, Q.; Harbottle, D.; Sjöblom, J.; Xu, Z.; Zeng, H., Molecular interactions of a polyaromatic surfactant C5Pe in aqueous solutions studied by a surface forces apparatus. *The Journal of Physical Chemistry B* **2012**, *116* (36), 11187-11196.
82. Chaisoontornyotin, W.; Haji-Akbari, N.; Fogler, H. S.; Hoepfner, M. P., Combined asphaltene aggregation and deposition investigation. *Energy & Fuels* **2016**, *30* (3), 1979-1986.
83. Shi, C.; Zhang, L.; Xie, L.; Lu, X.; Liu, Q.; Mantilla, C. A.; van den Berg, F. G.; Zeng, H., Interaction mechanism of oil-in-water emulsions with asphaltenes determined using droplet probe AFM. *Langmuir* **2016**, *32* (10), 2302-2310.
84. Mo, H.; Tay, K. G.; Ng, H. Y., Fouling of reverse osmosis membrane by protein (BSA): effects of pH, calcium, magnesium, ionic strength and temperature. *Journal of Membrane Science* **2008**, *315* (1-2), 28-35.
85. Elimelech, M.; Zhu, X.; Childress, A. E.; Hong, S., Role of membrane surface morphology in colloidal fouling of cellulose acetate and composite aromatic polyamide reverse osmosis membranes. *Journal of membrane science* **1997**, *127* (1), 101-109.
86. Hamza, A.; Pham, V.; Matsuura, T.; Santerre, J., Development of membranes with low surface energy to reduce the fouling in ultrafiltration applications. *Journal of Membrane Science* **1997**, *131* (1-2), 217-227.

Chapter 4 Probing the Interaction Mechanism Between Oil-in-Water Emulsions and Electroless Nickel-phosphorus (EN) Coating with Implications for Antifouling in Oil Production

4.1 Introduction

Fouling problems are highly undesirable in oil production, which can significantly impact the related production processes in negative ways: lowering the production efficiency and drastically increasing the cost of production and maintenance.¹⁻⁵ Fouling phenomena can occur at the various stages of oil production from extraction, transportation to storage processes,⁶⁻⁷ and the foulants are generally composed of both inorganic and organic materials such as sands, clays, asphaltenes, bitumen and products due to the corrosive reactions between the foulants and substrate materials.⁸⁻⁹ Fouling is believed to be initiated and driven by the attractive interactions between the substrate materials and the inorganic and organic components in the surrounding fluid media.¹⁰⁻¹² Surface mining and *in situ* extraction techniques such as steam assisted gravity drainage (SAGD) have been widely used by the Canadian oil sands industry for bitumen extraction.¹³⁻¹⁴ Warm water and high pressure steam are used in surface mining and SAGD operations, respectively, to extract the bitumen from the oil sands deposits. Water-in-oil (W/O), oil-in-water (O/W) and even more complex emulsions are commonly formed in these water/steam-assisted operations.¹⁵⁻¹⁶ The interactions between these emulsion drops and various substrate surfaces (e.g. pipeline surfaces)

can contribute to the fouling phenomena.

Understanding the fouling mechanisms and developing antifouling coating or strategies are of both fundamental and practical importance. Recently, fabricating protection and inert coatings on pipeline and reactor surfaces has attracted consideration attention in gas and oil industries, to achieve the anticorrosion, antifouling or anti-abrasion performances.¹⁷⁻¹⁹ For example, depositing electroless nickel-phosphorus alloy coating on steel surfaces has been widely used in various industries, due to its outstanding properties of high hardness and resistance to corrosion and abrasion.²⁰⁻²²

The deposition of electroless nickel-phosphorus coating was first developed by Wurtz in 1844.²³ In 1946, Brenner and Riddell accidentally re-discovered this technique and improved the bath coating process so that this deposition could be utilized in practical processes.²⁴⁻²⁵ Since then, EN coating has attracted much attention, which has been applied in different engineering areas.²⁶⁻³² Despite the much work reported on the preparation and characterization of EN coatings and related composite coatings, there is no work available on the fouling behaviors of emulsion drops on EN coatings as well as the fundamental interaction mechanisms involved. Understanding the fouling/antifouling performance and the interaction mechanism of EN coating in emulsion suspensions is of significant importance, which will facilitate the development of antifouling coatings for practical applications in oil production.

In this work, for the *first* time, the antifouling properties and interaction mechanisms of electron-beam deposited iron substrates with and without EN coatings have been

investigated in oil-in-water emulsion suspensions, with varying water chemistries such as salinity, pH and the presence of divalent ions, and with different asphaltenes concentrations. The interaction forces between oil drops (toluene used here as a model oil) and Fe or Fe/EN substrates have been directly measured using a drop probe atomic force microscope (AFM) technique in aqueous solutions. The classical Derjaguin-Landau-Verwey-Overbeek (DLVO) theory has been incorporated into a theoretical model based on the Reynolds lubrication equation and augmented Young-Laplace equation to analyze the measured surface force profiles, including van der Waals force and electric double layer interaction.³³⁻³⁷ Bulk fouling tests have also been conducted to evaluate the performance of EN coating in toluene-in-water emulsions in the presence of asphaltenes. Our results demonstrate that the EN coatings show excellent antifouling performance to the emulsions, with useful insights into the fundamental interaction forces and fouling/antifouling mechanisms involved.

4.2 Experimental Section

4.2.1 Materials.

Asphaltenes were extracted from Athabasca bitumen by following a procedure reported elsewhere.³⁸ Toluene (HPLC grade, Fisher Scientific, Canada) and ethanol (HPLC grade, Fisher Scientific, Canada) was used as received. Sodium chloride, calcium chloride, nickel sulphate, sodium hypophosphite, ammonium chloride, sodium acetate, citric acid, and ammonium hydroxide were purchased from Sigma-Aldrich and used as received. Milli-Q water with a resistivity of 18.2 M Ω •cm (BARNSTEAD

Smart2Pure, Thermo Scientific) was used to prepare aqueous solutions. Sodium hydroxide (ACS reagent, Sigma-Aldrich, Canada) and hydrochloric acid (certified ACS Plus, Fisher Scientific, Canada) were used to adjust the pH of aqueous solutions.

4.2.2 Preparation of iron and EN substrates.

The iron and EN substrates were prepared on silicon wafers. Firstly, layers of chromium (thickness 10 nm) and iron (thickness 90 nm) were deposited on a silicon wafer surface using electron beam evaporation (EBE) technique. The chromium layer was applied to strengthen the adhesion and stability of the iron layer on the wafer. Electroless nickel-phosphorus coating was deposited by following a reported bath process.³⁹⁻⁴⁰ The compositions of the reaction solution and deposition conditions are listed in Table 4.1.

Table 4.1 Bath compositions and environmental conditions for deposition of EN coating.

Composition	Concentration
NiSO₄·6H₂O	25 g/L
NaH₂PO₂·H₂O	16 g/L
NH₄Cl	40 g/L
CH₃COONa	10 g/L
Citric acid	15 g/L
Plating conditions:	
Temperature: 80~85 °C	
pH: 8~9	

Agitation: 200 rpm
Time: 30 min

4.2.3 Surface energies of Fe/EN substrates using Lifshitz-van der Waals Acid/Base approach.

The surface energies of deposited Fe and EN substrates were investigated using Lifshitz-van der Waals Acid/Base approach, which describes the surface energy with the polar and apolar components.⁴¹ The apolar component also contains the electron-donor and electron-acceptor parts. The total surface energy is given in Equation 1.

$$\gamma = \gamma^d + \gamma^p = \gamma^d + 2\sqrt{\gamma^+ \cdot \gamma^-} \quad (1)$$

where, γ is the total surface energy, γ^d and γ^p are apolar and polar components, γ^+ is the electron-acceptor part, and γ^- is the electron-donor part. The surface energy of a substrate can be obtained using the Equation 2.

$$\begin{bmatrix} 2\sqrt{\gamma_{L1}^d} & 2\sqrt{\gamma_{L1}^+} & 2\sqrt{\gamma_{L1}^-} \\ 2\sqrt{\gamma_{L2}^d} & 2\sqrt{\gamma_{L2}^+} & 2\sqrt{\gamma_{L2}^-} \\ 2\sqrt{\gamma_{L3}^d} & 2\sqrt{\gamma_{L3}^+} & 2\sqrt{\gamma_{L3}^-} \end{bmatrix} \cdot \begin{bmatrix} \sqrt{\gamma_s^d} \\ \sqrt{\gamma_s^-} \\ \sqrt{\gamma_s^+} \end{bmatrix} = \begin{bmatrix} \gamma_{L1}(1 + \cos\theta_{L1}) \\ \gamma_{L2}(1 + \cos\theta_{L2}) \\ \gamma_{L3}(1 + \cos\theta_{L3}) \end{bmatrix} \quad (2)$$

where, γ_s^d , γ_s^+ and γ_s^- are the surface energy components of the substrate, γ_L^d , γ_L^+ and γ_L^- are the surface energy components of the probe liquid, θ_L is the contact angle of probe liquid on the substrate in air. Thus, the surface energies of Fe and EN could be calculated from contact angles of the probe liquids. Here, three probe liquids with different polarities were chosen, including water (polar liquid), diiodomethane (DIM, nonpolar liquid), and dimethyl sulfoxide (DMSO, partially polar liquid). The surface energy components of water, DIM and DMSO are in Table 4.2.⁴²

Table 4.2 Surface energy components of water, DIM and DMSO.

	γ (mN/m)	γ^d (mN/m)	γ^p (mN/m)	γ^+ (mN/m)	γ^- (mN/m)
water	72.90	21.90	51.00	25.50	25.50
DIM	50.80	50.80	0	0	0
DMSO	44.00	36.00	8.00	0.50	32.00

4.2.4 Force measurements using drop probe AFM technique.

The interaction forces between an oil drop and Fe/EN substrates in aqueous solutions were measured using a MPF-3D AFM (Asylum Research, Santa Barbara, CA) with a custom-made rectangular silicon AFM cantilever as reported previously.³³ The cantilever had a circular gold patch on its one end, which was firstly hydrophobized in 50 mM 1-dodecanethiol in ethanol solution, and then calibrated using thermal tuning method to obtain its spring constant. During experiments, oil droplets were generated in a fluid cell filled with aqueous solutions and hydrophobized cantilever was moved to carefully pick up an oil droplet with a proper size, generating an oil drop probe. This cantilever-anchored oil droplet was then moved and placed above the substrate in aqueous solution.

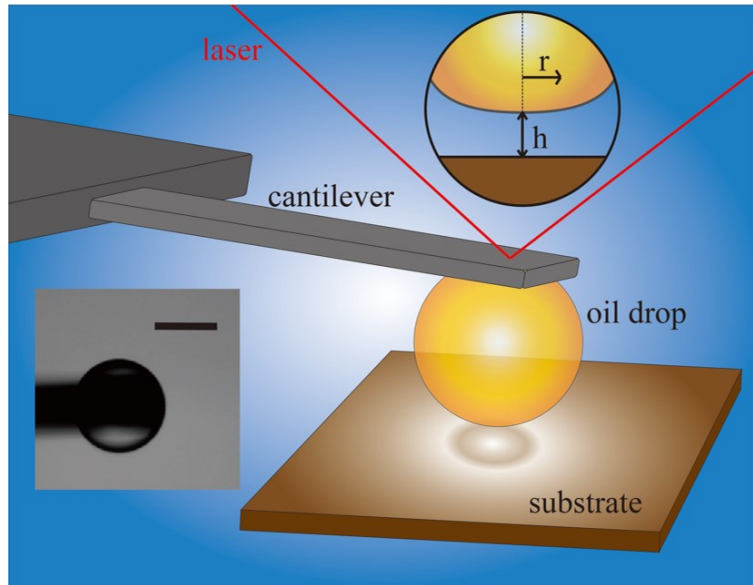


Figure 4.1 Schematic of experimental setup for surface force measurements between an oil drop and a substrate using the drop probe AFM technique. The inset (up) shows the central interaction region between an oil drop and a flat substrate, and the inset (left) shows a microscopic image of a typical drop probe prepared (Scale bar 100 μm).

In force measurements, the cantilever-anchored oil droplet was driven by a piezo to move towards the substrate at a velocity of 1 $\mu\text{m/s}$ till a certain deflection of the cantilever was achieved. Then, the cantilever was lifted up, as shown in Figure 4.1. The deflection of drop probe was detected by the reflected laser and recorded by the AFM software. Meanwhile, the piezo displacement was recorded with time to generate the force profiles.

4.2.5 Theoretical analysis of force profiles.

The measured force profiles were analyzed using a theoretical model based on the

Reynolds lubrication equation and augmented Young-Laplace equation.³³⁻³⁵ Emulsion drops could deform to respond to external pressures, such as hydrodynamic pressure and disjoining pressure. To describe the surface deformation of emulsion drops during force measurements, the augmented Young-Laplace equation was used.⁴³

$$\frac{\sigma}{r} \frac{\partial}{\partial r} \left(r \frac{\partial h}{\partial r} \right) = \frac{2\sigma}{R} - \Pi - p \quad (3)$$

Here, σ is the interfacial tension of the oil/water interface, r is the radial coordinate, h is the thickness of the water film confined between the drop and the substrate as shown in Figure 4.1, R is the radius of the drop, Π is the disjoining pressure and p is the excess hydrodynamic pressure. The overall disjoining pressure can generally arise from van der Waals (VDW) interaction, electric double layer (EDL) interaction and other surface interactions. Here, the VDW interaction Π_{VDW} is given by Equation 4.⁴⁴

$$\Pi_{VDW} = -\frac{A_H}{6\pi h^3} \quad (4)$$

where A_H is the Hamaker constant between oil drop and Fe/EN substrate in aqueous solutions, and h is the liquid film thickness between the oil drop and the substrate as shown in Figure 4.1. The EDL interaction Π_{EDL} between two asymmetric surfaces is given by Equation 5.⁴⁵⁻⁴⁶

$$\Pi_{EDL} = \frac{2\varepsilon\varepsilon_0\kappa^2[(e^{\kappa D} + e^{-\kappa D})\psi_1\psi_2 - (\psi_1^2 + \psi_2^2)]}{(e^{\kappa D} - e^{-\kappa D})^2} \quad (5)$$

where κ is the inverse of Debye length, Ψ is the surface potential of oil drop or substrates, ε_0 is the vacuum permittivity and ε is the dielectric constant of the liquid medium. The inverse of Debye length κ was calculated as:

$$\kappa = \sqrt{\frac{\sum \rho_0 e^2 z^2}{\epsilon \epsilon_0 k_B T}} \quad (6)$$

where ρ_0 is the number density of ions in aqueous solutions, e is the elementary charge, z is the valence of the ions, and k_B is the Boltzmann constant. During the approaching and withdrawing processes of the oil drop, the drainage of confined water film between the drop and flat substrate can be described by the Reynolds lubrication equation:⁴³

$$\frac{\partial h}{\partial t} = \frac{1}{12\mu r} \frac{\partial}{\partial r} (r h^3 \frac{\partial p}{\partial r}) \quad (7)$$

where t is time and μ is the viscosity of the aqueous solutions. The overall interaction $F(t)$ can be calculated from the integration of the hydrodynamic pressure and the disjoining pressure based on Derjaguin approximation.

$$F(t) = 2\pi \int_0^\infty [p(r, t) + \Pi(r, t)] r dr \quad (8)$$

4.2.6 Bulk fouling tests in oil-in-water emulsions with asphaltenes.

The oil-in-water emulsions with asphaltenes were prepared using a homogenizer to mix toluene, containing 100 ppm asphaltenes, and 100 mM NaCl aqueous solutions with a volume ratio of 3:2. The Fe and EN substrates were separately placed in 20 mL vials, which were then filled with the prepared oil-in-water emulsions. These vials were kept at room temperature (22 °C) for 24 hours. Then, the substrates were taken out, washed using DI water and ethanol, and dried using pure nitrogen. Images of the Fe/EN substrates were taken to show the fouling and antifouling performance on the substrates.

4.3 Results and Discussion

4.3.1 Surface properties of Fe/EN substrates.

The iron substrates were prepared using electron beam evaporation technique on silicon wafer, and electroless nickel-phosphorus coating was then conducted on this iron surface. This electron beam evaporation technique has been used to prepare iron substrate in reported works.⁴⁷⁻⁵⁰ The successful deposition of iron and EN coatings was characterized using AFM imaging, Scanning Electron Microscopy (SEM) and Energy Dispersive X-Ray Spectroscopy (EDX), as shown in Figure 4.2.

Figure 4.2A shows that the bare silicon wafer surface was very smooth with a root-mean-square (RMS) roughness less than 0.3 nm). The substrate became rougher after the deposition of thin iron layer, and turned even rougher after depositing the EN coating. Figure 4.2B and C show the RMS roughness of the deposited Fe and EN surfaces is 1.33 nm and 4.64 nm, respectively. This distinct change in surface morphology indicates the successful deposition of iron layer and EN coating on the substrate surfaces. The thickness of EN coating was measured through the SEM section image to be about 1.6 μm (Figure 4.2D). Figure 4.2E and F show the elemental EDX mapping images for the as-prepared Fe surface and EN coating, respectively, which confirmed that the silicon substrates have been uniformly covered with a thin layer of Fe or the EN coating.

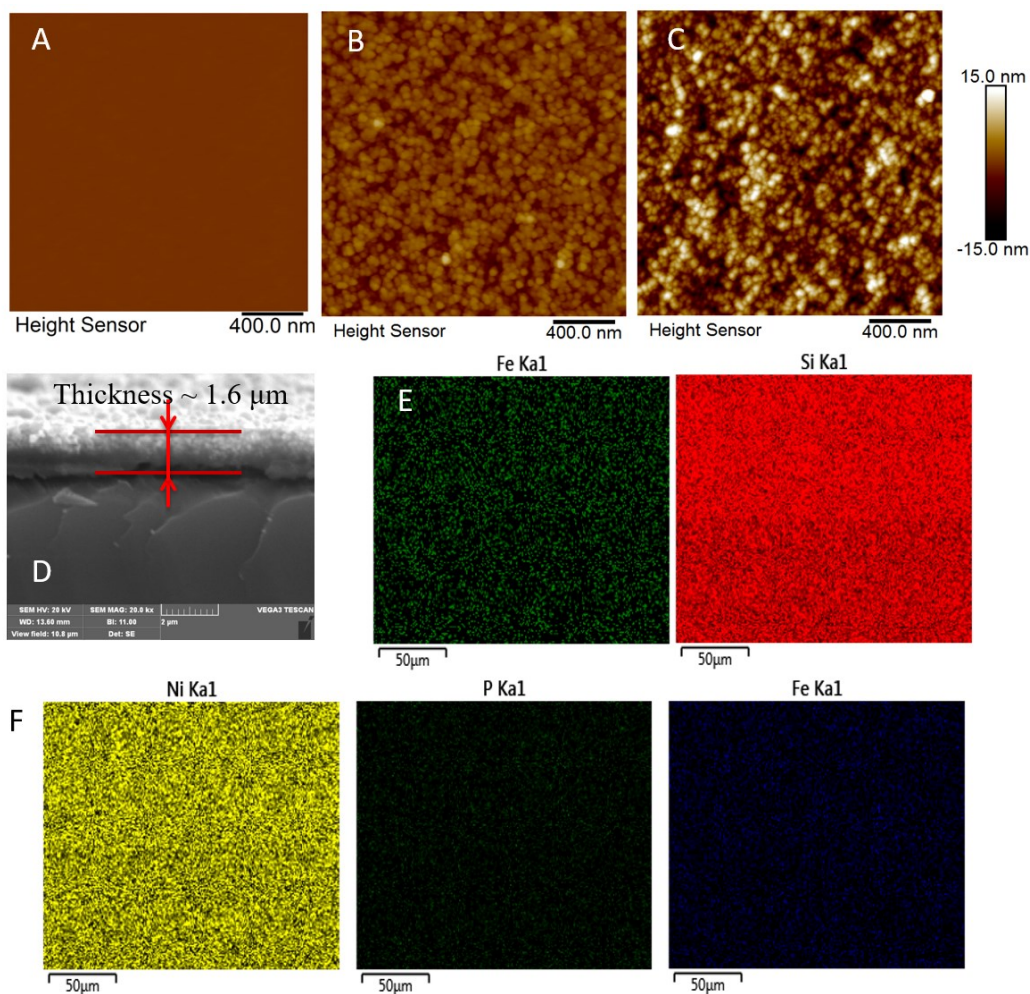


Figure 4.2 AFM topographic images of silicon wafer (A), iron substrate (B), and EN coating (C). (D) SEM section image of EN coating. The thickness of the EN coating is measured to be about 1.6 μm. (E) Elemental EDX mapping images of iron and silicon for deposited Fe substrate. (F) Elemental EDX mapping images of nickel, phosphate, and iron for the as-prepared EN substrate.

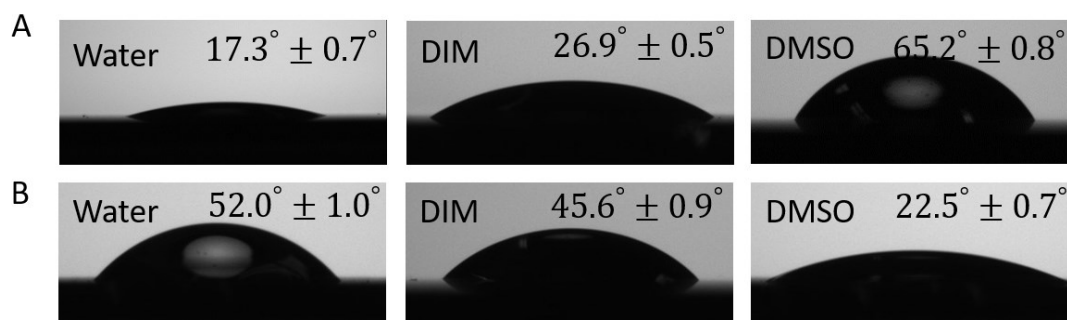


Figure 4.3 Contact angles of water, DIM, and DMSO on Fe substrate (A) and EN substrate (B) in air.

The surface energies of deposited Fe and EN substrates were investigated using Lifshitz-van der Waals Acid/Base approach, which describes the surface energy with the polar and apolar components.⁴¹ Figure 4.3 shows the contact angles of these three probe liquids on Fe and EN substrates in air. The surface energies of deposited Fe and EN substrates calculated from the contact angles are listed in Table 4.3. The overall surface energies of Fe and EN substrates are calculated to be 110.25 mN/m and 42.27 mN/m, respectively. The surface energies are a little low, which is due to the surface roughness, defects and potential contaminations. EN coating has a smaller surface energy than Fe surface.

Table 4.3 Calculated surface energies of Fe and EN substrates.

Substrate	γ (mN/m)	γ^d (mN/m)	γ^p (mN/m)	γ^+ (mN/m)	γ^- (mN/m)
Fe	110.25	45.45	64.80	8.92	117.69
EN	42.27	41.56	0.71	0.0038	33.08

4.3.2 Effects of salinity on surface forces.

The interaction forces between toluene drops and Fe or EN substrate in 1 mM and 100 mM NaCl solutions (pH 5.8, natural pH of the aqueous solutions due to the CO₂ dissolving from the atmosphere⁵¹) were measured using a drop probe AFM technique, as shown in Figure 4.4.

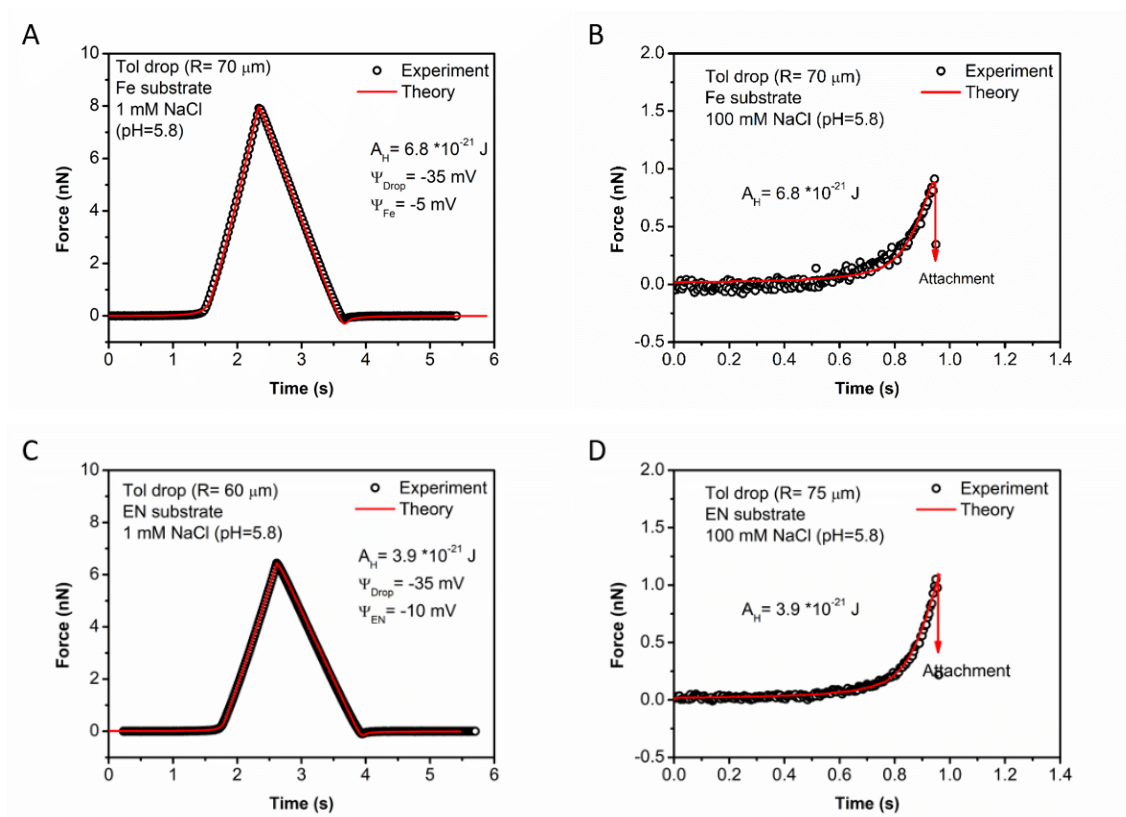


Figure 4.4 Interaction force profiles of a toluene drop and Fe substrate (A, B) and EN substrate (C, D) in 1 mM and 100 mM NaCl solutions (pH=5.8). The hollow black symbols were experiment data, and solid red lines were theoretical calculation results.

Figure 4.4A shows the approaching-separation force profile of a toluene drop and Fe substrate in 1 mM NaCl solution. No attachment behavior was observed, which was mainly due to the electric double layer repulsion of the toluene drop and Fe substrate in 1 mM NaCl, with a Debye length of 9.6 nm. Figure 4.4B shows that with increasing the solution salinity to 100 mM NaCl, attachment behavior was observed during the approaching process as the electric double layer was significantly suppressed with a Debye length < 1 nm. The attachment in Figure 4.4B was mainly driven by the attractive van der Waals interaction between the toluene drop and the Fe substrate in the aqueous

solution. For comparison, the force profiles between the toluene drop and EN coatings in 1 mM and 100 mM NaCl solutions are shown in Figure 4.4C and D, respectively. Similar interaction behavior were observed between toluene drop and EN coating, that pure repulsion was measured under low salinity condition (i.e. 1 mM NaCl) and attachment was observed under high salinity condition (i.e. 100 mM NaCl).

The theoretical model based on the Reynolds lubrication equation and augmented Young-Laplace equation has been used to analyze the measured force profiles, and the theoretical calculation results are shown as red lines in Figure 4.4. As discussed above, in high salinity solution (100 mM NaCl), the EDL force is significantly suppressed (with a Debye length < 1 nm) and the VDW force dominates the interactions. Therefore, for the 100 mM NaCl case, the disjoining pressure was mainly contributed by the van der Waals interactions. Fitting the experimental force profile using the theoretical model (Figure 4.4B) gives a Hamaker constant of 6.8×10^{-21} J for the interactions between toluene and Fe in 100 mM NaCl. Similarly, the theoretical fitting of the surface force profile between toluene drop and EN coating in 100 mM NaCl solution (Figure 4.4D) gives a Hamaker constant of 3.9×10^{-21} J. The Hamaker constant results are listed in Table 4.4. The theoretical Hamaker constant was calculated using the combining relations of the Hamaker constants of the different materials involved.⁴⁴ It is found that the fitted Hamaker constant values reasonably agree with the theoretical values.

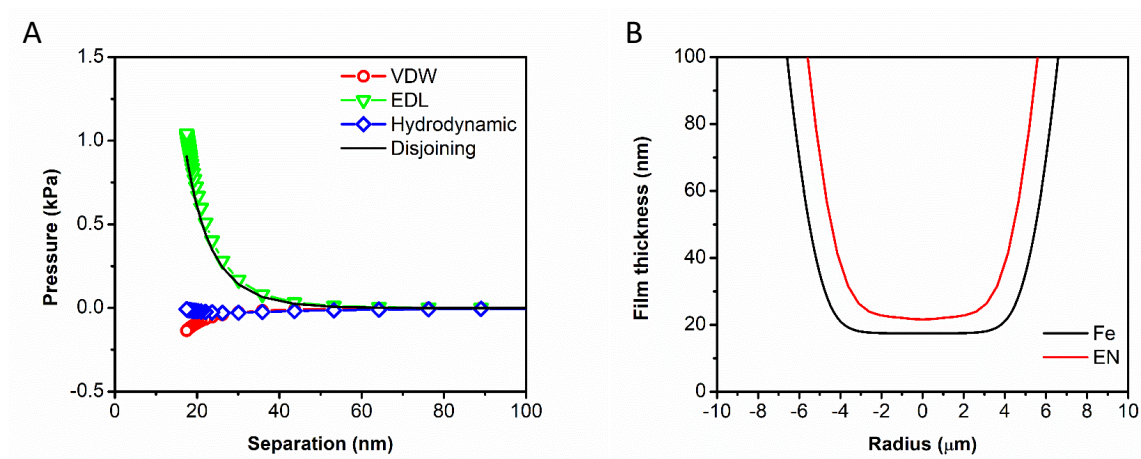
In low salinity of 1 mM NaCl solution, both electric double layer repulsion and attractive van der Waals force would contribute to the surface interactions and

disjoining pressure. The surface potential of toluene in 1 mM NaCl solution ($\Psi_{\text{drop}} = -35$ mV) was determined by fitting the force profile measured between two toluene drops in 1 mM NaCl solution as we reported previously.³³ Then, the force profile for the interaction between a toluene drop and Fe substrate in 1 mM NaCl solution is fitted using the theoretical model and the surface potential of the deposited Fe substrate is fitted to be $\Psi_{\text{Fe}} = -5$ mV (Figure 4.4A). Figure 4.5A shows the calculated disjoining pressure profiles contributed by the VDW, EDL and hydrodynamic interactions between a toluene drop and Fe substrate in 1 mM NaCl solution. Figure 4.5A clearly demonstrates that in 1 mM NaCl solution, the repulsive electric double layer interaction dominates the over surface interactions, which is much stronger than the VDW interactions; while the hydrodynamic force is very weak and also negligible due to the low driving velocity applied in this work. The force profile for the interactions between a toluene drop and EN coating in 1 mM NaCl solution has also been fitted using the theoretical model, which gives the surface potential of EN coating in the solution to be $\Psi_{\text{EN}} = -10$ mV. The more negatively charged surface potential of EN coating indicates stronger electric double layer repulsion with toluene drops than that of the Fe substrate. Figure 4.5B shows the calculated emulsion drop profiles and water film thickness confined between the toluene droplet and solid substrates (i.e., Fe, EN) in 1 mM NaCl solution under the maximum load conditions. The minimum separation distance between the toluene droplet and Fe and EN substrate is ~ 17.4 μm and ~ 21.6 μm , respectively, indicating stronger repulsion between the toluene droplet and EN substrate which is consistent with the stronger EDL repulsion due to the more negative surface

potential. The confined water films prevent the attachment between the oil drop and solid substrates. Figure 4.5C, D, E and F show the interaction force-separation curves of a toluene drop and Fe substrate and EN substrate in 1 mM and 100 mM NaCl solutions (pH=5.8).

Table 4.4 Theoretical fitted Hamaker constant (based on the surface force profiles measured in 100 mM NaCl) and theoretical Hamaker constant of a toluene drop and Fe/EN substrate in aqueous solutions.

Substrate	Fitted Hamaker constant A_{132}	Theoretical Hamaker constant A_{132}
Fe	6.8×10^{-21} J	7.2×10^{-21} J
EN	3.9×10^{-21} J	3.1×10^{-21} J



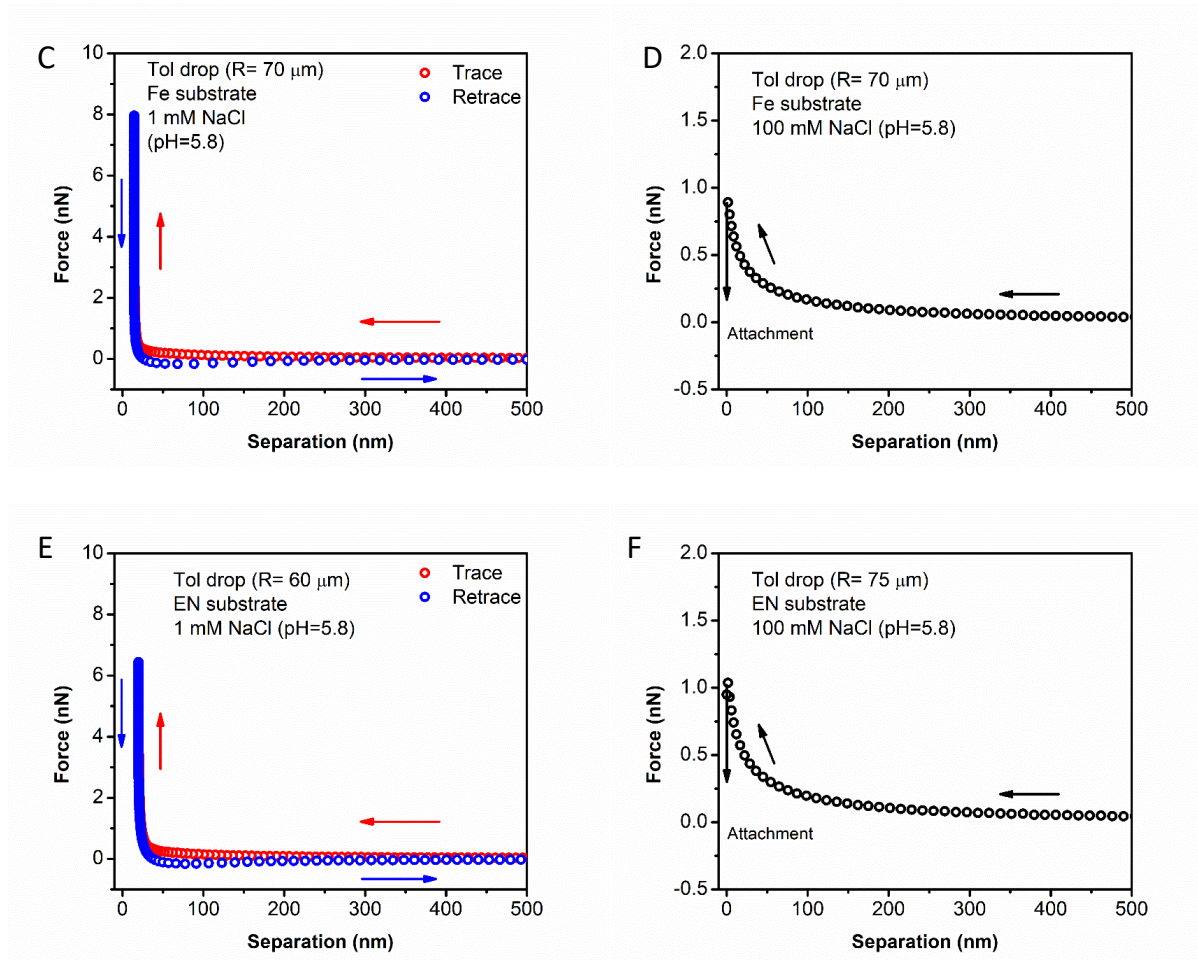
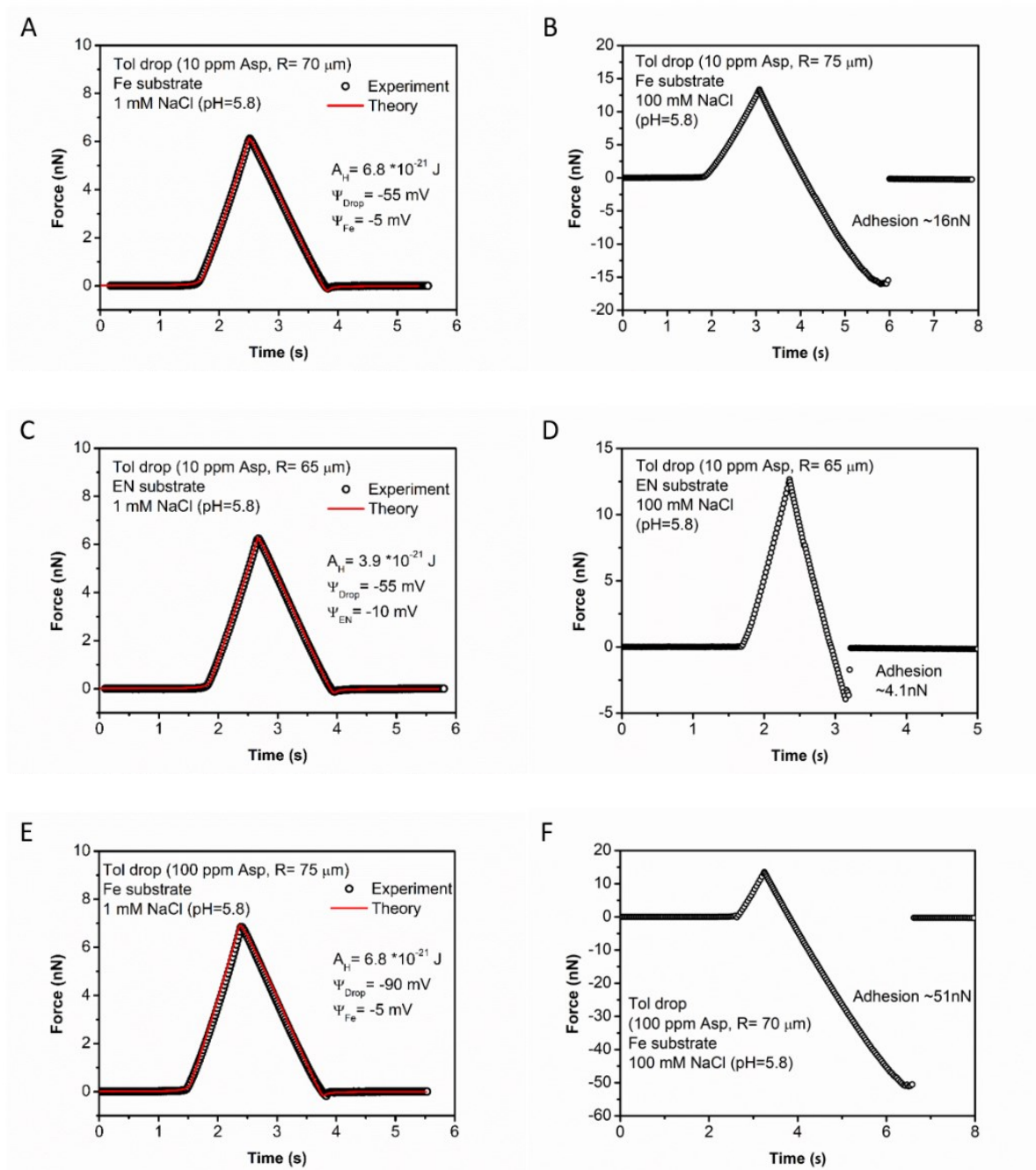


Figure 4.5 (A) Calculated profiles of VDW, EDL, hydrodynamic and disjoining pressures between a toluene drop and Fe substrate in 1 mM aqueous NaCl solution. (B) Calculated emulsion drop profile and confined water film thickness under maximum loading condition during force measurements between a toluene drop and solid substrates (i.e., Fe, EN) in 1 mM NaCl solution. (C, D, E, F) Interaction force-separation profiles of a toluene drop and Fe substrate (C, D) and EN substrate (E, F) in 1 mM and 100 mM NaCl solutions (pH=5.8).

4.3.3 Effects of asphaltenes.

The interaction forces between toluene drops with asphaltenes and Fe substrate or

EN coating were measured in 1 mM and 100 mM NaCl solutions (pH=5.8). The measured force profiles (black open symbols) and theoretical calculations (red solid lines) are shown in Figure 4.6.



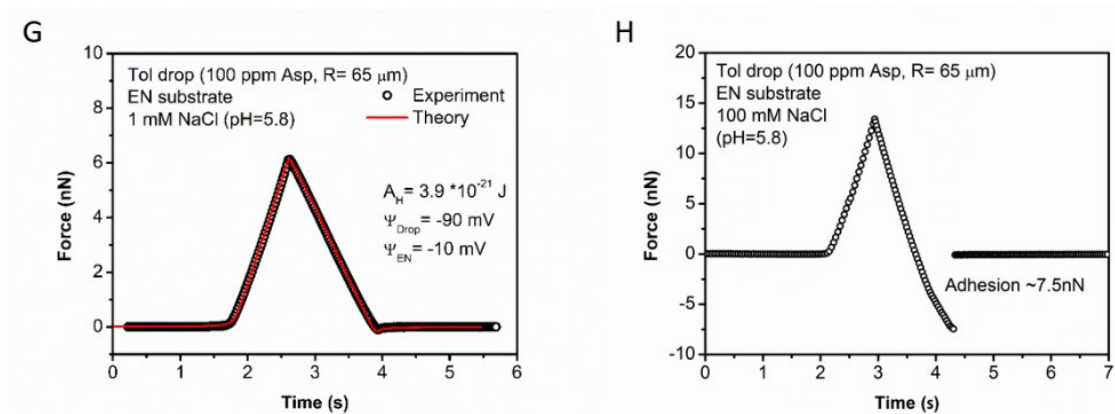


Figure 4.6 Interaction force profiles of a toluene drop and Fe substrate (A, B, E, F) and EN substrate (C, D, G, H) in the presence of 10 ppm and 100 ppm asphaltenes in 1 mM and 100 mM NaCl solutions.

Figure 4.6A shows the approaching-separation force profile of a toluene drop with 10 ppm asphaltenes and Fe substrate in 1 mM NaCl solution. With the effect of the strong electric double layer repulsion, no attachment was observed. Figure 4.6B shows that with increasing the salinity to 100 mM NaCl, strong adhesion was detected during separation, which was mainly due to the highly compressed electric double layer under such high salinity condition and the VDW attraction. However, unlike the force profile in Figure 4.4B, no attachment behavior was observed, which suggests that the toluene-water interface with the adsorption of asphaltenes becomes more rigid.⁵² The adsorbed asphaltenes could stack with each other to generate a relatively rigid and protective film due to intermolecular interactions of asphaltenes, such as van der Waals force, hydrophobic force, π - π interactions, and hydrogen bonding.⁵³⁻⁵⁶ The measured adhesion in Figure 4.6B originates from the attractive VDW force between the toluene drop with

asphaltenes and the Fe substrate. Figure 4.6C and D show the force profiles between asphaltenes-dissolved toluene drops and EN coating in 1 mM and 100 mM NaCl solutions, respectively. The general trends of the force profiles for the EN coating case (Figure 4.6C and D) are similar to those of the Fe substrate (Figure 4.6A and B), but with a much reduced adhesion measured for the EN coating case. Figure 4.6E and F show the measured force profiles between toluene drops dissolved with 100 ppm asphaltenes and Fe substrate in 1 mM and 100 mM NaCl solutions, respectively. Similarly, pure repulsion was measured under low salinity with no obvious attachment or adhesion detected. In 100 mM NaCl, much stronger adhesion was measured, as compared with the 10 ppm asphaltenes case (Figure 4.6B). Higher asphaltene concentration would lead to a more compact interfacial film at the toluene/water interface and much stronger adhesion with Fe substrate.

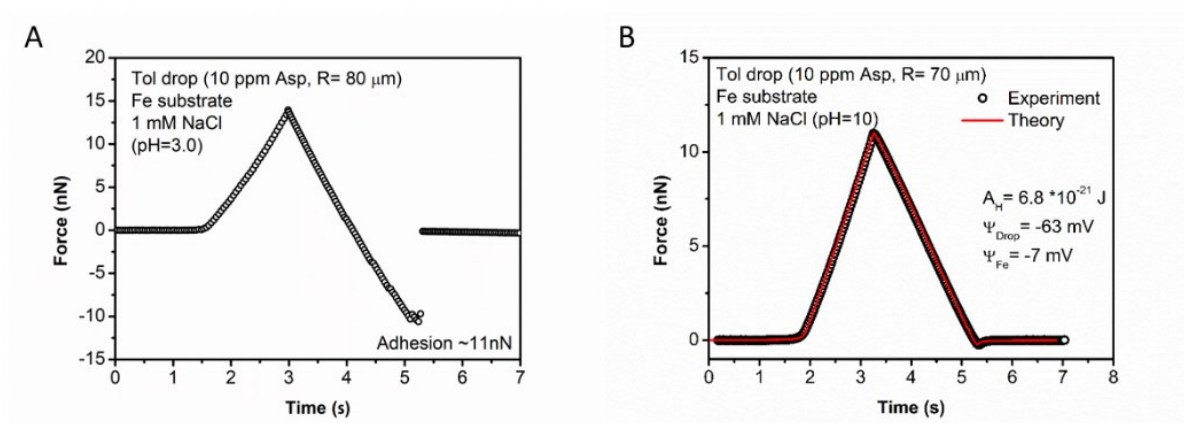
Figure 4.6G and H show similar force profiles of pure repulsion under low salinity (i.e. 1 mM NaCl) and adhesion behavior under high salinity (i.e. 100 mM NaCl) between the toluene drop with 100 ppm asphaltenes and the EN coating. The measured adhesion becomes stronger for the 100 ppm asphaltenes case (Figure 4.6H), which was increased by ~ 80% as compared with 10 ppm asphaltenes (Figure 4.6D). However, it is noted that the measured adhesions with EN coating for both 10 ppm and 100 ppm asphaltenes cases are much weaker than the adhesion with Fe substrate, demonstrate that the EN coating could significantly reduce the surface adhesion with oil-in-water emulsion drops with asphaltenes. Compared with Fe substrate, EN coating has metal nickel and nonmetal phosphorus elements on its surface. It has been reported that the

presence of phosphorus atoms in the coating structure causes the lattice disorder and the deposited EN coating would be amorphous.⁵⁷ Therefore, the surface energy of EN coating is much lower and the attractive VDW force with asphaltenes are also weaker than the Fe substrate.

The surface potentials of toluene drops dissolved with 10 ppm and 100 ppm asphaltenes in 1 mM NaCl solution were theoretically fitted to be $\Psi_{\text{drop}} = -55$ mV and -90 mV, respectively, agreeing with the previous studies.³³ The results indicate that oil/water interface becomes more negatively charged with more asphaltenes dissolved in the toluene phase, leading to a stronger electric double layer repulsion.

4.3.4 Effects of pHs.

Figure 4.7 shows the effects of pH on the interaction forces of toluene drops with 10 ppm asphaltenes with Fe (Figure 4.7A and B) and EN (Figure 4.7C and D) substrate in 1 mM NaCl solutions of pH 3 (Figure 4.7A and C) and pH 10 (Figure 4.7B and D).



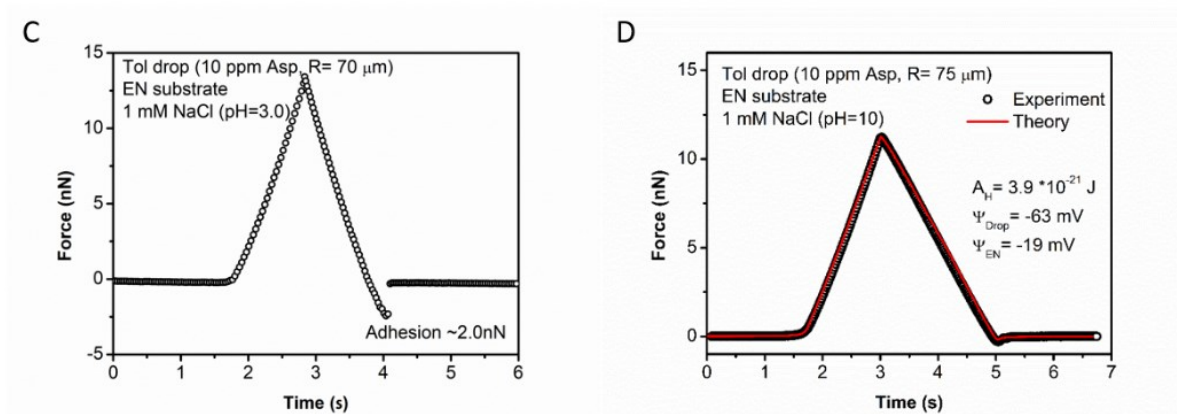


Figure 4.7 Interaction force profiles of a toluene drop (10 ppm asphaltenes) and Fe substrate (A, B) and EN substrate (C, D) in 1 mM NaCl solutions of pH of 3 (A, C) and pH 10 (B, D).

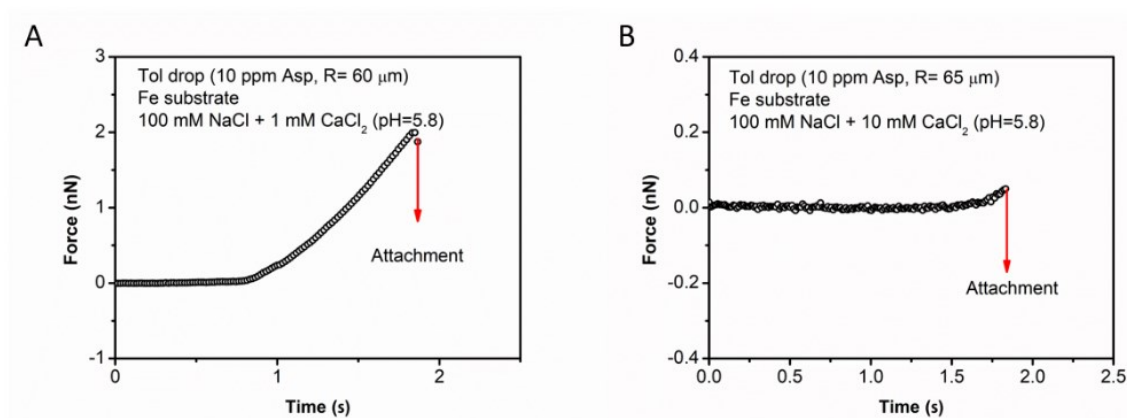
Figure 4.7A and B show the approaching-separating force profiles between toluene drops with 10 ppm asphaltenes and Fe substrate in 1 mM NaCl solutions of pH 3 and pH 10, respectively. Strong adhesion was detected at in acidic pH 3 while pure repulsion was detected in alkaline pH 10, which was due to the strengthened repulsive electric double layer force in alkaline solution. The functional groups on asphaltenes molecules can be deprotonated in alkaline solutions to carry more negative charges and therefore generate a more negative charged surface. The surface potential of toluene drop with 10 ppm asphaltenes $\Psi_{\text{drop}} = -63 \text{ mV}$ was determined from the theoretical modelling of the force profiles between two toluene drops with 10 ppm asphaltenes in 1 mM NaCl solutions of pH 10.³³ The surface potential of the Fe substrate in 1 mM NaCl solution of pH 10 was determined to be -7 mV.

For comparison, Figure 4.7C and D show the force profiles between toluene drops

with 10 ppm asphaltenes and EN coating in 1 mM NaCl solution of pH 3 and pH 10, respectively. Similarly, adhesion was measured under acidic pH (i.e. pH 3) and pure repulsion was detected in alkaline solution (pH 10). Compared with the adhesions for the Fe cases under acidic pH condition, the EN coating shows much weaker adhesion with toluene drop with 10 ppm asphaltenes. The surface potential of EN substrate in 1 mM NaCl solution of pH 10 was determined to be -19 mV, which is more negatively charged than the Fe substrate, contributing to a stronger electric double layer repulsion with the toluene drop.

4.3.5 Effects of Ca^{2+} ions.

Interaction forces of toluene drops with 10 ppm asphaltenes with Fe substrates and EN coating in 100 mM NaCl with the addition of 1 mM and 10 mM CaCl_2 have also been investigated, and the results are shown in Figure 4.8.



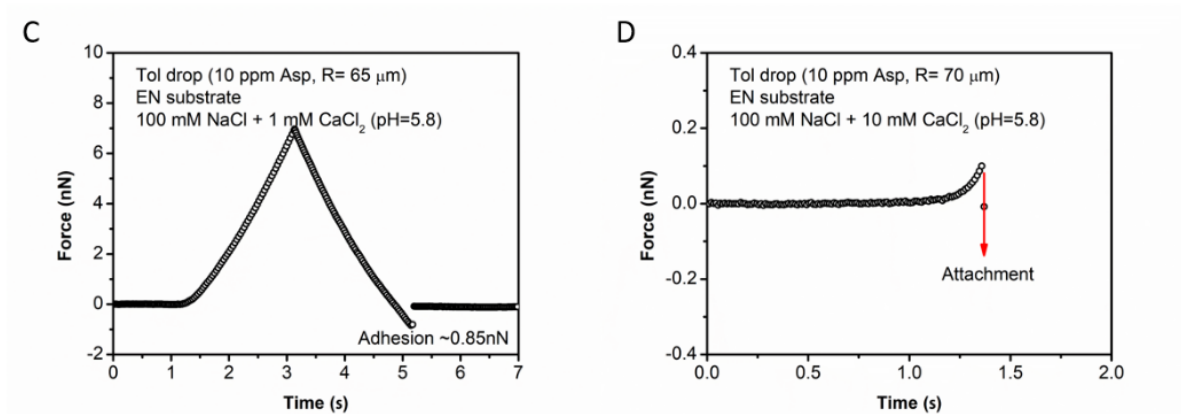


Figure 4.8 Interaction force profiles of a toluene drop (10 ppm asphaltene) and Fe substrate (A, B) and EN substrate (C, D) in 100 mM NaCl solutions with the addition of 1 mM and 10 mM CaCl_2 .

Both force profiles show that the toluene drops attached onto the Fe substrates during approaching, as shown in Figure 4.8A and B. With increasing the Ca^{2+} concentration from 1 mM to 10 mM, the repulsion before surface attachment was greatly reduced, indicating that the presence of divalent Ca^{2+} ions in the aqueous solutions could promote the attachment behavior. Ca^{2+} ions in the NaCl solutions could react with the carboxylic groups of the asphaltene,⁵⁷⁻⁵⁸ and therefore, induce the conformation changes of the asphaltene and asphaltene nanoaggregates adsorbed at toluene/water interface,⁵⁹⁻⁶¹ which could facilitate the droplet and substrate attachment.

Figure 4.8C and D show the force profiles between toluene drops with 10 ppm asphaltene and EN coating in 100 mM NaCl solutions with the addition of 1 mM and 10 mM Ca^{2+} ions, respectively. The force profile in NaCl solution with 1 mM Ca^{2+} ions was measured to have a weak adhesion with EN coating (Figure 4.8C) but without

strong attachment, while the strong attachment behavior was observed in NaCl solution with 10 mM Ca^{2+} ions.

4.3.6 Fouling tests in toluene-in-water emulsions.

Fouling tests of Fe and EN substrates in toluene-in-water emulsions were conducted to evaluate their fouling and antifouling performances. The toluene-in-water emulsions were prepared using toluene dissolved with 100 ppm asphaltenes and 100 mM NaCl solution (pH 5.8). Figure 4.9A shows the schematic fouling test process. Figure 4.9B and C show the images of Fe and EN substrates before and after the fouling test. Figure 4.9 clearly shows that the Fe substrate could be fouled in the toluene-in-water emulsion with asphaltenes; while the EN coating remained clean after the tests, which demonstrates that the EN coating possesses excellent antifouling property to the oil-in-water emulsions. These fouling test results are consistent with the AFM force measurements. It is noted that the EN coating shows higher surface roughness (RMS roughness 4.64 nm) than the Fe substrate (RMS roughness 1.33 nm). Previous study reported that larger surface roughness generally enhances the fouling process by providing larger surface area and higher contact possibilities between the foulants and the substrate.⁶² Despite its higher surface roughness in this work, the EN coating still shows better antifouling performance than Fe substrate, suggesting its good antifouling properties to emulsions.

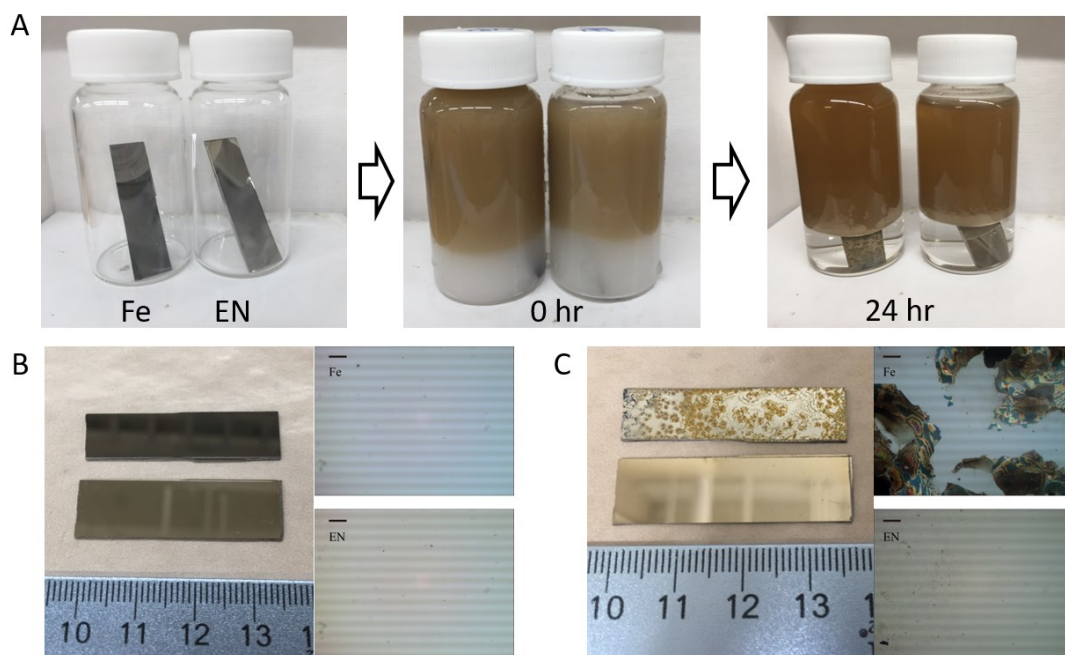


Figure 4.9 (A) Schematic process of fouling tests of selected substrates in oil-in-water emulsions based on toluene dissolved with 100 ppm asphaltenes and 100 mM NaCl solution (pH 5.8) at room temperature (22 °C) for 24 hours. Images of Fe and EN substrates before (B) and after (C) fouling test in the emulsions. (Scale bar 1 μm)

4.4 Conclusions

In this work, the drop probe AFM technique was applied for the *first* time to directly probe the interaction mechanisms of electron-beam deposited iron substrates with and without EN coating and the toluene-in-water emulsion drops in aqueous solutions of different water chemistries (e.g. salinity, pH, divalent ions). A theoretical model based on the Reynolds lubrication equation and augmented Young-Laplace equation has been applied to analyze the measured force profiles. Our results indicate that the attractive van der Waals force plays an important role in the fouling phenomena, particularly

under high salinity condition. The repulsive electric double layer interaction contributes to the antifouling properties. The presence of asphaltenes at the toluene-water interfaces could significantly increase the adhesion between the emulsion drops and substrates. Acidic pH condition leads to less negatively charged surfaces; while the alkaline pH promotes the deprotonation and strengthens the repulsive EDL forces. The addition of divalent Ca^{2+} ions in the solutions could promote the attachment behavior of emulsion drops on the substrates in aqueous solution, due to their influence on the conformation changes of asphaltene molecules and asphaltenes nanoaggregates adsorbed at the oil/water interfaces. EN coating owns metal nickel and nonmetal phosphorous elements and has a much weaker surface energy, thus showing weaker adhesion with asphaltenes and emulsion droplets than Fe substrate. Additionally, the fouling tests of Fe and EN substrates in toluene-in-water emulsions in the presence of asphaltenes have been conducted to evaluate the antifouling performance. The fouling tests clearly demonstrate that the EN coating possesses excellent antifouling performance to oil-in-water emulsions, even with the addition of asphaltenes. Our results also provide useful insights into the fundamental understanding of fouling and antifouling mechanisms of oil-in-water emulsions with asphaltenes in oil production processes, with implications to the development new antifouling coatings and strategies.

Reference

1. Ma, F.; Hanna, M. A., Biodiesel production: a review. *Bioresource technology* **1999**, *70* (1), 1-15.
2. Shams Ashaghi, K.; Ebrahimi, M.; Czermak, P., Ceramic ultra-and nanofiltration membranes for oilfield produced water treatment: a mini review. *Open Environmental Sciences* **2007**, *1* (1).
3. Fakhru'l-Razi, A.; Pendashteh, A.; Abdullah, L. C.; Biak, D. R. A.; Madaeni, S. S.; Abidin, Z. Z., Review of technologies for oil and gas produced water treatment. *Journal of hazardous materials* **2009**, *170* (2-3), 530-551.
4. Ochando-Pulido, J.; Stoller, M.; Bravi, M.; Martinez-Ferez, A.; Chianese, A., Batch membrane treatment of olive vegetation wastewater from two-phase olive oil production process by threshold flux based methods. *Separation and Purification Technology* **2012**, *101*, 34-41.
5. Macchietto, S.; Hewitt, G.; Coletti, F.; Crittenden, B. D.; Dugwell, D.; Galindo, A.; Jackson, G.; Kandiyoti, R.; Kazarian, S.; Luckham, P., Fouling in crude oil preheat trains: a systematic solution to an old problem. *Heat Transfer Engineering* **2011**, *32* (3-4), 197-215.
6. Pragma, N.; Pandey, K. K.; Sahoo, P., A review on harvesting, oil extraction and biofuels production technologies from microalgae. *Renewable and Sustainable Energy Reviews* **2013**, *24*, 159-171.
7. Martínez-Palou, R.; de Lourdes Mosqueira, M.; Zapata-Rendón, B.; Mar-Juárez, E.; Bernal-Huicochea, C.; de la Cruz Clavel-López, J.; Aburto, J., Transportation of

heavy and extra-heavy crude oil by pipeline: A review. *Journal of Petroleum Science and Engineering* **2011**, 75 (3-4), 274-282.

8. Zhao, B.; Shaw, J. M., Composition and size distribution of coherent nanostructures in Athabasca bitumen and Maya crude oil. *Energy & Fuels* **2007**, 21 (5), 2795-2804.

9. Watkinson, A. P., Deposition from crude oils in heat exchangers. *Heat transfer engineering* **2007**, 28 (3), 177-184.

10. Bacchin, P.; Aimar, P.; Sanchez, V., Model for colloidal fouling of membranes. *AIChE journal* **1995**, 41 (2), 368-376.

11. Mansoori, G. A.; Vazquez, D.; Shariaty-Niassar, M., Polydispersity of heavy organics in crude oils and their role in oil well fouling. *Journal of Petroleum Science and Engineering* **2007**, 58 (3-4), 375-390.

12. Hoepfner, M. P.; Limsakoune, V.; Chuenmeechao, V.; Maqbool, T.; Fogler, H. S., A fundamental study of asphaltene deposition. *Energy & fuels* **2013**, 27 (2), 725-735.

13. Visser, S.; Griffiths, C. L.; Parkinson, D., Effects of surface mining on the microbiology of a prairie site in Alberta, Canada. *Canadian Journal of Soil Science* **1983**, 63 (2), 177-189.

14. Jimenez, J. In *The field performance of SAGD projects in Canada*, International petroleum technology conference, International Petroleum Technology Conference: 2008.

15. Balsamo, V.; Nguyen, D.; Phan, J., Non-conventional techniques to characterize complex SAGD emulsions and dilution effects on emulsion stabilization. *Journal of*

Petroleum Science and Engineering **2014**, *122*, 331-345.

16. Noik, C.; Dalmazzone, C. S.; Goulay, C.; Glenat, P. In *Characterisation and emulsion behaviour of Athabasca extra heavy oil produced by SAGD*, SPE International Thermal Operations and Heavy Oil Symposium, Society of Petroleum Engineers: 2005.

17. Wang, G.; Zhu, L.; Liu, H.; Li, W., Galvanic corrosion of Ni–Cu–Al composite coating and its anti-fouling property for metal pipeline in simulated geothermal water. *Surface and Coatings Technology* **2012**, *206* (18), 3728-3732.

18. Zhao, Q.; Liu, C.; Su, X.; Zhang, S.; Song, W.; Wang, S.; Ning, G.; Ye, J.; Lin, Y.; Gong, W., Antibacterial characteristics of electroless plating Ni–P–TiO₂ coatings. *Applied Surface Science* **2013**, *274*, 101-104.

19. Crosby, T.; Wolodko, J.; Tsapraillis, H. In *Gap Analysis of Canadian Pipeline Coatings: A Review Study*, NACE International Corrosion Conference Proceedings, NACE International: 2016; p 1.

20. Farzaneh, A.; Ehteshamzadeh, M.; Can, M.; Mermer, O.; Okur, S., Effects of SiC particles size on electrochemical properties of electroless Ni-P-SiC nanocomposite coatings. *Protection of Metals and Physical Chemistry of Surfaces* **2016**, *52* (4), 632-636.

21. Azizi, A.; Mohammadi, M.; Sadrnezhad, S., End-closed NiCoFe-B nanotube arrays by electroless method. *Mater. Lett.* **2011**, *65* (2), 289-292.

22. Farzaneh, A.; Ehteshamzadeh, M.; Cobley, A. J., Modelling of surfactants and chemistry for electroless Ni-P plating. *Surf. Eng.* **2017**, 1-8.

23. Wurtz, A., Sur l'hydrure de cuivre. *CR Hebd. Seances Acad. Sci.* **1844**, *18*, 702-

704.

24. Brenner, A.; Riddell, G. E., Deposition of nickel and cobalt by chemical reduction.

J. Res. Nat. Bur. Stand **1947**, *39*, 385-395.

25. Drenner, A.; Couch, D.; Williams, E. K., Electrodeposition of Alloys of

Phosphorus and Nickel or Cobalt. *Plating* **1950**, *37*, 36-42.

26. Gutzeit, G., Catalytic nickel deposition from aqueous solution. I-IV. *Plating surface finishing* **1959**, *46*, 1158-1164.

27. John, S.; Shanmugham, N.; Shenoi, B., A Low-Temperature Autocatalytic(Electroless) Nickel Plating Process. *Metal Finishing* **1982**, *80* (4), 47-52.

28. Parker, K., The formulation of electroless nickel-phosphorus plating baths. *Plat. Surf. Finish.* **1987**, *74* (2), 60-65.

29. Bates, J., Why use electroless nickel today? *Plat. Surf. Finish.* **1998**, *85* (5), 14-16.

30. Apachitei, I.; Duszczuk, J.; Katgerman, L.; Overkamp, P., Electroless Ni-P composite coatings: the effect of heat treatment on the microhardness of substrate and coating. *Scripta Mater.* **1998**, *38* (9), 1347-1353.

31. Hajdu, J., Electroless plating: the past is prologue. *Plat. Surf. Finish.* **1996**, *83* (9), 29-33.

32. Hajdu, J., William Blum Lecture--Electroless Plating: What's Past is Prologue. *Plat. Surf. Finish.* **1996**, *83* (9), 29-33.

33. Shi, C.; Zhang, L.; Xie, L.; Lu, X.; Liu, Q.; Mantilla, C. A.; van den Berg, F. G.; Zeng, H., Interaction mechanism of oil-in-water emulsions with asphaltenes determined using droplet probe AFM. *Langmuir* **2016**, *32* (10), 2302-2310.

34. Shi, C.; Yan, B.; Xie, L.; Zhang, L.; Wang, J.; Takahara, A.; Zeng, H., Long - Range Hydrophilic Attraction between Water and Polyelectrolyte Surfaces in Oil. *Angewandte Chemie International Edition* **2016**, *55* (48), 15017-15021.
35. Shi, C.; Zhang, L.; Xie, L.; Lu, X.; Liu, Q.; He, J.; Mantilla, C. A.; Zeng, H., Surface Interaction of Water-in-Oil Emulsion Droplets with Interfacially Active Asphaltenes. *Langmuir* **2017**, *33* (5), 1265-1274.
36. Xie, L.; Shi, C.; Cui, X.; Zeng, H., Surface Forces and Interaction Mechanisms of Emulsion Drops and Gas Bubbles in Complex Fluids. *Langmuir* **2017**, *33* (16), 3911-3925.
37. Xie, L.; Shi, C.; Cui, X.; Huang, J.; Wang, J.; Liu, Q.; Zeng, H., Probing the Interaction Mechanism between Air Bubbles and Bitumen Surfaces in Aqueous Media Using Bubble Probe Atomic Force Microscopy. *Langmuir*.
38. Zhang, L. Y.; Lawrence, S.; Xu, Z.; Masliyah, J. H., Studies of Athabasca asphaltene Langmuir films at air–water interface. *Journal of colloid and interface science* **2003**, *264* (1), 128-140.
39. Kar, K. K.; Sathiyamoorthy, D., Influence of process parameters for coating of nickel–phosphorous on carbon fibers. *journal of materials processing technology* **2009**, *209* (6), 3022-3029.
40. Palaniappa, M.; Babu, G. V.; Balasubramanian, K., Electroless nickel–phosphorus plating on graphite powder. *Materials Science and Engineering: A* **2007**, *471* (1), 165-168.
41. Gao, Z.; Xie, L.; Cui, X.; Hu, Y.; Sun, W.; Zeng, H., Probing Anisotropic Surface

- Properties and Surface Forces of Fluorite Crystals. *Langmuir* **2018**, *34* (7), 2511-2521.
42. Radelczuk, H.; Hołysz, L.; Chibowski, E., Comparison of the Lifshitz–van der Waals/acid–base and contact angle hysteresis approaches for determination of solid surface free energy. *Journal of adhesion science and technology* **2002**, *16* (12), 1547-1568.
43. Chan, D. Y.; Klaseboer, E.; Manica, R., Film drainage and coalescence between deformable drops and bubbles. *Soft Matter* **2011**, *7* (6), 2235-2264.
44. Israelachvili, J. N., *Intermolecular and surface forces*. Academic press: 2011.
45. Cappella, B.; Dietler, G., Force-distance curves by atomic force microscopy. *Surf. Sci. Rep.* **1999**, *34* (1-3), 15-3104.
46. Yang, D.; Xie, L.; Bobicki, E.; Xu, Z.; Liu, Q.; Zeng, H., Probing anisotropic surface properties and interaction forces of chrysotile rods by atomic force microscopy and rheology. *Langmuir* **2014**, *30* (36), 10809-10817.
47. Hayashi, T.; Ohno, T.; Yatsuya, S.; Uyeda, R., Formation of ultrafine metal particles by gas-evaporation technique. IV. Crystal habits of iron and Fcc metals, Al, Co, Ni, Cu, Pd, Ag, In, Au and Pb. *Japanese Journal of Applied Physics* **1977**, *16* (5), 705.
48. Chen, C.; Idzerda, Y.; Lin, H.-J.; Smith, N.; Meigs, G.; Chaban, E.; Ho, G.; Pellegrin, E.; Sette, F., Experimental confirmation of the X-ray magnetic circular dichroism sum rules for iron and cobalt. *Physical review letters* **1995**, *75* (1), 152.
49. Miyazaki, T.; Tezuka, N., Giant magnetic tunneling effect in Fe/Al₂O₃/Fe junction. *Journal of Magnetism and Magnetic Materials* **1995**, *139* (3), L231-L234.

50. Pogrebnyak, A.; Bratushka, S.; Boyko, V.; Shamanin, I. V.; Tsvintarnaya, Y. V., A review of mixing processes in Ta/Fe and Mo/Fe systems treated by high current electron beams. *Nuclear Instruments and Methods in Physics Research Section B: Beam Interactions with Materials and Atoms* **1998**, *145* (3), 373-390.
51. Drever, J. I., *The geochemistry of natural waters*. Prentice-Hall Englewood Cliffs: 1982; Vol. 9.
52. Shi, C.; Zhang, L.; Xie, L.; Lu, X.; Liu, Q.; He, J.; Mantilla, C. A.; Van den Berg, F. G.; Zeng, H., Surface interaction of water-in-oil emulsion droplets with interfacially active asphaltenes. *Langmuir* **2017**, *33* (5), 1265-1274.
53. Murgich, J., Intermolecular forces in aggregates of asphaltenes and resins. *Petroleum Science and Technology* **2002**, *20* (9-10), 983-997.
54. Rocha, J.; Baydak, E.; Yarranton, H.; Sztukowski, D.; Ali-Marcano, V.; Gong, L.; Shi, C.; Zeng, H., Role of aqueous phase chemistry, interfacial film properties, and surface coverage in stabilizing water-in-bitumen emulsions. *Energy & Fuels* **2016**, *30* (7), 5240-5252.
55. Jian, C.; Tang, T.; Bhattacharjee, S., Probing the effect of side-chain length on the aggregation of a model asphaltene using molecular dynamics simulations. *Energy & Fuels* **2013**, *27* (4), 2057-2067.
56. Maqbool, T.; Raha, S.; Hoepfner, M. P.; Fogler, H. S., Modeling the aggregation of asphaltene nanoaggregates in crude oil– precipitant systems. *Energy & Fuels* **2011**, *25* (4), 1585-1596.
57. Kou, J.; Xu, S.; Sun, T.; Sun, C.; Guo, Y.; Wang, C., A study of sodium oleate

adsorption on Ca^{2+} activated quartz surface using quartz crystal microbalance with dissipation. *International Journal of Mineral Processing* **2016**, *154*, 24-34.

58. Yu, W.; Sun, T.; Kou, J.; Wei, Y.; Xu, C.; Liu, Z., The function of $\text{Ca}(\text{OH})_2$ and Na_2CO_3 as additive on the reduction of high-phosphorus oolitic hematite-coal mixed pellets. *ISIJ international* **2013**, *53* (3), 427-433.

59. Mullins, O. C.; Sabbah, H.; Eyssautier, J.; Pomerantz, A. E.; Barré, L.; Andrews, A. B.; Ruiz-Morales, Y.; Mostowfi, F.; McFarlane, R.; Goual, L., Advances in asphaltene science and the Yen–Mullins model. *Energy & Fuels* **2012**, *26* (7), 3986-4003.

60. Chaisoontornyotin, W.; Haji-Akbari, N.; Fogler, H. S.; Hoepfner, M. P., Combined asphaltene aggregation and deposition investigation. *Energy & Fuels* **2016**, *30* (3), 1979-1986.

61. Goual, L.; Firoozabadi, A., Measuring asphaltenes and resins, and dipole moment in petroleum fluids. *AIChE Journal* **2002**, *48* (11), 2646-2663.

62. Elimelech, M.; Zhu, X.; Childress, A. E.; Hong, S., Role of membrane surface morphology in colloidal fouling of cellulose acetate and composite aromatic polyamide reverse osmosis membranes. *Journal of membrane science* **1997**, *127* (1), 101-109.

Chapter 5 Surface Interactions between Water-in-Oil Emulsions with Asphaltenes and Electroless Nickel-phosphorus Coating

5.1 Introduction

Surface interactions between emulsion drops and substrate surfaces are involved in many processes and issues in various industries, such as the water or oil drop collection in chemical engineering and fouling problems in oil and gas industries. The interactions between water-in-oil emulsion drop and a substrate surface would induce the drop attachment on the substrate and potentially cause the fouling problems during oil production.¹⁻⁶ The crude oil components (e.g., bitumen or asphaltenes), mineral particles (e.g., silica and clay), and corrosive products (e.g., iron oxide) have been found to be the main compositions in the foulants.⁷⁻¹¹ The undesired deposition of these foulants on the facility surfaces can further lead to the plugging and breaking-down issues in oil transportation, storage and refinery processes,^{7, 12-16} which will eventually result in the damages of pipelines, malfunction of production facilities, reduction of the efficiency in oil production, and thereby, increase the oil production cost.^{10, 17} Thus, it is critical and urgent to find a solution to mitigate or even solve the fouling problems.

In the past decades, much attention has been focused on the investigation of surface fouling mechanisms along oil production. It is commonly believed that the interface-active asphaltenes, as the heaviest component in crude oil, have played an important role in the initiation and growing processes of the fouling.¹⁸⁻²² Asphaltenes are defined as solubility class, which is soluble in aromatic solvents (e.g., toluene) and insoluble in alkane solvents (e.g., heptane).^{19, 23-}

²⁴ Hence, toluene is commonly regarded as the good solvent to asphaltenes, and heptane is treated as the poor solvent. In the Yen-Mullins model, a typical asphaltene molecule consists of polyaromatic core with peripheral alkyl chains and functional polar groups containing nitrogen, oxygen and sulphur atoms.²⁵⁻²⁶ The strong intra- and inter- molecular interactions between the aromatic rings, alkyl chains and functional groups including π - π stacking, van der Waals (VDW), acid-base, and hydrogen bond interactions, could induce the instinctive aggregation behavior of asphaltenes.^{24, 27-29} Therefore, it is generally inaccurate to use one specific molecular structure to describe asphaltenes and analyze their physical and/or chemical properties. Instead, the bulk properties of asphaltene solution, such as the solubility and the distribution of asphaltene aggregation sizes, are usually used.¹⁹ Experiments have been designed and conducted to study the adsorption behaviors of asphaltenes onto various surfaces, including both solid surfaces (e.g., silica, steel and gold) and water/oil interfaces (e.g., water/toluene interface).³⁰⁻³⁵ It was found that the asphaltenes could irreversibly adsorb to the water/oil interface and form a protective layer to enhance the stability of the emulsion drops.^{29, 36-39} Meanwhile, the strong intermolecular interactions between asphaltenes could induce the agglomeration and flocculation of the water-in-oil emulsions,⁴⁰⁻⁴³ which would form complex mixture and finally lead to fouling problems. So far, the fouling mechanisms of water-in-oil emulsions with interfacially adsorbed asphaltenes on iron-based surfaces, as one of the most commonly used materials for pipelines and reactors in chemical engineering and oil industries, have not been thoroughly studied. Electroless nickel-phosphorus (EN) coating has been used to protect the facility surfaces (e.g., iron surfaces) from abrasion in different industries because of its excellent properties of uniform hardness and great resistance to corrosion,⁴⁴⁻⁴⁶ since the re-

discovery of this coating technique by Brenner and Riddell in 1946.⁴⁷ Meanwhile, growing studies have been conducted in order to improve the anti-corrosion and anti-abrasion performances of EN coating.⁴⁸⁻⁵² However, limited studies are available on the fouling phenomena of water-in-oil emulsions with asphaltenes on EN coating as well as the interaction mechanisms involved.

Over the past few years, the surface interactions between deformable bubbles or drops and various substrate surfaces in aqueous solutions or organic media have been quantitatively measured using the bubble/drop probe atomic force microscope (AFM) technique.^{18, 40, 53-56} The obtained results described the surface deformation of the bubbles or drops, deciphered the drop attachment process on hydrophilic or hydrophobic substrates, and revealed the stability mechanisms of emulsion drops and the contributions of various interactions (e.g., VDW, electric double layer, hydrophobic and steric interactions). It has been demonstrated that the asphaltenes at the water/oil interface could induce strong steric repulsion between water drops during surface approaching and interfacial adhesion during their separation, responsible for the stability and flocculation behavior of water-in-oil emulsions.¹⁸ It is expected that the interactions between asphaltenes at the water/oil interface and substrate surface could affect the stability and attachment behavior of water-in-oil emulsions on the substrates. To the best of our knowledge, the direct quantification of interaction forces between water-in-oil emulsion drops with asphaltenes and substrate surfaces has not been reported.

In this work, the surface interactions between water drops with interfacially adsorbed asphaltenes and Fe substrate with or without EN coating were directly measured in organic media (i.e., toluene, heptols and heptane) using the drop probe AFM technique. The effects of

asphaltene concentration, solvent type, aging time, contact time and loading force were investigated. Bulk fouling tests of Fe and EN substrates in water-in-oil emulsion stabilized with asphaltenes were also conducted to evaluate their fouling and antifouling performances. Our work quantifies the interaction forces between water-in-oil emulsion drops with interfacial asphaltenes and selected substrates (i.e., Fe and EN substrates) in organic media, which helps to elucidate the fundamental mechanisms in the fouling phenomena and facilitate the development of efficient antifouling strategies in related industrial applications.

5.2 Materials and Experimental Methods

5.2.1 Materials.

Asphaltenes were extracted from Athabasca bitumen by following the procedure reported elsewhere.⁵⁷ 10,000 mg/L asphaltene stock solution was prepared by dissolving asphaltenes in pure toluene (HPLC, Fisher Scientific, Canada) and sonicated for 30 min to ensure the complete dissolution. Prior to the experiments, the asphaltene solutions with different concentrations were prepared by diluting the stock solution with pure toluene, and sonicated for 15 min. Milli-Q water with a resistivity of 18.2 M Ω •cm (BARNSTEAD Smart2Pure, Thermo Scientific, Canada) was used throughout the experiment. To explore the effect of organic solvent to asphaltene stability and solubility, the heptols prepared by mixing toluene and heptane (HPLC grade, Fisher Scientific, Canada) with desired volume ratios have been used as the organic media in following experiments. Octadecyltrichlorosilane (OTS) was purchased from Sigma-Aldrich and used as received.

5.2.2 Preparation of Fe and EN coating substrates.

The Fe substrate was prepared by depositing a layer of iron with the thickness of 90 nm on a pre-treated silica wafer using the electron beam evaporation (EBE) technique, which has been reported previously.⁵⁸ A layer of chromium with the thickness of 10 nm was deposited between iron and silica to enhance the adhesion and stability, as shown in Figure 5.1A. The EN coating substrate was prepared on Fe substrate using the electroless bathing method as reported previously.^{52, 59} The electroless bath solution was prepared following the compositions shown in Table 1 and the pH of the solution was adjusted to around 8.5. Then, the solution was heated to 85 °C with the agitation of 250 rpm. The EN coating process started when the cleaned Fe substrate was immersed in the prepared bath solution. After 30 min, the prepared substrate was washed with DI water and ethanol, and dried using pure nitrogen. The successful deposition of EN coating on the Fe substrate was confirmed using the AFM surface image, Scanning Electron Microscopy (SEM) and Energy Dispersive X-ray Spectroscopy (EDS).

Table 5.1 The compositions of the bath solution for EN coating.

Composition	NiSO₄· 6H₂O	NaH₂PO₂· H₂O	NH₄Cl	CH₃COONa	Citric acid
Concentration	25 g/L	16 g/L	40 g/L	10 g/L	15 g/L

5.2.3 AFM force measurements.

The surface interaction between a water drop with asphaltenes adsorbed at water/oil interface

and Fe or EN substrate in various organic media were quantitatively measured to investigate the fouling and antifouling mechanisms using the drop probe AFM technique based on a MFP-3D-Bio AFM system (Asylum Research, Santa Barbara, CA). The detailed experimental procedure was reported in previous studies.^{18, 40, 60}

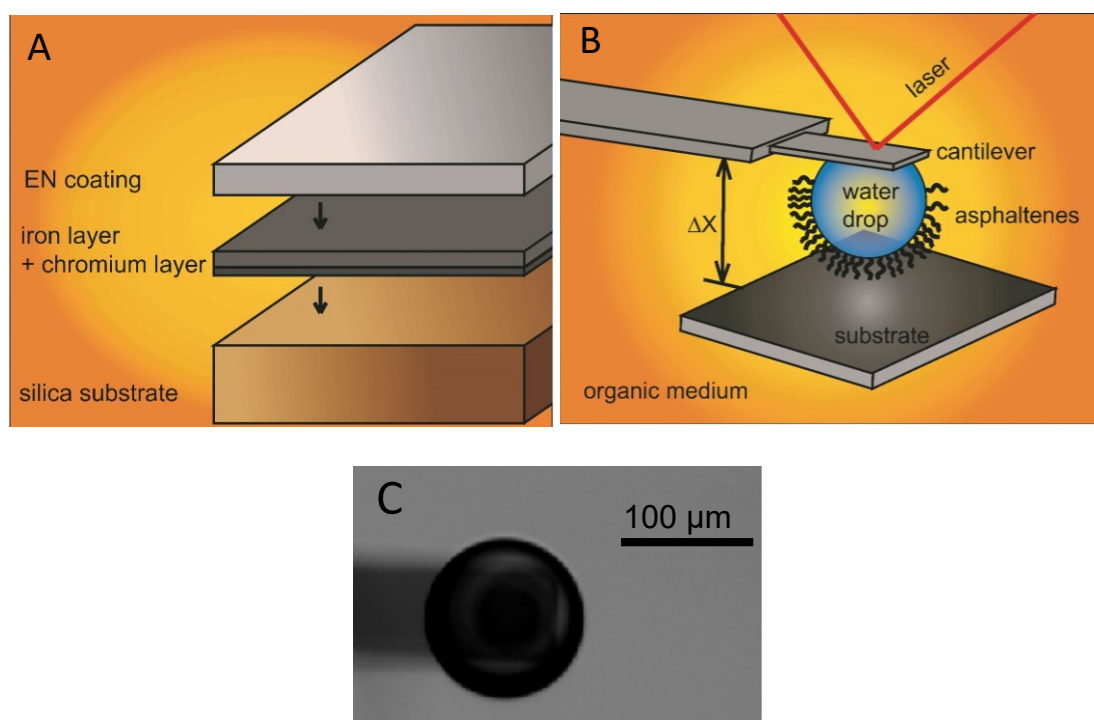


Figure 5.1 (A) The preparation of Fe and EN substrates. (B) The schematic of drop probe atomic force microscope (AFM) technique. The ΔX shows the piezo displacement. (C) A microscope image showing a water drop was anchored on the tipless AFM cantilever in toluene for the force measurements.

For each force measurement, the AFM fluid cell was firstly filled with asphaltene solution, and water drops were generated in the cell using a custom-made ultrasharp glass pipet. These water drops spontaneously settled down to the glass substrate of the fluid cell due to the relatively higher density of the water. The glass substrate was slightly hydrophobized in 5 mM

OTS solution to obtain a water contact angle in air of $\sim 90^\circ$ prior to the experiments, which facilitates the immobilization of the water drops on the glass substrate as well as the pick-up of water drops later. The water drops were aged in the asphaltenes solution for 5 min unless specified elsewhere. Afterwards, the asphaltenes solution was replaced by a large amount of organic solvent (e.g., toluene, heptane or heptol in this work) several times to wash off all the free asphaltenes in the surrounding solution and the pure solvent was used for force measurement. Thus, only the asphaltenes adsorbed at the water/oil interface were left and contributed to the measured interfacial interactions. A custom-made rectangular tipless silicon AFM cantilever ($400 \times 70 \times 2 \mu\text{m}$) was used to pick up a water drop with asphaltenes in the pure solvent to create the water drop probe, as shown in Figure 5.1C. Then, this drop probe was moved and placed above the Fe or EN substrate for the force measurements. A schematic illustration of the experimental setup was shown in Figure 5.1B. During the force measurement, the water drop anchored cantilever was driven by a piezo actuator to approach the substrate at a velocity of $1 \mu\text{m/s}$ till a certain maximum loading force was obtained. This loading force was kept at 4 nN unless specified elsewhere. Then, this probe was driven to retract. The spring constant of the AFM cantilever was calibrated using the thermal tune method in the solvent before picking up the water drop, and an optical laser beam system was used to monitor the deflection of the cantilever. Thus, the force was determined through the Hooke's law. For each experimental condition, at least 10 force measurements were conducted at different positions of each independently prepared substrate. To investigate the effect of contact time, the water drop probe was kept in contact with the substrate for a certain time after the maximum loading force of 4 nN was reached. The force profiles with respect to the piezo displacement ΔX were

obtained from the AFM software. The adhesion force data was collected and normalized by the radius of the water drop. In this work, the adhesion between the water drops with interfacial asphaltenes and Fe or EN substrate describes the difficulty for water drops and asphaltenes to be removed from the substrate surface. When the adhesion is strong, the removal process is difficult, which indicates the fouling phenomena. When the adhesion is weak, the removal process will be easy, which suggests the antifouling property. Thus, the antifouling property can be evaluated via the measured adhesion.

5.2.4 Bulk fouling tests.

The experimental setup for bulk fouling tests is shown in Figure 5.2. The emulsion solution was prepared by mixing 100 mg/L asphaltene-toluene solution and DI water with the volume fraction of 7:3 using a homogenizer. The as-prepared emulsion was settled for 1 hour. After the settlement, two phases were observed and the water-in-oil emulsion on the upper phase was transferred to 20 mL vials. Then, Fe and EN substrates were separately placed in the emulsions for 24 hours in room temperature. The Fe and EN substrates after the bulk fouling tests were cleaned using DI water and ethanol, dried with pure nitrogen and characterized with the optical microscope, AFM surface imaging and SEM-EDS characterization.

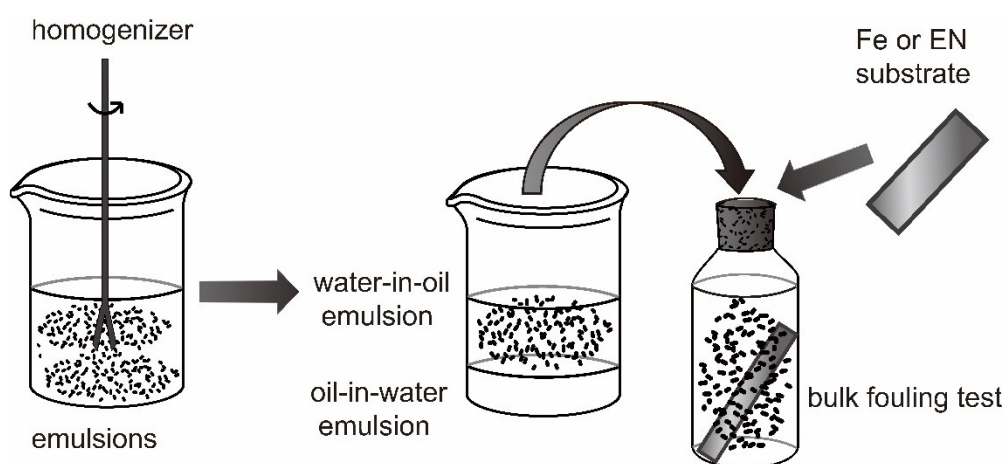


Figure 5.2 Schematic of bulk fouling tests for Fe and EN substrates in water-in-oil emulsions with asphaltenes.

5.3 Results and Discussion

5.3.1 Characterization of Fe and EN substrates.

The AFM topographic images of silica substrate, Fe substrate and EN substrate are shown in the supporting information in Figures 5.S1A-S1C, respectively, which exhibit that the silica surface is featureless and flat, while both Fe and EN substrates are much rougher with aggregate particles. The root-mean-square (rms) roughness for the silica surface, Fe substrate and EN substrate were 0.45 nm, 1.33 nm and 4.22 nm, respectively. Moreover, Figures 5.S1D-S1G show the SEM images and EDS element mapping results, demonstrating the presence of iron element on Fe substrate and nickel and phosphorus elements on EN substrate. These results prove the successful deposition of EN coating on Fe substrate. The thickness of the EN coating was measured to be about 1.6 μm from the SEM image from the cross section view (in Figure 5.S1H).⁶¹ As shown in Figure 5.3, the oil (i.e., toluene) contact angles (OCAs) in DI water for silica, Fe and EN substrates were measured to be $130.3^\circ \pm 1.3^\circ$, $121.1^\circ \pm 0.9^\circ$, and $146.3^\circ \pm 1.5^\circ$, respectively. The water contact angles (WCAs) in oil (i.e., toluene) for silica, Fe and EN substrates were also measured to be $64.0^\circ \pm 0.7^\circ$, $55.6^\circ \pm 1.1^\circ$, and $108.6^\circ \pm 1.0^\circ$, respectively. The OCA and WCA for EN substrate are bigger than those of Fe substrate, which suggests the possible antifouling property of EN coating.

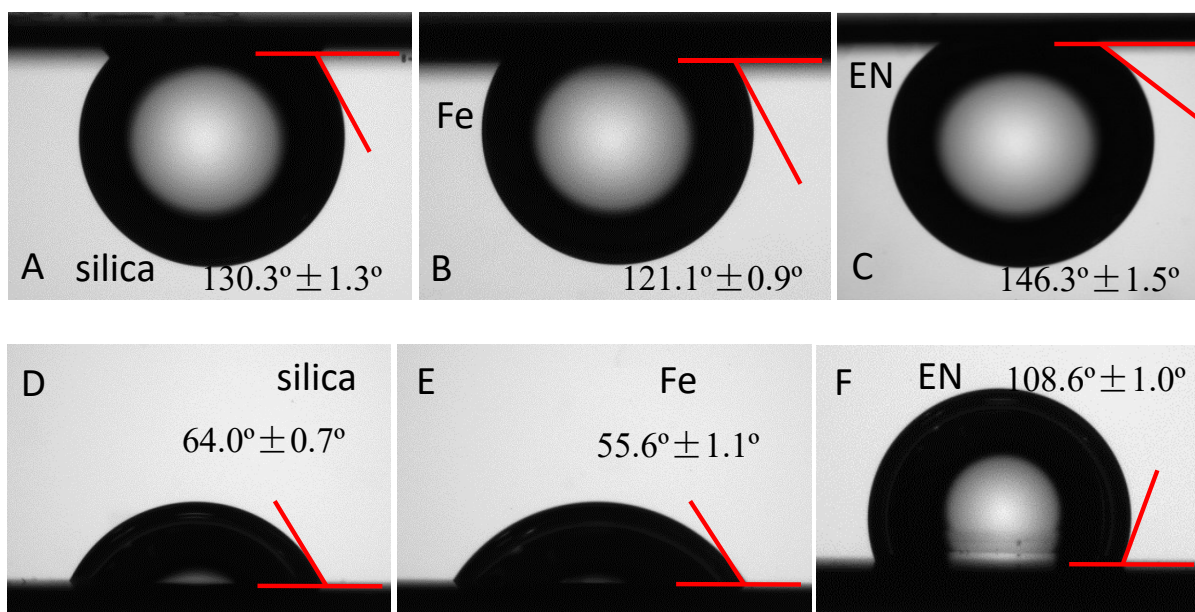


Figure 5.3 Oil contact angles (OCAs) in water for (A) silica substrate, (B) Fe substrate, (C) EN substrate. Water contact angles (WCAs) in oil for (D) silica substrate, (E) Fe substrate, (F) EN substrate.

5.3.2 Effect of asphaltene concentrations.

Figure 5.4 shows the measured force profiles between the water drops and Fe substrate in pure toluene, after the water drops were aged in asphaltene solutions with different concentrations for 5 min. It should be noted that the piezo displacement ΔX here is the relative movement of the AFM cantilever, not the true surface separation between the water drop and the Fe substrate.

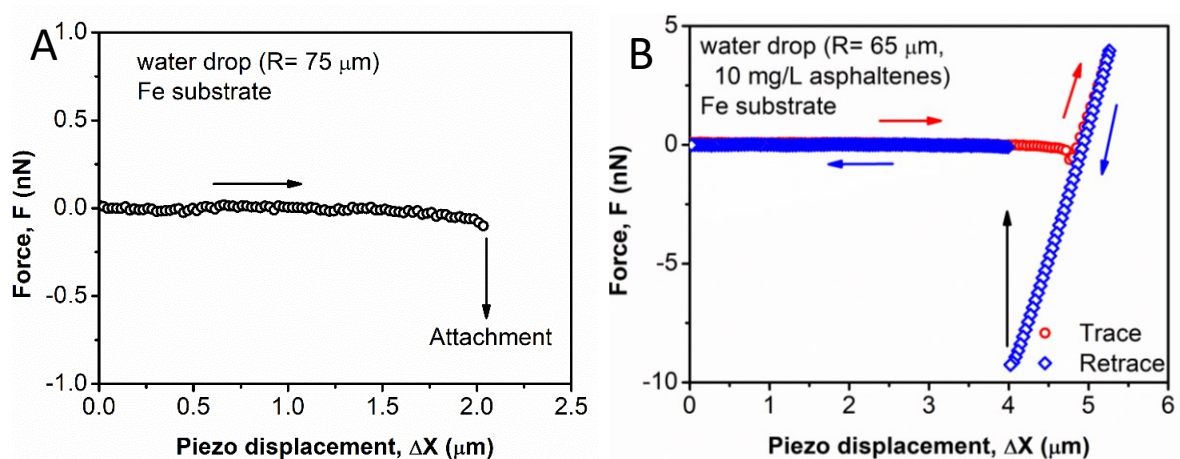


Figure 5.4 Measured force profiles between a water drop and Fe substrate in toluene after aged in (A) 0 and (B) 10 mg/L asphaltene solutions for 5 min. The open dots are experimental data. The arrows show the movements of water drops

Figure 5.4A shows the measured interaction between a water drop without asphaltenes and the Fe substrate in pure toluene. The obtained force curve was attractive as the water drop approached the substrate. When the water drop moved closer to the substrate, this attractive force became stronger till a sudden “jump-in” behavior was observed, indicating that the water drop jumped into contact with the Fe substrate. From the optical microscope, it was directly observed that the water drop detached from the AFM cantilever and attached onto the Fe substrate. This behavior was attributed to the strong VDW attraction between water drop and Fe substrate in toluene.⁶¹⁻⁶²

Figure 5.4B and Figure 5.S2 show the measured force results between water drops and Fe substrate in toluene after the water drops were aged in asphaltenes solutions with different concentrations of 10, 20, 50, 100, 200, and 500 mg/L. For all the cases, attraction was detected during approaching of the water to the Fe substrate and water drop jumped into contact with

the Fe substrate due to the VDW attraction, but no drop detachment from the cantilever was observed. Meanwhile, strong adhesion was measured when the water drop was retracted. Previous work showed that asphaltenes could irreversibly adsorb at water/oil interface and form a protect layer to enhance the stability of water drops in organic medium.^{38, 63} The measured adhesion was due to the attractive interactions between the interfacially adsorbed asphaltenes and iron surface, which was in consistence with the reported results that asphaltenes could interact with various metal surfaces, such as gold and stainless steel, via hydrogen bonding, VDW force, coordinate interaction and so on.⁶⁴⁻⁶⁶

Comparing the adhesion measured at different asphaltene concentrations (Figure 5.5), it could be noted that with increasing the asphaltene concentration, the adhesion between the water drop and Fe substrate became stronger. However, the measured adhesion was almost the same at the asphaltene concentrations of 200 mg/L and 500 mg/L. The adhesion change should be caused by the different amount of the asphaltenes adsorbed at the water/toluene interface. At relatively lower asphaltene concentration (<200 mg/L), increasing asphaltene concentration in the solution induced more asphaltenes adsorbed at the water/toluene interface. The increased amount of asphaltenes at the interface created more active sites to interact with the opposing Fe surface during force measurements, resulting in the stronger adhesion. However, as the asphaltene concentration kept increasing (>200 mg/L), the water/toluene interface could be fully covered by asphaltenes during the aging time, forming a protective layer. Thus, active sites on the interfacial asphaltene layer did not obviously increase with further increasing the asphaltene concentration, so the adhesion showed relatively weak dependence on the concentration (>200 mg/L).

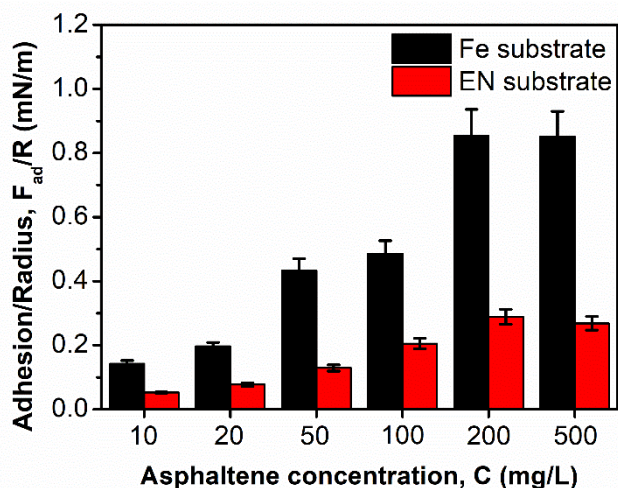


Figure 5.5 The normalized adhesion of a water drop on Fe substrate and EN coating substrate in toluene after aged in asphaltene solutions with different concentrations.

Figure 5.S3 show the measured force profiles between the water drops and EN substrate in toluene after being aged in asphaltene solutions with different concentrations. Figure 5.S3A shows that the interaction force between pure water drop and EN substrate had no obvious change when the water drop approached the substrate in toluene, till a sudden “jump-in” behavior was also observed, indicating the contact of water drop and EN substrate. From the optical microscope, the detachment of the water drop from the AFM cantilever and the following attachment on EN substrate were also directly observed, which was similar with the force measurement between pure water drop and Fe substrate in Figure 5.4A. This behavior could also be contributed by the VDW attraction between the water drop and EN substrate in toluene. However, the force profile for EN substrate didn’t show obvious attraction before the “jump-in” behavior occurred, suggesting that the VDW attraction between the water drop and EN substrate was relatively weaker than that between the water drop and Fe substrate.

Figure 5.S3B-G show the measured force profiles between the water drops with asphaltenes

and EN substrate in toluene after aged in asphaltene solutions at concentrations of 10, 20, 50, 100, 200 and 500 mg/L, respectively. For all the curves, attractive interaction force during approaching was observed. The tendency that the adhesion measured during retraction increased along with the increasing asphaltene concentration was also noticed. Similarly, the adhesion did not change significantly when the concentration was greater than 200 mg/L. The adhesion between the water drops with asphaltenes and Fe or EN substrates are compared as shown in Figure 5.5. It is obvious that the normalized adhesion between the water drop and EN substrate was much weaker than that with Fe surface, suggesting that asphaltenes on the EN substrate could be more easily removed than that on Fe surface. It is noted that EN substrate has a higher surface roughness (rms roughness 4.22 nm) than Fe substrate (rms roughness 1.33 nm). In reported literatures, the increased surface roughness could enhance the adhesion between two rough soft surfaces due to the large contact area, which thus led to the aggravated fouling phenomena.⁶⁷⁻⁷⁰ However, despite the relatively higher surface roughness of EN substrates, the weaker adhesion has been measured between the water drops with interfacial asphaltenes and EN substrate than that with Fe substrate, which further suggests the better antifouling property of EN coating.

5.3.3 Effect of solvent type.

The interactions between the water drop with asphaltenes and Fe or EN substrate were also investigated in heptols (i.e., mixtures of toluene and heptane) and heptane. Here, heptols with different volume fractions of toluene, i.e., 75%, 50% and 25% (denoted as 75% heptol, 50% heptol and 25% heptol) were used. In the experiments, after aged in the 100 mg/L asphaltene-

in-toluene solution for 5 min, a large amount of heptol or heptane was used to replace the asphaltene-in-toluene solution and wash off the free asphaltenes before the Fe or EN substrate was placed in the organic solvent. Due to the irreversible adsorption of asphaltenes,^{36, 38, 71} it was expected that the amount of asphaltenes at the water/oil interface for each water drop was almost the same, and the influences of asphaltenes dissolved in the solution or adsorbed on the substrate surface during the force measurements could be negligible.

Figure 5.S4 show the force results between the water drops with asphaltenes and Fe substrate in heptols (with toluene volume fraction of 75%, 50%, and 25%) and heptane. Similar to the force curve in pure toluene (Figure 5.S2C), attraction was observed during approach and strong adhesion was measured during retraction. It was evident that the adhesion was weakened by decreasing the volume fraction of toluene in heptol. Since heptane is a poor solvent to asphaltenes,^{36, 72-73 36, 72-73 36, 72-73 36, 72-73 36, 72-73 36, 72-73} the addition of heptane could enhance the solvophobic interaction and induce the strong aggregation between asphaltene molecules at the interface. The self-association of the active functional groups of aggregated asphaltenes could lead to less molecular mobility and lower amount of exposed active functional groups for surface adhesion. Therefore, the adhesion between water drop with interfacial asphaltenes and substrate became weakened. In pure heptane (Figure 5.S4D), the measured interaction force between water drop and Fe substrate was attractive and growing stronger during approaching. Finally, the “jump-in” behavior was observed, suggesting the contact of water drop on the Fe substrate. This distinctive “jump-in” behavior could be possibly due to the significantly enhanced aggregation of asphaltenes and their reduced molecular mobility in pure heptane than in heptols, which led to disruption of the protective asphaltene layer at oil/water interface.⁷⁴

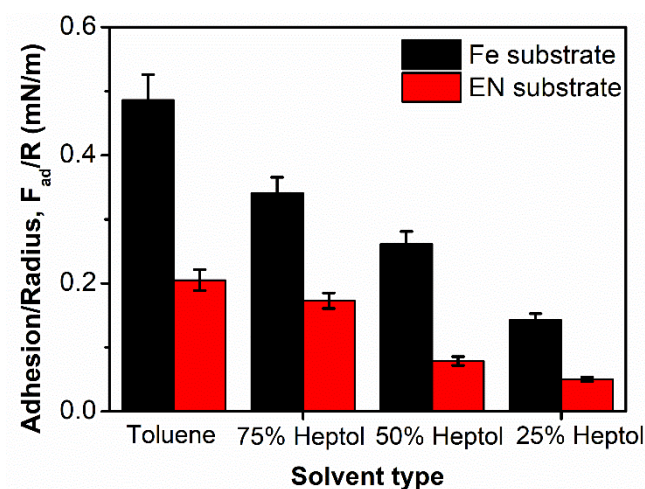


Figure 5.6 The normalized adhesion of a water drop on Fe substrate and EN coating substrate in toluene and heptol.

Figure 5.S5 show the measured force curves between the water drops with asphaltenes and EN substrate in heptols (with toluene volume fraction of 75%, 50%, and 25%) and heptane. Similar force results with Fe substrates in Figure 5.S4 were observed. In heptols, the measured adhesion also became weakened with the decreasing volume fraction of toluene, which was due to the molecular mobility of interfacial asphaltenes and their exposed active functional groups. In pure heptane, the “jump-in” behavior was also observed. The normalized adhesion between the water drop and Fe or EN substrate was summarized in Figure 5.6. It was noticed that the adhesion between water drop with interfacial asphaltenes and EN substrate was weaker than that for Fe substrate, suggesting that the asphaltenes on EN substrate could be more easily removed than that on Fe substrate in different organic solvents.

5.3.4 Effect of aging time.

The effect of aging time was also investigated here. Before force measurements, water drops

were aged in 100 mg/L asphaltene solution for 1, 2, 5, 10, 20 and 30 min, respectively, and 50% heptol was used to replace the solution. The obtained force profiles are shown in Figure 5.S6. All the measured force profiles exhibited adhesion during retraction, which was normalized and summarized in Figure 5.7A.

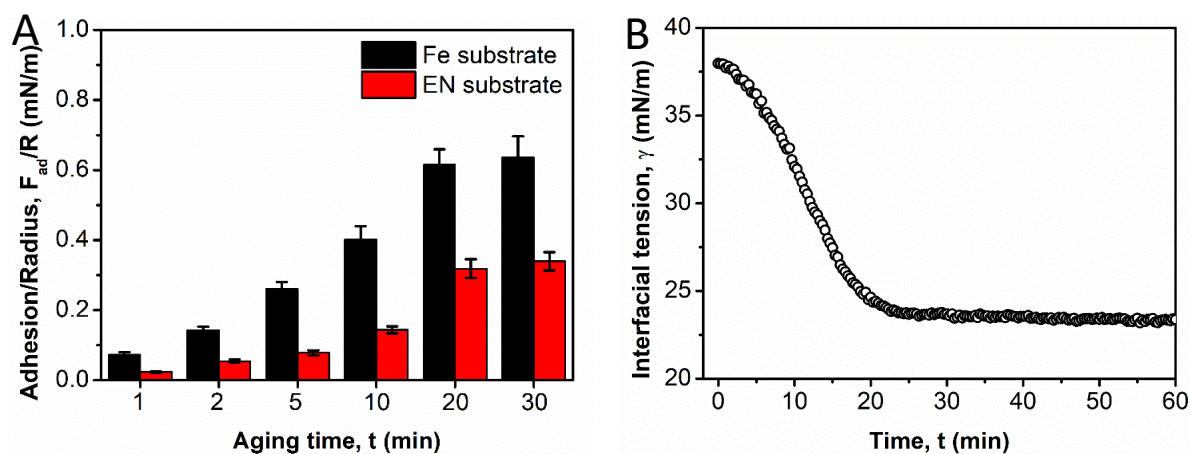


Figure 5.7 (A) The normalized adhesion of a water drop on Fe and EN substrate in 50% heptol after being aged in 100 mg/L asphaltene solution for 1, 2, 5, 10, 20 and 30 min, respectively. (B) Measured dynamic interfacial tension curve of water and 50% heptol with 100 mg/L asphaltenes dissolved.

It was noticed that longer aging time resulted in the stronger adhesion between water drop with interfacial asphaltenes and the Fe or EN substrate, which was caused by more asphaltenes adsorbed at water/oil interface during aging time. However, the adhesion didn't obviously change when the aging time was longer than 20 min for both Fe and EN substrates, which could be the consequence of the saturated adsorption of asphaltenes at water/oil interface. To demonstrate this statement, the adsorption behavior of asphaltenes (100 mg/L) at water/50% heptol interface was investigated by measuring the dynamic interfacial tension using a pendant

drop shape method and the result is shown in Figure 5.7B.⁷⁵ The obtained result showed that the interfacial tension of water/50% heptol interface decreased sharply within 15 min, indicating the rapid adsorption of asphaltenes at the interface. Then, to the decrease of the interfacial tension gradually slows down at 18 ~ 22 min, suggesting the lowered adsorption rate due to the limited interfacial area and steric hindrance of adsorbed asphaltenes.⁷⁵ After ~22 min, the interfacial tension reached a plateau, suggesting the saturated adsorption of asphaltenes at the water/50% heptol interface. Furthermore, Figure 5.7A also shows that the adhesion between water drops with interfacial asphaltenes and EN substrate is much weaker than that for Fe substrate.

5.3.5 Effect of contact time.

The contact time effect was investigated by measuring the force profiles between water drops with interfacial asphaltenes and Fe or EN substrate in 50% heptol, after aged in 100 mg/L asphaltenes solution for 5 min. The water drop probe was driven to approach the substrate till the maximum loading force of 4 nN was reached. Then, this cantilever was held for the contact time of 1, 2, 5 and 10 s, respectively, followed by the retraction from the substrate. The obtained force profiles are shown in Figure 5.S7. The normalized adhesion for both Fe substrate and EN coating substrate is shown in Figure 5.8A. Obviously, much weaker adhesion between water drop and EN substrate in the presence of interfacial asphaltenes was detected than that for Fe substrate under varying contact time. The results also showed that the adhesion was strengthened with longer contact time, which was most likely due to the conformational changes of confined asphaltenes thus leading to stronger contact with the substrate, as illustrated in

Figure 5.8B.

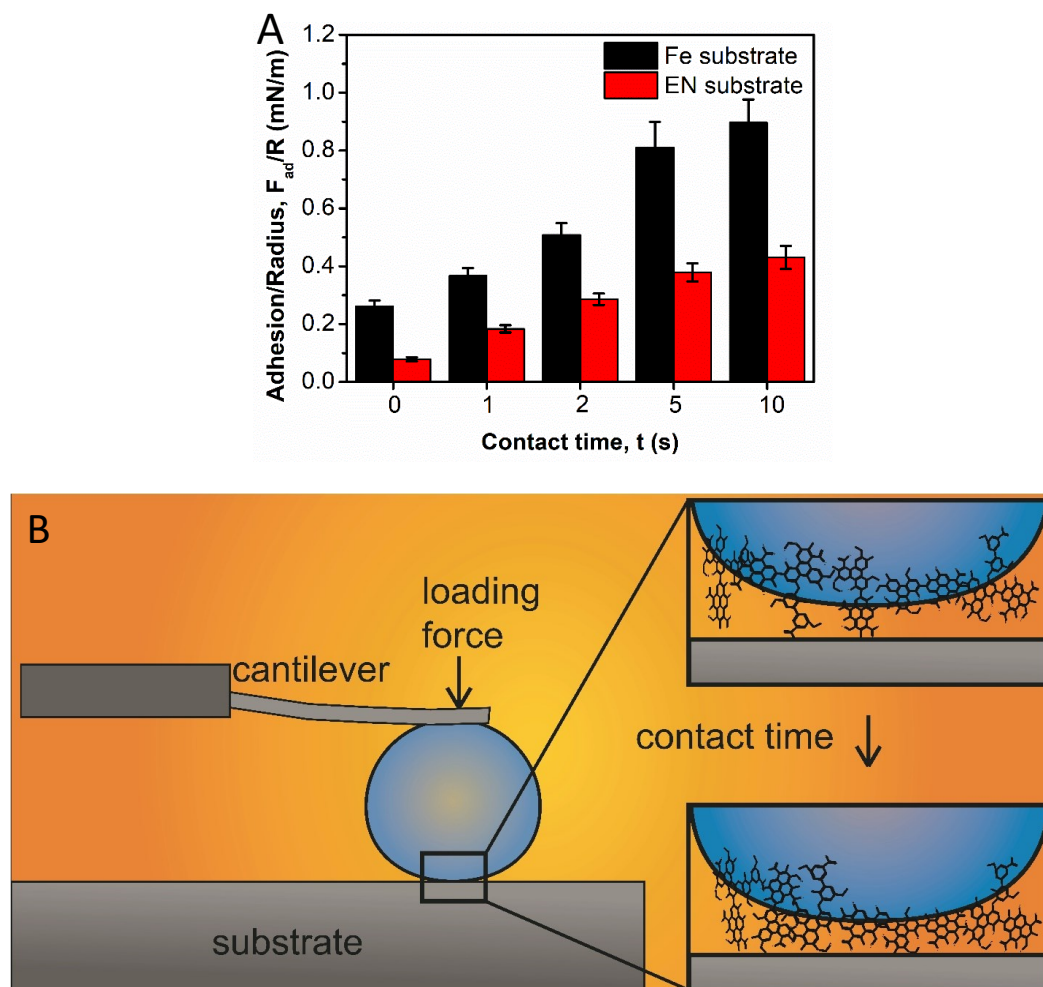


Figure 5.8 (A) The normalized adhesion between a water drop and Fe or EN substrate in 50% heptol after aged in 100 mg/L asphaltenes solutions for 5 min with the contact time of 0, 1, 2, 5 and 10 s, respectively. (B) Schematic of conformational change of confined asphaltenes during contact with the substrate.

5.3.6 Effect of loading force.

The effect of loading force was investigated between the water drop and Fe or EN substrate in 50% heptol after aged in 100 mg/L asphaltene solutions for 5 min with the loading force of

1, 2, 4, 10, 20 and 40 nN, respectively. The measured force profiles are shown in Figure 5.8. Figure 5.9 shows the normalized adhesion between water drops and Fe or EN substrate, which becomes stronger as the loading force increases. The strengthened adhesion is due to the enlarged contact area under higher loading force which facilitates stronger interactions between more confined asphaltenes and substrates. Figure 5.9 also demonstrates that the EN coating showed a weaker adhesion with water drop in the presence of asphaltenes than Fe substrate under different loading conditions.

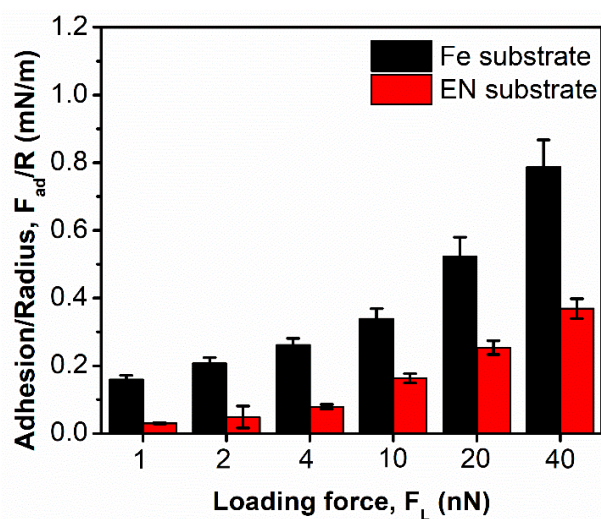


Figure 5.9 The normalized adhesion between the water drop and Fe or EN substrate in 50% heptol after aged in 100 mg/L asphaltenes solutions for 5 min under the loading force of 1, 2, 4, 10, 20 and 40 nN, respectively.

5.3.7 Bulk fouling tests.

To further evaluate the antifouling performances, the bulk fouling tests were conducted with both Fe and EN substrates. The obtained results are shown in Figure 5.10.

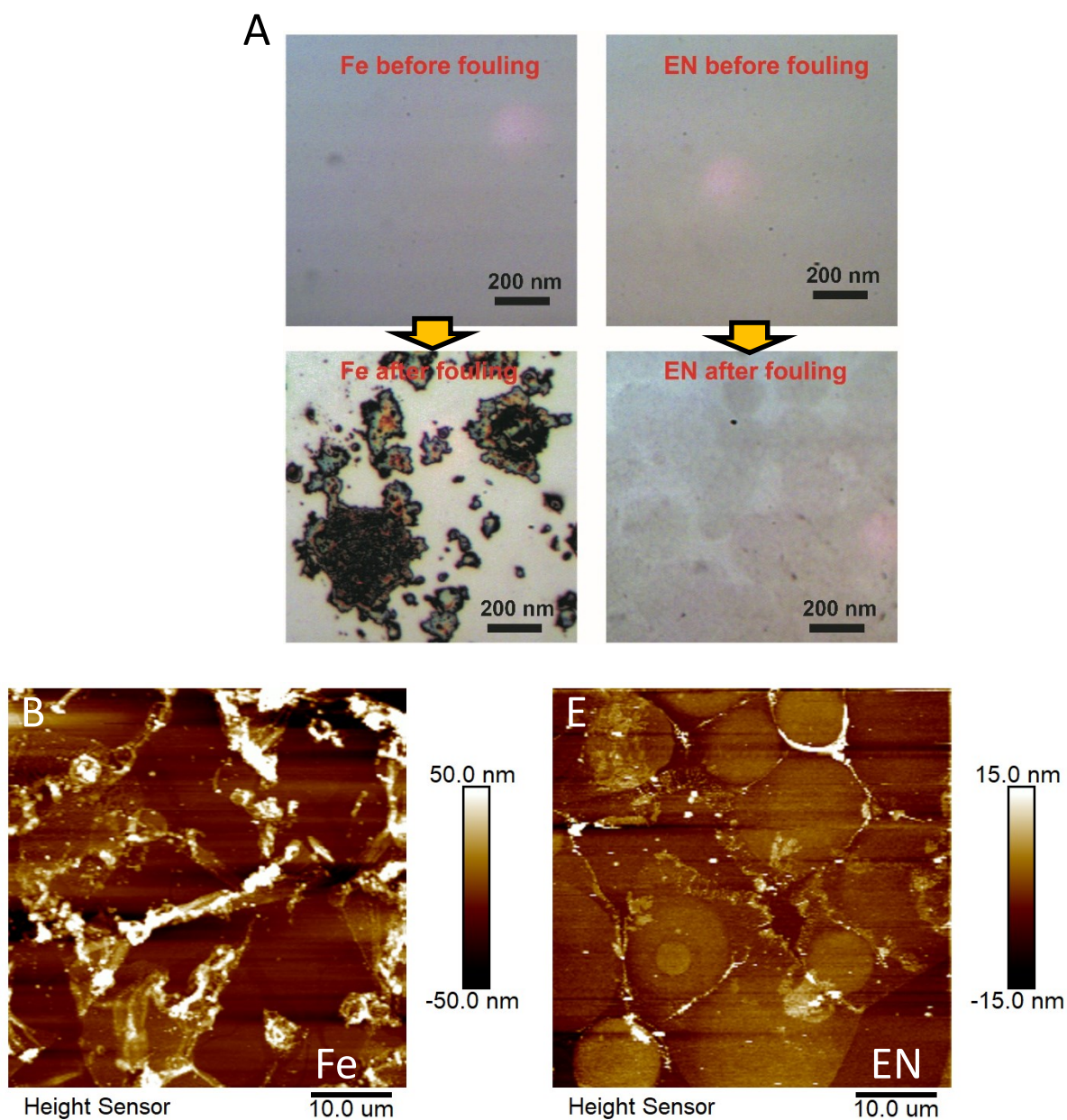


Figure 5.10 (A) Optical images of Fe and EN substrates before and after bulk fouling tests. AFM surface image of Fe (B) and EN (C) substrate after bulk fouling tests.

Figure 5.10A shows the optical images of Fe and EN substrates before and after the bulk fouling tests. Before bulk fouling tests, both Fe and EN substrates were flat and clean. After bulk fouling tests, obvious aggregates were found on the Fe substrate, indicating that Fe substrate could be easily fouled in the water-in-oil emulsion with asphaltenes. However, EN

substrate remained relatively clean with only some grey remnants on the surface. The AFM surface images in Figures 5.10B and C further show that there are a large number of aggregates deposited on the Fe substrate, suggesting the severe fouling phenomenon in the emulsions; whereas the EN substrate showed much less deposits. The rms roughness of the Fe and EN substrates after bulk fouling tests was found to increase to 23.7 nm and 6.4 nm, respectively. Furthermore, the SEM-EDS characterizations have been conducted and the obtained results show that much higher weight percentage for carbon element on Fe substrate has been detected than that on EN substrate (as shown in Figure 5.S9). The above bulk fouling tests demonstrate that EN coating possesses a good antifouling performance in water-in-oil emulsions, agreeing well with the adhesion results from the force measurements.

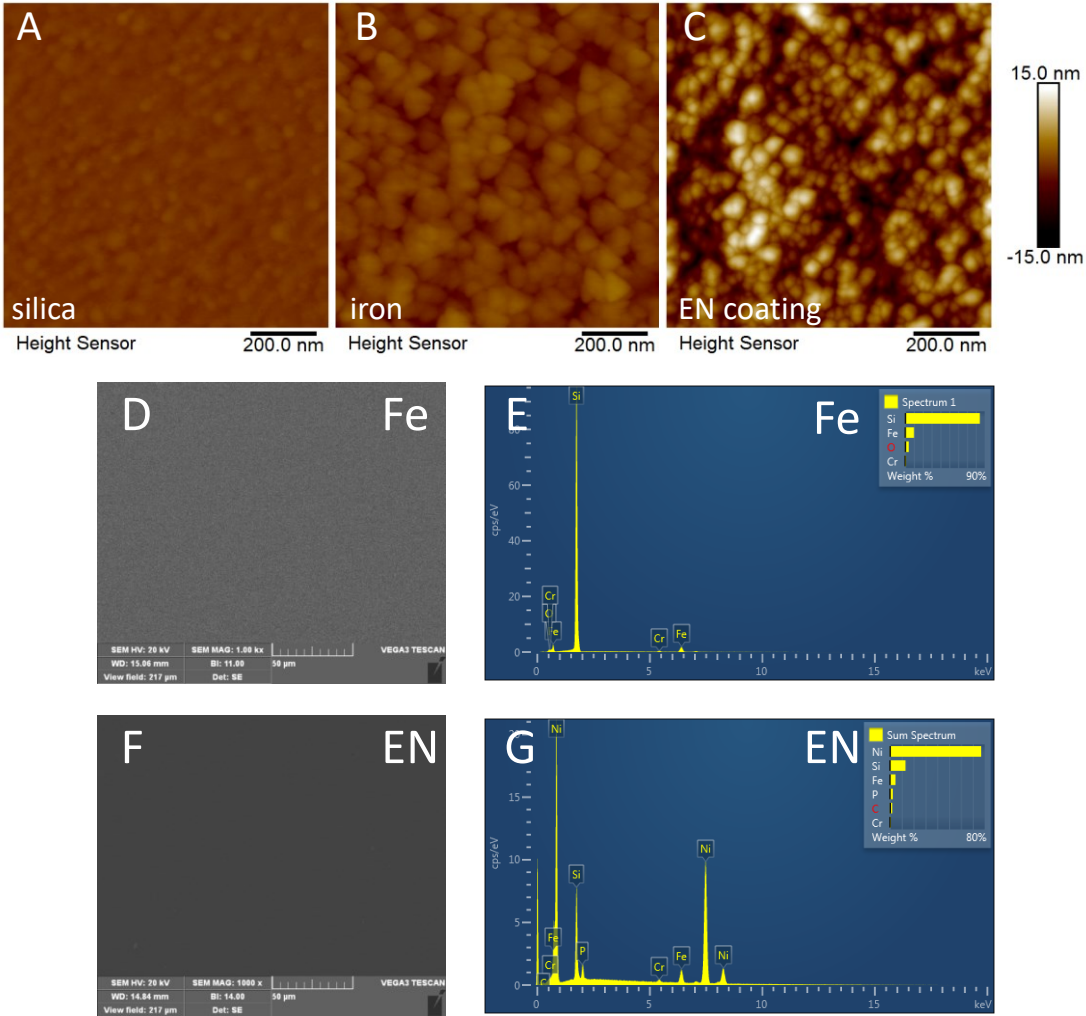
5.4 Conclusions

In this work, the drop probe AFM technique was used to directly measure the surface interaction forces between water drops with asphaltenes adsorbed at the water/oil interface and Fe or EN substrate in organic media. The effects of asphaltene concentration, solvent type, aging time, contact time and loading force were investigated. For bare water drops, the force results revealed that the drops could easily jump into contact with Fe or EN substrate during approaching in oil media because of the strong VDW attraction. For water drops in the presence of asphaltenes, the asphaltenes could form a protective layer at the water/oil interface. The functional groups of the interfacial asphaltenes could interact with the substrate, contributing to the measured adhesion during retraction. It was also noted that the higher asphaltene concentration and longer aging time during the aging process could result in more asphaltenes

adsorbed at the water/oil interface, which then lead to the stronger adhesion between water drop and the substrate. The addition of poor solvent (i.e., heptane) in the organic medium could cause the strong aggregation of asphaltenes, thus lowering the molecular mobility of interfacial asphaltenes and preventing the interactions between the functional groups of asphaltenes and the substrate. Consequently, the weaker adhesion was measured. In pure heptane, the aggregation of interfacial asphaltenes was so strong that the protective layer of interfacial asphaltenes would be disturbed and direct water-substrate contact could occur. Hence, “jump-in” behavior of the water drop on the substrate was observed. The longer contact time during the force measurements could allow interfacial asphaltenes to change their conformation and have stronger interaction with the substrate. The stronger loading force could enlarge the contact area of the water drop on the substrate and include more interfacial asphaltenes within the contact area, which thereby strengthened the adhesion between water drop and substrate. Meanwhile, much weaker adhesion was measured between water drop with interfacial asphaltenes and EN substrate than that for Fe substrate, suggesting that asphaltenes on EN substrate could be more easily removed than that on Fe substrate. Furthermore, the bulk fouling tests in water-in-oil emulsions also demonstrated that more significant fouling phenomenon was detected on Fe substrate than that on EN substrate, which agreed well with the force measurement results. This work improves the fundamental understanding of the surface interactions between water-in-oil emulsions with asphaltenes and iron substrate or EN coating, demonstrates the antifouling properties of EN coating, and provides useful information on the intermolecular and surface interactions contributing to the fouling phenomena in oil production. Such information helps the design and selection of coating materials and facilitates the

development of new efficient coatings with antifouling performances in related industrial applications.

5.5 Support information



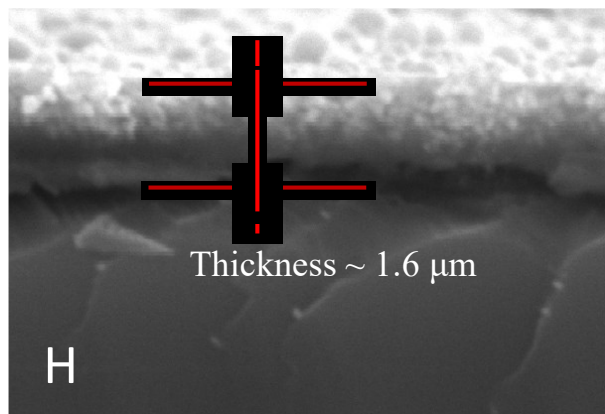
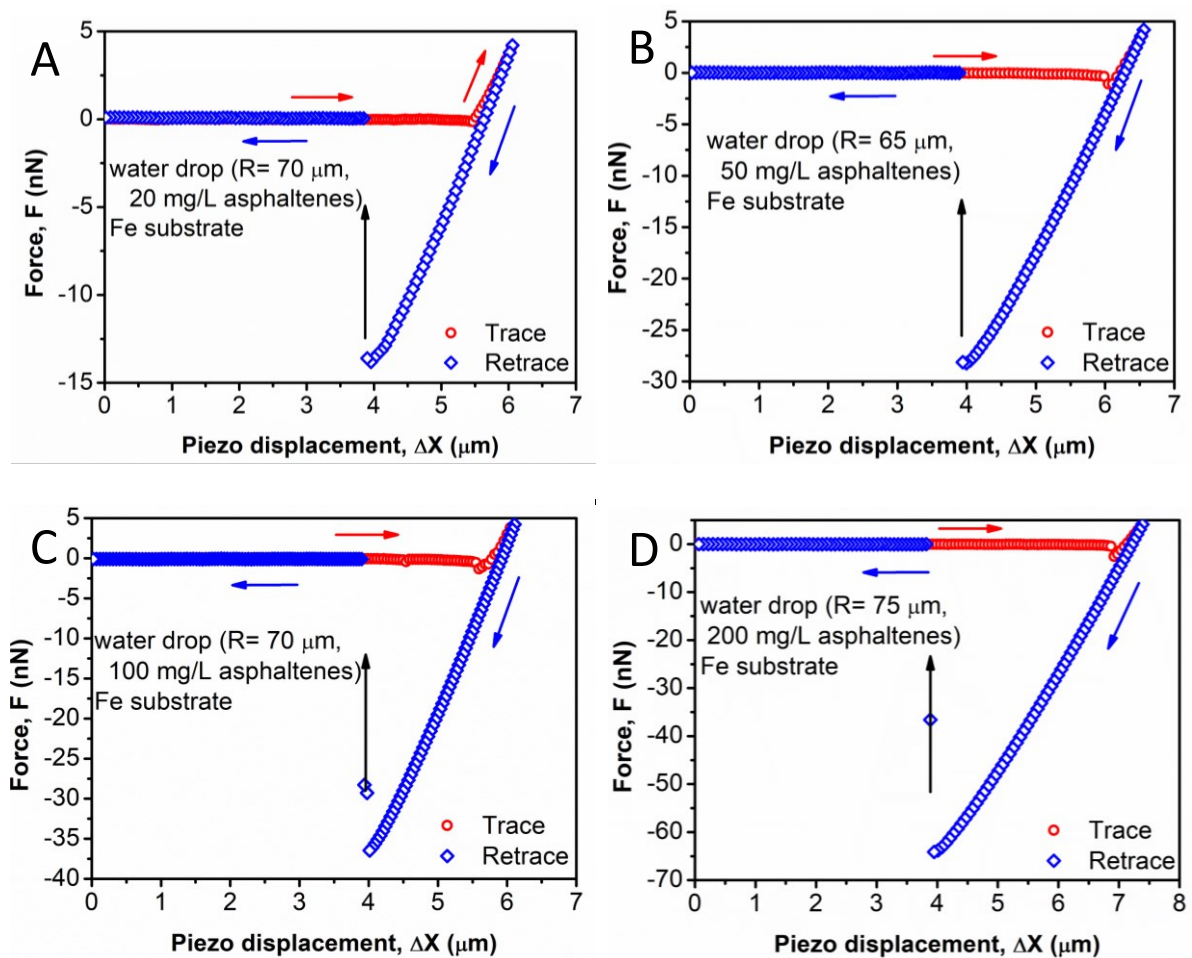


Figure 5.S1 AFM images of (A) silica substrate, (B) Fe substrate and (C) EN substrate. The SEM images (D, F) and EDS results (E, G) of Fe and EN substrate. (H) The SEM image of the cross section of EN substrate.



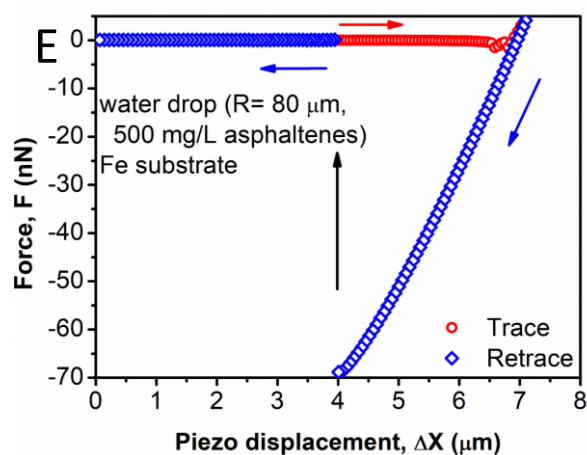
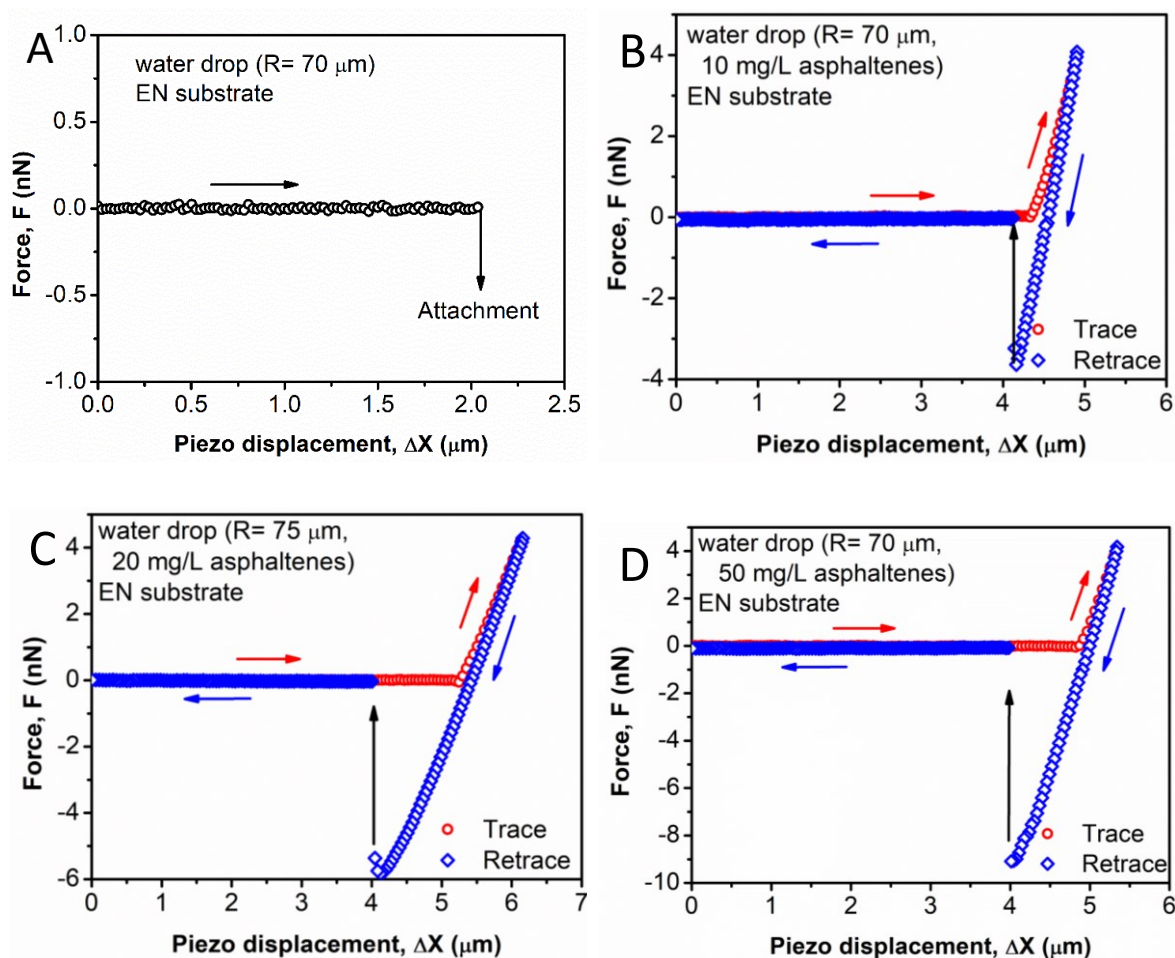


Figure 5.S2 Measured force profiles between a water drop and Fe substrate in toluene after aged in (A) 20, (B) 50, (C) 100, (D) 200, and (E) 500 mg/L asphaltene solutions for 5 min. The open dots are experimental data. The arrows show the movements of water drops.



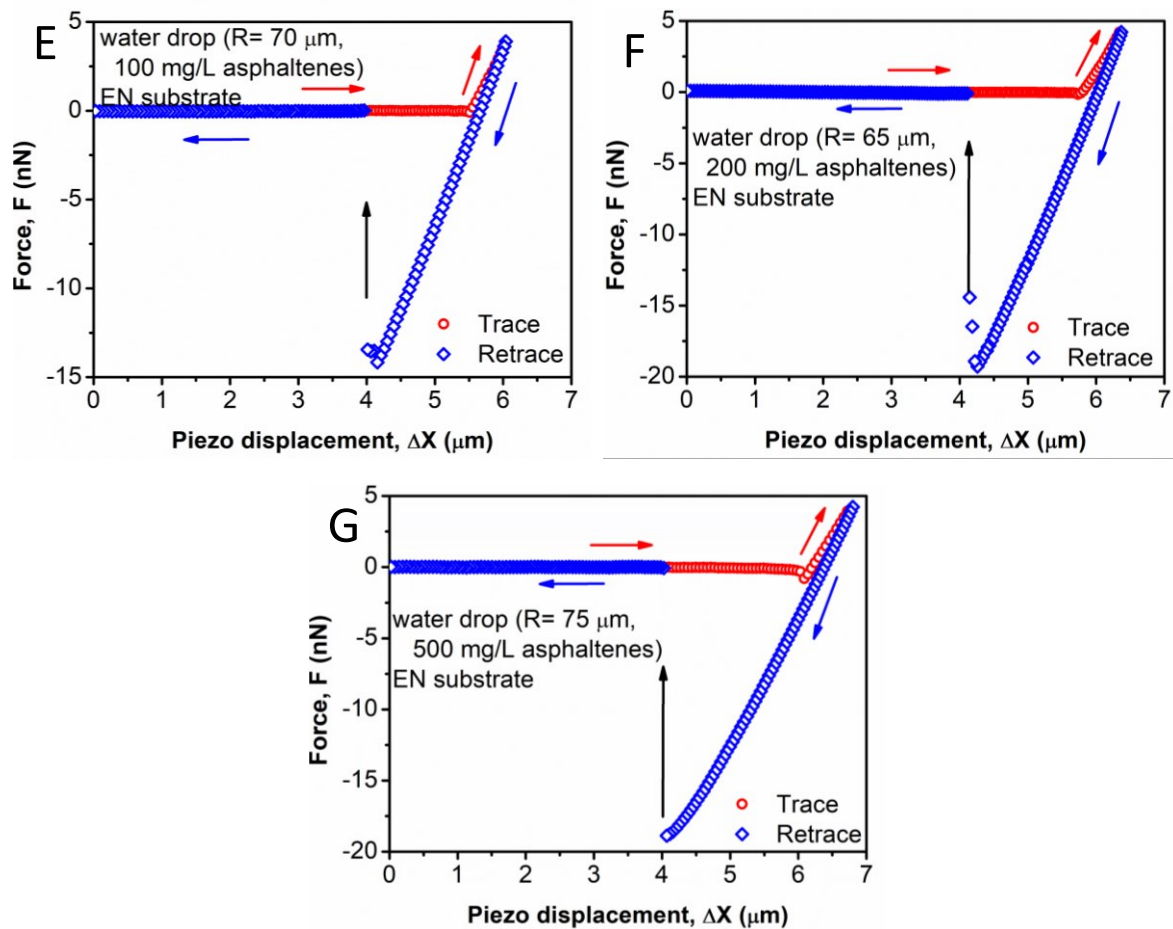
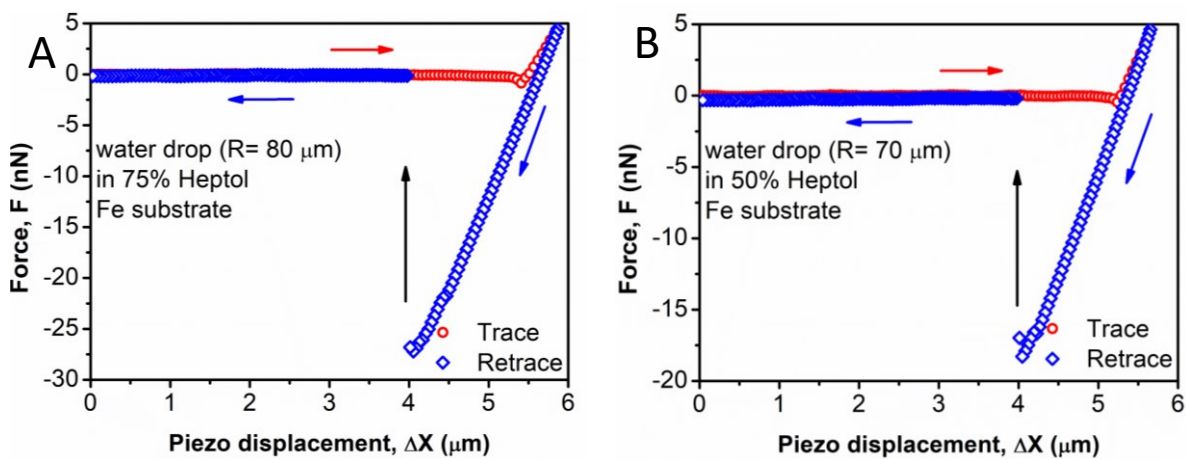


Figure 5.S3 Measured force profiles between a water drop and EN substrate in toluene after aged in (A) 0, (B) 10, (C) 20, (D) 50, (E) 100, (F) 200, and (G) 500 mg/L asphaltene solutions for 5 min.



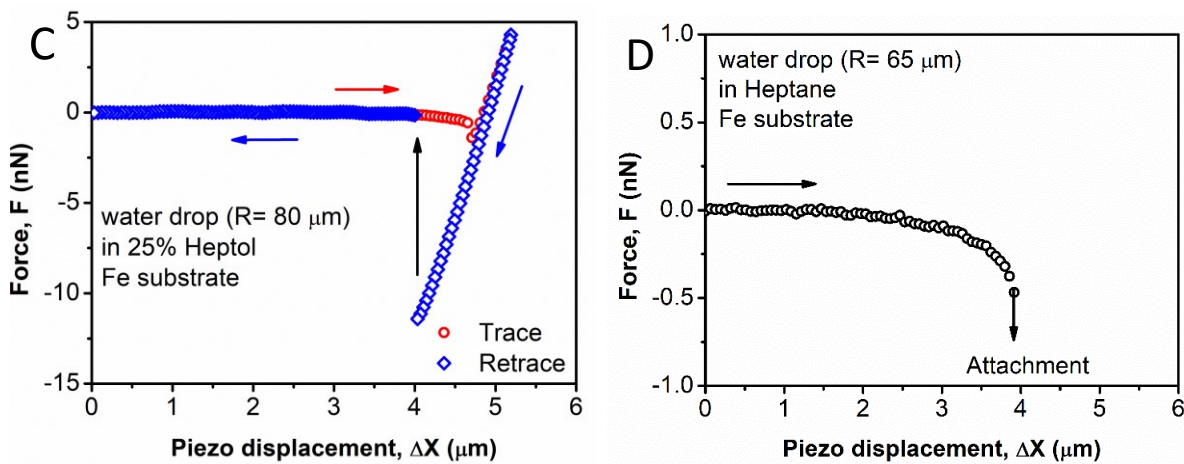
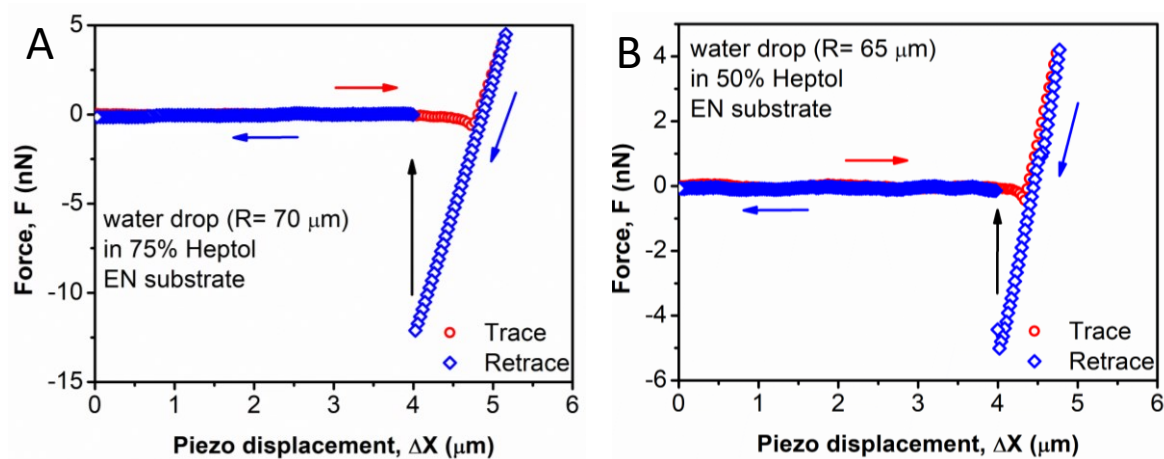


Figure 5.S4 Measured force profiles between a water drop and Fe substrate in (A) heptol with 75% volume fraction of toluene (denoted as 75% heptol), (B) 50% heptol, (C) 25% heptol and (D) heptane, after aged in 100 mg/L asphaltene solutions for 5 min. The percentage is the volume ratio of toluene.



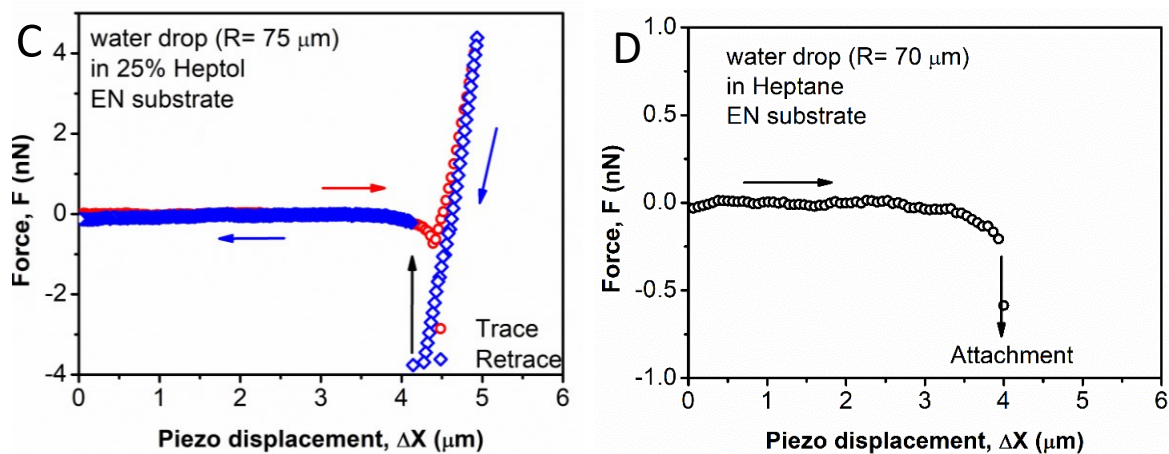
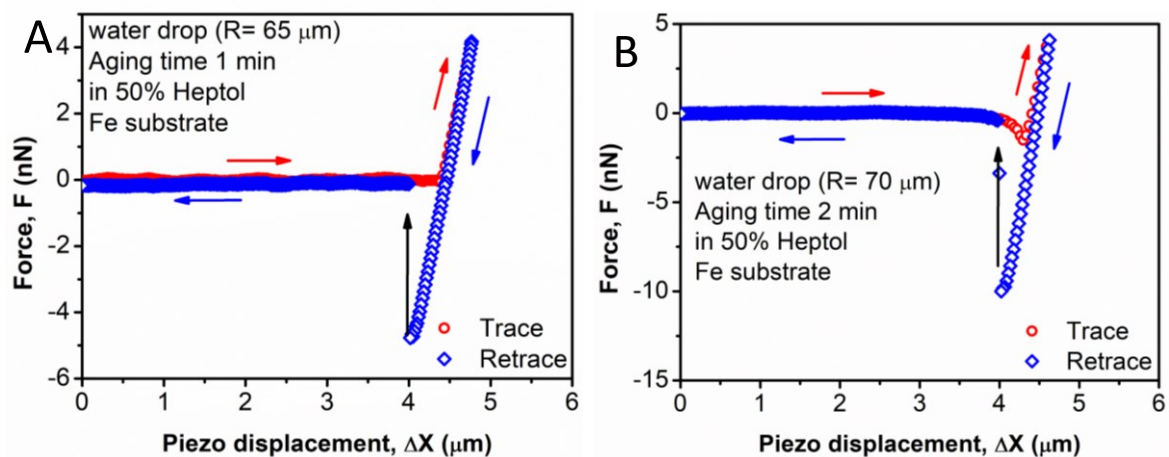
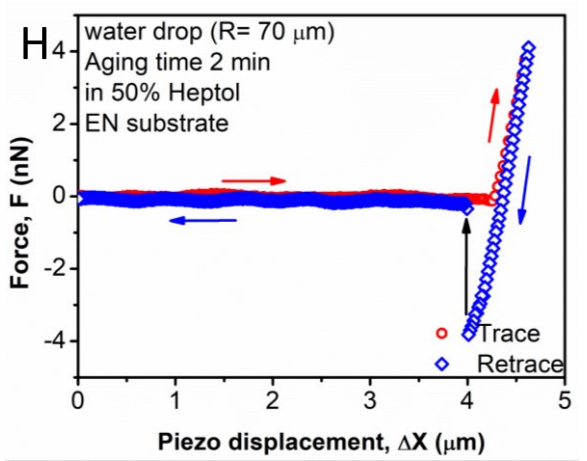
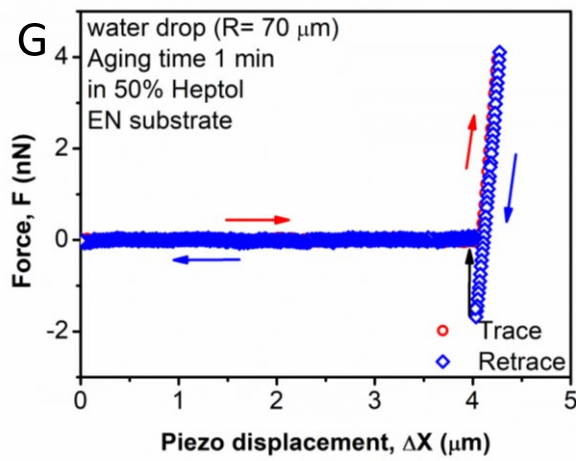
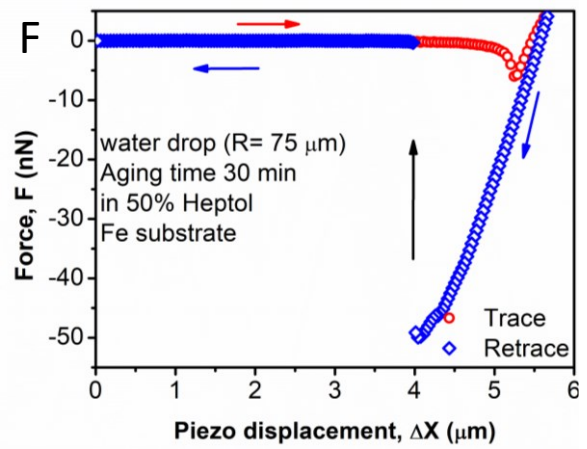
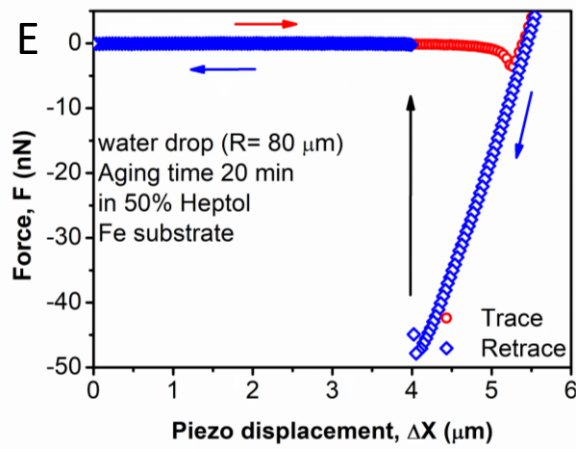
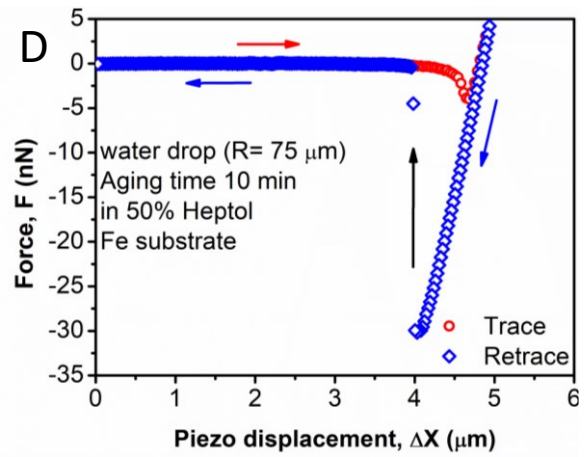
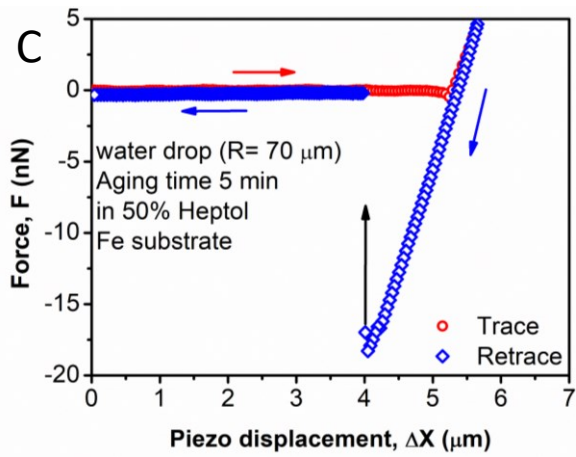


Figure 5.S5 Measured force profiles between the water drop and EN substrate in (A) heptol with 75% volume fraction of toluene (denoted as 75% heptol), (B) 50% heptol, (C) 25% heptol and (D) heptane, after aged in 100 mg/L asphaltene solutions for 5 min. The percentages in the figures are the volume ratios of toluene.





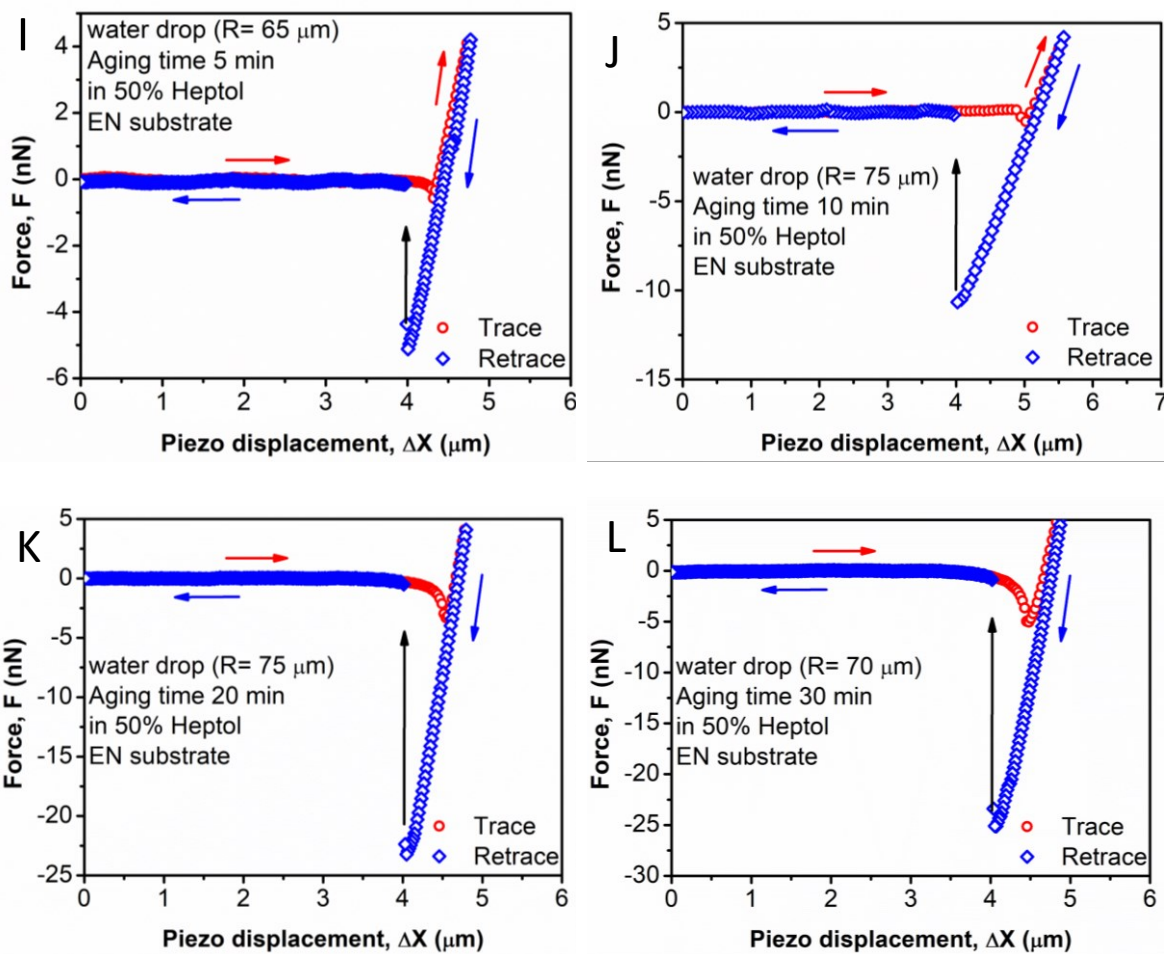
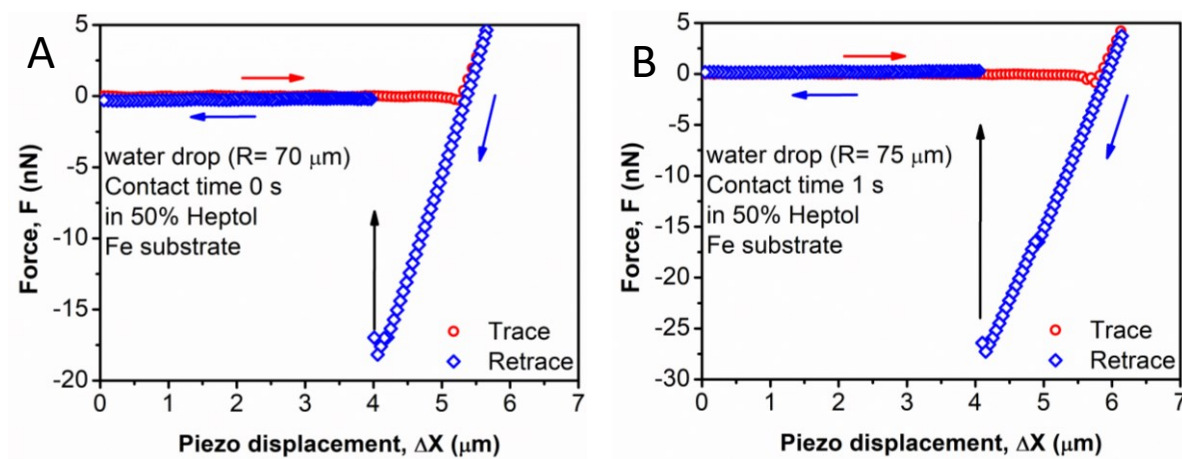
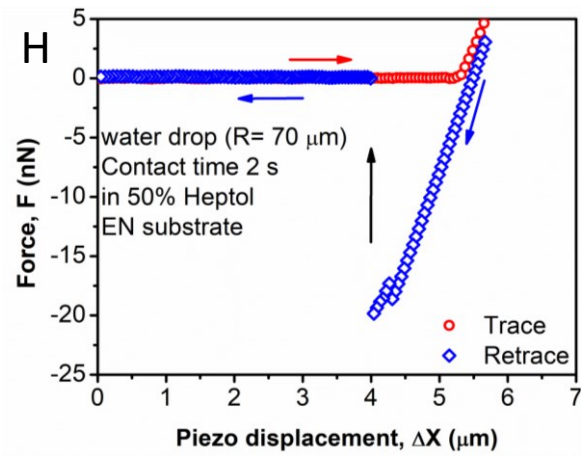
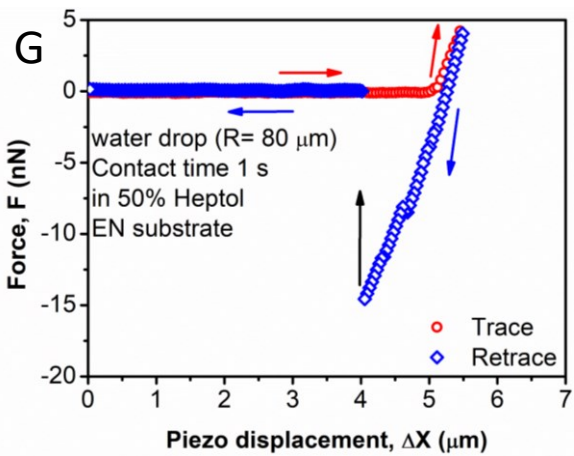
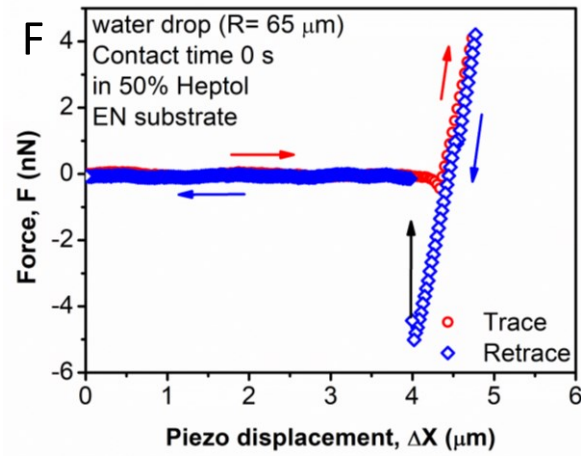
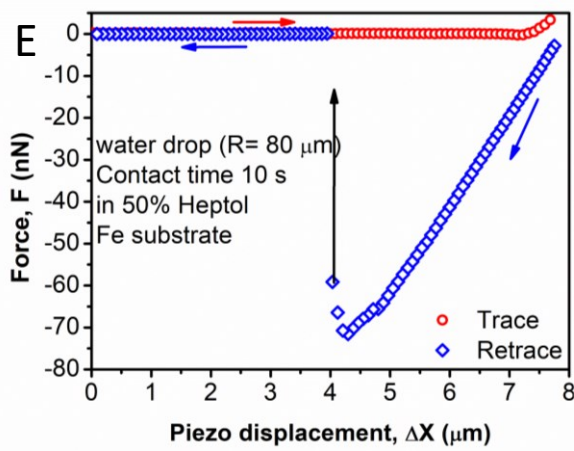
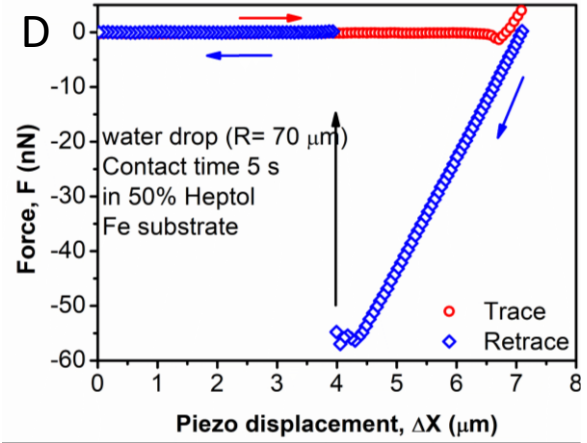
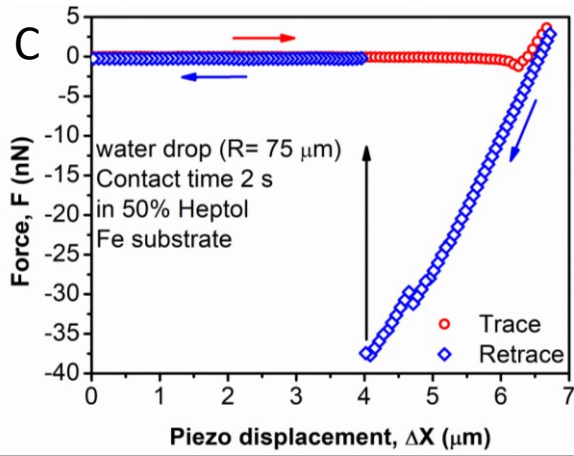


Figure 5.S6 Measured force profiles of a water drop with Fe substrate (A-F) and EN substrate (G-L) in 50% heptol, after aged in 100 mg/L asphaltenes solutions for 1, 2, 5, 10, 20 and 30 min.





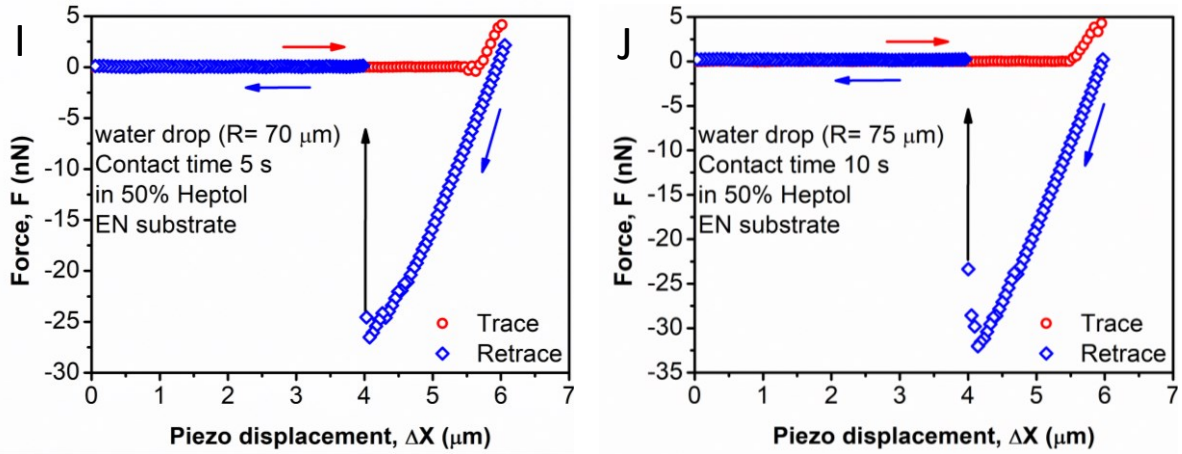
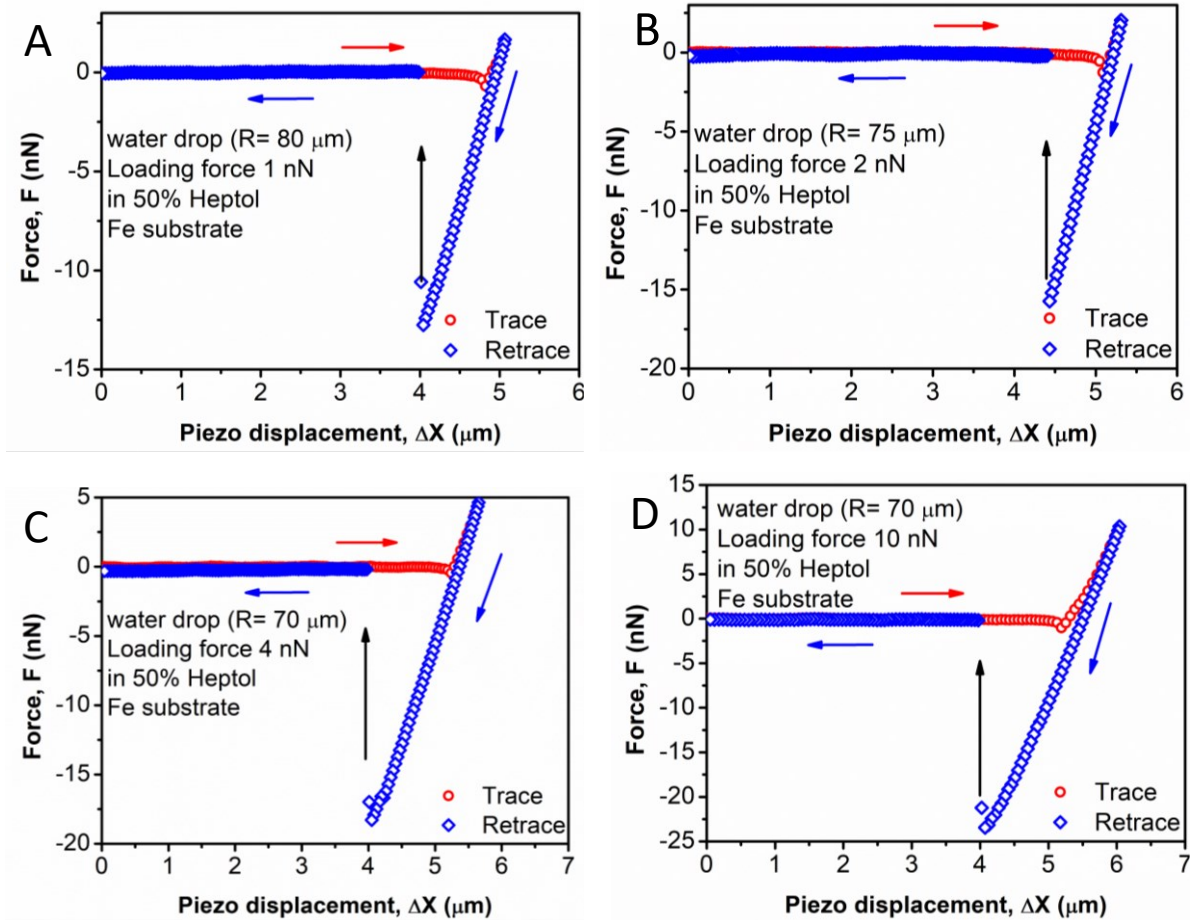
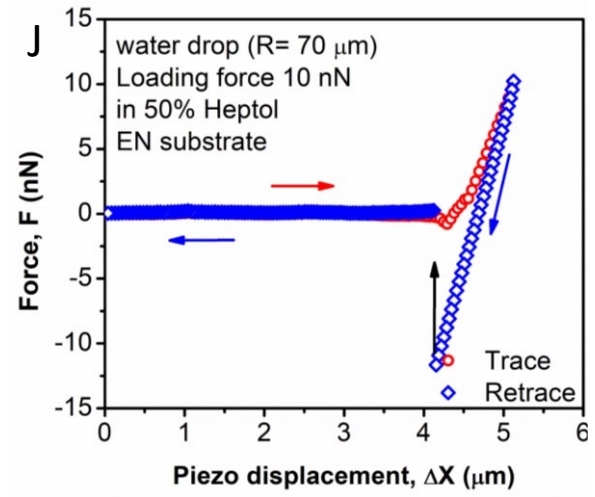
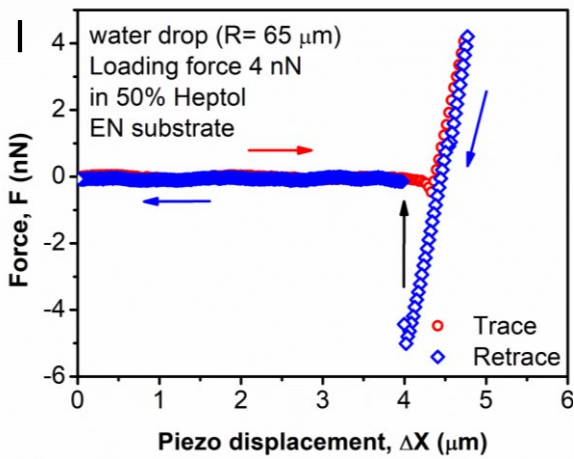
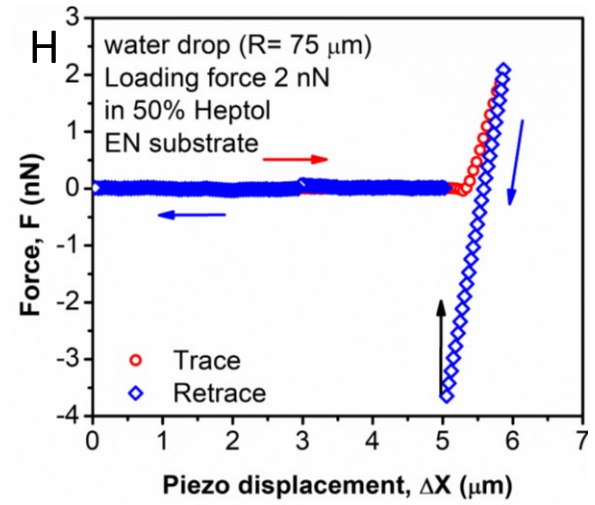
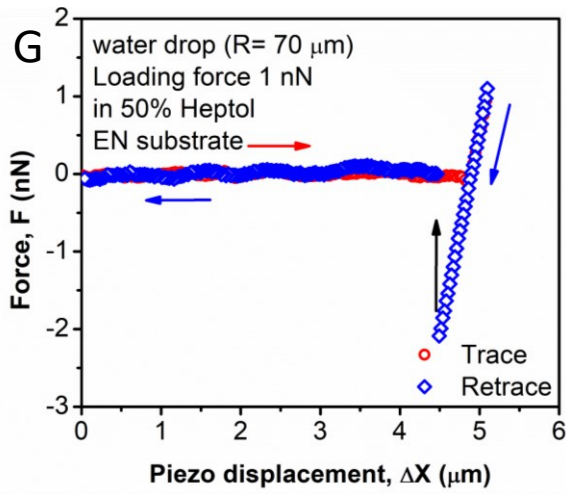
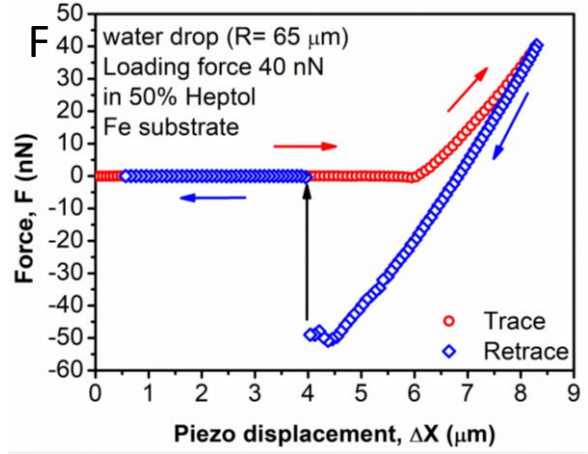
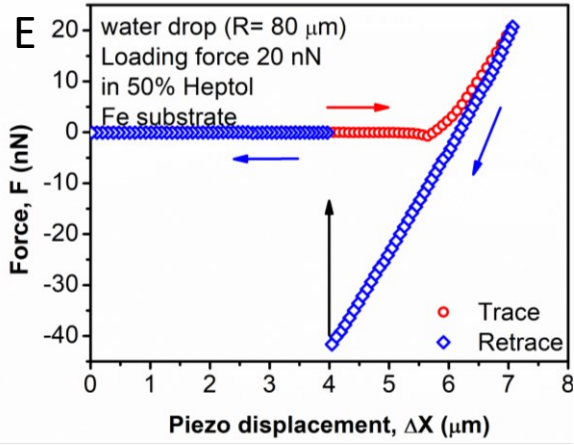


Figure 5.S7 Measured force profiles of a water drop with Fe substrate (A-E) and EN substrate (F-J) in 50% heptol, after aged in 100 mg/L asphaltenes solutions for 5 min, with the contact time of 0, 1, 2, 5 and 10 s.





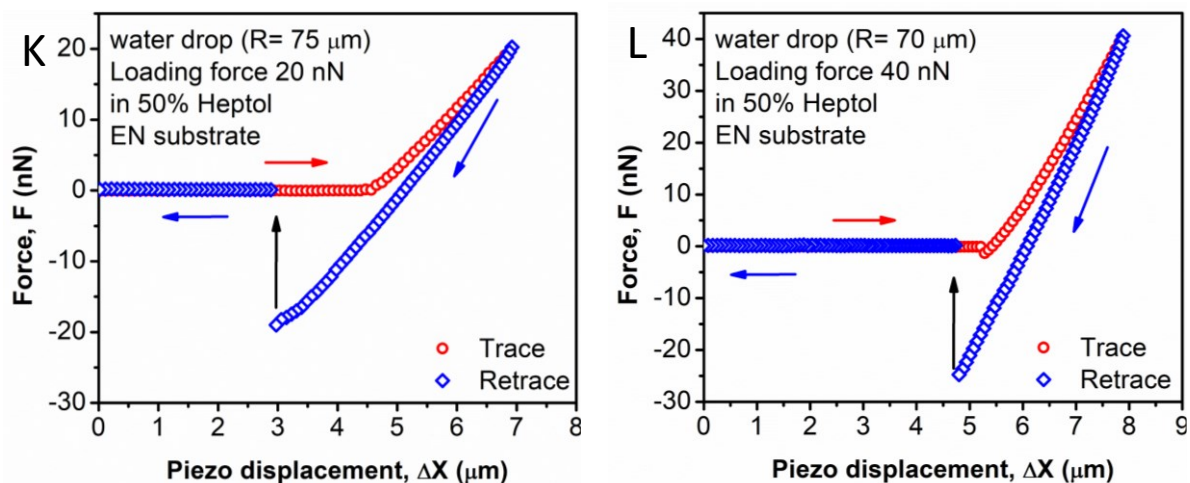


Figure 5.S8 Measured force profiles of a water drop with Fe substrate (A-F) and EN substrate (G-L) in 50% heptol, after aged in 100 mg/L asphaltenes solutions for 5 min, with the loading force of 1, 2, 4, 10, 20 and 40 nN.

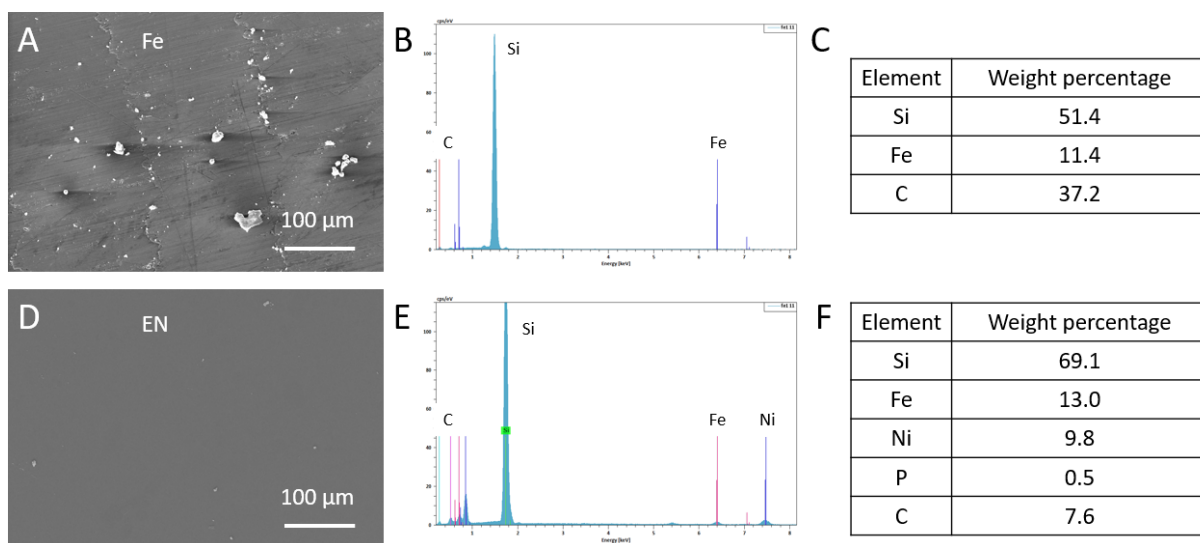


Figure 5.S9 SEM images, EDS element analysis and obtained elemental weight percentages for Fe (A, B and C) and EN (D, E and F) substrates after the bulk fouling tests.

Reference

1. Yang, F.; Tchoukov, P.; Dettman, H.; Teklebrhan, R. B.; Liu, L.; Dabros, T.; Czarnecki, J.; Masliyah, J.; Xu, Z., Asphaltene subfractions responsible for stabilizing water-in-crude oil emulsions. Part 2: Molecular representations and molecular dynamics simulations. *Energy & Fuels* **2015**, *29* (8), 4783-4794.
2. Czarnecki, J.; Tchoukov, P.; Dabros, T.; Xu, Z., Role of asphaltenes in stabilisation of water in crude oil emulsions. *The Canadian Journal of Chemical Engineering* **2013**, *91* (8), 1365-1371.
3. Li, M.; Xu, M.; Ma, Y.; Wu, Z.; Christy, A. A., Interfacial film properties of asphaltenes and resins. *Fuel* **2002**, *81* (14), 1847-1853.
4. Long, Y.; Dabros, T.; Hamza, H., Stability and settling characteristics of solvent-diluted bitumen emulsions. *Fuel* **2002**, *81* (15), 1945-1952.
5. Lu, Q.; Huang, J.; Maan, O.; Liu, Y.; Zeng, H., Probing molecular interaction mechanisms of organic fouling on polyamide membrane using a surface forces apparatus: implication for wastewater treatment. *Science of The Total Environment* **2018**, *622*, 644-654.
6. Xia, Y.; Adibnia, V.; Huang, R.; Murschel, F.; Faivre, J.; Xie, G.; Olszewski, M.; De Crescenzo, G.; Qi, W.; He, Z., Biomimetic Bottlebrush Polymer Coatings for Fabrication of Ultralow Fouling Surfaces. *Angewandte Chemie* **2019**, *131* (5), 1322-1328.
7. Srinivasan, M.; Watkinson, A., Fouling of some Canadian crude oils. *Heat transfer engineering* **2005**, *26* (1), 7-14.
8. Collins, I. In *A new model for mineral scale adhesion*, International Symposium on Oilfield Scale, Society of Petroleum Engineers: 2002.

9. Gentzis, T.; Parker, R.; McFarlane, R., Microscopy of fouling deposits in bitumen furnaces. *Fuel* **2000**, *79* (10), 1173-1184.
10. Bott, T., General fouling problems. In *Fouling Science and Technology*, Springer: 1988; pp 3-14.
11. Kazi, S.; Duffy, G.; Chen, X., Mineral scale formation and mitigation on metals and a polymeric heat exchanger surface. *Appl. Therm. Eng.* **2010**, *30* (14-15), 2236-2242.
12. Leontaritis, K. In *Asphaltene deposition: A comprehensive description of problem manifestations and modeling approaches*, SPE production operations symposium, Society of Petroleum Engineers: 1989.
13. Wiehe, I. A.; Kennedy, R. J.; Dickakian, G., Fouling of nearly incompatible oils. *Energy & fuels* **2001**, *15* (5), 1057-1058.
14. Bennett, C. A.; Kistler, R. S.; Nangia, K.; Al-Ghawas, W.; Al-Hajji, N.; Al-Jemaz, A., Observation of an isokinetic temperature and compensation effect for high-temperature crude oil fouling. *Heat Transfer Engineering* **2009**, *30* (10-11), 794-804.
15. Hammami, A.; Ratulowski, J., Precipitation and deposition of asphaltenes in production systems: A flow assurance overview. In *Asphaltenes, heavy oils, and petroleomics*, Springer: 2007; pp 617-660.
16. Asomaning, S. Heat exchanger fouling by petroleum asphaltenes. University of British Columbia, 1997.
17. Awad, M. M., Fouling of heat transfer surfaces. In *Heat Transfer-Theoretical Analysis, Experimental Investigations and Industrial Systems*, InTech: 2011.
18. Shi, C.; Zhang, L.; Xie, L.; Lu, X.; Liu, Q.; He, J.; Mantilla, C. A.; Van den Berg, F. G.;

- Zeng, H., Surface interaction of water-in-oil emulsion droplets with interfacially active asphaltenes. *Langmuir* **2017**, *33* (5), 1265-1274.
19. Adams, J. J., Asphaltene adsorption, a literature review. *Energy & Fuels* **2014**, *28* (5), 2831-2856.
20. Rana, M. S.; Samano, V.; Ancheyta, J.; Diaz, J., A review of recent advances on process technologies for upgrading of heavy oils and residua. *Fuel* **2007**, *86* (9), 1216-1231.
21. Mendoza de la Cruz, J. L.; Argüelles-Vivas, F. J.; Matías-Pérez, V. c.; Durán-Valencia, C. d. l. A.; López-Ramírez, S. n., Asphaltene-induced precipitation and deposition during pressure depletion on a porous medium: an experimental investigation and modeling approach. *Energy & Fuels* **2009**, *23* (11), 5611-5625.
22. Drummond, C.; Israelachvili, J., Fundamental studies of crude oil–surface water interactions and its relationship to reservoir wettability. *Journal of Petroleum Science and Engineering* **2004**, *45* (1-2), 61-81.
23. Natarajan, A.; Xie, J.; Wang, S.; Liu, Q.; Masliyah, J.; Zeng, H.; Xu, Z., Understanding molecular interactions of asphaltenes in organic solvents using a surface force apparatus. *The Journal of Physical Chemistry C* **2011**, *115* (32), 16043-16051.
24. Shi, C.; Zhang, L.; Xie, L.; Lu, X.; Liu, Q.; He, J.; Mantilla, C. A.; Zeng, H., Surface Interaction of Water-in-Oil Emulsion Droplets with Interfacially Active Asphaltenes. *Langmuir* **2017**, *33* (5), 1265-1274.
25. Mullins, O. C., The asphaltenes. *Annual review of analytical chemistry* **2011**, *4*, 393-418.
26. Mullins, O. C.; Sheu, E. Y., *Structures and dynamics of asphaltenes*. Springer Science & Business Media: 2013.

27. Gray, M. R.; Tykwinski, R. R.; Stryker, J. M.; Tan, X., Supramolecular assembly model for aggregation of petroleum asphaltenes. *Energy & Fuels* **2011**, *25* (7), 3125-3134.
28. Langevin, D.; Argillier, J.-F., Interfacial behavior of asphaltenes. *Advances in colloid and interface science* **2016**, *233*, 83-93.
29. Eyssautier, J. l.; Levitz, P.; Espinat, D.; Jestin, J.; Gummel, J. r. m.; Grillo, I.; Barré, L. c., Insight into asphaltene nanoaggregate structure inferred by small angle neutron and X-ray scattering. *J. Phys. Chem. B* **2011**, *115* (21), 6827-6837.
30. Visser, J., Particle adhesion and removal: A review. *Particulate science and technology* **1995**, *13* (3-4), 169-196.
31. Faille, C.; Jullien, C.; Fontaine, F.; Bellon-Fontaine, M.-N.; Slomianny, C.; Benezech, T., Adhesion of Bacillus spores and Escherichia coli cells to inert surfaces: role of surface hydrophobicity. *Can. J. Microbiol.* **2002**, *48* (8), 728-738.
32. Lee, S.; Elimelech, M., Relating organic fouling of reverse osmosis membranes to intermolecular adhesion forces. *Environmental science & technology* **2006**, *40* (3), 980-987.
33. Choo, K.-H.; Lee, C.-H., Understanding membrane fouling in terms of surface free energy changes. *J. Colloid Interface Sci.* **2000**, *226* (2), 367-370.
34. Bartels, L., Tailoring molecular layers at metal surfaces. *Nature chemistry* **2010**, *2* (2), 87.
35. Ye, Q.; Zhou, F.; Liu, W., Bioinspired catecholic chemistry for surface modification. *Chemical Society Reviews* **2011**, *40* (7), 4244-4258.
36. Mikami, Y.; Liang, Y.; Matsuoka, T.; Boek, E. S., Molecular dynamics simulations of asphaltenes at the oil–water interface: from nanoaggregation to thin-film formation. *Energy & Fuels* **2013**, *27* (4), 1838-1845.

37. Alvarez, G.; Jestin, J.; Argillier, J.; Langevin, D., Small-angle neutron scattering study of crude oil emulsions: Structure of the oil– water interfaces. *Langmuir* **2009**, *25* (7), 3985-3990.
38. Tchoukov, P.; Yang, F.; Xu, Z.; Dabros, T.; Czarnecki, J.; Sjöblom, J., Role of asphaltenes in stabilizing thin liquid emulsion films. *Langmuir* **2014**, *30* (11), 3024-3033.
39. Yarranton, H. W.; Hussein, H.; Masliyah, J. H., Water-in-hydrocarbon emulsions stabilized by asphaltenes at low concentrations. *J. Colloid Interface Sci.* **2000**, *228* (1), 52-63.
40. Shi, C.; Zhang, L.; Xie, L.; Lu, X.; Liu, Q.; Mantilla, C. A.; van den Berg, F. G.; Zeng, H., Interaction mechanism of oil-in-water emulsions with asphaltenes determined using droplet probe AFM. *Langmuir* **2016**, *32* (10), 2302-2310.
41. Rocha, J.; Baydak, E.; Yarranton, H.; Sztukowski, D.; Ali-Marcano, V.; Gong, L.; Shi, C.; Zeng, H., Role of aqueous phase chemistry, interfacial film properties, and surface coverage in stabilizing water-in-bitumen emulsions. *Energy & Fuels* **2016**, *30* (7), 5240-5252.
42. Zhang, L.; Shi, C.; Lu, Q.; Liu, Q.; Zeng, H., Probing molecular interactions of asphaltenes in heptol using a surface forces apparatus: Implications on stability of water-in-oil emulsions. *Langmuir* **2016**, *32* (19), 4886-4895.
43. Zhang, L.; Xie, L.; Shi, C.; Huang, J.; Liu, Q.; Zeng, H., Mechanistic Understanding of Asphaltene Surface Interactions in Aqueous Media. *Energy & Fuels* **2016**, *31* (4), 3348-3357.
44. Huang, Y.; Zeng, X.; Hu, X.; Liu, F., Corrosion resistance properties of electroless nickel composite coatings. *Electrochim. Acta* **2004**, *49* (25), 4313-4319.
45. Rabizadeh, T.; Allahkaram, S. R.; Zarebidaki, A., An investigation on effects of heat treatment on corrosion properties of Ni–P electroless nano-coatings. *Materials & Design* **2010**, *31* (7), 3174-3179.

46. Sahoo, P.; Das, S. K., Tribology of electroless nickel coatings—a review. *Materials & Design* **2011**, *32* (4), 1760-1775.
47. Brenner, A.; Riddell, G. E., Deposition of nickel and cobalt by chemical reduction. *J. Res. Nat. Bur. Stand* **1947**, *39*, 385-395.
48. Grosjean, A.; Rezrazi, M.; Takadoum, J.; Bercot, P., Hardness, friction and wear characteristics of nickel-SiC electroless composite deposits. *Surf. Coat. Technol.* **2001**, *137* (1), 92-96.
49. Chen, C.; Feng, H.; Lin, H.; Hon, M.-H., The effect of heat treatment on the microstructure of electroless Ni–P coatings containing SiC particles. *Thin Solid Films* **2002**, *416* (1-2), 31-37.
50. Sudagar, J.; Lian, J.; Sha, W., Electroless nickel, alloy, composite and nano coatings—A critical review. *J. Alloys Compd.* **2013**, *571*, 183-204.
51. Chen, X.; Chen, C.; Xiao, H.; Liu, H.; Zhou, L.; Li, S.; Zhang, G., Dry friction and wear characteristics of nickel/carbon nanotube electroless composite deposits. *Tribology international* **2006**, *39* (1), 22-28.
52. Luo, H.; Leitch, M.; Behnamian, Y.; Ma, Y.; Zeng, H.; Luo, J.-L., Development of electroless Ni–P/nano-WC composite coatings and investigation on its properties. *Surface and Coatings Technology* **2015**, *277*, 99-106.
53. Shi, C.; Chan, D. Y.; Liu, Q.; Zeng, H., Probing the hydrophobic interaction between air bubbles and partially hydrophobic surfaces using atomic force microscopy. *The Journal of Physical Chemistry C* **2014**, *118* (43), 25000-25008.
54. Shi, C.; Cui, X.; Xie, L.; Liu, Q.; Chan, D. Y.; Israelachvili, J. N.; Zeng, H., Measuring forces and spatiotemporal evolution of thin water films between an air bubble and solid surfaces

of different hydrophobicity. *ACS nano* **2014**, *9* (1), 95-104.

55. Khodakarami, M.; Alagha, L.; Burnett, D. J., Probing Surface Characteristics of Rare Earth Minerals Using Contact Angle Measurements, Atomic Force Microscopy, and Inverse Gas Chromatography. *ACS omega* **2019**, *4* (8), 13319-13329.

56. Gao, Z.; Xie, L.; Cui, X.; Hu, Y.; Sun, W.; Zeng, H., Probing Anisotropic Surface Properties and Surface Forces of Fluorite Crystals. *Langmuir* **2018**, *34* (7), 2511-2521.

57. Zhang, L. Y.; Lawrence, S.; Xu, Z.; Masliyah, J. H., Studies of Athabasca asphaltene Langmuir films at air–water interface. *Journal of colloid and interface science* **2003**, *264* (1), 128-140.

58. Hayashi, T.; Ohno, T.; Yatsuya, S.; Uyeda, R., Formation of ultrafine metal particles by gas-evaporation technique. IV. Crystal habits of iron and Fcc metals, Al, Co, Ni, Cu, Pd, Ag, In, Au and Pb. *Japanese Journal of Applied Physics* **1977**, *16* (5), 705.

59. Kar, K. K.; Sathiyamoorthy, D., Influence of process parameters for coating of nickel–phosphorous on carbon fibers. *journal of materials processing technology* **2009**, *209* (6), 3022-3029.

60. Shi, C.; Yan, B.; Xie, L.; Zhang, L.; Wang, J.; Takahara, A.; Zeng, H., Long - Range Hydrophilic Attraction between Water and Polyelectrolyte Surfaces in Oil. *Angewandte Chemie International Edition* **2016**, *55* (48), 15017-15021.

61. Gong, L.; Qiu, X.; Zhang, L.; Huang, J.; Hu, W.; Xiang, L.; Zhu, D.; Sabbagh, R.; Mahmoudi, M.; Fattahpour, V., Probing the Interaction Mechanism between Oil-in-Water Emulsions and Electroless Nickel–Phosphorus Coating with Implications for Antifouling in Oil Production. *Energy & Fuels* **2018**.

62. Israelachvili, J. N., *Intermolecular and surface forces*. Academic press: 2011.
63. Wu, X., Investigating the stability mechanism of water-in-diluted bitumen emulsions through isolation and characterization of the stabilizing materials at the interface. *Energy & fuels* **2003**, *17* (1), 179-190.
64. Rudrake, A.; Karan, K.; Horton, J. H., A combined QCM and XPS investigation of asphaltene adsorption on metal surfaces. *Journal of colloid and interface science* **2009**, *332* (1), 22-31.
65. Abdallah, W.; Taylor, S., Surface characterization of adsorbed asphaltene on a stainless steel surface. *Nuclear Instruments and Methods in Physics Research Section B: Beam Interactions with Materials and Atoms* **2007**, *258* (1), 213-217.
66. Wang, J.; Buckley, J. S.; Creek, J. L., Asphaltene deposition on metallic surfaces. *Journal of dispersion science and technology* **2004**, *25* (3), 287-298.
67. Zhong, Z.; Li, D.; Zhang, B.; Xing, W., Membrane surface roughness characterization and its influence on ultrafine particle adhesion. *Separation and purification technology* **2012**, *90*, 140-146.
68. Hoek, E. M.; Bhattacharjee, S.; Elimelech, M., Effect of membrane surface roughness on colloid– membrane DLVO interactions. *Langmuir* **2003**, *19* (11), 4836-4847.
69. Bowen, W. R.; Doneva, T. A., Atomic force microscopy studies of membranes: Effect of surface roughness on double-layer interactions and particle adhesion. *Journal of colloid and interface science* **2000**, *229* (2), 544-549.
70. Crittenden, B.; Alderman, N., Negative fouling resistances: the effect of surface roughness. *Chemical engineering science* **1988**, *43* (4), 829-838.

71. Eyssautier, J.; Levitz, P.; Espinat, D.; Jestin, J.; Gummel, J.; Grillo, I.; Barré, L., Insight into asphaltene nanoaggregate structure inferred by small angle neutron and X-ray scattering. *The Journal of Physical Chemistry B* **2011**, *115* (21), 6827-6837.
72. McLean, J. D.; Kilpatrick, P. K., Effects of asphaltene solvency on stability of water-in-crude-oil emulsions. *J. Colloid Interface Sci.* **1997**, *189* (2), 242-253.
73. McLean, J. D.; Kilpatrick, P. K., Effects of asphaltene aggregation in model heptane–toluene mixtures on stability of water-in-oil emulsions. *J. Colloid Interface Sci.* **1997**, *196* (1), 23-34.
74. Destribats, M.; Lapeyre, V.; Wolfs, M.; Sellier, E.; Leal-Calderon, F.; Ravaine, V.; Schmitt, V., Soft microgels as Pickering emulsion stabilisers: role of particle deformability. *Soft Matter* **2011**, *7* (17), 7689-7698.
75. Zhang, S.; Zhang, L.; Lu, X.; Shi, C.; Tang, T.; Wang, X.; Huang, Q.; Zeng, H., Adsorption kinetics of asphaltenes at oil/water interface: Effects of concentration and temperature. *Fuel* **2018**, *212*, 387-394.

Chapter 6 Conclusions and Future Works

6.1 Major conclusions

In this study, the interaction mechanisms among asphaltenes, fine solids, water-oil emulsions and substrate surfaces have been directly quantified using the atomic force microscope (AFM) colloidal and drop probe technique to understand the fouling mechanisms and the antifouling properties in oil production. The typical constructive material of pipeline (i.e., iron substrate) and the popular industrial coating (i.e., EN coating) have been used in this project. The corresponding bulk fouling tests have also been conducted to confirm the fouling and antifouling performances. The major conclusions from this study are summarized below.

(1) The interaction forces between the silica particles or asphaltenes-coated silica particles and L80 or EN substrates in NaCl solutions were investigated using the AFM colloidal probe technique under the effects of salinity, pH and Ca^{2+} ions. According to the classic DLVO theory, the attractive VDW force led to the attachment of particles on the substrates, and the repulsive EDL force contributed to the antifouling properties. High salinity in the solution could lead to the compressed electric double layer. Acidic pH resulted to the less negative surface potentials of silica and metal surfaces. The presence of Ca^{2+} ions caused the neutralization of the negative surface charges due to greater charge density of divalent ions. Therefore, high salinity, acidic pH and Ca^{2+} ions weakened EDL repulsion and aggravated the fouling processes. The obtained adhesions

from the force profiles also demonstrated that the adhesion did not change obviously with the varying salinity, but became stronger in acidic pH and Ca^{2+} ions, which was due to the neutralized surface charges and bridging effect. The asphaltenes adsorbed on the silica surface could have a more negatively charged surface and stronger adhesion with metal substrates due to the functional groups of asphaltenes. Besides, compared with L80 substrate, the EN coating showed weaker attraction with asphaltenes and silica particles. The bulk fouling tests in silica and asphaltenes-coated silica suspensions were conducted and the results were in consistence with force results.

(2) The interaction forces between oil drops with the presence of asphaltenes and iron or EN substrate in NaCl solutions have been investigated using the AFM drop probe technique under the effects of salinity, pH and Ca^{2+} ions. Measured force profiles were analyzed using the theoretical model incorporated with augmented Young-Laplace equation and Reynolds lubrication theory. The results indicated that the high salinity, acidic pH and Ca^{2+} ions could weaken the EDL repulsion and cause the contact of oil drops on substrate surfaces. The presence of asphaltenes at water-oil interface could render more negative surface potential and enhance the adhesions between oil drops and iron or EN surfaces because of the functional groups of asphaltenes. It was also noticed that the surface potential of EN coating in NaCl solutions was more negative than that of iron surface, which would arise stronger EDL repulsion with oil drops and lead to better antifouling property. The fouling tests in water-oil emulsions with asphaltenes were also conducted to confirm the better antifouling performances of EN coating.

(3) The interaction forces between water drops and iron or EN coating in organic media (i.e. toluene, heptane and heptol) with interfacially adsorbed asphaltenes were investigated using the AFM drop probe technique under the effect of asphaltenes concentration, aging time, solvent type, loading force and contact time. The adhesion between the water drops with interfacial asphaltenes and iron or EN coating surface were analyzed and the results showed that before the saturation of asphaltenes adsorbed at the water-oil interfaces, the adhesion became stronger with the higher asphaltenes concentration and longer aging time due to more interfacial asphaltenes. After the saturation, the asphaltenes concentration and aging time had almost no influence on the measured adhesion. When the organic solvent became bad to asphaltenes by increasing the heptane ratio, the adhesion was weakened because of the aggregation and the conformational change of asphaltenes. Longer contact time during force measurements could allow asphaltenes to have a better conformation to form stronger interactions with the opposite substrate. The adhesion became stronger with greater loading force due to a larger contact area. Besides, the adhesion measured between water drops and EN coating surface was much weaker than that with iron surface, indicating the relatively easy removal of asphaltenes from EN coating. The conducted bulk fouling tests in water-in-oil emulsions exhibited less asphaltenes on EN coating, which agreed well with force measurement results.

6.2 Original contributions

It was the first time to directly and quantitatively investigate the interaction

mechanisms among asphaltenes, fine solids, emulsion drops and pipeline surfaces, which provided the fundamental information on the fouling phenomena in oil production. Comparing the force measurement results of iron substrate and EN coating could provide the fundamental understandings on the antifouling properties and help in the development of new efficient antifouling coatings and strategies. Furthermore, the theoretical models were applied to analyze the force results to determine the major driving forces in fouling and antifouling processes.

In the case of interactions between silica particles and L80/EN substrates in aqueous solutions, the attractive VDW force contributed to the fouling problems. The repulsive EDL force in the aqueous solutions prevented the attachment of silica particles on metal surfaces, which was also regarded as the antifouling property. Therefore, strengthening the EDL repulsion could improve the antifouling performances of the industrial coatings. For example, diluting the concentration of the electrolytes, increasing the pH to alkaline, and decreasing the ions with multiple charges could result in the strong EDL repulsion. Besides, measured adhesion, which described the difficulty of removing attached particles from the substrate surfaces, indicated the significant importance of asphaltenes-substrate interactions and asphaltenes-asphaltene interactions.

In the case of interactions between stabilized emulsions (oil-in-water emulsions and water-in-oil emulsions) and iron or EN surface with the presence of interfacially adsorbed asphaltenes, the deformation of water or oil drops generated larger contact area when the drops approached substrate surface under the loading force. The functional groups of interfacial asphaltenes could create a more negatively charged

surface potential of oil drops in aqueous solutions and form strong interaction with the opposite substrate, such as hydrogen bonds and acid-base interactions. The combination of all these interactions accounted for the fouling phenomena or the antifouling properties of emulsions on iron or EN surfaces. It was also interesting to discover that the interactions between asphaltenes and iron or EN surface became more attractive in bad solvent (i.e., heptane), which was due to the aggregation and conformational change of asphaltenes.

Furthermore, the application of AFM force measurement techniques, including the colloidal and drop probe techniques, provided the direct and quantitative results to investigate the practical and complex fouling problems in oil production. The surface interactions among asphaltenes, silica particles, water drops, oil drops and substrate surfaces revealed the fundamental mechanisms of fouling phenomena and antifouling properties in nano-scale. Instead of testing the fouling and antifouling performances in a practical facility, AFM force measurement techniques were direct, underspent, fast, and easy to conduct to evaluate and predict the fouling and antifouling performances.

This work directly and quantitatively investigates the surface interactions among asphaltenes, silica particles, water drops, oil drops and pipeline surfaces to shed the fundamental insights in the fouling mechanisms and antifouling properties in oil sands production, which could provide the valuable guidance to the material selection in industries and further facilitate the development efficient antifouling coatings.

6.3 Suggestions for future work

(1) The fouling problems in practical industries are extremely complex, and the foulants contain various components in different industries and processes. In this work, only asphaltenes, silica and water-oil emulsions have been investigated. In other specific process, the foulants, such as calcium carbonate particles (inorganic material) and resins (organic materials), are important. It is significant to identify the components of foulants in the specific process and investigate the interaction and fouling mechanisms.

(2) In this work, the metal surfaces of carbon steel L80, iron and EN coating have been investigated due to the common usage of these materials. It is obvious that a plenty of metal and alloy materials are used in our life and industries, such as the copper and aluminum alloy. Besides, a variety of coatings have been applied to protect the metal materials from abrasion, erosion, corrosion and fouling. Probing the interactions between the fouling materials and these metal substrates is of practical and fundamental importance to design antifouling strategies accordingly and improve antifouling performances.

(3) The conditions used in this work are the room temperature, normal pressure, commonly used solvent (i.e. water, toluene and heptane) and electrolytes (i.e. NaCl and CaCl₂), which is almost impossible in practical industries. The high temperature, high pressure, multiple electrolytes and complicated solvent mixtures provide a much more complex system for the fouling problems, which might also lead to other synergic mechanisms. Studying the interactions in practical or near-real conditions provides the

comprehensive understandings to the fouling issues.

(4) It has been discovered that the fouling and corrosion are synergic. It is believed that the corrosion on metal surface caused by the chemical and electrochemical reactions provide the interaction sites for the foulants to firmly attach. Investigating the fouling mechanisms under the influence of corrosion is also a good topic.

(5) The surface microstructure of metal surface has not been investigated in this work, which is demonstrated to have significant effect on the interactions between two surfaces. Creating the surface pattern is also a useful method to protect the metal surface. It is useful and important to study the interfacial interactions under the effect of surface microstructure.

(6) Nowadays, other force fields, including electric field and magnetic field, have been applied and discovered in some industries to reduce the fouling phenomena, even though the intrinsic mechanisms have not been clearly understood. Investigating the interaction and adsorption mechanisms of foulants on substrate surface with the application of electric field or magnetic field is an interesting and promising project.

Bibliography

1. Campbell, C. J., The assessment and importance of oil depletion. *Energy exploration & exploitation* **2002**, 20 (6), 407-435.
2. Kokal, S.; Al-Kaabi, A., Enhanced oil recovery: challenges & opportunities. *World Petroleum Council: Official Publication* **2010**, 64.
3. Hirschberg, A.; DeJong, L.; Schipper, B.; Meijer, J., Influence of temperature and pressure on asphaltene flocculation. *Society of Petroleum Engineers Journal* **1984**, 24 (03), 283-293.
4. Bentley, R. W., Global oil & gas depletion: an overview. *Energy policy* **2002**, 30 (3), 189-205.
5. Méjean, A.; Hope, C., Modelling the costs of non-conventional oil: A case study of Canadian bitumen. *Energy Policy* **2008**, 36 (11), 4205-4216.
6. Sorrell, S.; Speirs, J.; Bentley, R.; Brandt, A.; Miller, R., Global oil depletion: A review of the evidence. *Energy Policy* **2010**, 38 (9), 5290-5295.
7. Owen, N. A.; Inderwildi, O. R.; King, D. A., The status of conventional world oil reserves—Hype or cause for concern? *Energy policy* **2010**, 38 (8), 4743-4749.
8. Stringham, G., Energy developments in Canada's oil sands. In *Developments in Environmental Science*, Elsevier: 2012; Vol. 11, pp 19-34.
9. Söderbergh, B.; Robelius, F.; Aleklett, K., A crash programme scenario for the Canadian oil sands industry. *Energy policy* **2007**, 35 (3), 1931-1947.
10. Giacchetta, G.; Leporini, M.; Marchetti, B., Economic and environmental analysis

- of a Steam Assisted Gravity Drainage (SAGD) facility for oil recovery from Canadian oil sands. *Applied Energy* **2015**, *142*, 1-9.
11. Isaacs, E., Canadian Oil Sands: development and future outlook. *Alberta Energy Research Institute, Calgary* **2005**.
 12. Shin, H.; Polikar, M. In *Optimizing the SAGD process in three major Canadian oil-sands areas*, SPE Annual Technical Conference and Exhibition, Society of Petroleum Engineers: 2005.
 13. McLennan, A.; Deutsch, C. V., SAGD reservoir characterization using geostatistics: Application to the Athabasca oil sands, Alberta, Canada. *Canadian Heavy Oil Association handbook, 2d ed.: Canadian Heavy Oil Association* **2005**, 321-340.
 14. Schneider, R.; Dyer, S., *Death by a thousand cuts: impacts of in situ oil sands development on Alberta's boreal forest*. Pembina Institute Calgary, AB, Canada: 2006.
 15. Shin, H.; Polikar, M., Fast-SAGD application in the Alberta oil sands areas. *Journal of Canadian Petroleum Technology* **2006**, *45* (09).
 16. Stalder, J. L. In *Test of SAGD Flow Distribution Control Liner System, Surmont Field, Alberta, Canada*, SPE Western Regional Meeting, Society of Petroleum Engineers: 2012.
 17. Edmunds, N.; Chhina, H., Economic optimum operating pressure for SAGD projects in Alberta. *Journal of Canadian Petroleum Technology* **2001**, *40* (12).
 18. Jimenez, J. In *The field performance of SAGD projects in Canada*, International petroleum technology conference, International Petroleum Technology Conference:

2008.

19. Lightbown, V., New SAGD technologies show promise in reducing environmental impact of oil sand production. *Journal of Environmental Solutions for Oil, Gas, and Mining* **2015**, *1* (1), 47-58.
20. Pugsley, T.; Pernitsky, D.; Grundler, J.; Johnsen, E. In *Fouling of heat transfer surfaces in a steam assisted gravity drainage (SAGD) in situ facility for the recovery of oil sands bitumen*, International Conference on Heat Exchanger Fouling and Clearing, 2013.
21. Acosta, E., Achieving sustainable, optimal SAGD operations. *Journal of Petroleum Technology* **2010**, *62* (11), 24-28.
22. Zhu, D.; Uzcategui, A.; Gong, L.; Qiu, X.; Huang, J.; Sun, C.; Luo, J.-L.; Zeng, H. In *Investigation of Electroless Nickel-Phosphorus Coating as an Alternative to Corrosion/Fouling Resistant Alloys in Downhole Service*, OTC Brasil, Offshore Technology Conference: 2017.
23. Alipour, M.; Kurian, V.; Dhir, S.; Gupta, R., Analysis of syngas cooler fouling from asphaltene gasification. *Fuel Processing Technology* **2016**, *152*, 7-14.
24. Thibault, Y.; McEvoy, J. G.; Mortazavi, S.; Smith, D.; Doiron, A., Characterization of fouling processes in ceramic membranes used for the recovery and recycle of oil sands produced water. *Journal of Membrane Science* **2017**, *540*, 307-320.
25. Bell, I. H.; Groll, E. A., Air-side particulate fouling of microchannel heat exchangers: experimental comparison of air-side pressure drop and heat transfer with plate-fin heat exchanger. *Applied Thermal Engineering* **2011**, *31* (5), 742-749.

26. Sarafraz, M.; Hormozi, F., Heat transfer, pressure drop and fouling studies of multi-walled carbon nanotube nano-fluids inside a plate heat exchanger. *Experimental Thermal and Fluid Science* **2016**, *72*, 1-11.
27. Hesselgreaves, J., An approach to fouling allowances in the design of compact heat exchangers. *Applied Thermal Engineering* **2002**, *22* (7), 755-762.
28. Little, B.; Wagner, P.; Mansfeld, F., Microbiologically influenced corrosion of metals and alloys. *International Materials Reviews* **1991**, *36* (1), 253-272.
29. Lee, W.; Lewandowski, Z.; Nielsen, P. H.; Hamilton, W. A., Role of sulfate - reducing bacteria in corrosion of mild steel: a review. *Biofouling* **1995**, *8* (3), 165-194.
30. Somerscales, E. F., Fundamentals of corrosion fouling. *Experimental thermal and fluid science* **1997**, *14* (4), 335-355.
31. Finnie, I., Erosion of surfaces by solid particles. *wear* **1960**, *3* (2), 87-103.
32. Safaei, M.; Mahian, O.; Garoosi, F.; Hooman, K.; Karimipour, A.; Kazi, S.; Gharehkhani, S., Investigation of micro-and nanosized particle erosion in a 90 pipe bend using a two-phase discrete phase model. *The scientific world journal* **2014**, *2014*.
33. Barton, D.; Wallace, R., Effects of eroding oil sand and periodic flooding on benthic macroinvertebrate communities in a brown-water stream in northeastern Alberta, Canada. *Canadian Journal of Zoology* **1979**, *57* (3), 533-541.
34. Heggs, P., Heat exchanger fouling-mitigation and cleaning technologies by Hans Muller-Steinhager. *TCE CHEMICAL ENGINEER* **2001**, 49-49.

35. Egan, S.; James, S.; Kjelleberg, S., Identification and characterization of a putative transcriptional regulator controlling the expression of fouling inhibitors in *Pseudoalteromonas tunicata*. *Appl. Environ. Microbiol.* **2002**, *68* (1), 372-378.
36. Müller-Steinhagen, H.; Malayeri, M.; Watkinson, A., Heat exchanger fouling: environmental impacts. Taylor & Francis: 2009.
37. Chen, T.; Chan, S.-H., Novel biological inhibitors of fouling and scale formation on heat transfer surfaces through genetic engineering. *Microscale Thermophysical Engineering* **2000**, *4* (2), 103-108.
38. Gönder, Z. B.; Kaya, Y.; Vergili, I.; Barlas, H., Capacity loss in an organically fouled anion exchanger. *Desalination* **2006**, *189* (1-3), 303-307.
39. Ming, F.; Howell, J.; Acosta, F.; Hubble, J., Study on separation of conalbumin and lysozyme from high concentration fresh egg white at high flow rates by a novel ion - exchanger. *Biotechnology and bioengineering* **1993**, *42* (9), 1086-1090.
40. Wang, Y.; Babchin, J.; Chernyi, L.; Chow, R.; Sawatzky, R., Rapid onset of calcium carbonate crystallization under the influence of a magnetic field. *Water Research* **1997**, *31* (2), 346-350.
41. Vermeiren, T., Magnetic treatment of liquids for scale and corrosion prevention. *Anti-Corrosion Methods and Materials* **1958**, *5* (7), 215-219.
42. Cho, Y.; Choi, B.-G., Validation of an electronic anti-fouling technology in a single-tube heat exchanger. *International Journal of Heat and Mass Transfer* **1999**, *42* (8), 1491-1499.
43. Cho, Y. I.; Fan, C.; Choi, B.-G., Use of electronic anti-fouling technology with

- filtration to prevent fouling in a heat exchanger. *International journal of heat and mass transfer* **1998**, *41* (19), 2961-2966.
44. Kobayashi, T.; Chai, X.; Fujii, N., Ultrasound enhanced cross-flow membrane filtration. *Separation and Purification Technology* **1999**, *17* (1), 31-40.
45. Chen, D.; Weavers, L. K.; Walker, H. W. In *Using ultrasound to reduce ceramic membrane fouling by silica particles*, National Meeting of the American Chemical Society, Orlando, USA, 2002; pp 166-169.
46. Pan, Y.; Wang, T.; Sun, H.; Wang, W., Preparation and application of titanium dioxide dynamic membranes in microfiltration of oil-in-water emulsions. *Separation and purification technology* **2012**, *89*, 78-83.
47. Bates, D.; Patist, A., Industrial applications of high power ultrasonics in the food, beverage and wine industry. In *Case Studies in Novel Food Processing Technologies*, Elsevier: 2010; pp 119-138.
48. Zhang, H.; Chiao, M., Anti-fouling coatings of poly (dimethylsiloxane) devices for biological and biomedical applications. *Journal of medical and biological engineering* **2015**, *35* (2), 143-155.
49. Förster, M.; Augustin, W.; Bohnet, M., Influence of the adhesion force crystal/heat exchanger surface on fouling mitigation. *Chemical Engineering and Processing: Process Intensification* **1999**, *38* (4-6), 449-461.
50. Müller-Steinhagen, H.; Zhao, Q., Investigation of low fouling surface alloys made by ion implantation technology. *Chemical Engineering Science* **1997**, *52* (19), 3321-3332.

51. Allen, E. W., Process water treatment in Canada's oil sands industry: I. Target pollutants and treatment objectives. *Journal of Environmental Engineering and Science* **2008**, 7 (2), 123-138.
52. Duyvesteyn, W. P.; Budden, J. R.; Picavet, M. A., Extraction of bitumen from bitumen froth and biotreatment of bitumen froth tailings generated from tar sands. Google Patents: 1999.
53. Epstein, N. In *Fouling in heat exchangers*, Sixth International Heat Transfer Conference., 1977; pp 235-253.
54. Speight, J. G., *Fouling in refineries*. Gulf Professional Publishing: 2015.
55. Wu, X.; Chung, K., Hydrotreater feed filter fouling and its remedy. *Energy & fuels* **2007**, 21 (3), 1212-1216.
56. Irani, M. In *On Subcool Control in the SAGD Producers. Part II: Localized Hot Spots Effects and Optimization of Flow-Control-Devices*, SPE Thermal Well Integrity and Design Symposium, Society of Petroleum Engineers: 2018.
57. Ezeuko, C. C.; Wang, J.; Gates, I. D., Investigation of emulsion flow in steam-assisted gravity drainage. *SPE Journal* **2013**, 18 (03), 440-447.
58. Kar, T.; Williamson, M.; Hascakir, B. In *The role of asphaltenes in emulsion formation for steam assisted gravity drainage (SAGD) and expanding solvent-SAGD (ES-SAGD)*, SPE Heavy and Extra Heavy Oil Conference: Latin America, Society of Petroleum Engineers: 2014.
59. Edwards, Y.; Isacson, U., Wax in bitumen: part 1—classifications and general aspects. *Road materials and pavement design* **2005**, 6 (3), 281-309.

60. Sheu, E. Y., Petroleum asphaltene properties, characterization, and issues. *Energy & Fuels* **2002**, *16* (1), 74-82.
61. Lee, R. F., Agents which promote and stabilize water-in-oil emulsions. *Spill Science & Technology Bulletin* **1999**, *5* (2), 117-126.
62. Langevin, D.; Poteau, S.; Hénaut, I.; Argillier, J., Crude oil emulsion properties and their application to heavy oil transportation. *Oil & gas science and technology* **2004**, *59* (5), 511-521.
63. Watkinson, A.; Wilson, D., Chemical reaction fouling: A review. *Experimental Thermal and Fluid Science* **1997**, *14* (4), 361-374.
64. Wiehe, I. A.; Kennedy, R. J.; Dickakian, G., Fouling of nearly incompatible oils. *Energy & fuels* **2001**, *15* (5), 1057-1058.
65. Stark, J. L.; Asomaning, S., Crude oil blending effects on asphaltene stability in refinery fouling. *Petroleum science and technology* **2003**, *21* (3-4), 569-579.
66. Bennett, C. A., A theory describing asphaltene adhesion fouling inside heat exchanger tubes. *Heat Transfer Engineering* **2012**, *33* (15), 1246-1250.
67. FAN, M.; SUN, X.-w.; XU, Z.-m.; ZHAO, S.-q., Characterization of Residue (C5-C7) Asphaltene (Soluble in n-Heptane but Insoluble in n-Pentane)[J]. *Journal of Petrochemical Universities* **2011**, *3*.
68. Goual, L., Petroleum asphaltenes. In *Crude Oil Emulsions-Composition Stability and Characterization*, InTech: 2012.
69. Dufour, J.; Calles, J. A.; Marugán, J.; Giménez-Aguirre, R.; Peña, J. L.; Merino-García, D., Influence of hydrocarbon distribution in crude oil and residues on

- asphaltene stability. *Energy & Fuels* **2009**, *24* (4), 2281-2286.
70. Strausz, O. P.; Jha, K. N.; Montgomery, D. S., Chemical composition of gases in Athabasca bitumen and in low-temperature thermolysis of oil sand, asphaltene and maltene. *Fuel* **1977**, *56* (2), 114-120.
71. Adams, J. J., Asphaltene adsorption, a literature review. *Energy & Fuels* **2014**, *28* (5), 2831-2856.
72. Mullins, O. C.; Sabbah, H.; Eyssautier, J.; Pomerantz, A. E.; Barré, L.; Andrews, A. B.; Ruiz-Morales, Y.; Mostowfi, F.; McFarlane, R.; Goual, L., Advances in asphaltene science and the Yen–Mullins model. *Energy & Fuels* **2012**, *26* (7), 3986-4003.
73. Mullins, O. C., The asphaltenes. *Annual review of analytical chemistry* **2011**, *4*, 393-418.
74. Ancheyta, J.; Centeno, G.; Trejo, F.; Marroquin, G.; Garcia, J.; Tenorio, E.; Torres, A., Extraction and characterization of asphaltenes from different crude oils and solvents. *Energy & Fuels* **2002**, *16* (5), 1121-1127.
75. Alboudwarej, H.; Beck, J.; Svrcek, W.; Yarranton, H.; Akbarzadeh, K., Sensitivity of asphaltene properties to separation techniques. *Energy & Fuels* **2002**, *16* (2), 462-469.
76. Dutta Majumdar, R.; Gerken, M.; Mikula, R.; Hazendonk, P., Validation of the Yen–Mullins model of Athabasca oil-sands asphaltenes using solution-state ¹H NMR relaxation and 2D HSQC spectroscopy. *Energy & Fuels* **2013**, *27* (11), 6528-6537.

77. Mullins, O. C.; Seifert, D. J.; Zuo, J. Y.; Zeybek, M., Clusters of asphaltene nanoaggregates observed in oilfield reservoirs. *Energy & Fuels* **2012**, *27* (4), 1752-1761.
78. Mullins, O. C., The modified Yen model. *Energy & Fuels* **2010**, *24* (4), 2179-2207.
79. Simon, S.; Jestin, J.; Palermo, T.; Barré, L. c., Relation between solution and interfacial properties of asphaltene aggregates. *Energy & Fuels* **2008**, *23* (1), 306-313.
80. Long, J.; Xu, Z.; Masliyah, J. H., Single molecule force spectroscopy of asphaltene aggregates. *Langmuir* **2007**, *23* (11), 6182-6190.
81. Moschopedis, S. E.; Speight, J. G., Investigation of hydrogen bonding by oxygen functions in Athabasca bitumen. *Fuel* **1976**, *55* (3), 187-192.
82. Lopez-Chavez, E.; Pacheco-Sánchez, J.-H.; Martínez-Magadán, J.-M.; Castillo-Alvarado, F. d. L.; Soto-Figueroa, C.; Garcia-Cruz, I., Methodology for predicting the phase envelope of a heavy crude oil and its asphaltene deposition onset. *Petroleum science and technology* **2007**, *25* (1-2), 19-39.
83. Sparks, B.; Kotlyar, L.; O'Carroll, J.; Chung, K., Athabasca oil sands: effect of organic coated solids on bitumen recovery and quality. *Journal of Petroleum Science and Engineering* **2003**, *39* (3-4), 417-430.
84. Masliyah, J.; Zhou, Z. J.; Xu, Z.; Czarnecki, J.; Hamza, H., Understanding water - based bitumen extraction from Athabasca oil sands. *The Canadian Journal of Chemical Engineering* **2004**, *82* (4), 628-654.
85. Yan, N.; Gray, M. R.; Masliyah, J. H., On water-in-oil emulsions stabilized by fine

- solids. *Colloids and Surfaces A: Physicochemical and Engineering Aspects* **2001**, *193* (1-3), 97-107.
86. Kotlyar, L.; Sparks, B.; Woods, J.; Chung, K., Solids associated with the asphaltene fraction of oil sands bitumen. *Energy & fuels* **1999**, *13* (2), 346-350.
87. Jada, A.; Debih, H., Hydrophobation of clay particles by asphaltene adsorption. *Composite Interfaces* **2009**, *16* (2-3), 219-235.
88. Binks, B. P.; Desforges, A.; Duff, D. G., Synergistic stabilization of emulsions by a mixture of surface-active nanoparticles and surfactant. *Langmuir* **2007**, *23* (3), 1098-1106.
89. Bensebaa, F.; Kotlyar, L. S.; Sparks, B. D.; Chung, K. H., Organic coated solids in Athabasca bitumen: Characterization and process implications. *The Canadian Journal of Chemical Engineering* **2000**, *78* (4), 610-616.
90. Nikakhtari, H.; Wolf, S.; Choi, P.; Liu, Q.; Gray, M. R., Migration of fine solids into product bitumen from solvent extraction of Alberta oilsands. *Energy & Fuels* **2014**, *28* (5), 2925-2932.
91. Abraham, T.; Christendat, D.; Karan, K.; Xu, Z.; Masliyah, J., Asphaltene– Silica Interactions in Aqueous Solutions: Direct Force Measurements Combined with Electrokinetic Studies. *Industrial & engineering chemistry research* **2002**, *41* (9), 2170-2177.
92. Liu, J.; Zhang, L.; Xu, Z.; Masliyah, J., Colloidal interactions between asphaltene surfaces in aqueous solutions. *Langmuir* **2006**, *22* (4), 1485-1492.
93. Fritschy, G.; Papirer, E., Interactions between a bitumen, its components and model

- fillers. *Fuel* **1978**, 57 (11), 701-704.
94. Liu, J.; Xu, Z.; Masliyah, J., Interaction forces in bitumen extraction from oil sands. *Journal of colloid and interface science* **2005**, 287 (2), 507-520.
95. Wang, S.; Liu, J.; Zhang, L.; Masliyah, J.; Xu, Z., Interaction forces between asphaltene surfaces in organic solvents. *Langmuir* **2009**, 26 (1), 183-190.
96. Wang, J.; Li, C.; Zhang, L.; Que, G.; Li, Z., The properties of asphaltenes and their interaction with amphiphiles. *Energy & Fuels* **2009**, 23 (7), 3625-3631.
97. Peltonen, P. V., Road aggregate choice based on silicate quality and bitumen adhesion. *Journal of transportation engineering* **1992**, 118 (1), 50-61.
98. Long, J.; Zhang, L.; Xu, Z.; Masliyah, J. H., Colloidal interactions between Langmuir–Blodgett bitumen films and fine solid particles. *Langmuir* **2006**, 22 (21), 8831-8839.
99. Jada, A.; Chaou, A. A.; Bertrand, Y.; Moreau, O., Adsorption and surface properties of silica with transformer insulating oils. *Fuel* **2002**, 81 (9), 1227-1232.
100. Wang, S.; Segin, N.; Wang, K.; Masliyah, J. H.; Xu, Z., Wettability control mechanism of highly contaminated hydrophilic silica/alumina surfaces by ethyl cellulose. *The Journal of Physical Chemistry C* **2011**, 115 (21), 10576-10587.
101. Cortés, F. B.; Mejía, J. M.; Ruiz, M. A.; Benjumea, P.; Riffel, D. B., Sorption of asphaltenes onto nanoparticles of nickel oxide supported on nanoparticulated silica gel. *Energy & Fuels* **2012**, 26 (3), 1725-1730.
102. Zahabi, A.; Gray, M. R.; Dabros, T., Kinetics and properties of asphaltene adsorption on surfaces. *Energy & Fuels* **2012**, 26 (2), 1009-1018.

103. Becher, P.; Hamor, W. A., *Emulsions: theory and practice*. Reinhold New York: 1957; Vol. 135.
104. Berg, J. C., *An introduction to interfaces & colloids: the bridge to nanoscience*. World Scientific: 2010.
105. Khristov, K.; Taylor, S.; Czarnecki, J.; Masliyah, J., Thin liquid film technique—application to water–oil–water bitumen emulsion films. *Colloids and Surfaces A: Physicochemical and Engineering Aspects* **2000**, *174* (1-2), 183-196.
106. Yan, Z.; Elliott, J. A.; Masliyah, J. H., Roles of various bitumen components in the stability of water-in-diluted-bitumen emulsions. *Journal of colloid and interface science* **1999**, *220* (2), 329-337.
107. Gao, S.; Moran, K.; Xu, Z.; Masliyah, J., Role of bitumen components in stabilizing water-in-diluted oil emulsions. *Energy & Fuels* **2009**, *23* (5), 2606-2612.
108. Freer, E.; Radke, C., Relaxation of asphaltenes at the toluene/water interface: diffusion exchange and surface rearrangement. *The Journal of Adhesion* **2004**, *80* (6), 481-496.
109. Acevedo, S.; Ranaudo, M. A.; García, C.; Castillo, J.; Fernández, A., Adsorption of asphaltenes at the toluene– silica interface: A kinetic study. *Energy & fuels* **2003**, *17* (2), 257-261.
110. Langevin, D.; Argillier, J.-F., Interfacial behavior of asphaltenes. *Advances in colloid and interface science* **2016**, *233*, 83-93.
111. Tsamantakis, C.; Masliyah, J.; Yeung, A.; Gentzis, T., Investigation of the interfacial properties of water-in-diluted-bitumen emulsions using micropipette

- techniques. *Journal of colloid and interface science* **2005**, *284* (1), 176-183.
- 112.Kralova, I.; Sjöblom, J.; Øye, G.; Simon, S.; Grimes, B. A.; Paso, K., Heavy crude oils/particle stabilized emulsions. *Advances in colloid and interface science* **2011**, *169* (2), 106-127.
- 113.Natarajan, A.; Xie, J.; Wang, S.; Liu, Q.; Masliyah, J.; Zeng, H.; Xu, Z., Understanding molecular interactions of asphaltenes in organic solvents using a surface force apparatus. *The Journal of Physical Chemistry C* **2011**, *115* (32), 16043-16051.
- 114.Shi, C.; Zhang, L.; Xie, L.; Lu, X.; Liu, Q.; Mantilla, C. A.; van den Berg, F. G.; Zeng, H., Interaction mechanism of oil-in-water emulsions with asphaltenes determined using droplet probe AFM. *Langmuir* **2016**, *32* (10), 2302-2310.
- 115.Zhang, L.; Shi, C.; Lu, Q.; Liu, Q.; Zeng, H., Probing molecular interactions of asphaltenes in heptol using a surface forces apparatus: Implications on stability of water-in-oil emulsions. *Langmuir* **2016**, *32* (19), 4886-4895.
- 116.Shi, C.; Zhang, L.; Xie, L.; Lu, X.; Liu, Q.; He, J.; Mantilla, C. A.; Van den Berg, F. G.; Zeng, H., Surface interaction of water-in-oil emulsion droplets with interfacially active asphaltenes. *Langmuir* **2017**, *33* (5), 1265-1274.
- 117.Natarajan, A.; Kuznicki, N.; Harbottle, D.; Masliyah, J.; Zeng, H.; Xu, Z., Understanding mechanisms of asphaltene adsorption from organic solvent on mica. *Langmuir* **2014**, *30* (31), 9370-9377.
- 118.Bott, T. R., Aspects of crystallization fouling. *Experimental thermal and fluid science* **1997**, *14* (4), 356-360.

119. Fernandez-Torres, M.; Fitzgerald, A.; Paterson, W.; Wilson, D., A theoretical study of freezing fouling: limiting behaviour based on a heat and mass transfer analysis. *Chemical Engineering and Processing: Process Intensification* **2001**, *40* (4), 335-344.
120. Rogel, E.; Ovalles, C.; Vien, J.; Moir, M., Asphaltene characterization of paraffinic crude oils. *Fuel* **2016**, *178*, 71-76.
121. MacAdam, J.; Parsons, S. A., Calcium carbonate scale formation and control. *Re/Views in Environmental Science & Bio/Technology* **2004**, *3* (2), 159-169.
122. Chen, T.; Neville, A.; Yuan, M., Calcium carbonate scale formation—assessing the initial stages of precipitation and deposition. *Journal of Petroleum Science and Engineering* **2005**, *46* (3), 185-194.
123. Ramstad, K.; Tydal, T.; Askvik, K. M.; Fotland, P., Predicting carbonate scale in oil producers from high temperature reservoirs. *SPE Journal* **2005**, *10* (04), 363-373.
124. Jones, T.; Neustadter, E.; Whittingham, K., Water-in-crude oil emulsion stability and emulsion destabilization by chemical demulsifiers. *Journal of Canadian Petroleum Technology* **1978**, *17* (02).
125. Kokal, S. L., Crude oil emulsions: A state-of-the-art review. *SPE Production & facilities* **2005**, *20* (01), 5-13.
126. Gillis, P. L., Assessing the toxicity of sodium chloride to the glochidia of freshwater mussels: Implications for salinization of surface waters. *Environmental Pollution* **2011**, *159* (6), 1702-1708.

127. Blanchard, G.; Maunaye, M.; Martin, G., Removal of heavy metals from waters by means of natural zeolites. *Water research* **1984**, *18* (12), 1501-1507.
128. Hem, J. D.; Survey, G., Study and interpretation of the chemical characteristics of natural water. **1989**.
129. Fattahpour, V.; Mahmoudi, M.; Roostaei, M.; Cheung, S.; Gong, L.; Qiu, X.; Huang, J.; Velayati, A.; Kyanpour, M.; Alkough, A. In *Evaluation of the Scaling Resistance of Different Coating and Material for Thermal Operations*, SPE International Heavy Oil Conference and Exhibition, Society of Petroleum Engineers: 2018.
130. Sullivan, A. P.; Kilpatrick, P. K., The effects of inorganic solid particles on water and crude oil emulsion stability. *Industrial & Engineering Chemistry Research* **2002**, *41* (14), 3389-3404.
131. Nassar, N. N., Asphaltene adsorption onto alumina nanoparticles: kinetics and thermodynamic studies. *Energy & Fuels* **2010**, *24* (8), 4116-4122.
132. Mohammadi, M.; Sedighi, M.; Hashemi Kiasari, H.; Hosseini, S. M., Genetic algorithm development for prediction of modified Langmuir isotherm parameters of asphaltene adsorption onto metal surfaces: using novel quartz crystal nanobalance. *Journal of Dispersion Science and Technology* **2015**, *36* (3), 384-392.
133. Alboudwarej, H.; Pole, D.; Svrcek, W. Y.; Yarranton, H. W., Adsorption of asphaltenes on metals. *Industrial & engineering chemistry research* **2005**, *44* (15), 5585-5592.
134. Rudrake, A. Investigations of Asphaltene-Metal Interactions. 2008.
135. Ekholm, P.; Blomberg, E.; Claesson, P.; Auflem, I. H.; Sjöblom, J.; Kornfeldt, A.,

- A quartz crystal microbalance study of the adsorption of asphaltenes and resins onto a hydrophilic surface. *Journal of colloid and interface science* **2002**, *247* (2), 342-350.
136. Goual, L.; Horváth-Szabó, G.; Masliyah, J. H.; Xu, Z., Adsorption of bituminous components at oil/water interfaces investigated by quartz crystal microbalance: Implications to the stability of water-in-oil emulsions. *Langmuir* **2005**, *21* (18), 8278-8289.
137. Rudrake, A.; Karan, K.; Horton, J. H., A combined QCM and XPS investigation of asphaltene adsorption on metal surfaces. *Journal of colloid and interface science* **2009**, *332* (1), 22-31.
138. Abdallah, W.; Taylor, S., Surface characterization of adsorbed asphaltene on a stainless steel surface. *Nuclear Instruments and Methods in Physics Research Section B: Beam Interactions with Materials and Atoms* **2007**, *258* (1), 213-217.
139. Balabin, R. M.; Syunyaev, R. Z.; Schmid, T.; Stadler, J.; Lomakina, E. I.; Zenobi, R., Asphaltene adsorption onto an iron surface: combined near-infrared (NIR), Raman, and AFM study of the kinetics, thermodynamics, and layer structure. *Energy & Fuels* **2010**, *25* (1), 189-196.
140. Karan, K.; Hammami, A.; Flannery, M.; Artur Stankiewicz, B., Evaluation of asphaltene instability and a chemical control during production of live oils. *Petroleum science and technology* **2003**, *21* (3-4), 629-645.
141. Papadimitriou, N.; Romanos, G.; Charalambopoulou, G. C.; Kainourgiakis, M.; Katsaros, F.; Stubos, A., Experimental investigation of asphaltene deposition

- mechanism during oil flow in core samples. *Journal of petroleum science and engineering* **2007**, *57* (3-4), 281-293.
- 142.Eskin, D.; Ratulowski, J.; Akbarzadeh, K.; Pan, S., Modelling asphaltene deposition in turbulent pipeline flows. *The Canadian Journal of Chemical Engineering* **2011**, *89* (3), 421-441.
- 143.Buckley, J. S., Asphaltene deposition. *Energy & Fuels* **2012**, *26* (7), 4086-4090.
- 144.Kermani, M.; Harrop, D., The impact of corrosion on oil and gas industry. *SPE Production & Facilities* **1996**, *11* (03), 186-190.
- 145.Wu, S.; Cui, Z.; Zhao, G.; Yan, M.; Zhu, S.; Yang, X., EIS study of the surface film on the surface of carbon steel from supercritical carbon dioxide corrosion. *Applied Surface Science* **2004**, *228* (1-4), 17-25.
- 146.Finšgar, M.; Jackson, J., Application of corrosion inhibitors for steels in acidic media for the oil and gas industry: a review. *Corrosion Science* **2014**, *86*, 17-41.
- 147.Migahed, M.; Mohamed, H.; Al-Sabagh, A., Corrosion inhibition of H-11 type carbon steel in 1 M hydrochloric acid solution by N-propyl amino lauryl amide and its ethoxylated derivatives. *Materials chemistry and physics* **2003**, *80* (1), 169-175.
- 148.Ren, C.; Liu, D.; Bai, Z.; Li, T., Corrosion behavior of oil tube steel in simulant solution with hydrogen sulfide and carbon dioxide. *Materials chemistry and physics* **2005**, *93* (2-3), 305-309.
- 149.Nasr, T.; Beaulieu, G.; Golbeck, H.; Heck, G. In *Novel expanding solvent-SAGD process "ES-SAGD"*, Canadian International Petroleum Conference, Petroleum Society of Canada: 2002.

150. Singh, D.; Sirkar, K. K., Desalination of brine and produced water by direct contact membrane distillation at high temperatures and pressures. *Journal of Membrane Science* **2012**, *389*, 380-388.
151. Droes, S. R.; Kodas, T. T.; Hampden-Smith, M. J., Plasma-Enhanced Chemical Vapor Deposition (PECVD). In *Carbide, Nitride and Boride Materials Synthesis and Processing*, Springer: 1997; pp 579-603.
152. Schultz, M. P., Frictional resistance of antifouling coating systems. *Transactions of the ASME-I-Journal of Fluids Engineering* **2004**, *126* (6), 1039-1047.
153. Müller-Steinhagen, H.; Zhao, Q., Investigation of low fouling surface alloys made by ion implantation technology. *Chemical Engineering Science* **1997**, *52* (19), 3321-3332.
154. Alayo, M.; Pereyra, I.; Scopel, W. L.; Fantini, M. C. d. A., On the nitrogen and oxygen incorporation in plasma-enhanced chemical vapor deposition (PECVD) SiO_xN_y films. *Thin Solid Films* **2002**, *402* (1-2), 154-161.
155. Miyajima, S.; Irikawa, J.; Yamada, A.; Konagai, M., High quality aluminum oxide passivation layer for crystalline silicon solar cells deposited by parallel-plate plasma-enhanced chemical vapor deposition. *Applied Physics Express* **2009**, *3* (1), 012301.
156. Park, K. C.; Moon, J. H.; Jang, J.; Oh, M. H., Deposition of hydrogen - free diamond - like carbon film by plasma enhanced chemical vapor deposition. *Applied physics letters* **1996**, *68* (25), 3594-3595.
157. Wang, Y.; Fei, W.; An, L., Oxidation/Corrosion of Polymer - Derived SiAlCN

- Ceramics in Water Vapor. *Journal of the American Ceramic Society* **2006**, *89* (3), 1079-1082.
158. Marcus, P., *Corrosion mechanisms in theory and practice*. CRC press: 2011.
159. Mansfeld, F. B., *Corrosion mechanisms*. CRC Press: 1986; Vol. 28.
160. Wang, W.; Booske, J.; Baum, C.; Clothier, C.; Zjaba, N.; Zhang, L., Modification of bearing steel surface by nitrogen plasma source ion implantation for corrosion protection. *Surface and Coatings Technology* **1999**, *111* (1), 97-102.
161. Stroosnijder, M., Ion implantation for high temperature corrosion protection. *Surface and Coatings Technology* **1998**, *100*, 196-201.
162. Karimi, M. V.; Sinha, S.; Kothari, D.; Khanna, A.; Tyagi, A., Effect of ion implantation on corrosion resistance and high temperature oxidation resistance of Ti deposited 316 stainless steel. *Surface and Coatings Technology* **2002**, *158*, 609-614.
163. Smidt, F., Recent advances in the application of ion implantation to corrosion and wear protection. *Nuclear Instruments and Methods in Physics Research Section B: Beam Interactions with Materials and Atoms* **1985**, *10*, 532-538.
164. Cheng, Y.; Zou, Y.; Cheng, L.; Liu, W., Effect of the microstructure on the anti-fouling property of the electroless Ni-P coating. *Materials letters* **2008**, *62* (27), 4283-4285.
165. Barish, J. A.; Goddard, J. M., Anti-fouling surface modified stainless steel for food processing. *Food and Bioproducts processing* **2013**, *91* (4), 352-361.
166. Zhao, Q.; Liu, Y.; Müller-Steinhagen, H.; Liu, G., Graded Ni-P-PTFE coatings

- and their potential applications. *Surface and Coatings Technology* **2002**, *155* (2-3), 279-284.
- 167.Keong, K.; Sha, W.; Malinov, S., Crystallisation kinetics and phase transformation behaviour of electroless nickel–phosphorus deposits with high phosphorus content. *Journal of Alloys and Compounds* **2002**, *334* (1-2), 192-199.
- 168.Keong, K.; Sha, W.; Malinov, S., Hardness evolution of electroless nickel–phosphorus deposits with thermal processing. *Surface and Coatings Technology* **2003**, *168* (2-3), 263-274.
- 169.Brown, R. J.; Brewer, P. J.; Milton, M. J., The physical and chemical properties of electroless nickel–phosphorus alloys and low reflectance nickel–phosphorus black surfaces. *Journal of Materials Chemistry* **2002**, *12* (9), 2749-2754.
- 170.Wurtz, A., Hebd. *Sciences Acad. Sci* **1844**, *18*, 702.
- 171.Brenner, A.; Riddell, G. E., Deposition of nickel and cobalt by chemical reduction. *J. Res. Nat. Bur. Stand* **1947**, *39*, 385-395.
- 172.Brenner, A.; Riddell, G. E., Nickel plating on steel by chemical reduction. *Plating and surface finishing* **1998**, *85* (8), 54-55.
- 173.Ashassi-Sorkhabi, H.; Rafizadeh, S. H., Effect of coating time and heat treatment on structures and corrosion characteristics of electroless Ni–P alloy deposits. *Surface and coatings Technology* **2004**, *176* (3), 318-326.
- 174.Dai, K.; Xiong, Y.; Yin, J., Electroless Ni - P coating on Cu substrate with strike nickel activation and its corrosion resistance. *Materialwissenschaft und Werkstofftechnik* **2013**, *44* (11), 918-921.

- 175.Cui, G.; Li, N.; Li, D.; Zheng, J.; Wu, Q., The physical and electrochemical properties of electroless deposited nickel–phosphorus black coatings. *Surface and Coatings Technology* **2006**, *200* (24), 6808-6814.
- 176.Mai, Q.; Daniels, R.; Harpalani, H., Structural changes induced by heating in electroless nickel-phosphorus alloys. *Thin Solid Films* **1988**, *166*, 235-247.
- 177.Lambert, M. R.; Duquette, D. J., A study of electroless nickel coatings containing low phosphorus. *Thin Solid Films* **1989**, *177* (1-2), 207-223.
- 178.Kumar, P. S.; Nair, P. K., Studies on crystallization of electroless Ni P deposits. *Journal of Materials Processing Technology* **1996**, *56* (1-4), 511-520.
- 179.Erming, M.; Shoufu, L.; Pengxing, L., A transmission electron microscopy study on the crystallization of amorphous Ni-P electroless deposited coatings. *Thin Solid Films* **1988**, *166*, 273-280.
- 180.Wang, J. J.; Li, S. R.; Su, X. J.; Hou, G. L.; Song, B.; Liu, C. H. In *Study on Wear Resistance of Two Types of Low Phosphorus Electroless Nickel Plating on 30CrMnSi*, Advanced Materials Research, Trans Tech Publ: 2017; pp 178-182.
- 181.Balaraju, J.; Seshadri, S., Synthesis and characterization of electroless nickel-high phosphorus coatings. *Metal Finishing* **1999**, *97* (7), 8-13.
- 182.Wang, Y.; Shu, X.; Wei, S.; Liu, C.; Gao, W.; Shakoor, R.; Kahraman, R., Duplex Ni–P–ZrO₂/Ni–P electroless coating on stainless steel. *Journal of Alloys and Compounds* **2015**, *630*, 189-194.
- 183.Karthikeyan, S.; Ramamoorthy, B., Effect of reducing agent and nano Al₂O₃ particles on the properties of electroless Ni–P coating. *Applied Surface Science*

2014, 307, 654-660.

184. Bigdeli, F.; Allahkaram, S. R., An investigation on corrosion resistance of as-applied and heat treated Ni-P/nanoSiC coatings. *Materials & Design* **2009**, 30 (10), 4450-4453.
185. Xu, H.; Yang, Z.; Li, M.-K.; Shi, Y.-L.; Huang, Y.; Li, H.-L., Synthesis and properties of electroless Ni-P-Nanometer Diamond composite coatings. *Surface and coatings technology* **2005**, 191 (2-3), 161-165.
186. Ranganatha, S.; Venkatesha, T.; Vathsala, K., Process and properties of electroless Ni-Cu-P-ZrO₂ nanocomposite coatings. *Materials Research Bulletin* **2012**, 47 (3), 635-645.
187. Sadreddini, S.; Afshar, A., Corrosion resistance enhancement of Ni-P-nano SiO₂ composite coatings on aluminum. *Applied Surface Science* **2014**, 303, 125-130.
188. Araghi, A.; Paydar, M., Electroless deposition of Ni-W-P-B₄C nanocomposite coating on AZ91D magnesium alloy and investigation on its properties. *Vacuum* **2013**, 89, 67-70.
189. Luo, H.; Leitch, M.; Behnamian, Y.; Ma, Y.; Zeng, H.; Luo, J.-L., Development of electroless Ni-P/nano-WC composite coatings and investigation on its properties. *Surface and Coatings Technology* **2015**, 277, 99-106.
190. Tsai, Y.-Y.; Wu, F.-B.; Chen, Y.-I.; Peng, P.-J.; Duh, J.-G.; Tsai, S.-Y., Thermal stability and mechanical properties of Ni-W-P electroless deposits. *Surface and Coatings Technology* **2001**, 146, 502-507.
191. Balaraju, J.; Rajam, K., Influence of particle size on the microstructure, hardness

- and corrosion resistance of electroless Ni–P–Al₂O₃ composite coatings. *Surface and Coatings Technology* **2006**, *200* (12-13), 3933-3941.
192. Zielińska, K.; Stankiewicz, A.; Szczygieł, I., Electroless deposition of Ni–P–nano-ZrO₂ composite coatings in the presence of various types of surfactants. *Journal of colloid and interface science* **2012**, *377* (1), 362-367.
193. Zhu, D.; Leitch, M.; Wang, J.; Shi, X.; Gong, L.; Aghaie, E.; Luo, J.-l.; Zeng, H. In *Evaluation of an Advanced Metal Bonded Coating Technology for Improved SAGD Performance*, SPE Latin America and Caribbean Heavy and Extra Heavy Oil Conference, Society of Petroleum Engineers: 2016.
194. Buckley, J.; Morrow, N. In *Characterization of crude oil wetting behavior by adhesion tests*, SPE/DOE Enhanced Oil Recovery Symposium, Society of Petroleum Engineers: 1990.
195. Buckley, J. S. In *Chemistry of the crude oil/brine interface*, Proc. 3 rd International Symposium on Evaluation of Reservoir Wettability and Its Effect on Oil Recovery, 1994; pp 33-38.
196. Buckley, J.; Liu, Y.; Monsterleet, S., Mechanisms of wetting alteration by crude oils. *SPE journal* **1998**, *3* (01), 54-61.
197. Abudu, A.; Goual, L., Adsorption of crude oil on surfaces using quartz crystal microbalance with dissipation (QCM-D) under flow conditions. *Energy & Fuels* **2008**, *23* (3), 1237-1248.
198. Xie, K.; Karan, K., Kinetics and thermodynamics of asphaltene adsorption on metal surfaces: A preliminary study. *Energy & fuels* **2005**, *19* (4), 1252-1260.

199. Harbottle, D.; Chen, Q.; Moorthy, K.; Wang, L.; Xu, S.; Liu, Q.; Sjöblom, J.; Xu, Z., Problematic stabilizing films in petroleum emulsions: Shear rheological response of viscoelastic asphaltene films and the effect on drop coalescence. *Langmuir* **2014**, *30* (23), 6730-6738.
200. Wang, J.; van der Tuuk Opedal, N.; Lu, Q.; Xu, Z.; Zeng, H.; Sjöblom, J., Probing molecular interactions of an asphaltene model compound in organic solvents using a surface forces apparatus (SFA). *Energy & Fuels* **2011**, *26* (5), 2591-2599.
201. Zhang, L.; Xie, L.; Shi, C.; Huang, J.; Liu, Q.; Zeng, H., Mechanistic Understanding of Asphaltene Surface Interactions in Aqueous Media. *Energy & Fuels* **2016**, *31* (4), 3348-3357.
202. Wang, S.; Liu, J.; Zhang, L.; Xu, Z.; Masliyah, J., Colloidal interactions between asphaltene surfaces in toluene. *Energy & Fuels* **2008**, *23* (2), 862-869.
203. Xie, L.; Shi, C.; Cui, X.; Huang, J.; Wang, J.; Liu, Q.; Zeng, H., Probing the interaction mechanism between air bubbles and bitumen surfaces in aqueous media using bubble probe atomic force microscopy. *Langmuir* **2017**, *34* (3), 729-738.
204. Liu, J.; Wang, J.; Huang, J.; Cui, X.; Tan, X.; Liu, Q.; Zeng, H., Heterogeneous Distribution of Adsorbed Bitumen on Fine Solids from Solvent-Based Extraction of Oil Sands Probed by AFM. *Energy & Fuels* **2017**, *31* (9), 8833-8842.
205. Mao, X.; Gong, L.; Xie, L.; Qian, H.; Wang, X.; Zeng, H., Novel Fe₃O₄ based superhydrophilic core-shell microspheres for breaking asphaltene-stabilized water-in-oil emulsion. *Chemical Engineering Journal* **2019**, *358*, 869-877.
206. Gong, L.; Wang, J.; Zhang, L.; Fattahpour, V.; Mamoudi, M.; Roostaei, M.;

- Fermaniuk, B.; Luo, J.-L.; Zeng, H., Fouling mechanisms of asphaltenes and fine solids on bare and electroless nickel-phosphorus coated carbon steel. *Fuel* **2019**, *252*, 188-199.
- 207.Liu, J.; Xu, Z.; Masliyah, J., Studies on bitumen– silica interaction in aqueous solutions by atomic force microscopy. *Langmuir* **2003**, *19* (9), 3911-3920.
- 208.Hutter, J. L.; Bechhoefer, J., Calibration of atomic - force microscope tips. *Review of Scientific Instruments* **1993**, *64* (7), 1868-1873.
- 209.Meyer, G.; Amer, N. M., Novel optical approach to atomic force microscopy. *Applied physics letters* **1988**, *53* (12), 1045-1047.
- 210.Giessibl, F. J., Advances in atomic force microscopy. *Reviews of modern physics* **2003**, *75* (3), 949.
- 211.Chan, D. Y.; Klaseboer, E.; Manica, R., Dynamic deformations and forces in soft matter. *Soft Matter* **2009**, *5* (15), 2858-2861.
- 212.Chan, D. Y.; Klaseboer, E.; Manica, R., Film drainage and coalescence between deformable drops and bubbles. *Soft Matter* **2011**, *7* (6), 2235-2264.
- 213.Chan, D. Y.; Klaseboer, E.; Manica, R., Theory of non-equilibrium force measurements involving deformable drops and bubbles. *Advances in colloid and interface science* **2011**, *165* (2), 70-90.
- 214.Shi, C.; Cui, X.; Xie, L.; Liu, Q.; Chan, D. Y.; Israelachvili, J. N.; Zeng, H., Measuring forces and spatiotemporal evolution of thin water films between an air bubble and solid surfaces of different hydrophobicity. *ACS nano* **2014**, *9* (1), 95-104.

215. Brant, J. A.; Childress, A. E., Membrane–colloid interactions: comparison of extended DLVO predictions with AFM force measurements. *Environmental Engineering Science* **2002**, *19* (6), 413-427.
216. Dorobantu, L. S.; Bhattacharjee, S.; Foght, J. M.; Gray, M. R., Analysis of force interactions between AFM tips and hydrophobic bacteria using DLVO theory. *Langmuir* **2009**, *25* (12), 6968-6976.
217. Freitas, A. M.; Sharma, M. M., Detachment of particles from surfaces: an AFM study. *Journal of colloid and interface science* **2001**, *233* (1), 73-82.
218. Israelachvili, J. N., *Intermolecular and surface forces*. Academic press: 2011.
219. Cappella, B.; Dietler, G., Force-distance curves by atomic force microscopy. *Surface science reports* **1999**, *34* (1-3), 1-104.
220. Butt, H.-J.; Kappl, M.; Mueller, H.; Raiteri, R.; Meyer, W.; R uhe, J., Steric forces measured with the atomic force microscope at various temperatures. *Langmuir* **1999**, *15* (7), 2559-2565.
221. Biggs, S., Steric and bridging forces between surfaces bearing adsorbed polymer: an atomic force microscopy study. *Langmuir* **1995**, *11* (1), 156-162.
222. Liu, J.; Cui, X.; Huang, J.; Xie, L.; Tan, X.; Liu, Q.; Zeng, H., Understanding the stabilization mechanism of bitumen-coated fine solids in organic media from non-aqueous extraction of oil sands. *Fuel* **2019**, *242*, 255-264.
223. Tamiz Bakhtiari, M.; Harbottle, D.; Curran, M.; Ng, S.; Spence, J.; Siy, R.; Liu, Q.; Masliyah, J.; Xu, Z., Role of caustic addition in bitumen–clay interactions. *Energy & Fuels* **2015**, *29* (1), 58-69.

224. Vogt, B. D.; Lin, E. K.; Wu, W.-I.; White, C. C., Effect of film thickness on the validity of the Sauerbrey equation for hydrated polyelectrolyte films. *The Journal of Physical Chemistry B* **2004**, *108* (34), 12685-12690.
225. Malmström, J.; Agheli, H.; Kingshott, P.; Sutherland, D. S., Viscoelastic Modeling of Highly Hydrated Laminin Layers at Homogeneous and Nanostructured Surfaces: Quantification of Protein Layer Properties Using QCM-D and SPR. *Langmuir* **2007**, *23* (19), 9760-9768.
226. Wu, W.; Giese, R. F., Jr.; van Oss, C. J., Evaluation of the Lifshitz-van der Waals/Acid-Base Approach To Determine Surface Tension Components. *Langmuir* **1995**, *11* (1), 379-382.
227. Park, S.; Jang, E.; An, H.; Choi, W.; Kim, J.-H.; Lee, J.-H.; Choi, J.; Lee, J. S., The Lifshitz-van der Waals acid-base theory assisted fabrication of MFI-containing mixed matrix membranes for gas separations. *Microporous and Mesoporous Materials* **2018**, *264*, 60-69.
228. Watkinson, A. P., Deposition from crude oils in heat exchangers. *Heat transfer engineering* **2007**, *28* (3), 177-184.
229. Hu, B.; Scott, K., Microfiltration of water in oil emulsions and evaluation of fouling mechanism. *Chemical Engineering Journal* **2008**, *136* (2-3), 210-220.
230. Amin, I. N. H. M.; Mohammad, A. W., Adsorptive fouling of organic solutes simulating sweetwater solutions on ultrafiltration membranes. *Chemical Engineering Journal* **2015**, *264*, 470-478.
231. Munoz, V.; Elliott, G.; Afara, M.; Mikula, R., Microscopy of Heat Exchanger

- Fouling During SAGD Operations. *Microsc. Microanal.* **2011**, 17 (S2), 1906.
232. MacAdam, J.; Parsons, S. A., Calcium carbonate scale formation and control. *Re/Views in Environmental Science & Bio/Technology* **2004**, 3 (2), 159-169.
233. Das, S. K.; Butler, R. M., Mechanism of the vapor extraction process for heavy oil and bitumen. *Journal of Petroleum Science and Engineering* **1998**, 21 (1), 43-59.
234. Srinivasan, M. Heat exchanger fouling of some Canadian crude oils. University of British Columbia, 2008.
235. Lalchan, C. A.; Wiggins, C. B.; Moriyama, C. In *Formulation of an Emulsified Thermal Acid Blend for SAGD Applications in Eastern Alberta*, Canadian Unconventional Resources Conference, Society of Petroleum Engineers: 2011.
236. Yarranton, H. W.; Masliyah, J. H., Molar mass distribution and solubility modeling of asphaltenes. *AIChE Journal* **1996**, 42 (12), 3533-3543.
237. Hoepfner, M. P.; Limsakoune, V.; Chuenmeechao, V.; Maqbool, T.; Fogler, H. S., A fundamental study of asphaltene deposition. *Energy & fuels* **2013**, 27 (2), 725-735.
238. Goual, L.; Firoozabadi, A., Measuring asphaltenes and resins, and dipole moment in petroleum fluids. *AIChE Journal* **2002**, 48 (11), 2646-2663.
239. Wang, J.; Buckley, J. S.; Creek, J. L., Asphaltene deposition on metallic surfaces. *J. Dispersion Sci. Technol.* **2004**, 25 (3), 287-298.
240. Deshannavar, U.; Rafeen, M.; Ramasamy, M.; Subbarao, D., Crude oil fouling: A review. *Journal of Applied Sciences (Faisalabad)* **2010**, 10 (24), 3167-3174.
241. Rocha, J.; Baydak, E.; Yarranton, H.; Sztukowski, D.; Ali-Marcano, V.; Gong, L.;

- Shi, C.; Zeng, H., Role of aqueous phase chemistry, interfacial film properties, and surface coverage in stabilizing water-in-bitumen emulsions. *Energy & Fuels* **2016**, *30* (7), 5240-5252.
242. Mullins, O. C.; Sheu, E. Y., *Structures and dynamics of asphaltenes*. Springer Science & Business Media: 2013.
243. Harji, A.; Koppel, P.; Mazurek, W.; Meysami, P. In *Processing Options for Bitumen Upgrading*, Canadian International Petroleum Conference, Petroleum Society of Canada: 2003.
244. Jian, C.; Tang, T.; Bhattacharjee, S., Probing the effect of side-chain length on the aggregation of a model asphaltene using molecular dynamics simulations. *Energy & Fuels* **2013**, *27* (4), 2057-2067.
245. Jian, C.; Zeng, H.; Liu, Q.; Tang, T., Probing the Adsorption of Polycyclic Aromatic Compounds onto Water Droplets Using Molecular Dynamics Simulations. *The Journal of Physical Chemistry C* **2016**, *120* (26), 14170-14179.
246. Goual, L.; Sedghi, M.; Zeng, H.; Mostowfi, F.; McFarlane, R.; Mullins, O. C., On the formation and properties of asphaltene nanoaggregates and clusters by DC-conductivity and centrifugation. *Fuel* **2011**, *90* (7), 2480-2490.
247. Kim, S.-H.; Kim, K.-D.; Lee, H.; Lee, Y.-K., Beneficial roles of H-donors as diluent and H-shuttle for asphaltenes in catalytic upgrading of vacuum residue. *Chemical Engineering Journal* **2017**, *314*, 1-10.
248. Thompson, D.; Taylor, A.; Graham, D., Emulsification and demulsification related to crude oil production. *Colloids and Surfaces* **1985**, *15*, 175-189.

249. Bobicki, E. R.; Liu, Q.; Xu, Z., Ligand-promoted dissolution of serpentine in ultramafic nickel ores. *Minerals Engineering* **2014**, *64*, 109-119.
250. Chalaturnyk, R. J.; Don Scott, J.; Özüm, B., Management of oil sands tailings. *Petroleum Science and Technology* **2002**, *20* (9-10), 1025-1046.
251. Carew, J.; Al-Sayegh, A.; Al-Hashem, A. In *The effect of water-cut on the corrosion behaviour L80 carbon steel under downhole conditions*, CORROSION-NATIONAL ASSOCIATION OF CORROSION ENGINEERS ANNUAL CONFERENCE-, NACE: 2000.
252. Choi, H. J.; Warnken, D.; Al Beheiri, F. I.; Al-Bannai, N. S. In *Field Corrosion Assessment of L80 Carbon Steel Downhole Production Tubing at Khuff Gas Wells*, CORROSION 2006, NACE International: 2006.
253. Sun, W.; Pugh, D.; Ling, S.; Reddy, R.; Pacheco, J.; Nisbet, R.; Nor, N.; Kersey, M.; Morshidi, L. In *Understanding and quantifying corrosion of L80 carbon steel in sour environments*, CORROSION 2011, NACE International: 2011.
254. Deyab, M. A. M., Corrosion Inhibition and Adsorption Behavior of Sodium Lauryl Ether Sulfate on L80 Carbon Steel in Acetic Acid Solution and Its Synergism with Ethanol. *Journal of Surfactants and Detergents* **2015**, *18* (3), 405-411.
255. Ye, Y.; Liu, Z.; Liu, W.; Zhang, D.; Zhao, H.; Wang, L.; Li, X., Superhydrophobic oligoaniline-containing electroactive silica coating as pre-process coating for corrosion protection of carbon steel. *Chemical Engineering Journal* **2018**, *348*, 940-951.
256. Lalande, M.; Tissier, J.-P.; Corrieu, G., Fouling of a plate heat exchanger used in

- ultra-high-temperature sterilization of milk. *Journal of Dairy Research* **1984**, *51* (04), 557-568.
257. Changani, S.; Belmar-Beiny, M.; Fryer, P., Engineering and chemical factors associated with fouling and cleaning in milk processing. *Exp. Therm Fluid Sci.* **1997**, *14* (4), 392-406.
258. Visser, J.; Jeurink, T. J., Fouling of heat exchangers in the dairy industry. *Exp. Therm Fluid Sci.* **1997**, *14* (4), 407-424.
259. Bansal, B.; Chen, X. D., A critical review of milk fouling in heat exchangers. *Comprehensive reviews in food science and food safety* **2006**, *5* (2), 27-33.
260. Genzer, J.; Marmur, A., Biological and synthetic self-cleaning surfaces. *MRS Bull.* **2008**, *33* (08), 742-746.
261. Mérian, T.; Goddard, J. M., Advances in nonfouling materials: perspectives for the food industry. *J. Agric. Food. Chem.* **2012**, *60* (12), 2943-2957.
262. Beuf, M.; Rizzo, G.; Leuliet, J.; Müller-Steinhagen, H.; Yiantsios, S.; Karabelas, A.; Benezech, T., Fouling and cleaning of modified stainless steel plate heat exchangers processing milk products. **2003**.
263. Rosmaninho, R.; Melo, L. F., Calcium phosphate deposition from simulated milk ultrafiltrate on different stainless steel-based surfaces. *International Dairy Journal* **2006**, *16* (1), 81-87.
264. Premathilaka, S.; Hyland, M.; Chen, X.; Bansal, B., A study of the effects of surface chemistry on the initial deposition mechanisms of dairy fouling. *Food and bioproducts processing* **2006**, *84* (4), 265-273.

265. Rosmaninho, R.; Santos, O.; Nylander, T.; Paulsson, M.; Beuf, M.; Benezech, T.; Yiantsios, S.; Andritsos, N.; Karabelas, A.; Rizzo, G., Modified stainless steel surfaces targeted to reduce fouling—evaluation of fouling by milk components. *J. Food Eng.* **2007**, *80* (4), 1176-1187.
266. Balasubramanian, S.; Puri, V., Thermal energy savings in pilot-scale plate heat exchanger system during product processing using modified surfaces. *J. Food Eng.* **2009**, *91* (4), 608-611.
267. Lin, J.; Wang, C.; Wang, S.; Chen, Y.; He, W.; Xiao, D., Initiation electroless nickel plating by atomic hydrogen for PCB final finishing. *Chemical Engineering Journal* **2016**, *306*, 117-123.
268. Gu, C.; Lian, J.; Li, G.; Niu, L.; Jiang, Z., High corrosion-resistant Ni-P/Ni/Ni-P multilayer coatings on steel. *Surf. Coat. Technol.* **2005**, *197* (1), 61-67.
269. Wu, Y.; Liu, T.; Luo, S., Corrosion characteristics of electroless Ni - P coating in sulfur - bearing solution. *Mater. Corros.* **2009**, *60* (12), 987-990.
270. Karthikeyan, S.; Ramamoorthy, B., Effect of reducing agent and nano Al₂O₃ particles on the properties of electroless Ni-P coating. *Appl. Surf. Sci.* **2014**, *307*, 654-660.
271. Ranganatha, S.; Venkatesha, T.; Vathsala, K., Process and properties of electroless Ni-Cu-P-ZrO₂ nanocomposite coatings. *Mater. Res. Bull.* **2012**, *47* (3), 635-645.
272. Sadreddini, S.; Afshar, A., Corrosion resistance enhancement of Ni-P-nano SiO₂ composite coatings on aluminum. *Appl. Surf. Sci.* **2014**, *303*, 125-130.
273. Zhang, L. Y.; Lawrence, S.; Xu, Z.; Masliyah, J. H., Studies of Athabasca

- asphaltene Langmuir films at air–water interface. *Journal of colloid and interface science* **2003**, *264* (1), 128-140.
274. Kar, K. K.; Sathiyamoorthy, D., Influence of process parameters for coating of nickel–phosphorous on carbon fibers. *journal of materials processing technology* **2009**, *209* (6), 3022-3029.
275. Xie, L.; Wang, J.; Shi, C.; Huang, J.; Zhang, H.; Liu, Q.; Liu, Q.; Zeng, H., Probing surface interactions of electrochemically active galena mineral surface using atomic force microscopy. *The Journal of Physical Chemistry C* **2016**, *120* (39), 22433-22442.
276. Wang, J.; Li, J.; Xie, L.; Shi, C.; Liu, Q.; Zeng, H., Interactions between elemental selenium and hydrophilic/hydrophobic surfaces: Direct force measurements using AFM. *Chemical Engineering Journal* **2016**, *303*, 646-654.
277. Xie, L.; Wang, J.; Shi, C.; Cui, X.; Huang, J.; Zhang, H.; Liu, Q.; Liu, Q.; Zeng, H., Mapping the nanoscale heterogeneity of surface hydrophobicity on the sphalerite mineral. *The Journal of Physical Chemistry C* **2017**, *121* (10), 5620-5628.
278. Wang, J.; Xie, L.; Zhang, H.; Liu, Q.; Liu, Q.; Zeng, H., Probing interactions between sphalerite and hydrophobic/hydrophilic surfaces: Effect of water chemistry. *Powder Technology* **2017**, *320*, 511-518.
279. Yang, D.; Xie, L.; Bobicki, E.; Xu, Z.; Liu, Q.; Zeng, H., Probing anisotropic surface properties and interaction forces of chrysotile rods by atomic force microscopy and rheology. *Langmuir* **2014**, *30* (36), 10809-10817.

280. Gao, Z.; Xie, L.; Cui, X.; Hu, Y.; Sun, W.; Zeng, H., Probing Anisotropic Surface Properties and Surface Forces of Fluorite Crystals. *Langmuir* **2018**, *34* (7), 2511-2521.
281. Tulpar, A.; Walz, J., Simultaneous measurement of structural and hydrodynamic forces between colloidal surfaces in complex fluids. *Colloids Surf., A* **2007**, *300* (3), 268-280.
282. Prieve, D. C.; Russel, W. B., Simplified predictions of Hamaker constants from Lifshitz theory. *Journal of Colloid and Interface Science* **1988**, *125* (1), 1-13.
283. Bergstrom, L.; Meurk, A.; Arwin, H.; Rowcliffe, D. J., Estimation of Hamaker constants of ceramic materials from optical data using Lifshitz theory. *Journal of the American Ceramic Society* **1996**, *79* (2), 339-348.
284. Wang, M.; Revil, A., Electrochemical charge of silica surfaces at high ionic strength in narrow channels. *Journal of colloid and interface science* **2010**, *343* (1), 381-386.
285. Chen, G.; Warmack, R.; Huang, A.; Thundat, T., Harmonic response of near - contact scanning force microscopy. *Journal of Applied Physics* **1995**, *78* (3), 1465-1469.
286. Boulangé-Petermann, L.; Doren, A.; Baroux, B.; Bellon-Fontaine, M.-N., Zeta potential measurements on passive metals. *Journal of colloid and interface science* **1995**, *171* (1), 179-186.
287. Gong, L.; Qiu, X.; Zhang, L.; Huang, J.; Hu, W.; Xiang, L.; Zhu, D.; Sabbagh, R.; Mahmoudi, M.; Fattahpour, V., Probing the Interaction Mechanism between Oil-

- in-Water Emulsions and Electroless Nickel–Phosphorus Coating with Implications for Antifouling in Oil Production. *Energy & Fuels* **2018**.
288. Wu, J.; Prausnitz, J. M.; Firoozabadi, A., Molecular thermodynamics of asphaltene precipitation in reservoir fluids. *AIChE journal* **2000**, *46* (1), 197-209.
289. Das, S.; Thundat, T.; Mitra, S. K., Analytical model for zeta potential of asphaltene. *Fuel* **2013**, *108*, 543-549.
290. Wang, J.; Lu, Q.; Harbottle, D.; Sjöblom, J.; Xu, Z.; Zeng, H., Molecular interactions of a polyaromatic surfactant C5Pe in aqueous solutions studied by a surface forces apparatus. *The Journal of Physical Chemistry B* **2012**, *116* (36), 11187-11196.
291. Chaisoontornyotin, W.; Haji-Akbari, N.; Fogler, H. S.; Hoepfner, M. P., Combined asphaltene aggregation and deposition investigation. *Energy & Fuels* **2016**, *30* (3), 1979-1986.
292. Mo, H.; Tay, K. G.; Ng, H. Y., Fouling of reverse osmosis membrane by protein (BSA): effects of pH, calcium, magnesium, ionic strength and temperature. *Journal of Membrane Science* **2008**, *315* (1-2), 28-35.
293. Elimelech, M.; Zhu, X.; Childress, A. E.; Hong, S., Role of membrane surface morphology in colloidal fouling of cellulose acetate and composite aromatic polyamide reverse osmosis membranes. *Journal of membrane science* **1997**, *127* (1), 101-109.
294. Hamza, A.; Pham, V.; Matsuura, T.; Santerre, J., Development of membranes with low surface energy to reduce the fouling in ultrafiltration applications. *Journal of*

- Membrane Science* **1997**, *131* (1-2), 217-227.
295. Ma, F.; Hanna, M. A., Biodiesel production: a review. *Bioresource technology* **1999**, *70* (1), 1-15.
296. Shams Ashaghi, K.; Ebrahimi, M.; Czermak, P., Ceramic ultra-and nanofiltration membranes for oilfield produced water treatment: a mini review. *Open Environmental Sciences* **2007**, *1* (1).
297. Fakhru'l-Razi, A.; Pendashteh, A.; Abdullah, L. C.; Biak, D. R. A.; Madaeni, S. S.; Abidin, Z. Z., Review of technologies for oil and gas produced water treatment. *Journal of hazardous materials* **2009**, *170* (2-3), 530-551.
298. Ochando-Pulido, J.; Stoller, M.; Bravi, M.; Martinez-Ferez, A.; Chianese, A., Batch membrane treatment of olive vegetation wastewater from two-phase olive oil production process by threshold flux based methods. *Separation and Purification Technology* **2012**, *101*, 34-41.
299. Macchietto, S.; Hewitt, G.; Coletti, F.; Crittenden, B. D.; Dugwell, D.; Galindo, A.; Jackson, G.; Kandiyoti, R.; Kazarian, S.; Luckham, P., Fouling in crude oil preheat trains: a systematic solution to an old problem. *Heat Transfer Engineering* **2011**, *32* (3-4), 197-215.
300. Pragya, N.; Pandey, K. K.; Sahoo, P., A review on harvesting, oil extraction and biofuels production technologies from microalgae. *Renewable and Sustainable Energy Reviews* **2013**, *24*, 159-171.
301. Martínez-Palou, R.; de Lourdes Mosqueira, M.; Zapata-Rendón, B.; Mar-Juárez, E.; Bernal-Huicochea, C.; de la Cruz Clavel-López, J.; Aburto, J., Transportation

- of heavy and extra-heavy crude oil by pipeline: A review. *Journal of Petroleum Science and Engineering* **2011**, 75 (3-4), 274-282.
302. Zhao, B.; Shaw, J. M., Composition and size distribution of coherent nanostructures in Athabasca bitumen and Maya crude oil. *Energy & Fuels* **2007**, 21 (5), 2795-2804.
303. Bacchin, P.; Aimar, P.; Sanchez, V., Model for colloidal fouling of membranes. *AIChE journal* **1995**, 41 (2), 368-376.
304. Mansoori, G. A.; Vazquez, D.; Shariaty-Niassar, M., Polydispersity of heavy organics in crude oils and their role in oil well fouling. *Journal of Petroleum Science and Engineering* **2007**, 58 (3-4), 375-390.
305. Visser, S.; Griffiths, C. L.; Parkinson, D., Effects of surface mining on the microbiology of a prairie site in Alberta, Canada. *Canadian Journal of Soil Science* **1983**, 63 (2), 177-189.
306. Balsamo, V.; Nguyen, D.; Phan, J., Non-conventional techniques to characterize complex SAGD emulsions and dilution effects on emulsion stabilization. *Journal of Petroleum Science and Engineering* **2014**, 122, 331-345.
307. Noik, C.; Dalmazzone, C. S.; Goulay, C.; Glenat, P. In *Characterisation and emulsion behaviour of Athabasca extra heavy oil produced by SAGD*, SPE International Thermal Operations and Heavy Oil Symposium, Society of Petroleum Engineers: 2005.
308. Wang, G.; Zhu, L.; Liu, H.; Li, W., Galvanic corrosion of Ni–Cu–Al composite coating and its anti-fouling property for metal pipeline in simulated geothermal

- water. *Surface and Coatings Technology* **2012**, 206 (18), 3728-3732.
309. Zhao, Q.; Liu, C.; Su, X.; Zhang, S.; Song, W.; Wang, S.; Ning, G.; Ye, J.; Lin, Y.; Gong, W., Antibacterial characteristics of electroless plating Ni-P-TiO₂ coatings. *Applied Surface Science* **2013**, 274, 101-104.
310. Crosby, T.; Wolodko, J.; Tsaprailis, H. In *Gap Analysis of Canadian Pipeline Coatings: A Review Study*, NACE International Corrosion Conference Proceedings, NACE International: 2016; p 1.
311. Farzaneh, A.; Ehteshamzadeh, M.; Can, M.; Mermer, O.; Okur, S., Effects of SiC particles size on electrochemical properties of electroless Ni-P-SiC nanocomposite coatings. *Protection of Metals and Physical Chemistry of Surfaces* **2016**, 52 (4), 632-636.
312. Azizi, A.; Mohammadi, M.; Sadrnezhaad, S., End-closed NiCoFe-B nanotube arrays by electroless method. *Mater. Lett.* **2011**, 65 (2), 289-292.
313. Farzaneh, A.; Ehteshamzadeh, M.; Cobley, A. J., Modelling of surfactants and chemistry for electroless Ni-P plating. *Surf. Eng.* **2017**, 1-8.
314. Wurtz, A., Sur l'hydrure de cuivre. *CR Hebd. Seances Acad. Sci.* **1844**, 18, 702-704.
315. Drenner, A.; Couch, D.; Williams, E. K., Electrodeposition of Alloys of Phosphorus and Nickel or Cobalt. *Plating* **1950**, 37, 36-42.
316. Gutzeit, G., Catalytic nickel deposition from aqueous solution. I-IV. *Plating surface finishing* **1959**, 46, 1158-1164.
317. John, S.; Shanmugham, N.; Shenoi, B., A Low-Temperature

- Autocatalytic(Electroless) Nickel Plating Process. *Metal Finishing* **1982**, 80 (4), 47-52.
- 318.Parker, K., The formulation of electroless nickel-phosphorus plating baths. *Plat. Surf. Finish.* **1987**, 74 (2), 60-65.
- 319.Bates, J., Why use electroless nickel today? *Plat. Surf. Finish.* **1998**, 85 (5), 14-16.
- 320.Apachitei, I.; Duszczyk, J.; Katgerman, L.; Overkamp, P., Electroless Ni-P composite coatings: the effect of heat treatment on the microhardness of substrate and coating. *Scripta Mater.* **1998**, 38 (9), 1347-1353.
- 321.Hajdu, J., Electroless plating: the past is prologue. *Plat. Surf. Finish.* **1996**, 83 (9), 29-33.
- 322.Hajdu, J., William Blum Lecture--Electroless Plating: What's Past is Prologue. *Plat. Surf. Finish.* **1996**, 83 (9), 29-33.
- 323.Shi, C.; Yan, B.; Xie, L.; Zhang, L.; Wang, J.; Takahara, A.; Zeng, H., Long - Range Hydrophilic Attraction between Water and Polyelectrolyte Surfaces in Oil. *Angewandte Chemie International Edition* **2016**, 55 (48), 15017-15021.
- 324.Shi, C.; Zhang, L.; Xie, L.; Lu, X.; Liu, Q.; He, J.; Mantilla, C. A.; Zeng, H., Surface Interaction of Water-in-Oil Emulsion Droplets with Interfacially Active Asphaltenes. *Langmuir* **2017**, 33 (5), 1265-1274.
- 325.Xie, L.; Shi, C.; Cui, X.; Zeng, H., Surface Forces and Interaction Mechanisms of Emulsion Drops and Gas Bubbles in Complex Fluids. *Langmuir* **2017**, 33 (16), 3911-3925.
- 326.Xie, L.; Shi, C.; Cui, X.; Huang, J.; Wang, J.; Liu, Q.; Zeng, H., Probing the

Interaction Mechanism between Air Bubbles and Bitumen Surfaces in Aqueous Media Using Bubble Probe Atomic Force Microscopy. *Langmuir*.

327. Palaniappa, M.; Babu, G. V.; Balasubramanian, K., Electroless nickel–phosphorus plating on graphite powder. *Materials Science and Engineering: A* **2007**, *471* (1), 165-168.
328. Radelczuk, H.; Hołysz, L.; Chibowski, E., Comparison of the Lifshitz–van der Waals/acid–base and contact angle hysteresis approaches for determination of solid surface free energy. *Journal of adhesion science and technology* **2002**, *16* (12), 1547-1568.
329. Cappella, B.; Dietler, G., Force-distance curves by atomic force microscopy. *Surf. Sci. Rep.* **1999**, *34* (1-3), 15-3104.
330. Hayashi, T.; Ohno, T.; Yatsuya, S.; Uyeda, R., Formation of ultrafine metal particles by gas-evaporation technique. IV. Crystal habits of iron and Fcc metals, Al, Co, Ni, Cu, Pd, Ag, In, Au and Pb. *Japanese Journal of Applied Physics* **1977**, *16* (5), 705.
331. Chen, C.; Idzerda, Y.; Lin, H.-J.; Smith, N.; Meigs, G.; Chaban, E.; Ho, G.; Pellegrin, E.; Sette, F., Experimental confirmation of the X-ray magnetic circular dichroism sum rules for iron and cobalt. *Physical review letters* **1995**, *75* (1), 152.
332. Miyazaki, T.; Tezuka, N., Giant magnetic tunneling effect in Fe/Al₂O₃/Fe junction. *Journal of Magnetism and Magnetic Materials* **1995**, *139* (3), L231-L234.
333. Pogrebnyak, A.; Bratushka, S.; Boyko, V.; Shamanin, I. V.; Tsvintarnaya, Y. V., A review of mixing processes in Ta/Fe and Mo/Fe systems treated by high current

- electron beams. *Nuclear Instruments and Methods in Physics Research Section B: Beam Interactions with Materials and Atoms* **1998**, 145 (3), 373-390.
334. Drever, J. I., *The geochemistry of natural waters*. Prentice-Hall Englewood Cliffs: 1982; Vol. 9.
335. Murgich, J., Intermolecular forces in aggregates of asphaltenes and resins. *Petroleum Science and Technology* **2002**, 20 (9-10), 983-997.
336. Maqbool, T.; Raha, S.; Hoepfner, M. P.; Fogler, H. S., Modeling the aggregation of asphaltene nanoaggregates in crude oil– precipitant systems. *Energy & Fuels* **2011**, 25 (4), 1585-1596.
337. Kou, J.; Xu, S.; Sun, T.; Sun, C.; Guo, Y.; Wang, C., A study of sodium oleate adsorption on Ca²⁺ activated quartz surface using quartz crystal microbalance with dissipation. *International Journal of Mineral Processing* **2016**, 154, 24-34.
338. Yu, W.; Sun, T.; Kou, J.; Wei, Y.; Xu, C.; Liu, Z., The function of Ca (OH) 2 and Na₂CO₃ as additive on the reduction of high-phosphorus oolitic hematite-coal mixed pellets. *ISIJ international* **2013**, 53 (3), 427-433.
339. Yang, F.; Tchoukov, P.; Dettman, H.; Teklebrhan, R. B.; Liu, L.; Dabros, T.; Czarnecki, J.; Masliyah, J.; Xu, Z., Asphaltene subfractions responsible for stabilizing water-in-crude oil emulsions. Part 2: Molecular representations and molecular dynamics simulations. *Energy & Fuels* **2015**, 29 (8), 4783-4794.
340. Czarnecki, J.; Tchoukov, P.; Dabros, T.; Xu, Z., Role of asphaltenes in stabilisation of water in crude oil emulsions. *The Canadian Journal of Chemical Engineering* **2013**, 91 (8), 1365-1371.

- 341.Li, M.; Xu, M.; Ma, Y.; Wu, Z.; Christy, A. A., Interfacial film properties of asphaltenes and resins. *Fuel* **2002**, *81* (14), 1847-1853.
- 342.Long, Y.; Dabros, T.; Hamza, H., Stability and settling characteristics of solvent-diluted bitumen emulsions. *Fuel* **2002**, *81* (15), 1945-1952.
- 343.Lu, Q.; Huang, J.; Maan, O.; Liu, Y.; Zeng, H., Probing molecular interaction mechanisms of organic fouling on polyamide membrane using a surface forces apparatus: implication for wastewater treatment. *Science of The Total Environment* **2018**, *622*, 644-654.
- 344.Xia, Y.; Adibnia, V.; Huang, R.; Murschel, F.; Faivre, J.; Xie, G.; Olszewski, M.; De Crescenzo, G.; Qi, W.; He, Z., Biomimetic Bottlebrush Polymer Coatings for Fabrication of Ultralow Fouling Surfaces. *Angewandte Chemie* **2019**, *131* (5), 1322-1328.
- 345.Srinivasan, M.; Watkinson, A., Fouling of some Canadian crude oils. *Heat transfer engineering* **2005**, *26* (1), 7-14.
- 346.Collins, I. In *A new model for mineral scale adhesion*, International Symposium on Oilfield Scale, Society of Petroleum Engineers: 2002.
- 347.Gentzis, T.; Parker, R.; McFarlane, R., Microscopy of fouling deposits in bitumen furnaces. *Fuel* **2000**, *79* (10), 1173-1184.
- 348.Bott, T., General fouling problems. In *Fouling Science and Technology*, Springer: 1988; pp 3-14.
- 349.Kazi, S.; Duffy, G.; Chen, X., Mineral scale formation and mitigation on metals and a polymeric heat exchanger surface. *Appl. Therm. Eng.* **2010**, *30* (14-15), 2236-

2242.

350. Leontaritis, K. In *Asphaltene deposition: A comprehensive description of problem manifestations and modeling approaches*, SPE production operations symposium, Society of Petroleum Engineers: 1989.
351. Bennett, C. A.; Kistler, R. S.; Nangia, K.; Al-Ghawas, W.; Al-Hajji, N.; Al-Jemaz, A., Observation of an isokinetic temperature and compensation effect for high-temperature crude oil fouling. *Heat Transfer Engineering* **2009**, *30* (10-11), 794-804.
352. Hammami, A.; Ratulowski, J., Precipitation and deposition of asphaltenes in production systems: A flow assurance overview. In *Asphaltenes, heavy oils, and petroleomics*, Springer: 2007; pp 617-660.
353. Asomaning, S. Heat exchanger fouling by petroleum asphaltenes. University of British Columbia, 1997.
354. Awad, M. M., Fouling of heat transfer surfaces. In *Heat Transfer-Theoretical Analysis, Experimental Investigations and Industrial Systems*, InTech: 2011.
355. Rana, M. S.; Samano, V.; Ancheyta, J.; Diaz, J., A review of recent advances on process technologies for upgrading of heavy oils and residua. *Fuel* **2007**, *86* (9), 1216-1231.
356. Mendoza de la Cruz, J. L.; Argüelles-Vivas, F. J.; Matías-Pérez, V. c.; Durán-Valencia, C. d. l. A.; López-Ramírez, S. n., Asphaltene-induced precipitation and deposition during pressure depletion on a porous medium: an experimental investigation and modeling approach. *Energy & Fuels* **2009**, *23* (11), 5611-5625.

357. Drummond, C.; Israelachvili, J., Fundamental studies of crude oil–surface water interactions and its relationship to reservoir wettability. *Journal of Petroleum Science and Engineering* **2004**, *45* (1-2), 61-81.
358. Gray, M. R.; Tykwinski, R. R.; Stryker, J. M.; Tan, X., Supramolecular assembly model for aggregation of petroleum asphaltenes. *Energy & Fuels* **2011**, *25* (7), 3125-3134.
359. Eyssautier, J. l.; Levitz, P.; Espinat, D.; Jestin, J.; Gummel, J. r. m.; Grillo, I.; Barré, L. c., Insight into asphaltene nanoaggregate structure inferred by small angle neutron and X-ray scattering. *J. Phys. Chem. B* **2011**, *115* (21), 6827-6837.
360. Visser, J., Particle adhesion and removal: A review. *Particulate science and technology* **1995**, *13* (3-4), 169-196.
361. Faille, C.; Jullien, C.; Fontaine, F.; Bellon-Fontaine, M.-N.; Slomianny, C.; Benezech, T., Adhesion of Bacillus spores and Escherichia coli cells to inert surfaces: role of surface hydrophobicity. *Can. J. Microbiol.* **2002**, *48* (8), 728-738.
362. Lee, S.; Elimelech, M., Relating organic fouling of reverse osmosis membranes to intermolecular adhesion forces. *Environmental science & technology* **2006**, *40* (3), 980-987.
363. Choo, K.-H.; Lee, C.-H., Understanding membrane fouling in terms of surface free energy changes. *J. Colloid Interface Sci.* **2000**, *226* (2), 367-370.
364. Bartels, L., Tailoring molecular layers at metal surfaces. *Nature chemistry* **2010**, *2* (2), 87.
365. Ye, Q.; Zhou, F.; Liu, W., Bioinspired catecholic chemistry for surface modification.

Chemical Society Reviews **2011**, *40* (7), 4244-4258.

366. Mikami, Y.; Liang, Y.; Matsuoka, T.; Boek, E. S., Molecular dynamics simulations of asphaltenes at the oil–water interface: from nanoaggregation to thin-film formation. *Energy & Fuels* **2013**, *27* (4), 1838-1845.
367. Alvarez, G.; Jestin, J.; Argillier, J.; Langevin, D., Small-angle neutron scattering study of crude oil emulsions: Structure of the oil– water interfaces. *Langmuir* **2009**, *25* (7), 3985-3990.
368. Tchoukov, P.; Yang, F.; Xu, Z.; Dabros, T.; Czarnecki, J.; Sjöblom, J., Role of asphaltenes in stabilizing thin liquid emulsion films. *Langmuir* **2014**, *30* (11), 3024-3033.
369. Yarranton, H. W.; Hussein, H.; Masliyah, J. H., Water-in-hydrocarbon emulsions stabilized by asphaltenes at low concentrations. *J. Colloid Interface Sci.* **2000**, *228* (1), 52-63.
370. Huang, Y.; Zeng, X.; Hu, X.; Liu, F., Corrosion resistance properties of electroless nickel composite coatings. *Electrochim. Acta* **2004**, *49* (25), 4313-4319.
371. Rabizadeh, T.; Allahkaram, S. R.; Zarebidaki, A., An investigation on effects of heat treatment on corrosion properties of Ni–P electroless nano-coatings. *Materials & Design* **2010**, *31* (7), 3174-3179.
372. Sahoo, P.; Das, S. K., Tribology of electroless nickel coatings—a review. *Materials & Design* **2011**, *32* (4), 1760-1775.
373. Grosjean, A.; Rezrazi, M.; Takadoun, J.; Bercot, P., Hardness, friction and wear characteristics of nickel-SiC electroless composite deposits. *Surf. Coat. Technol.*

2001, *137* (1), 92-96.

- 374.Chen, C.; Feng, H.; Lin, H.; Hon, M.-H., The effect of heat treatment on the microstructure of electroless Ni–P coatings containing SiC particles. *Thin Solid Films* **2002**, *416* (1-2), 31-37.
- 375.Sudagar, J.; Lian, J.; Sha, W., Electroless nickel, alloy, composite and nano coatings—A critical review. *J. Alloys Compd.* **2013**, *571*, 183-204.
- 376.Chen, X.; Chen, C.; Xiao, H.; Liu, H.; Zhou, L.; Li, S.; Zhang, G., Dry friction and wear characteristics of nickel/carbon nanotube electroless composite deposits. *Tribology international* **2006**, *39* (1), 22-28.
- 377.Shi, C.; Chan, D. Y.; Liu, Q.; Zeng, H., Probing the hydrophobic interaction between air bubbles and partially hydrophobic surfaces using atomic force microscopy. *The Journal of Physical Chemistry C* **2014**, *118* (43), 25000-25008.
- 378.Khodakarami, M.; Alagha, L.; Burnett, D. J., Probing Surface Characteristics of Rare Earth Minerals Using Contact Angle Measurements, Atomic Force Microscopy, and Inverse Gas Chromatography. *ACS omega* **2019**, *4* (8), 13319-13329.
- 379.Wu, X., Investigating the stability mechanism of water-in-diluted bitumen emulsions through isolation and characterization of the stabilizing materials at the interface. *Energy & fuels* **2003**, *17* (1), 179-190.
- 380.Zhong, Z.; Li, D.; Zhang, B.; Xing, W., Membrane surface roughness characterization and its influence on ultrafine particle adhesion. *Separation and purification technology* **2012**, *90*, 140-146.

- 381.Hoek, E. M.; Bhattacharjee, S.; Elimelech, M., Effect of membrane surface roughness on colloid– membrane DLVO interactions. *Langmuir* **2003**, *19* (11), 4836-4847.
- 382.Bowen, W. R.; Doneva, T. A., Atomic force microscopy studies of membranes: Effect of surface roughness on double-layer interactions and particle adhesion. *Journal of colloid and interface science* **2000**, *229* (2), 544-549.
- 383.Crittenden, B.; Alderman, N., Negative fouling resistances: the effect of surface roughness. *Chemical engineering science* **1988**, *43* (4), 829-838.
- 384.Eyssautier, J.; Levitz, P.; Espinat, D.; Jestin, J.; Gummel, J.; Grillo, I.; Barré, L., Insight into asphaltene nanoaggregate structure inferred by small angle neutron and X-ray scattering. *The Journal of Physical Chemistry B* **2011**, *115* (21), 6827-6837.
- 385.McLean, J. D.; Kilpatrick, P. K., Effects of asphaltene solvency on stability of water-in-crude-oil emulsions. *J. Colloid Interface Sci.* **1997**, *189* (2), 242-253.
- 386.McLean, J. D.; Kilpatrick, P. K., Effects of asphaltene aggregation in model heptane–toluene mixtures on stability of water-in-oil emulsions. *J. Colloid Interface Sci.* **1997**, *196* (1), 23-34.
- 387.Destribats, M.; Lapeyre, V.; Wolfs, M.; Sellier, E.; Leal-Calderon, F.; Ravaine, V.; Schmitt, V., Soft microgels as Pickering emulsion stabilisers: role of particle deformability. *Soft Matter* **2011**, *7* (17), 7689-7698.
- 388.Zhang, S.; Zhang, L.; Lu, X.; Shi, C.; Tang, T.; Wang, X.; Huang, Q.; Zeng, H., Adsorption kinetics of asphaltenes at oil/water interface: Effects of concentration and temperature. *Fuel* **2018**, *212*, 387-394.